Mechanistic Determinations of Enhanced Heat Transfer Occurring in Stagnant and Flowing Microfibrous Entrapped Catalytic Reactors

by

Phillip Michael Martin

A dissertation submitted to the Graduate Faculty of
Auburn University
in partial fulfillment of the
requirements for the Degree of
Doctor of Philosophy

Auburn, Alabama
August 3, 2024

Keywords: microfibrous media, heat transfer, effective thermal conductivity

Approved by

Bruce Tatarchuk, Chair, Charles E. Gavin III Professor of Chemical Engineering
William Ashurst, Uthlaut Family Associate Professor of Chemical Engineering
Maria Auad, Charles Gavin Distinguished Professor of Chemical Engineering
Daniel Harris, Associate Professor of Mechanical Engineering

Abstract

Microfibrous media (MFM) is a fibrous material made via traditional paper-making techniques resulting in a media that is preferentially oriented within a single plane (but random within that plane). Metal MFMs, particularly copper MFM (Cu-MFM), are used in catalytic beds and are known to exhibit superior heat transfer performance to packed beds. To investigate the mechanisms for this, experiments were conducted in an $\frac{1}{8}$-inch alumina pellet packed bed and a Cu-MFM bed composed of 17 mm diameter x 6 mm long fibers and 6 mm diameter x 3 mm long fibers. Heat transfer experiments were performed both with stagnant and flowing gasses as well as under vacuum. Existing literature models were compared to the experimental results and various resistance networks and unit cells are presented for modelling MFM. What was found is that the the presence of a gas within an MFM bed plays a substantial role in its effective thermal conductivity. Additionally, as has been previously shown for packed beds, as the thermal conductivity of the gas within an MFM bed increases, the effective thermal conductivity of the bed increases. It was found that if two fibers are modelled with a gas-filled gap, the length of the gap has a large impact on the effective thermal conductivity of the system. Therefore, it is proposed that the superior heat transfer performance of MFM over packed beds is due in part to the preferential orientation of the fibers as appears in prior literature, and in part due to many short gaps between fibers within the media that, when a fluid is present, provide excellent heat-transfer pathways.

Acknowledgments

I would like to acknowledge several people for their support and help in completing this work. Foremost, the Auburn University Chemical Engineering department; my advisor, Dr. Bruce Tatarchuk; and my committee for giving me the opportunity to pursue this degree and for their assistance provided along the way. Likewise, Intramicron in Auburn, AL was essential to this work as they provided the microfibrous media (MFM) for this work as well as lending their expertise, time, and resources.

Next, My research group who has always been willing to lend a hand when needed. Especially, Dr. Zenda Davis and Dr. Xinquan Cheng who have been a great friends who have continued to help me long after completing their times in the group.

Within the Auburn University Chemical Engineering department, I would like to thank a few people specifically. Brian Schwieker who provided great assistance with equipment and materials as well as much discussion of ideas for this work. Also, Dwight Cahela who provided various kinds of help whenever needed and shared his knowledge. Lastly, Emma Goodlett and Elaine Manning who provided constant help with completing this degree.

In addition to the chemical engineering department, Auburn University Engineering Network Services has been an indispensable resource ranging from help with programming, repairing damaged computers, and giving advice and ideas on how to solve problems. I would like to especially thank Nabeel Rawajfih of Engineering Network Services who has provided more help than there is thanks to give.

Finally, I thank my friends and family who have provided support financially, through allowing me to discuss ideas with them, and through physically helping me in lab.

Table of Contents

Abstract 2

Acknowledgments 3

List of Tables 10

List of Figures 12

List of Abbreviations and Nomenclature 35

1 Introduction and Background 38

1.1 Overview of Microfibrous Media Research 39

2 Effective Thermal Conductivity of a Microfibrous Media Bed Containing Stagnant Gas 41

2.1 Experimental 41

2.1.1 Multi-Point Thermocouple Description 41

2.1.2 Thermocouple Support Description 43

2.1.3 Packed Bed Description 45

2.1.4 Microfibrous Media Bed Description 51

2.1.5 Microfibrous Media Used for Packing 58

2.2 Alumina Packed Bed Experimental Results 61

2.3 Microfibrous Media Bed Experimental Results 65

2.4 Computational Model of Experiments with stagnant Gas 71

2.4.1 Energy Equation in One Dimensions 72

2.4.2 von Neumann Analysis of the Energy Equation in One Dimensions . 73

2.4.3 Virial Coefficients 75

2.4.4 Properties of Select Gasses 79

2.5 Parameter Estimation 80

2.6 Alumina Packed Bed Parameter Estimates 82

2.7 Comparison of Alumina Packed Bed Experimental Data and Model Fits . . 90

2.8 Experimental and Model Comparisons for an Alumina Packed Bed Containing Stagnant Argon Taken from Approximately 0 °C and Submerged in a 19 °C Water Bath 91

2.9 Experimental and Model Comparisons for an Alumina Packed Bed Containing Stagnant Argon Taken from Approximately 22 °C and Submerged in a 0 °C Ice-Water Bath 93

2.10 Experimental and Model Comparisons for an Alumina Packed Bed Containing Stagnant Helium Taken from Approximately 0 °C and Submerged in a 21 °C Water Bath 96

2.11 Experimental and Model Comparisons for an Alumina Packed Bed Containing Stagnant Helium Taken from Approximately 21 °C and Submerged in a 0 °C Ice-Water Bath 99

2.12 Experimental and Model Comparisons for an Alumina Packed Bed Containing Stagnant Hydrogen Taken from Approximately 0 °C and Submerged in a 19 °C Water Bath 102

2.13 Experimental and Model Comparisons for an Alumina Packed Bed Containing Stagnant Hydrogen Taken from Approximately 21 °C and Submerged in a 0 °C Ice-Water Bath 105

2.14 Experimental and Model Comparisons for experiment 1 for an Alumina Packed Bed Containing Stagnant Nitrogen Taken from Approximately 0 °C and Submerged in a 19 °C Water Bath 108

2.15 Experimental and Model Comparisons for experiment 1 for an Alumina Packed Bed Containing Stagnant Nitrogen Taken from Approximately 21 °C and Submerged in a 0 °C Ice-Water Bath 111

2.16 Experimental and Model Comparisons for experiment 2 for an Alumina Packed Bed Containing Stagnant Nitrogen Taken from Approximately 0 °C and Submerged in a 19 °C Water Bath 113

2.17 Experimental and Model Comparisons for experiment 2 for an Alumina Packed Bed Containing Stagnant Nitrogen Taken from Approximately 21 °C and Submerged in a 0 °C Ice-Water Bath 116

2.18 Experimental and Model Comparisons for experiment 3 for an Alumina Packed Bed Containing Stagnant Nitrogen Taken from Approximately 0 °C and Submerged in a 19 °C Water Bath 118

2.19 Experimental and Model Comparisons for experiment 3 for an Alumina Packed Bed Containing Stagnant Nitrogen Taken from Approximately 21 °C and Submerged in a 0 °C Ice-Water Bath 121

2.20 Experimental and Model Comparisons for an Alumina Packed Bed Containing Stagnant Oxygen Taken from Approximately 0 °C and Submerged in a 19 °C Water Bath 123

2.21 Experimental and Model Comparisons for an Alumina Packed Bed Containing Stagnant Oxygen Taken from Approximately 0 °C and Submerged in a 19 °C Water Bath 125

2.22 Microfibrous Media Bed Parameter Estimates 127

2.23 Comparison of Microfibrous Media Bed Experimental Data and Model Fits 134

2.24 Experimental and Model Comparisons for a Microfibrous Media (MFM) Bed Containing Stagnant Argon Taken from Approximately 21 °C and Submerged in a 71 °C Water Bath 135

2.25 Experimental and Model Comparisons for a Microfibrous Media (MFM) Bed Containing Stagnant Argon Taken from Approximately 71 °C and Submerged in a 20 °C Water Bath 138

2.26 Experimental and Model Comparisons for a Microfibrous Media (MFM) Bed Containing Stagnant Argon Taken from Approximately 0 °C and Submerged in a 30 °C Water Bath 141

2.27 Experimental and Model Comparisons for a Microfibrous Media (MFM) Bed Containing Stagnant Argon Taken from Approximately 21 °C and Submerged in a 0 °C Ice-Water Bath 144

2.28 Experimental and Model comparisons for a Microfibrous Media (MFM) Bed Containing Stagnant Carbon Dioxide Taken from Approximately 21 °C and Submerged in a 71 °C Water Bath 147

2.29 Experimental and Model comparisons for a Microfibrous Media (MFM) Bed Containing Stagnant Carbon Dioxide Taken from Approximately 70 °C and Submerged in a 20 °C Water Bath 150

2.30 Experimental and Model comparisons for a Microfibrous Media (MFM) Bed Containing Stagnant Carbon Dioxide Taken from Approximately 0 °C and Submerged in a 21 °C Water Bath 153

2.31 Experimental and Model comparisons for a Microfibrous Media (MFM) Bed Containing Stagnant Carbon Dioxide Taken from Approximately 21 °C and Submerged in a 0 °C Ice-Water Bath 156

2.32 Experimental and Model Comparisons for a Microfibrous Media (MFM) Bed Containing Stagnant Helium Taken from Approximately 21 °C and Submerged in a 71 °C Water Bath 159

2.33 Experimental and Model Comparisons for a Microfibrous Media (MFM) Bed Containing Stagnant Helium Taken from Approximately 71 °C and Submerged in a 20 °C Water Bath 162

2.34 Experimental and Model Comparisons for a Microfibrous Media (MFM) Bed Containing Stagnant Helium Taken from Approximately 0 °C and Submerged in a 22 °C Water Bath 165

2.35 Experimental and Model Comparisons for a Microfibrous Media (MFM) Bed Containing Stagnant Helium Taken from Approximately 21 °C and Submerged in a 0 °C Ice-Water Bath 168

2.36 Experimental and Model Comparisons for a Microfibrous Media (MFM) Bed Containing Stagnant Hydrogen Taken from Approximately 21 °C and Submerged in a 69 °C Water Bath 171

2.37 Experimental and Model Comparisons for a Microfibrous Media (MFM) Bed Containing Stagnant Hydrogen Taken from Approximately 69 °C and Submerged in a 20 °C Water Bath 174

2.38 Experimental and Model Comparisons for a Microfibrous Media (MFM) Bed Containing Stagnant Hydrogen Taken from Approximately 0 °C and Submerged in a 19 °C Water Bath 177

2.39 Experimental and Model Comparisons for a Microfibrous Media (MFM) Bed Containing Stagnant Hydrogen Taken from Approximately 21 °C and Submerged in a 0 °C Ice-Water Bath 180

2.40 Experimental and Model Comparisons for a Microfibrous Media (MFM) Bed Containing Stagnant Oxygen Taken from Approximately 21 °C and Submerged in a 75 °C Water Bath 183

2.41 Experimental and Model Comparisons for a Microfibrous Media (MFM) Bed Containing Stagnant Oxygen Taken from Approximately 78 °C and Submerged in a 20 °C Water Bath 186

2.42 Experimental and Model Comparisons for a Microfibrous Media (MFM) Bed Containing Stagnant Oxygen Taken from Approximately 0 °C and Submerged in a 20 °C Water Bath 189

2.43 Experimental and Model Comparisons for a Microfibrous Media (MFM) Bed Containing Stagnant Oxygen Taken from Approximately 20 °C and Submerged in a 0 °C Ice-Water Bath 192

2.44 Experimental and Model Comparisons for a Microfibrous Media (MFM) Bed Reduced to Vacuum and Taken from Approximately 22 °C and Submerged in a 70 °C Water Bath 195

2.45 Experimental and Model Comparisons for a Microfibrous Media (MFM) Bed Reduced to Vacuum and Taken from Approximately 70 °C and Submerged in a 19 °C Water Bath 198

2.46 Experimental and Model Comparisons for a Microfibrous Media (MFM) Bed Reduced to Vacuum and Taken from Approximately 0 °C and Submerged in a 19 °C Water Bath 200

2.47 Experimental and Model Comparisons for a Microfibrous Media (MFM) Bed Reduced to Vacuum and Taken from Approximately 22 °C and Submerged in a 0 °C Ice-Water Bath 203

2.48 Stagnant Effective Thermal Conductivity 205

2.49 Discussion and Conclusions 209

3 Effect of Flowing Gas on Heat Transfer in Microfibrous Media 210

3.1 Sutherland Constants 212

3.2 Results 216

3.2.1 Steady State Temperature Data for Heat Transfer Experiments in a Microfibrous Media Bed with Flowing Argon 217

3.2.2 Steady State Temperature Data for Heat Transfer Experiments in a Microfibrous Media Bed with Flowing Helium 220

3.2.3 Steady State Temperature Data for Heat Transfer Experiments in a Microfibrous Media Bed with Flowing Oxygen 223

3.3 Discussion 226

3.3.1 Computational Model of Microfibrous Media Bed Experiments with Flowing Gas 226

3.3.2 Effective Thermal Conductivity of a Bed with Flow 231

4 Future Work 234

4.1 Introduction to Future Work 234

4.2 Resistance Networks for Microfibrous Media 235

4.3 Unit Cells for Microfibrous Media 238

4.3.1 Microfibrous Media (MFM) Fiber gap 242

4.4 Proposed Computational Model of a Unit Cell of Microfibrous Media . . . 246

Bibliography 250

List of Tables

2.1 Thermocouple support thickness for microfibrous media bed as measured with Mitutoyo calipers at arbitrary locations. 44

2.2 Alumina pellet size used in packed bed. 48

2.3 Sanitary tube diameter for microfibrous media experiments. 51

2.4 Microfibrous media bed packing 55

2.5 MFM fiber fractions measured from 0.25-inch disks. 59

2.6 MFM fiber fractions measured from 0.5-inch disks. 60

2.7 MFM fiber fractions measured from 2.400-inch disks. 60

2.8 Parameters for the second virial coefficient and square-well potential. 78

2.9 Properties of selected gases at 300 K [a] 79

2.10 Estimated thermal parameters for a packed bed of 11.7% aluminum oxide by volume and pressurized to 40 psi gauge with argon. 83

2.11 Estimated thermal parameters for a packed bed of 11.7% aluminum oxide by volume and pressurized to 40 psi gauge with helium. 84

2.12 Estimated thermal parameters for a packed bed of 11.7% aluminum oxide by volume and pressurized to 40 psi gauge with hydrogen. 85

2.13 Estimated thermal parameters for experiment 1 for a packed bed of 11.7% aluminum oxide by volume and pressurized to 40 psi gauge with nitrogen. . 86

2.14 Estimated thermal parameters for experiment 2 for a packed bed of 11.7% aluminum oxide by volume and pressurized to 40 psi gauge with nitrogen. . 87

2.15 Estimated thermal parameters for experiment 3 for a packed bed of 11.7% aluminum oxide by volume and pressurized to 40 psi gauge with nitrogen. . 88

2.16 Estimated thermal parameters for a packed bed of 11.7% aluminum oxide by volume and pressurized to 40 psi gauge with oxygen. 89

2.17 Estimated thermal parameters for a microfibrous media bed of 4.8% copper by volume and pressurized to 50 psi gauge with argon. 128

2.18 Estimated thermal parameters for a microfibrous media bed of 4.8% copper by volume and pressurized to 50 psi gauge with carbon dioxide. 129

2.19 Estimated thermal parameters for a microfibrous media bed of 4.8% copper by volume and pressurized to 50 psi gauge with helium. 130

2.20 Estimated thermal parameters for a microfibrous media bed of 4.8% copper by volume and pressurized to 50 psi gauge with hydrogen. 131

2.21 Estimated thermal parameters for a microfibrous media bed of 4.8% copper by volume and pressurized to 50 psi gauge with oxygen. 132

2.22 Estimated thermal parameters for a microfibrous media bed of 4.8% copper by volume and reduced to vacuum. 133

2.23 Models for stagnant effective thermal conductivity of beds of solids within a fluid phase. 206

2.24 Estimated stagnant effective thermal conductivity in $\frac{W}{m \cdot K}$ of a packed bed consisting of 11.7% $\frac{1}{8}$-in gamma alumina pellets and 88.3% void of various gasses. 208

2.25 Estimated stagnant effective thermal conductivity in $\frac{W}{m \cdot K}$ of a microfibrous bed consisting of 4.8% copper fibers and 95.2% void of various gasses. . . . 208

3.1 Sutherland constants for gases presented in "Viscosity of gases" [64]. 214

3.2 Sutherland constants for gases presented in "Viscosity of gases" [64] (cont.). 215

3.3 Models for effective radial thermal conductivity with flow of porous beds [49]. [a] 232

3.4 Simple models for effective radial thermal conductivity with flow of porous beds 233

3.5 Models for effective axial thermal conductivity with flow of porous beds. . . 233

List of Figures

2.1 Dimensional drawing (top view) for $\frac{3}{16}$-inch holes for thermocouples in $1\frac{1}{2}$-inch male NPT hex head plug. 42

2.2 Thermocouple support template. 46

2.3 Thermocouple support with attached thermocouples. 46

2.4 Diagram of the reactor used in packed bed experiments. 47

2.5 Tools used for loading packed beds. Two slotted push rods with head diameters of approximately $58.7\,\mathrm{mm}$ with caps that can be be clamped to a 3.5-inch sanitary flange and stop collars with thumb screws; these push rods will be referred to as clamping push rods. One push rod with a head diameter of approximately $55.5\,\mathrm{mm}$. 48

2.6 Flat slotted push-rod head with diameter of approximately $58.7\,\mathrm{mm}$. 49

2.7 Slotted sanitary cap for push rod. Fits with a 3.5-inch sanitary flange. 49

2.8 Diagram of the reactor used in microfibrous media experiments. 51

2.9 Tools used for the microfibrous media bed. Two slotted push rods with head diameters of approximately $58.7\,\mathrm{mm}$ with caps that can be be clamped to a 3.5-inch sanitary flange and stop collars with thumb screws; these push rods will be referred to as clamping push rods. One push rod with a head diameter of approximately $55.5\,\mathrm{mm}$. A push rod with a concave head with a diameter of approximately $59.5\,\mathrm{mm}$. A rod with a cap that can be clamped to a 3.5-inch sanitary flange and stop collars with thumb screw. A thin metal rod with a hooked end. 52

2.10 Slotted concave push-rod head with a diameter of approximately $59.5\,\mathrm{mm}$. . 53

2.11 Placement of first thermocouple support in microfibrous media bed. 54

2.12 Microfibrous media that has been cut but not compressed stored in a plastic tub. 56

2.13 Two pieces of microfibrous media (MFM) shown to depict variance in the media used. The pieces are as cut from sheets of MFM and have not been compressed. The two pieces shown are extreme examples, and the lines drawn are approximately how thick the pieces are as there is variance within each piece. 56

2.14 Microfibrous media that was compressed in the same tube used for microfibrous media beds in this work. 56

2.15 Microfibrous media bed being loaded. 57

2.16 Thermocouple support C inside of the microfibrous media bed. 57

2.17 Temperature readings at the center radially and center axially of an $\frac{1}{8}$-inch alumina pellet packed bed that begins at 0 °C and is submerged in a room-temperature-water bath of approximately 20 °C. The bed is approximately $304.8\,\mathrm{mm}$ (12 inches) in length and $61.5\,\mathrm{mm}$ (2.42 inches) in diameter. Data is recorded from the bed filled with various gases at 40 psi gauge. This data is truncated to all begin at 20.0 °C. The bed is packed at 11.7% alumina by volume. 63

2.18 Temperature readings at the center radially and center axially of an $\frac{1}{8}$-inch alumina pellet packed bed that begins at near 20.0 °C and is submerged in an ice-water bath of approximately 0.0 °C. The bed is approximately $304.8\,\mathrm{mm}$ (12 inches) in length and $61.5\,\mathrm{mm}$ (2.42 inches) in diameter. Data is recorded from the bed filled with various gases at 40 psi gauge. This data is truncated to all begin at 20.0 °C before it was normalized. The bed is packed at 11.7% alumina by volume. 64

2.19 Temperature readings at the center radially and center axially of a microfibrous media bed reaching a steady state temperature when the bed at approximately 0 °C is submerged in an room-temperature-water bath of approximately 20 °C. MFM only data was recorded at $0.029\,\mathrm{mbar}$ vacuum. . . 67

2.20 Temperature readings at the center radially and center axially of a microfibrous media bed reaching a steady state temperature when the bed at approximately 20 °C is submerged in an ice-water bath at approximately 0 °C. MFM only data was recorded at $0.029\,\mathrm{mbar}$ vacuum. 68

2.21 Temperature readings at the center radially and center axially of a microfibrous media bed reaching a steady state temperature when the bed at approximately 20 °C is submerged in an heated-water bath of approximately 70 °C. MFM only data was recorded at $0.033\,\mathrm{mbar}$ vacuum. 69

2.22 Temperature readings at the center radially and center axially of a microfibrous media bed reaching a steady state temperature when the bed at approximately 70 °C is submerged in a room-temperature-water bath of approximately 70 °C. MFM only data was recorded at $0.033\,\mathrm{mbar}$ vacuum. . . 70

2.23 Experimental temperature data of support C of an alumina packed bed compared with a model fit of the data as the bed is taken from approximately 0 °C and submerged in an approximately 19 °C water bath. The bed was pressurized to 40 psi gauge with argon at room temperature. 91

2.24 Experimental temperature data of support D of an alumina packed bed compared with a model fit of the data as the bed is taken from approximately 0 °C and submerged in an approximately 19 °C water bath. The bed was pressurized to 40 psi gauge with argon at room temperature. 92

2.25 Experimental temperature data of support E of an alumina packed bed compared with a model fit of the data as the bed is taken from approximately 0 °C and submerged in an approximately 19 °C water bath. The bed was pressurized to 40 psi gauge with argon at room temperature. 92

2.26 Experimental temperature data of support A of an alumina packed bed compared with a model fit of the data as the bed is taken from approximately 22 °C and submerged in an approximately 0 °C ice-water bath. The bed was pressurized to 40 psi gauge with argon at room temperature. 93

2.27 Experimental temperature data of support C of an alumina packed bed compared with a model fit of the data as the bed is taken from approximately 22 °C and submerged in an approximately 0 °C ice-water bath. The bed was pressurized to 40 psi gauge with argon at room temperature. 94

2.28 Experimental temperature data of support D of an alumina packed bed compared with a model fit of the data as the bed is taken from approximately 22 °C and submerged in an approximately 0 °C ice-water bath. The bed was pressurized to 40 psi gauge with argon at room temperature. 94

2.29 Experimental temperature data of support E of an alumina packed bed compared with a model fit of the data as the bed is taken from approximately 22 °C and submerged in an approximately 0 °C ice-water bath. The bed was pressurized to 40 psi gauge with argon at room temperature. 95

2.30 Experimental temperature data of support A of an alumina packed bed compared with a model fit of the data as the bed is taken from approximately 0 °C and submerged in an approximately 21 °C water bath. The bed was pressurized to 40 psi gauge with helium at room temperature. 96

2.31 Experimental temperature data of support C of an alumina packed bed compared with a model fit of the data as the bed is taken from approximately 0 °C and submerged in an approximately 21 °C water bath. The bed was pressurized to 40 psi gauge with helium at room temperature. 97

2.32 Experimental temperature data of support D of an alumina packed bed compared with a model fit of the data as the bed is taken from approximately 0 °C and submerged in an approximately 21 °C water bath. The bed was pressurized to 40 psi gauge with helium at room temperature. 97

2.33 Experimental temperature data of support E of an alumina packed bed compared with a model fit of the data as the bed is taken from approximately 0 °C and submerged in an approximately 21 °C water bath. The bed was pressurized to 40 psi gauge with helium at room temperature. 98

2.34 Experimental temperature data of support A of an alumina packed bed compared with a model fit of the data as the bed is taken from approximately 21 °C and submerged in an approximately 0 °C ice-water bath. The bed was pressurized to 40 psi gauge with helium at room temperature. 99

2.35 Experimental temperature data of support C of an alumina packed bed compared with a model fit of the data as the bed is taken from approximately 21 °C and submerged in an approximately 0 °C ice-water bath. The bed was pressurized to 40 psi gauge with helium at room temperature. 100

2.36 Experimental temperature data of support D of an alumina packed bed compared with a model fit of the data as the bed is taken from approximately 21 °C and submerged in an approximately 0 °C ice-water bath. The bed was pressurized to 40 psi gauge with helium at room temperature. 100

2.37 Experimental temperature data of support E of an alumina packed bed compared with a model fit of the data as the bed is taken from approximately 21 °C and submerged in an approximately 0 °C ice-water bath. The bed was pressurized to 40 psi gauge with helium at room temperature. 101

2.38 Experimental temperature data of support A of an alumina packed bed compared with a model fit of the data as the bed is taken from approximately 0 °C and submerged in an approximately 19 °C water bath. The bed was pressurized to 40 psi gauge with hydrogen at room temperature. 102

2.39 Experimental temperature data of support C of an alumina packed bed compared with a model fit of the data as the bed is taken from approximately 0 °C and submerged in an approximately 19 °C water bath. The bed was pressurized to 40 psi gauge with hydrogen at room temperature. 103

2.40 Experimental temperature data of support D of an alumina packed bed compared with a model fit of the data as the bed is taken from approximately 0 °C and submerged in an approximately 19 °C water bath. The bed was pressurized to 40 psi gauge with hydrogen at room temperature. 103

2.41 Experimental temperature data of support E of an alumina packed bed compared with a model fit of the data as the bed is taken from approximately 0 °C and submerged in an approximately 19 °C water bath. The bed was pressurized to 40 psi gauge with hydrogen at room temperature. 104

2.42 Experimental temperature data of support A of an alumina packed bed compared with a model fit of the data as the bed is taken from approximately 21 °C and submerged in an approximately 0 °C ice-water bath. The bed was pressurized to 40 psi gauge with hydrogen at room temperature. 105

2.43 Experimental temperature data of support C of an alumina packed bed compared with a model fit of the data as the bed is taken from approximately 21 °C and submerged in an approximately 0 °C ice-water bath. The bed was pressurized to 40 psi gauge with hydrogen at room temperature. 106

2.44 Experimental temperature data of support D of an alumina packed bed compared with a model fit of the data as the bed is taken from approximately 21 °C and submerged in an approximately 0 °C ice-water bath. The bed was pressurized to 40 psi gauge with hydrogen at room temperature. 106

2.45 Experimental temperature data of support E of an alumina packed bed compared with a model fit of the data as the bed is taken from approximately 21 °C and submerged in an approximately 0 °C ice-water bath. The bed was pressurized to 40 psi gauge with hydrogen at room temperature. 107

2.46 Experimental temperature data of support A of an alumina packed bed compared with a model fit of the data as the bed is taken from approximately 0 °C and submerged in an approximately 19 °C water bath. The bed was pressurized to 40 psi gauge with nitrogen at room temperature. 108

2.47 Experimental temperature data of support C of an alumina packed bed compared with a model fit of the data as the bed is taken from approximately 0 °C and submerged in an approximately 19 °C water bath. The bed was pressurized to 40 psi gauge with nitrogen at room temperature. 109

2.48 Experimental temperature data of support D of an alumina packed bed compared with a model fit of the data as the bed is taken from approximately 0 °C and submerged in an approximately 19 °C water bath. The bed was pressurized to 40 psi gauge with nitrogen at room temperature. 109

2.49 Experimental temperature data of support E of an alumina packed bed compared with a model fit of the data as the bed is taken from approximately 0 °C and submerged in an approximately 19 °C water bath. The bed was pressurized to 40 psi gauge with nitrogen at room temperature. 110

2.50 Experimental temperature data of support C of an alumina packed bed compared with a model fit of the data as the bed is taken from approximately 21 °C and submerged in an approximately 0 °C ice-water bath. The bed was pressurized to 40 psi gauge with nitrogen at room temperature. 111

2.51 Experimental temperature data of support D of an alumina packed bed compared with a model fit of the data as the bed is taken from approximately 21 °C and submerged in an approximately 0 °C ice-water bath. The bed was pressurized to 40 psi gauge with nitrogen at room temperature. 112

2.52 Experimental temperature data of support E of an alumina packed bed compared with a model fit of the data as the bed is taken from approximately 21 °C and submerged in an approximately 0 °C ice-water bath. The bed was pressurized to 40 psi gauge with nitrogen at room temperature. 112

2.53 Experimental temperature data of support A of an alumina packed bed compared with a model fit of the data as the bed is taken from approximately 0 °C and submerged in an approximately 18 °C water bath. The bed was pressurized to 40 psi gauge with nitrogen at room temperature. 113

2.54 Experimental temperature data of support C of an alumina packed bed compared with a model fit of the data as the bed is taken from approximately 0 °C and submerged in an approximately 18 °C water bath. The bed was pressurized to 40 psi gauge with nitrogen at room temperature. 114

2.55 Experimental temperature data of support D of an alumina packed bed compared with a model fit of the data as the bed is taken from approximately 0 °C and submerged in an approximately 18 °C water bath. The bed was pressurized to 40 psi gauge with nitrogen at room temperature. 114

2.56 Experimental temperature data of support E of an alumina packed bed compared with a model fit of the data as the bed is taken from approximately 0 °C and submerged in an approximately 18 °C water bath. The bed was pressurized to 40 psi gauge with nitrogen at room temperature. 115

2.57 Experimental temperature data of support C of an alumina packed bed compared with a model fit of the data as the bed is taken from approximately 18 °C and submerged in an approximately 0 °C ice-water bath. The bed was pressurized to 40 psi gauge with nitrogen at room temperature. 116

2.58 Experimental temperature data of support D of an alumina packed bed compared with a model fit of the data as the bed is taken from approximately 18 °C and submerged in an approximately 0 °C ice-water bath. The bed was pressurized to 40 psi gauge with nitrogen at room temperature. 117

2.59 Experimental temperature data of support E of an alumina packed bed compared with a model fit of the data as the bed is taken from approximately 18 °C and submerged in an approximately 0 °C ice-water bath. The bed was pressurized to 40 psi gauge with nitrogen at room temperature. 117

2.60 Experimental temperature data of support A of an alumina packed bed compared with a model fit of the data as the bed is taken from approximately 0 °C and submerged in an approximately 19 °C water bath. The bed was pressurized to 40 psi gauge with nitrogen at room temperature. 118

2.61 Experimental temperature data of support C of an alumina packed bed compared with a model fit of the data as the bed is taken from approximately 0 °C and submerged in an approximately 19 °C water bath. The bed was pressurized to 40 psi gauge with nitrogen at room temperature. 119

2.62 Experimental temperature data of support D of an alumina packed bed compared with a model fit of the data as the bed is taken from approximately 0 °C and submerged in an approximately 19 °C water bath. The bed was pressurized to 40 psi gauge with nitrogen at room temperature. 119

2.63 Experimental temperature data of support E of an alumina packed bed compared with a model fit of the data as the bed is taken from approximately 0 °C and submerged in an approximately 19 °C water bath. The bed was pressurized to 40 psi gauge with nitrogen at room temperature. 120

2.64 Experimental temperature data of support C of an alumina packed bed compared with a model fit of the data as the bed is taken from approximately 21 °C and submerged in an approximately 0 °C ice-water bath. The bed was pressurized to 40 psi gauge with nitrogen at room temperature. 121

2.65 Experimental temperature data of support D of an alumina packed bed compared with a model fit of the data as the bed is taken from approximately 21 °C and submerged in an approximately 0 °C ice-water bath. The bed was pressurized to 40 psi gauge with nitrogen at room temperature. 122

2.66 Experimental temperature data of support E of an alumina packed bed compared with a model fit of the data as the bed is taken from approximately 21 °C and submerged in an approximately 0 °C ice-water bath. The bed was pressurized to 40 psi gauge with nitrogen at room temperature. 122

2.67 Experimental temperature data of support C of an alumina packed bed compared with a model fit of the data as the bed is taken from approximately 0 °C and submerged in an approximately 19 °C water bath. The bed was pressurized to 40 psi gauge with oxygen at room temperature. 123

2.68 Experimental temperature data of support D of an alumina packed bed compared with a model fit of the data as the bed is taken from approximately 0 °C and submerged in an approximately 19 °C water bath. The bed was pressurized to 40 psi gauge with oxygen at room temperature. 124

2.69 Experimental temperature data of support E of an alumina packed bed compared with a model fit of the data as the bed is taken from approximately 0 °C and submerged in an approximately 19 °C water bath. The bed was pressurized to 40 psi gauge with oxygen at room temperature. 124

2.70 Experimental temperature data of support C of an alumina packed bed compared with a model fit of the data as the bed is taken from approximately 21 °C and submerged in an approximately 0 °C ice-water bath. The bed was pressurized to 40 psi gauge with oxygen at room temperature. 125

2.71 Experimental temperature data of support D of an alumina packed bed compared with a model fit of the data as the bed is taken from approximately 21 °C and submerged in an approximately 0 °C ice-water bath. The bed was pressurized to 40 psi gauge with oxygen at room temperature. 126

2.72 Experimental temperature data of support E of an alumina packed bed compared with a model fit of the data as the bed is taken from approximately 21 °C and submerged in an approximately 0 °C ice-water bath. The bed was pressurized to 40 psi gauge with oxygen at room temperature. 126

2.73 Experimental temperature data of support A of a microfibrous media bed compared with a model fit of the data as the bed is taken from approximately 21 °C and submerged in an approximately 71 °C water bath. The bed was pressurized to 50 psi gauge with argon at room temperature. 135

2.74 Experimental temperature data of support B of a microfibrous media bed compared with a model fit of the data as the bed is taken from approximately 21 °C and submerged in an approximately 71 °C water bath. The bed was pressurized to 50 psi gauge with argon at room temperature. 136

2.75 Experimental temperature data of support C of a microfibrous media bed compared with a model fit of the data as the bed is taken from approximately 21 °C and submerged in an approximately 71 °C water bath. The bed was pressurized to 50 psi gauge with argon at room temperature. 136

2.76 Experimental temperature data of support D of a microfibrous media bed compared with a model fit of the data as the bed is taken from approximately 21 °C and submerged in an approximately 71 °C water bath. The bed was pressurized to 50 psi gauge with argon at room temperature. 137

2.77 Experimental temperature data of support E of a microfibrous media bed compared with a model fit of the data as the bed is taken from approximately 21 °C and submerged in an approximately 71 °C water bath. The bed was pressurized to 50 psi gauge with argon at room temperature. 137

2.78 Experimental temperature data of support A of a microfibrous media bed compared with a model fit of the data as the bed is taken from approximately 71 °C and submerged in an approximately 20 °C water bath. The bed was pressurized to 50 psi gauge with argon at room temperature. 138

2.79 Experimental temperature data of support B of a microfibrous media bed compared with a model fit of the data as the bed is taken from approximately 71 °C and submerged in an approximately 20 °C water bath. The bed was pressurized to 50 psi gauge with argon at room temperature. 139

2.80 Experimental temperature data of support C of a microfibrous media bed compared with a model fit of the data as the bed is taken from approximately 71 °C and submerged in an approximately 20 °C water bath. The bed was pressurized to 50 psi gauge with argon at room temperature. 139

2.81 Experimental temperature data of support D of a microfibrous media bed compared with a model fit of the data as the bed is taken from approximately 71 °C and submerged in an approximately 20 °C water bath. The bed was pressurized to 50 psi gauge with argon at room temperature. 140

2.82 Experimental temperature data of support E of a microfibrous media bed compared with a model fit of the data as the bed is taken from approximately 71 °C and submerged in an approximately 20 °C water bath. The bed was pressurized to 50 psi gauge with argon at room temperature. 140

2.83 Experimental temperature data of support A of a microfibrous media bed compared with a model fit of the data as the bed is taken from approximately 0 °C and submerged in an approximately 20 °C water bath. The bed was pressurized to 50 psi gauge with argon at room temperature. 141

2.84 Experimental temperature data of support B of a microfibrous media bed compared with a model fit of the data as the bed is taken from approximately 0 °C and submerged in an approximately 20 °C water bath. The bed was pressurized to 50 psi gauge with argon at room temperature. 142

2.85 Experimental temperature data of support C of a microfibrous media bed compared with a model fit of the data as the bed is taken from approximately 0 °C and submerged in an approximately 20 °C water bath. The bed was pressurized to 50 psi gauge with argon at room temperature. 142

2.86 Experimental temperature data of support D of a microfibrous media bed compared with a model fit of the data as the bed is taken from approximately 0 °C and submerged in an approximately 20 °C water bath. The bed was pressurized to 50 psi gauge with argon at room temperature. 143

2.87 Experimental temperature data of support E of a microfibrous media bed compared with a model fit of the data as the bed is taken from approximately 0 °C and submerged in an approximately 20 °C water bath. The bed was pressurized to 50 psi gauge with argon at room temperature. 143

2.88 Experimental temperature data of support A of a microfibrous media bed compared with a model fit of the data as the bed is taken from approximately 21 °C and submerged in an approximately 0 °C ice-water bath. The bed was pressurized to 50 psi gauge with argon at room temperature. 144

2.89 Experimental temperature data of support B of a microfibrous media bed compared with a model fit of the data as the bed is taken from approximately 21 °C and submerged in an approximately 0 °C ice-water bath. The bed was pressurized to 50 psi gauge with argon at room temperature. 145

2.90 Experimental temperature data of support C of a microfibrous media bed compared with a model fit of the data as the bed is taken from approximately 21 °C and submerged in an approximately 0 °C ice-water bath. The bed was pressurized to 50 psi gauge with argon at room temperature. 145

2.91 Experimental temperature data of support D of a microfibrous media bed compared with a model fit of the data as the bed is taken from approximately 21 °C and submerged in an approximately 0 °C ice-water bath. The bed was pressurized to 50 psi gauge with argon at room temperature. 146

2.92 Experimental temperature data of support E of a microfibrous media bed compared with a model fit of the data as the bed is taken from approximately 21 °C and submerged in an approximately 0 °C ice-water bath. The bed was pressurized to 50 psi gauge with argon at room temperature. 146

2.93 Experimental temperature data of support A of a microfibrous media bed compared with a model fit of the data as the bed is taken from approximately 21 °C and submerged in an approximately 70 °C water bath. The bed was pressurized to 50 psi gauge with carbon dioxide at room temperature. 147

2.94 Experimental temperature data of support B of a microfibrous media bed compared with a model fit of the data as the bed is taken from approximately 21 °C and submerged in an approximately 70 °C water bath. The bed was pressurized to 50 psi gauge with carbon dioxide at room temperature. 148

2.95 Experimental temperature data of support C of a microfibrous media bed compared with a model fit of the data as the bed is taken from approximately 21 °C and submerged in an approximately 70 °C water bath. The bed was pressurized to 50 psi gauge with carbon dioxide at room temperature. 148

2.96 Experimental temperature data of support D of a microfibrous media bed compared with a model fit of the data as the bed is taken from approximately 21 °C and submerged in an approximately 70 °C water bath. The bed was pressurized to 50 psi gauge with carbon dioxide at room temperature. 149

2.97 Experimental temperature data of support E of a microfibrous media bed compared with a model fit of the data as the bed is taken from approximately 21 °C and submerged in an approximately 70 °C water bath. The bed was pressurized to 50 psi gauge with carbon dioxide at room temperature. 149

2.98 Experimental temperature data of support A of a microfibrous media bed compared with a model fit of the data as the bed is taken from approximately 70 °C and submerged in an approximately 20 °C water bath. The bed was pressurized to 50 psi gauge with carbon dioxide at room temperature. 150

2.99 Experimental temperature data of support B of a microfibrous media bed compared with a model fit of the data as the bed is taken from approximately 70 °C and submerged in an approximately 20 °C water bath. The bed was pressurized to 50 psi gauge with carbon dioxide at room temperature. 151

2.100 Experimental temperature data of support C of a microfibrous media bed compared with a model fit of the data as the bed is taken from approximately 70 °C and submerged in an approximately 20 °C water bath. The bed was pressurized to 50 psi gauge with carbon dioxide at room temperature. 151

2.101 Experimental temperature data of support D of a microfibrous media bed compared with a model fit of the data as the bed is taken from approximately 70 °C and submerged in an approximately 20 °C water bath. The bed was pressurized to 50 psi gauge with carbon dioxide at room temperature. 152

2.102 Experimental temperature data of support E of a microfibrous media bed compared with a model fit of the data as the bed is taken from approximately 70 °C and submerged in an approximately 20 °C water bath. The bed was pressurized to 50 psi gauge with carbon dioxide at room temperature. 152

2.103 Experimental temperature data of support A of a microfibrous media bed compared with a model fit of the data as the bed is taken from approximately 0 °C and submerged in an approximately 21 °C water bath. The bed was pressurized to 50 psi gauge with carbon dioxide at room temperature. . 153

2.104Experimental temperature data of support B of a microfibrous media bed compared with a model fit of the data as the bed is taken from approximately 0 °C and submerged in an approximately 21 °C water bath. The bed was pressurized to 50 psi gauge with carbon dioxide at room temperature. . 154

2.105Experimental temperature data of support C of a microfibrous media bed compared with a model fit of the data as the bed is taken from approximately 0 °C and submerged in an approximately 21 °C water bath. The bed was pressurized to 50 psi gauge with carbon dioxide at room temperature. . 154

2.106Experimental temperature data of support D of a microfibrous media bed compared with a model fit of the data as the bed is taken from approximately 0 °C and submerged in an approximately 21 °C water bath. The bed was pressurized to 50 psi gauge with carbon dioxide at room temperature. . 155

2.107Experimental temperature data of support E of a microfibrous media bed compared with a model fit of the data as the bed is taken from approximately 0 °C and submerged in an approximately 21 °C water bath. The bed was pressurized to 50 psi gauge with carbon dioxide at room temperature. . 155

2.108Experimental temperature data of support A of a microfibrous media bed compared with a model fit of the data as the bed is taken from approximately 21 °C and submerged in an approximately 0 °C ice-water bath. The bed was pressurized to 50 psi gauge with carbon dioxide at room temperature. 156

2.109Experimental temperature data of support B of a microfibrous media bed compared with a model fit of the data as the bed is taken from approximately 21 °C and submerged in an approximately 0 °C ice-water bath. The bed was pressurized to 50 psi gauge with carbon dioxide at room temperature. 157

2.110Experimental temperature data of support C of a microfibrous media bed compared with a model fit of the data as the bed is taken from approximately 21 °C and submerged in an approximately 0 °C ice-water bath. The bed was pressurized to 50 psi gauge with carbon dioxide at room temperature. 157

2.111Experimental temperature data of support D of a microfibrous media bed compared with a model fit of the data as the bed is taken from approximately 21 °C and submerged in an approximately 0 °C ice-water bath. The bed was pressurized to 50 psi gauge with carbon dioxide at room temperature. 158

2.112Experimental temperature data of support E of a microfibrous media bed compared with a model fit of the data as the bed is taken from approximately 21 °C and submerged in an approximately 0 °C ice-water bath. The bed was pressurized to 50 psi gauge with carbon dioxide at room temperature. 158

2.113Experimental temperature data of support A of a microfibrous media bed compared with a model fit of the data as the bed is taken from approximately 21 °C and submerged in an approximately 71 °C water bath. The bed was pressurized to 50 psi gauge with helium at room temperature. . . . 159

2.114Experimental temperature data of support B of a microfibrous media bed compared with a model fit of the data as the bed is taken from approximately 21 °C and submerged in an approximately 71 °C water bath. The bed was pressurized to 50 psi gauge with helium at room temperature. . . . 160

2.115Experimental temperature data of support C of a microfibrous media bed compared with a model fit of the data as the bed is taken from approximately 21 °C and submerged in an approximately 71 °C water bath. The bed was pressurized to 50 psi gauge with helium at room temperature. . . . 160

2.116Experimental temperature data of support D of a microfibrous media bed compared with a model fit of the data as the bed is taken from approximately 21 °C and submerged in an approximately 71 °C water bath. The bed was pressurized to 50 psi gauge with helium at room temperature. . . . 161

2.117Experimental temperature data of support E of a microfibrous media bed compared with a model fit of the data as the bed is taken from approximately 21 °C and submerged in an approximately 71 °C water bath. The bed was pressurized to 50 psi gauge with helium at room temperature. . . . 161

2.118Experimental temperature data of support A of a microfibrous media bed compared with a model fit of the data as the bed is taken from approximately 71 °C and submerged in an approximately 20 °C water bath. The bed was pressurized to 50 psi gauge with helium at room temperature. . . . 162

2.119Experimental temperature data of support B of a microfibrous media bed compared with a model fit of the data as the bed is taken from approximately 71 °C and submerged in an approximately 20 °C water bath. The bed was pressurized to 50 psi gauge with helium at room temperature. . . . 163

2.120Experimental temperature data of support C of a microfibrous media bed compared with a model fit of the data as the bed is taken from approximately 71 °C and submerged in an approximately 20 °C water bath. The bed was pressurized to 50 psi gauge with helium at room temperature. . . . 163

2.121Experimental temperature data of support D of a microfibrous media bed compared with a model fit of the data as the bed is taken from approximately 71 °C and submerged in an approximately 20 °C water bath. The bed was pressurized to 50 psi gauge with helium at room temperature. . . . 164

2.122Experimental temperature data of support E of a microfibrous media bed compared with a model fit of the data as the bed is taken from approximately 71 °C and submerged in an approximately 20 °C water bath. The bed was pressurized to 50 psi gauge with helium at room temperature. . . . 164

2.123Experimental temperature data of support A of a microfibrous media bed compared with a model fit of the data as the bed is taken from approximately 0 °C and submerged in an approximately 22 °C water bath. The bed was pressurized to 50 psi gauge with helium at room temperature. 165

2.124Experimental temperature data of support B of a microfibrous media bed compared with a model fit of the data as the bed is taken from approximately 0 °C and submerged in an approximately 22 °C water bath. The bed was pressurized to 50 psi gauge with helium at room temperature. 166

2.125Experimental temperature data of support C of a microfibrous media bed compared with a model fit of the data as the bed is taken from approximately 0 °C and submerged in an approximately 22 °C water bath. The bed was pressurized to 50 psi gauge with helium at room temperature. 166

2.126Experimental temperature data of support D of a microfibrous media bed compared with a model fit of the data as the bed is taken from approximately 0 °C and submerged in an approximately 22 °C water bath. The bed was pressurized to 50 psi gauge with helium at room temperature. 167

2.127Experimental temperature data of support E of a microfibrous media bed compared with a model fit of the data as the bed is taken from approximately 0 °C and submerged in an approximately 22 °C water bath. The bed was pressurized to 50 psi gauge with helium at room temperature. 167

2.128Experimental temperature data of support A of a microfibrous media bed compared with a model fit of the data as the bed is taken from approximately 21 °C and submerged in an approximately 0 °C ice-water bath. The bed was pressurized to 50 psi gauge with helium at room temperature. . . . 168

2.129Experimental temperature data of support B of a microfibrous media bed compared with a model fit of the data as the bed is taken from approximately 21 °C and submerged in an approximately 0 °C ice-water bath. The bed was pressurized to 50 psi gauge with helium at room temperature. . . . 169

2.130Experimental temperature data of support C of a microfibrous media bed compared with a model fit of the data as the bed is taken from approximately 21 °C and submerged in an approximately 0 °C ice-water bath. The bed was pressurized to 50 psi gauge with helium at room temperature. . . . 169

2.131Experimental temperature data of support D of a microfibrous media bed compared with a model fit of the data as the bed is taken from approximately 21 °C and submerged in an approximately 0 °C ice-water bath. The bed was pressurized to 50 psi gauge with helium at room temperature. . . . 170

2.132Experimental temperature data of support E of a microfibrous media bed compared with a model fit of the data as the bed is taken from approximately 21 °C and submerged in an approximately 0 °C ice-water bath. The bed was pressurized to 50 psi gauge with helium at room temperature. . . . 170

2.133Experimental temperature data of support A of a microfibrous media bed compared with a model fit of the data as the bed is taken from approximately 69 °C and submerged in an approximately 20 °C water bath. The bed was pressurized to 50 psi gauge with hydrogen at room temperature. . . 171

2.134Experimental temperature data of support B of a microfibrous media bed compared with a model fit of the data as the bed is taken from approximately 69 °C and submerged in an approximately 20 °C water bath. The bed was pressurized to 50 psi gauge with hydrogen at room temperature. . . 172

2.135Experimental temperature data of support C of a microfibrous media bed compared with a model fit of the data as the bed is taken from approximately 69 °C and submerged in an approximately 20 °C water bath. The bed was pressurized to 50 psi gauge with hydrogen at room temperature. . . 172

2.136Experimental temperature data of support D of a microfibrous media bed compared with a model fit of the data as the bed is taken from approximately 69 °C and submerged in an approximately 20 °C water bath. The bed was pressurized to 50 psi gauge with hydrogen at room temperature. . . 173

2.137Experimental temperature data of support E of a microfibrous media bed compared with a model fit of the data as the bed is taken from approximately 69 °C and submerged in an approximately 20 °C water bath. The bed was pressurized to 50 psi gauge with hydrogen at room temperature. . . 173

2.138Experimental temperature data of support A of a microfibrous media bed compared with a model fit of the data as the bed is taken from approximately 69 °C and submerged in an approximately 20 °C water bath. The bed was pressurized to 50 psi gauge with hydrogen at room temperature. . . 174

2.139Experimental temperature data of support B of a microfibrous media bed compared with a model fit of the data as the bed is taken from approximately 69 °C and submerged in an approximately 20 °C water bath. The bed was pressurized to 50 psi gauge with hydrogen at room temperature. . . 175

2.140Experimental temperature data of support C of a microfibrous media bed compared with a model fit of the data as the bed is taken from approximately 69 °C and submerged in an approximately 20 °C water bath. The bed was pressurized to 50 psi gauge with hydrogen at room temperature. . . 175

2.141Experimental temperature data of support D of a microfibrous media bed compared with a model fit of the data as the bed is taken from approximately 69 °C and submerged in an approximately 20 °C water bath. The bed was pressurized to 50 psi gauge with hydrogen at room temperature. . . 176

2.142Experimental temperature data of support E of a microfibrous media bed compared with a model fit of the data as the bed is taken from approximately 69 °C and submerged in an approximately 20 °C water bath. The bed was pressurized to 50 psi gauge with hydrogen at room temperature. . . 176

2.143Experimental temperature data of support A of a microfibrous media bed compared with a model fit of the data as the bed is taken from approximately 0 °C and submerged in an approximately 19 °C water bath. The bed was pressurized to 50 psi gauge with hydrogen at room temperature. 177

2.144Experimental temperature data of support B of a microfibrous media bed compared with a model fit of the data as the bed is taken from approximately 0 °C and submerged in an approximately 19 °C water bath. The bed was pressurized to 50 psi gauge with hydrogen at room temperature. 178

2.145Experimental temperature data of support D of a microfibrous media bed compared with a model fit of the data as the bed is taken from approximately 0 °C and submerged in an approximately 19 °C water bath. The bed was pressurized to 50 psi gauge with hydrogen at room temperature. 178

2.146Experimental temperature data of support E of a microfibrous media bed compared with a model fit of the data as the bed is taken from approximately 0 °C and submerged in an approximately 19 °C water bath. The bed was pressurized to 50 psi gauge with hydrogen at room temperature. 179

2.147Experimental temperature data of support A of a microfibrous media bed compared with a model fit of the data as the bed is taken from approximately 21 °C and submerged in an approximately 0 °C ice-water bath. The bed was pressurized to 50 psi gauge with hydrogen at room temperature. . . 180

2.148Experimental temperature data of support B of a microfibrous media bed compared with a model fit of the data as the bed is taken from approximately 21 °C and submerged in an approximately 0 °C ice-water bath. The bed was pressurized to 50 psi gauge with hydrogen at room temperature. . . 181

2.149Experimental temperature data of support C of a microfibrous media bed compared with a model fit of the data as the bed is taken from approximately 21 °C and submerged in an approximately 0 °C ice-water bath. The bed was pressurized to 50 psi gauge with hydrogen at room temperature. . . 181

2.150Experimental temperature data of support D of a microfibrous media bed compared with a model fit of the data as the bed is taken from approximately 21 °C and submerged in an approximately 0 °C ice-water bath. The bed was pressurized to 50 psi gauge with hydrogen at room temperature. . . 182

2.151Experimental temperature data of support E of a microfibrous media bed compared with a model fit of the data as the bed is taken from approximately 21 °C and submerged in an approximately 0 °C ice-water bath. The bed was pressurized to 50 psi gauge with hydrogen at room temperature. . . 182

2.152Experimental temperature data of support A of a microfibrous media bed compared with a model fit of the data as the bed is taken from approximately 21 °C and submerged in an approximately 75 °C water bath. The bed was pressurized to 50 psi gauge with oxygen at room temperature. . . . 183

2.153Experimental temperature data of support B of a microfibrous media bed compared with a model fit of the data as the bed is taken from approximately 21 °C and submerged in an approximately 75 °C water bath. The bed was pressurized to 50 psi gauge with oxygen at room temperature. . . . 184

2.154Experimental temperature data of support C of a microfibrous media bed compared with a model fit of the data as the bed is taken from approximately 21 °C and submerged in an approximately 75 °C water bath. The bed was pressurized to 50 psi gauge with oxygen at room temperature. . . . 184

2.155Experimental temperature data of support D of a microfibrous media bed compared with a model fit of the data as the bed is taken from approximately 21 °C and submerged in an approximately 75 °C water bath. The bed was pressurized to 50 psi gauge with oxygen at room temperature. . . . 185

2.156Experimental temperature data of support E of a microfibrous media bed compared with a model fit of the data as the bed is taken from approximately 21 °C and submerged in an approximately 75 °C water bath. The bed was pressurized to 50 psi gauge with oxygen at room temperature. . . . 185

2.157Experimental temperature data of support A of a microfibrous media bed compared with a model fit of the data as the bed is taken from approximately 78 °C and submerged in an approximately 20 °C water bath. The bed was pressurized to 50 psi gauge with oxygen at room temperature. . . . 186

2.158Experimental temperature data of support B of a microfibrous media bed compared with a model fit of the data as the bed is taken from approximately 78 °C and submerged in an approximately 20 °C water bath. The bed was pressurized to 50 psi gauge with oxygen at room temperature. . . . 187

2.159Experimental temperature data of support C of a microfibrous media bed compared with a model fit of the data as the bed is taken from approximately 78 °C and submerged in an approximately 20 °C water bath. The bed was pressurized to 50 psi gauge with oxygen at room temperature. . . . 187

2.160Experimental temperature data of support D of a microfibrous media bed compared with a model fit of the data as the bed is taken from approximately 78 °C and submerged in an approximately 20 °C water bath. The bed was pressurized to 50 psi gauge with oxygen at room temperature. . . . 188

2.161Experimental temperature data of support E of a microfibrous media bed compared with a model fit of the data as the bed is taken from approximately 78 °C and submerged in an approximately 20 °C water bath. The bed was pressurized to 50 psi gauge with oxygen at room temperature. . . . 188

2.162Experimental temperature data of support A of a microfibrous media bed compared with a model fit of the data as the bed is taken from approximately 0 °C and submerged in an approximately 20 °C water bath. The bed was pressurized to 50 psi gauge with oxygen at room temperature. 189

2.163Experimental temperature data of support B of a microfibrous media bed compared with a model fit of the data as the bed is taken from approximately 0 °C and submerged in an approximately 20 °C water bath. The bed was pressurized to 50 psi gauge with oxygen at room temperature. 190

2.164Experimental temperature data of support C of a microfibrous media bed compared with a model fit of the data as the bed is taken from approximately 0 °C and submerged in an approximately 20 °C water bath. The bed was pressurized to 50 psi gauge with oxygen at room temperature. 190

2.165Experimental temperature data of support D of a microfibrous media bed compared with a model fit of the data as the bed is taken from approximately 0 °C and submerged in an approximately 20 °C water bath. The bed was pressurized to 50 psi gauge with oxygen at room temperature. 191

2.166Experimental temperature data of support E of a microfibrous media bed compared with a model fit of the data as the bed is taken from approximately 0 °C and submerged in an approximately 20 °C water bath. The bed was pressurized to 50 psi gauge with oxygen at room temperature. 191

2.167Experimental temperature data of support A of a microfibrous media bed compared with a model fit of the data as the bed is taken from approximately 20 °C and submerged in an approximately 0 °C ice-water bath. The bed was pressurized to 50 psi gauge with oxygen at room temperature. . . . 192

2.168Experimental temperature data of support B of a microfibrous media bed compared with a model fit of the data as the bed is taken from approximately 20 °C and submerged in an approximately 0 °C ice-water bath. The bed was pressurized to 50 psi gauge with oxygen at room temperature. . . . 193

2.169Experimental temperature data of support C of a microfibrous media bed compared with a model fit of the data as the bed is taken from approximately 20 °C and submerged in an approximately 0 °C ice-water bath. The bed was pressurized to 50 psi gauge with oxygen at room temperature. . . . 193

2.170Experimental temperature data of support D of a microfibrous media bed compared with a model fit of the data as the bed is taken from approximately 20 °C and submerged in an approximately 0 °C ice-water bath. The bed was pressurized to 50 psi gauge with oxygen at room temperature. . . . 194

2.171Experimental temperature data of support E of a microfibrous media bed compared with a model fit of the data as the bed is taken from approximately 20 °C and submerged in an approximately 0 °C ice-water bath. The bed was pressurized to 50 psi gauge with oxygen at room temperature. . . . 194

2.172Experimental temperature data of support A of a microfibrous media bed compared with a model fit of the data as the bed is taken from approximately 22 °C and submerged in an approximately 70 °C water bath. The bed was reduced to 0.0033 mbar vacuum at room temperature. 195

2.173Experimental temperature data of support B of a microfibrous media bed compared with a model fit of the data as the bed is taken from approximately 22 °C and submerged in an approximately 70 °C water bath. The bed was reduced to 0.0033 mbar vacuum at room temperature. 196

2.174Experimental temperature data of support C of a microfibrous media bed compared with a model fit of the data as the bed is taken from approximately 22 °C and submerged in an approximately 70 °C water bath. The bed was reduced to 0.0033 mbar vacuum at room temperature. 196

2.175Experimental temperature data of support D of a microfibrous media bed compared with a model fit of the data as the bed is taken from approximately 22 °C and submerged in an approximately 70 °C water bath. The bed was reduced to 0.0033 mbar vacuum at room temperature. 197

2.176Experimental temperature data of support E of a microfibrous media bed compared with a model fit of the data as the bed is taken from approximately 22 °C and submerged in an approximately 70 °C water bath. The bed was reduced to 0.0033 mbar vacuum at room temperature. 197

2.177Experimental temperature data of support C of a microfibrous media bed compared with a model fit of the data as the bed is taken from approximately 70 °C and submerged in an approximately 19 °C water bath. The bed was reduced to 0.0033 mbar vacuum at room temperature. 198

2.178Experimental temperature data of support E of a microfibrous media bed compared with a model fit of the data as the bed is taken from approximately 70 °C and submerged in an approximately 19 °C water bath. The bed was reduced to 0.0033 mbar vacuum at room temperature. 199

2.179Experimental temperature data of support A of a microfibrous media bed compared with a model fit of the data as the bed is taken from approximately 0 °C and submerged in an approximately 19 °C water bath. The bed was reduced to 0.0029 mbar vacuum at room temperature. 200

2.180Experimental temperature data of support B of a microfibrous media bed compared with a model fit of the data as the bed is taken from approximately 0 °C and submerged in an approximately 19 °C water bath. The bed was reduced to 0.0029 mbar vacuum at room temperature. 201

2.181Experimental temperature data of support C of a microfibrous media bed compared with a model fit of the data as the bed is taken from approximately 0 °C and submerged in an approximately 19 °C water bath. The bed was reduced to 0.0029 mbar vacuum at room temperature. 201

2.182Experimental temperature data of support D of a microfibrous media bed compared with a model fit of the data as the bed is taken from approximately 0 °C and submerged in an approximately 19 °C water bath. The bed was reduced to 0.0029 mbar vacuum at room temperature. 202

2.183Experimental temperature data of support E of a microfibrous media bed compared with a model fit of the data as the bed is taken from approximately 0 °C and submerged in an approximately 19 °C water bath. The bed was reduced to 0.0029 mbar vacuum at room temperature. 202

2.184Experimental temperature data of support C of a microfibrous media bed compared with a model fit of the data as the bed is taken from approximately 22 °C and submerged in an approximately 0 °C ice-water bath. The bed was reduced to 0.0029 mbar vacuum at room temperature. 203

2.185Experimental temperature data of support D of a microfibrous media bed compared with a model fit of the data as the bed is taken from approximately 22 °C and submerged in an approximately 0 °C ice-water bath. The bed was reduced to 0.0029 mbar vacuum at room temperature. 204

2.186Experimental temperature data of support E of a microfibrous media bed compared with a model fit of the data as the bed is taken from approximately 22 °C and submerged in an approximately 0 °C ice-water bath. The bed was reduced to 0.0029 mbar vacuum at room temperature. 204

2.187Models of stagnant effective thermal conductivity with solid thermal conductivity $k_s = 30\frac{W}{mK}$ and void fraction $\varepsilon = 0.8$. 207

3.1 Characteristic length of microfibrous media composed of two layers of fibers with the top layer consisting of $17\,\mu m$ diameter by $6\,mm$ long fibers and the bottom layer consisting of $6\,\mu m$ diameter by $3\,mm$ long fibers. . . . 211

3.2 Steady state temperatures at the center line for a microfibrous (MFM) bed with various flow rates of argon. The bed is submerged in a hot water bath at approximately 70 °C. 217

3.3 Steady state temperatures at 15 mm from the center line for a microfibrous (MFM) bed with various flow rates of argon. The bed is submerged in a hot water bath at approximately 70 °C. 218

3.4 Steady state temperatures at 22.5 mm from the center line for a microfibrous (MFM) bed with various flow rates of argon. The bed is submerged in a hot water bath at approximately 70 °C. 219

3.5 Steady state temperatures at the center line for a microfibrous (MFM) bed with various flow rates of helium. The bed is submerged in a hot water bath at approximately 70 °C. 220

3.6 Steady state temperatures at 15 mm from the center line for a microfibrous (MFM) bed with various flow rates of helium. The bed is submerged in a hot water bath at approximately 70 °C. 221

3.7 Steady state temperatures at 22.5 mm from the center line for a microfibrous (MFM) bed with various flow rates of helium. The bed is submerged in a hot water bath at approximately 70 °C. 222

3.8 Steady state temperatures at the center line for a microfibrous (MFM) bed with various flow rates of oxygen. The bed is submerged in a hot water bath at approximately 70 °C. 223

3.9 Steady state temperatures at 15 mm from the center line for a microfibrous (MFM) bed with various flow rates of oxygen. The bed is submerged in a hot water bath at approximately 70 °C. 224

3.10 Steady state temperatures at 22.5 mm from the center line for a microfibrous (MFM) bed with various flow rates of oxygen. The bed is submerged in a hot water bath at approximately 70 °C. 225

4.1 Grid of resistances for fibers and fluid within microfibrous media. Four unit cells of resistances are show with one cell highlighted. Resistance labels containing 'f' refer to fluid, and those containing 's' refer to fiber (solid). Labels containing 'v' refer to vertical (parallel to the direction of heat flow) and 'h' refer to horizontal (perpendicular to the direction of heat flow). . . . 236

4.2 Single cell of resistances within microfibrous media with simplified fluid resistances in parallel. 237

4.3 Diagram of a wheatstone bridge. RS_b is the bridge resistance. 238

4.4 Simplified resistance diagram of resistances within microfibrous media with fluid. 239

4.5 Representative square fiber compared to circular fiber and mesh cage size. . 239

4.6 Cube unit cell of 1 fiber in fluid. 240

4.7 Cube unit cell for microfibrous media. 241

4.8 Cube unit cell for microfibrous media incorporating fiber junction. 242

4.9 Rectangle unit cell for microfibrous media incorporating fiber junction. . . . 242

4.10 Effective thermal conductivity of a system of two fibers separated by a gap as a function of the length of the gap. Each fiber is $1000\,\mu\mathrm{m}$ in length and $15.625\,\mu\mathrm{m}$ in diameter. The fibers have a thermal conductivity of $400\,\frac{\mathrm{W}}{\mathrm{m\cdot K}}$. . 244

4.11 Effective thermal conductivity of a system of two fibers separated by a gap as a function of the length of the gap. Each fiber is $1000\,\mu\mathrm{m}$ in length and $15.625\,\mu\mathrm{m}$ in diameter. The fibers have a thermal conductivity of $400\,\frac{\mathrm{W}}{\mathrm{m\cdot K}}$. The mean free path of hydrogen is added for comparison against the gap distance. 245

4.12 A two-dimensional cell consisting of a single fiber, surrounding materials, and walls. 246

4.13 A representation of a discretized grid for Figure 4.12 with the positions used for calculating k_{eq} circled. 247

4.14 A visual representation of how the average heat flux is determined at $\xi = 1$. 249

List of Abbreviations and Nomenclature

CS	Cage size
D_f	Diameter of circular-fiber cross-section
F_v	Volume fraction of solids
L	Length
R	Radius or Resistance depending on context
Rf_h	Horizontal resistance of fluid
Rf_v	Vertical resistance of fluid
Rs	Resistance of solid (fiber)
S	Surface area
S_f	Side length of square-fiber cross-section
S_v	Specific surface
U_{id}	Overall heat transfer coefficient
V	Volume
W	Width
Δ	Difference between two points
α	Thermal diffusivity
ϵ	Void fraction
η	Non-dimensional z direction (down the axis) when discussing radial coordinates, and non-dimensional x direction when discussing Cartesian coordinates

$\mathcal{O}$ Order of accuracy

μ Dynamic viscosity

ϕ Solid volume fraction or junction factor

ρ Density

τ Non-dimensional time

θ Non-dimensional temperature

ξ Non-dimensional radial direction when discussing radial coordinates, and non-dimensional y direction when discussing Cartesian coordinates

q Heat flux

u Superficial velocity

u Thermal conductivity

Abbreviations

AWG American wire gauge

Cu-MFM Copper microfibrous media

MFEC Microfibrous entrapped catalyst

MFES Microfibrous entrapped sorbent

MFM Microfibrous media

NPT National pipe taper

psi Pounds per square inch

PTFE Polytetrafluoroethylene

Dimensionless Numbers

Bi	Biot number
Pe	Péclet number
Pr	Prandtl number
Re	Reynolds number

Subscripts

c	Characteristic
c	Particle based
ea	Effective axial
eq	Equivalent
er	Effective radial
f	Fiber or fluid depending on context
g	Gap
i	Position in xi direction
j	Position in eta direction
s	Solid

Superscripts

n	Position in tau (dimensionless time)

Chapter 1

Introduction and Background

Microfibrous media (MFM) is a nonwoven fibrous material composed of one or more types of fibers preferentially oriented in a single plane. These fibers may be of many materials including copper, nickel, stainless steel, polymers, and more. Frequently MFM is made in two layers, the main layer and a much smaller barrier layer made of smaller diameter fibers. This fiber structure can be used as-is, or it can be combined with other components to make derivative materials. Furthermore, the void volume of MFM is highly variable and tunable. Being versatile in both composition and void fraction makes MFM a useful material for a variety of applications, including filtration, catalytic beds, and sorbent beds.

MFM is made and the preferential orientation achieved through the use of traditional paper-making techniques. A mixture including the chosen fibers and cellulose is used to create green media in the same way that paper would be made. This green media is then heated in an oven to burn off the cellulose and sinter the media fibers.

MFM was developed at Auburn University in the lab of Dr. Bruce Tatarchuk. It was described in 1990 for use in producing electrodes by Kohler et al. [1] and Zabasajja et al. [2]. It was then originally patented in 1992 [3]. It is now manufactured by Intramicron Inc. in Auburn, AL.

One use of MFM is as a heat transfer device within reactors. Catalyst or sorbent can be entrapped within the MFM to make a material known as microfibrous entrapped catalyst

(MFEC) or microfibrous entrapped sorbent (MFES), respectively. This material can then be loaded into a reactor to serve as both the catalyst/sorbent bed and a heat transfer medium.

MFM greatly enhances heat transfer in the plane of its preferential orientation as compared to a packed bed. This allows for better temperature control in an MFM bed than in a packed bed. This was investigated by Sheng et al. [4]. Furthermore, MFM has been used in conjunction with paraffin wax to create a material called microfibrous media phase change material (MFM-PCM). This material has been successfully used as a battery cooling medium.

1.1 Overview of Microfibrous Media Research

Initially created for use as electrodes as described by Kohler et el. [1], Kohler et al. [5], and Zabasajja et al. [2], further research revealed MFM was substantially useful in multiple applications. It was found that materials such as catalysts and sorbents could be trapped inside the microfibrous media. Initially, these microfibrous materials with entrapped particles were produced by including the particles in the slurry during the wet-lay process [6]. Later, it was found that a better method of entrapment was to create the MFM, then entrap pre-made catalysts in the material after it had been sintered; this is because the entrapped materials can become poisoned during the MFM production process [7]. Duggirala et al. [8] found that microfibrous entrapped sorbents (MFES) were able to outperform tested packed beds for desulferization via higher conversion rates. Cheng et al. [9] found that microfibrous entrapped catalyst (MFEC) exhibited a much flatter radial temperature profile for Fischer-Tropsch synthesis than tested packed beds (approximately 5 °C vs 54 °C temperature difference across the radius). Punde and Tatarchuk [10, 11] found that a nickel microfibrous entrapped catalyst (Ni-MFEC) bed outperformed a comparable packed bed for CO oxidation. Gu et al. [12] used computational models to study pressure drop in MFM, MFM with entrapped particles, and pleated MFM, while Cahela and Tatarchuk [13] proposed the porous media permeability equation (PMP equation) for calculating pressure

drop through microfibrous materials. Sheng et al. [14] studied the heat transfer properties of microfibrous entrapped catalysts and packed beds through simulation. Sheng et al. [15] tested comparable MFEC and packed bed reactors 41 millimeters in diameter and reported a maximum radial temperature difference of 6.4 °C for the MFEC reactor and 460 °C for the packed bed reactor. Zhu et al. [16] used microfibrous media phase change material active thermal management (MFM-PCM/ATM) to make cooling structures for Li-ion battery cells. This structure proved to be effective at controlling the temperature of the cells and mitigating damage to surrounding cells in the event of a failure of one cell.

This work continues the research into the heat transfer properties of microfibrous media. In fact, this work can be thought of as an almost direct continuation of the work of Min Sheng [4, 17, 18]. Here is presented work on the effective thermal conductivity of microfibrous media beds containing stagnant gas, the effect of flowing gas on the heat transfer properties of a microfibrous media bed, and potential resistance networks and unit cells to model microfibrous media.

Chapter 2

Effective Thermal Conductivity of a Microfibrous Media Bed Containing Stagnant Gas

2.1 Experimental

An alumina packed bed and a microfibrous media (MFM) bed were constructed in 2.5-inch (outer diameter) 304 stainless steel sanitary tubes. Two sanitary tubes were used; one for the packed bed, and the other for the MFM bed. The beds were used to collect temperature data for estimating effective thermal conductivities and overall heat transfer coefficients.

2.1.1 Multi-Point Thermocouple Description

A 15-point thermocouple was constructed. It was desired that this thermocouple be composed of the finest wires possible and be as hermetic as possible. Various epoxies were tested for sealing the thermocouple inside a housing, but this proved to not seal hermetically with gas escaping around (and it seemed through the inside channel of) the thermocouple wire insulation. It was then tested to etch the insulation of the thermocouples with FluoroEtch to improve adhesion of the epoxy against the insulation, but this also proved ineffective. A method was developed to remove a small section of insulation and seal against the bare metal wires of the thermocouples.

To facilitate this, 15 Type-T fine-wire thermocouples were made. Type-T thermocouples were constructed from Type-T thermocouple duplex wire puchased from Omega Engineering. The thermocouple wire had a polyimide conductor insulation and polyimide

overall insulation, and a wire gauge of 30 AWG ($0.254\,\mathrm{mm}$ diameter [19]). These thermocouples were fitted with miniature male type-T thermocouple connectors of various models.

A housing was constructed for the 15 thermocouples from a 304 stainless steel class 150 $1\frac{1}{2}$-inch male NPT hex head plug and a 304 stainless steel class 150 $1\frac{1}{2}$-inch female NPT x $\frac{3}{8}$-inch female NPT reducing coupling. The hex head plug was filled with J-B Weld Plastic Bonder that was allowed to cure overnight. The top of the hex head plug was then faced and had 15 $\frac{3}{16}$-inch holes drilled through it (and the plastic bonder) as shown in Figure 2.1.

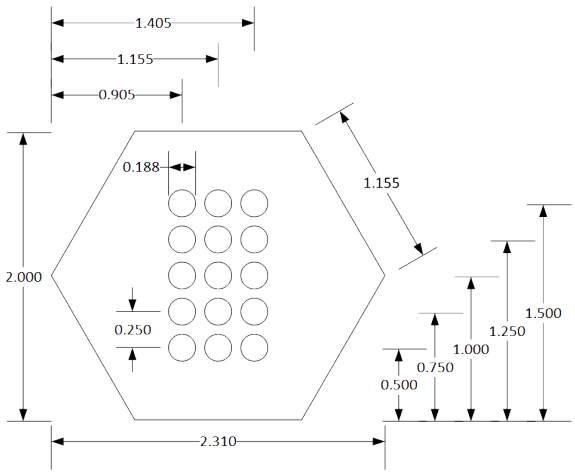

Figure 2.1: Dimensional drawing (top view) for $\frac{3}{16}$-inch holes for thermocouples in $1\frac{1}{2}$-inch male NPT hex head plug.

Using a craft knife, an approximately $\frac{1}{2}$-inch long section of insulation was stripped away approximately five inches from the connector of each of the 15 individual thermocouples. Both the conductor and overall insulation were stripped leaving a short section of bare wire. The two bare sections of thermocouple wire were slightly bowed away from each other to ensure that they would not touch.

The thermocouples were then sat on a sheet of plastic (assumed to be polypropylene) such that the bare sections of wire were on the plastic. The thermocouples were then taped to the table on either side of the plastic such that the thermocouples would not move. A

small amount of plastic bonder was then applied to each of these bare sections of wire. This was done so that in the following steps of the construction, the bare wires would not be able to touch.

Each of the thermocouples was then fed through one of the holes in the hex head plug such that the section now coated in plastic bonder was inside the filling of plastic bonder inside the plug and the connector was on the side of the top of the plug. Tape was then used to secure the sections of thermocouple wire on the top of the plug flat against the top of the plug. The plug assembly was then secured upside down on a ring stand the the long sections of thermocouple wire at the bottom of the plug bundled together and secured above the plug. A small syringe without a needle was then used to fill the holes in the plug and plastic bonder filling with plastic bonder. This was allowed to cure overnight.

A $\frac{3}{8}$-inch male NPT x $\frac{3}{8}$-inch male Swagelok tube fitting was then attached to the bottom of the reducing coupling using $\frac{1}{2}$-inch copper-filled PTFE tape. This reducing coupling assembly was then slid over the long sides of the thermocouples (protruding from the bottom of the hex head plug), and it was secured to the hex head plug using $\frac{1}{2}$-inch copper-filled PTFE tape. This completed the construction of the 15-point thermocouple.

The individual thermocouples were then passed through a series of tubes and fittings to pass through a thermometer cap that sealed one side of the sanitary tube containing the test bed. The thermometer cap was a sanitary cap tapped for $\frac{3}{4}$-inch NPT fitting. A tee was used to attach a second tube to the line containing the thermocouples. This second tube had a Swagelok quick disconnect attached to it for connecting to gas cylinders.

2.1.2 Thermocouple Support Description

Fifteen thermocouples were placed in each bed with three each attached to supports placed at the front of the bed, the end of the bed, and approximately at the $\frac{1}{4}$, $\frac{1}{2}$, and $\frac{3}{4}$ axial lengths of the bed. The thermocouple supports were made from PTFE-coated fiberglass fabric sheet (PTFE being polytetrafluoroethylene). The supports were labeled A through E and

were located at each end of the bed, the midpoint, and one-quarter the bed length from each end. The fabric sheet used was specified as 0.030 inches thick with an opening height and width of $\frac{3}{16}$ inch.

A template set was designed in SOLIDWORKS and 3d printed in PLA (polylactic acid) to both create and utilize the thermocouple supports. This template set is depicted in Figure 2.2 and consists of an inset (Figure 2.2a) and a shell (Figure 2.2b) that are separate pieces. Both pieces have holes at the center (labeled as position 1), $7.5\,\mathrm{mm}$ from center (approximately $\frac{1}{4}$ radius), $15\,\mathrm{mm}$ from center (approximately half radius; labeled as position 2), and $22.5\,\mathrm{mm}$ from center (approximately $\frac{3}{4}$ radius; labeled as position 3). The holes in the inset are $1.5\,\mathrm{mm}$ in diameter, and the holes in the shell are $6.0\,\mathrm{mm}$ in diameter. The two pieces have interlocking keys that were used both for aligning the pieces as well as providing channels on the supports for running thermocouple wires through the supports.

To create the supports, the template inset had one side covered in double-sided clear tape and was adhered to the fiberglass fabric with the holes aligned along fibers of the fabric. A craft knife was then used to cut the fabric to the shape of the template inset. The thickness of the thermocouple supports used in the microfibrous media bed was measured and is shown in Figure 2.1.

Table 2.1: Thermocouple support thickness for microfibrous media bed as measured with Mitutoyo calipers at arbitrary locations.

Support	Measurement 1 (mm)	Measurement 2 (mm)	Measurement 3 (mm)	Average (mm)
A	0.96	0.94	0.92	0.94
B	0.97	0.95	0.98	0.97
C	0.92	0.91	0.94	0.92
D	0.92	0.95	0.93	0.93
E	0.94	0.91	0.94	0.93

To prepare for attaching thermocouples to a support, the support was placed inside the template shell with fibers of the support aligning with the holes of the shell, and the template

inset was pressed into the shell sealing the support inside. Using a sewing needle, 0.014-inch ($0.36\,\mathrm{mm}$) PTFE-coated fiberglass thread was threaded through through the support via three holes in the inset at position 1, position 2, and position 3 in a single line. The support is then removed from the template with the threads remaining in the support. An object smaller than $6.0\,\mathrm{mm}$ in diameter can be used to pass through a hole in the shell and push the inset out of the shell. The object used by the author was a pen with the point retracted.

All three thermocouples on a support are attached on the same side. The side with the thermocouples will be referred to as the front, and the opposite side referred to as the back. To attach a thermocouple to the support, the end of a thread on the front of the support was passed between the wires of the thermocouple directly below the tip. Then, using a needle, the thread was then passed through the support to the back so that both ends of the thread are at the back of the support. Both ends of the thread were then passed back through the support next to each other so that both thread ends were then at the front of the support (not through any existing places where the thread passed through). The two thread ends were finally tied into a knot and excess thread length trimmed. The purpose of passing the thread through the support multiple times was to make it less likely for the thermocouple to become detached from the support if the knot were to come undone.

After all three thermocouples were attached to a support, they were run out from the support in a single line and a thread was tied around them as depicted in Figure 2.3. At a few points along the lengths of the three thermocouples, they were again tied together with the same thread. This was done to make handling and placing the support in the bed easier. These processes were repeated for all five thermocouple supports.

2.1.3 Packed Bed Description

Two packed beds were constructed. One used $\frac{1}{8}$-inch-diameter gamma alumina cylindrical pellets described in Table 2.2. The other used 100-mesh (approximately 150 micron)

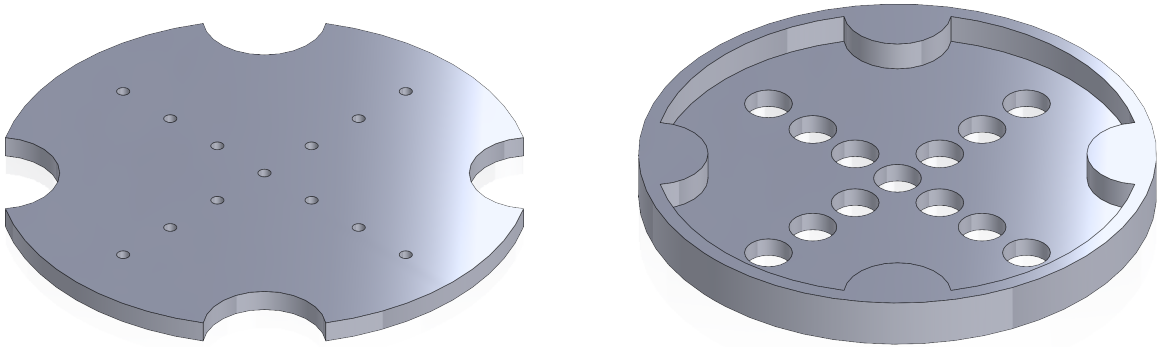

(a) Inset (b) Shell

Figure 2.2: Thermocouple support template.

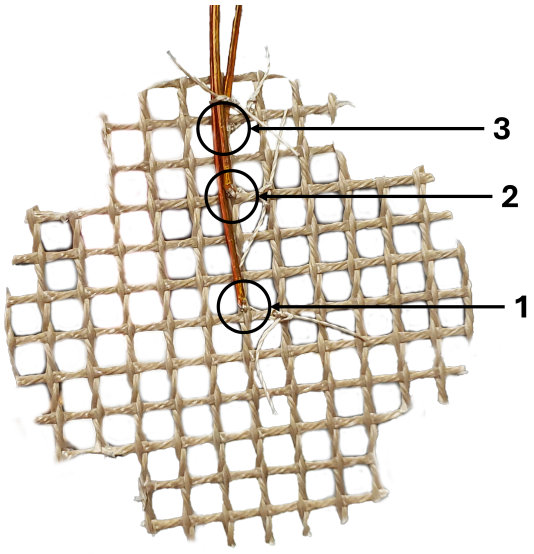

Figure 2.3: Thermocouple support with attached thermocouples.

gamma alumina powder. Both beds were packed in the same sanitary tube. The tube inside diameter (bed diameter) is approximately $61.5\,\mathrm{mm}$ as measured from one opening end with calipers.. For both, thermocouple were placed during loading at the front of the bed, the end of the bed, and approximately at the $\frac{1}{4}$, $\frac{1}{2}$, and $\frac{3}{4}$ axial lengths of the bed. The same sanitary tube and the same process was used for loading both of the packed beds.

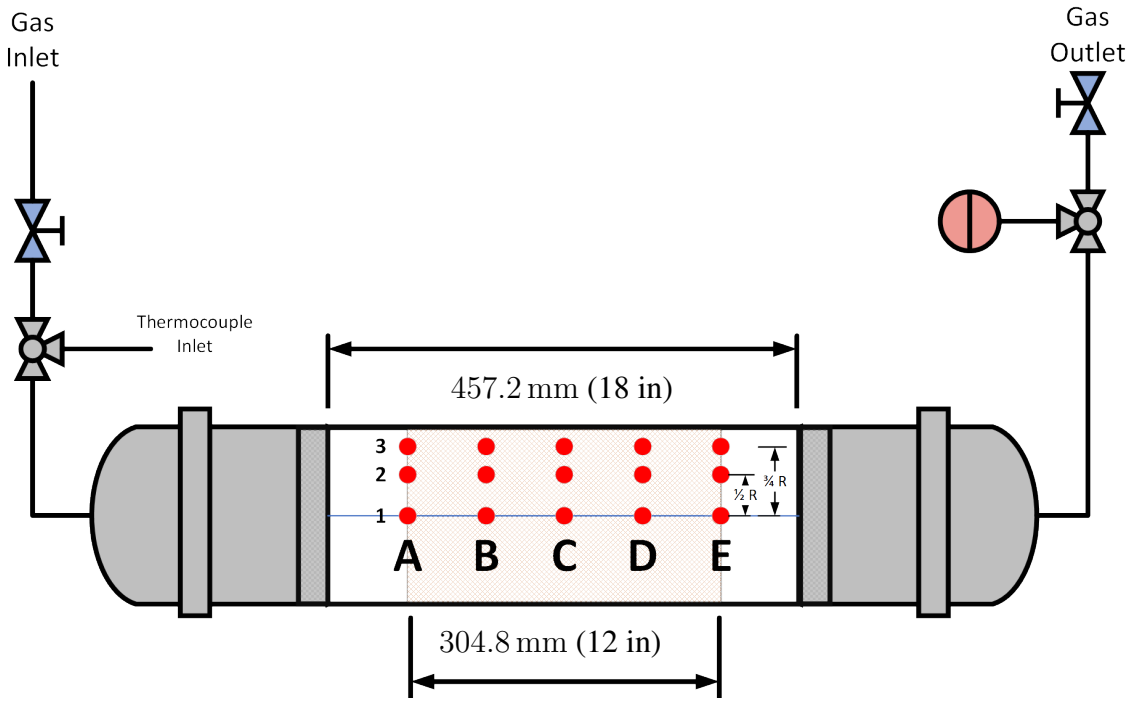

Figure 2.4: Diagram of the reactor used in packed bed experiments.

Tools used to load the packed bed are shown in Figure 2.5 and include two slotted-head push rods approximately $58.7\,\mathrm{mm}$ in diameter with caps that can be be clamped to a 3.5-inch sanitary flange and stop collars with thumb screws; these push rods will be referred to as clamping push rods, and the major parts of these clamping push rods can be seen in Figure 2.6 and Figure 2.7. One of the clamping push rods is used as a stop rod to set the position of one end of the bed, and the other is used to compact the bed. The slots in the push rod heads were to give passageways for any thermocouples already in the tube to facilitate loading without damaging thermocouples. Another flat-head pusher rod approximately $55.5\,\mathrm{mm}$ in diameter was also used to help compact the packed bed and

Table 2.2: Alumina pellet size used in packed bed.

Pellet	Diameter (mm)	Length (mm)
1	3.42	4.19
2	3.51	3.26
3	3.42	2.48
4	3.50	3.64
5	3.47	5.08
6	3.44	3.35
7	3.58	3.78
8	3.45	3.31
9	3.46	2.85
10	3.47	3.12
Average	3.47	3.51

[1] $\frac{1}{8}$-inch pellet Aluminum oxide, gamma-phase, catalyst support, high surface area, bimodal
[2] Measured with Mitutoyo calipers model 500-197-30.
[3] Caliper accuracy: $\pm\, 0.02\,\mathrm{mm}$
[4] 10 pellets chosen arbitrarily from 1 kg lot.

ensure the top of the bed was flat when measurements were taken. Lastly, a tape measure was used to measure the height of the bed for adding the thermocouple supports.

Figure 2.5: Tools used for loading packed beds. Two slotted push rods with head diameters of approximately $58.7\,\mathrm{mm}$ with caps that can be be clamped to a 3.5-inch sanitary flange and stop collars with thumb screws; these push rods will be referred to as clamping push rods. One push rod with a head diameter of approximately $55.5\,\mathrm{mm}$.

To begin loading, double-sided tape was attached to the head of one of the clamping push rods, then the rod was set at a length of three inches ($76.2\,\mathrm{mm}$) from one end of the sanitary tube and locked in place. This rod will be referred to as the stop rod. The purpose

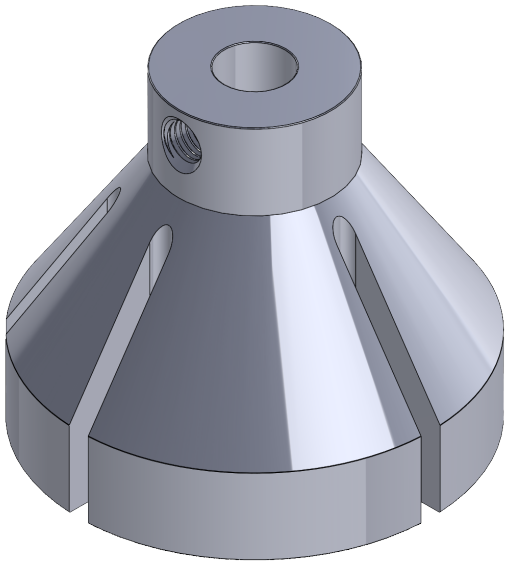

Figure 2.6: Flat slotted push-rod head with diameter of approximately $58.7\,\mathrm{mm}$.

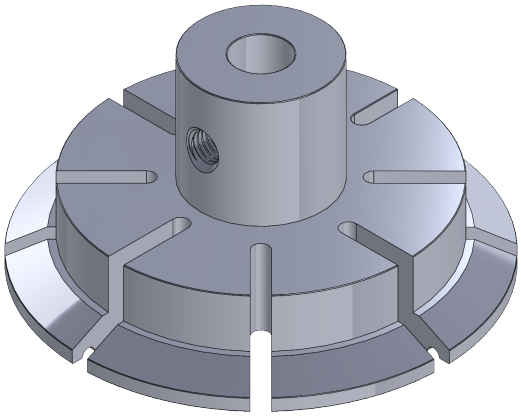

Figure 2.7: Slotted sanitary cap for push rod. Fits with a 3.5-inch sanitary flange.

of the tape was to hold the first thermocouple support in place until the packed bed could do so.

The sanitary tube with stop rod in place was then attached to a ring stand vertically using three chain clamps. The sanitary tube is oriented with the stop rod at the bottom and the open end at the top. A piece of polymer tubing was place around the chain of the chain clamps to avoid marring the outside of the tube.

With the sanitary tube prepared for loading, a thermocouple support (support E) was placed in the tube, and a push rod was used to adhere it to the doubled-sided tape on the stop rod. Packing was then weighed in a weighing boat and added to the tube. While adding packing to the tube, it was attempted to keep thermocouples at approximately the same radial position along their length through the tube. The height of the bed was measured using a tape measure repeatedly during packing. When the height of the bed reached three inches ($76.2\,\mathrm{mm}$) from the stop rod, another thermocouple support was placed at that location. A metal rod was used to hold this thermocouple support in place until enough packing was added on top of the support to hold it in place. This process was then repeated with thermocouple supports placed at 6 inches ($152.4\,\mathrm{mm}$), 9 inches ($228.6\,\mathrm{mm}$), and 12 inches ($304.8\,\mathrm{mm}$) from the stop rod.

After the bed was packed and the final thermocouple support was placed, 8 - $15\,\mu\mathrm{m}$ quartz wool was packed into the tube around the thermocouple wires. This was done to both insulate the bed and hold the bed in place. The remaining length of thermocouples was then pushed into the tube outside of the quartz wool, and the bed was sealed on that end. The sanitary tube was then flipped so that the stop rod was facing upward and the sealed end of the tube was facing downward. The stop rod was then removed and then end of the tube packed with quartz wool. This end was then also sealed completing the packing process.

2.1.4 Microfibrous Media Bed Description

The microfibrous media (MFM) was loaded into a 2.5-inch sanitary tube. The average tube diameter was $60.01\,\mathrm{mm}$ as measured with a bore gauge from inside the tube past where the flanges would have been welded. The media was loaded at approximately 4.8% solid by volume in 28 sections to allow the media to be more evenly compressed throughout the bed. Thermocouple supports were placed during loading at the front of the bed, the end of the bed, and approximately at the $\frac{1}{4}$, $\frac{1}{2}$, and $\frac{3}{4}$ axial length of the bed.

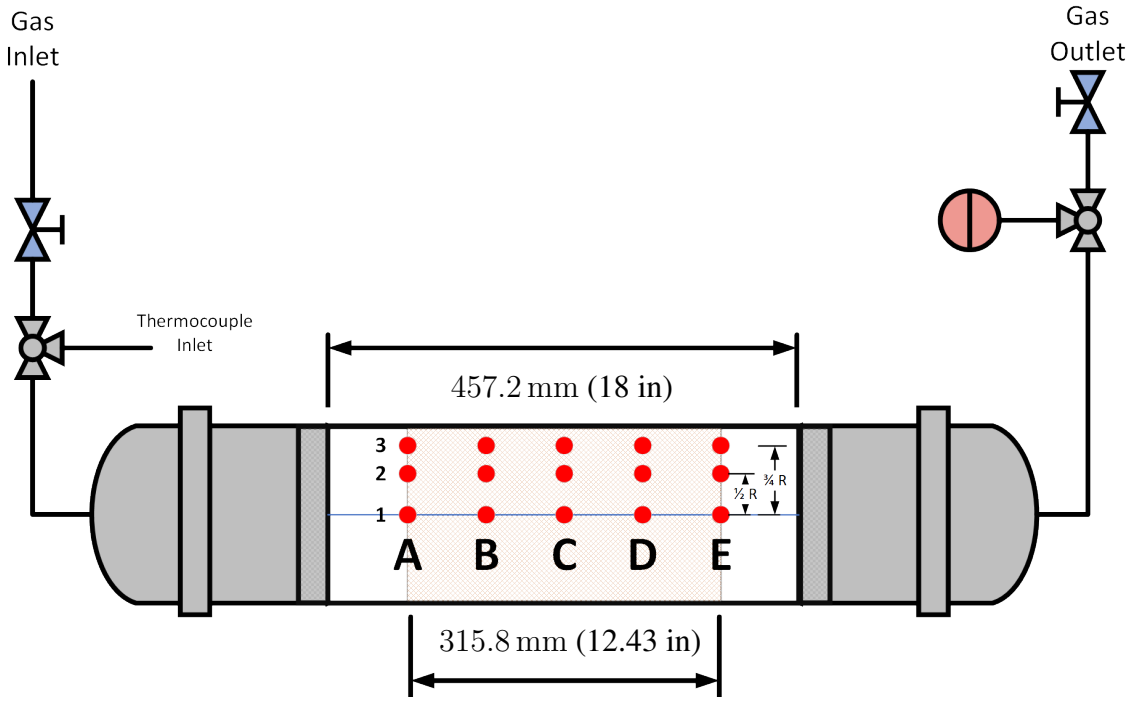

Figure 2.8: Diagram of the reactor used in microfibrous media experiments.

Table 2.3: Sanitary tube diameter for microfibrous media experiments.

6.0010 cm	average tube diameter
6.0109 cm	max tube diameter
5.9891 cm	min tube diameter

Tools used to load the MFM bed are shown in Figure 2.9 and include two slotted-head push rods approximately $58.7\,\mathrm{mm}$ in diameter with caps that can be be clamped to a 3.5-inch sanitary flange and stop collars with thumb screws; these push rods will be referred to as clamping push rods, and the major parts of these clamping push rods can be seen in Figure 2.6 and Figure 2.7. One of the clamping push rods is used as a stop rod to set the position of one end of the bed, and the other is used to compress the microfibrous media. The slots in the push rod heads were to give passageways for any thermocouples already in the tube to facilitate loading without damaging thermocouples. In addition to the flat clamping push rods, a concave push rod approximately $59.5\,\mathrm{mm}$ in diameter (the head of which is shown in Figure 2.10) was used to place disks of microfibrous media in their approximate location. A flat-head pusher rod approximately $55.5\,\mathrm{mm}$ in diameter and a thin metal rod with a right-angle hooked end were used to align the disks in their location. A rod with a cap that can be clamped to a 3.5-inch sanitary flange and stop collars with thumb screws was used as a depth gauge. Finally, a tape measure and a set of digital calipers were used for various measurements while loading the MFM bed.

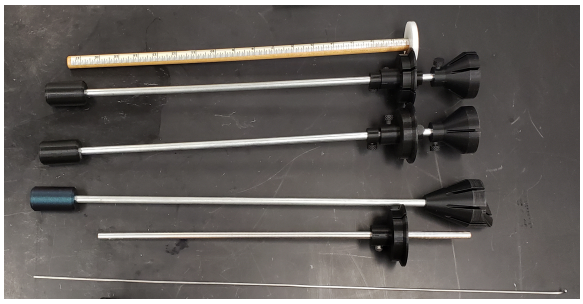

Figure 2.9: Tools used for the microfibrous media bed. Two slotted push rods with head diameters of approximately $58.7\,\mathrm{mm}$ with caps that can be be clamped to a 3.5-inch sanitary flange and stop collars with thumb screws; these push rods will be referred to as clamping push rods. One push rod with a head diameter of approximately $55.5\,\mathrm{mm}$. A push rod with a concave head with a diameter of approximately $59.5\,\mathrm{mm}$. A rod with a cap that can be clamped to a 3.5-inch sanitary flange and stop collars with thumb screw. A thin metal rod with a hooked end.

To begin loading, double-sided clear tape was attached to the head of one of the clamping push rods, then the rod was set at a length of three inches ($76.2\,\mathrm{mm}$) from one end of

Figure 2.10: Slotted concave push-rod head with a diameter of approximately $59.5\,\mathrm{mm}$.

the sanitary tube and locked in place. This rod will be referred to as the stop rod. The purpose of the tape was to hold the first thermocouple support in place until the MFM bed could do so.

The sanitary tube with stop rod in place was then attached to a ring stand vertically using three chain clamps. The sanitary tube is oriented with the stop rod at the bottom and the open end at the top. A piece of polymer tubing was place around the chain of the chain clamps to avoid marring the outside of the tube. The first thermocouple support was then inserted and attached to the double-sided clear tape is shown in Figure 2.11.

Disks of microfibrous media were loaded into the sanitary tube one at a time. To load a disk of media, it was first slightly folded and placed onto the head of the concave push rod with the head oriented so that the media could be placed upon it and not fall off. The push rod was then gently pushed into the tube until it came into contact with material. The concave push rod was removed leaving the disk of microfibrous media in the tube. With

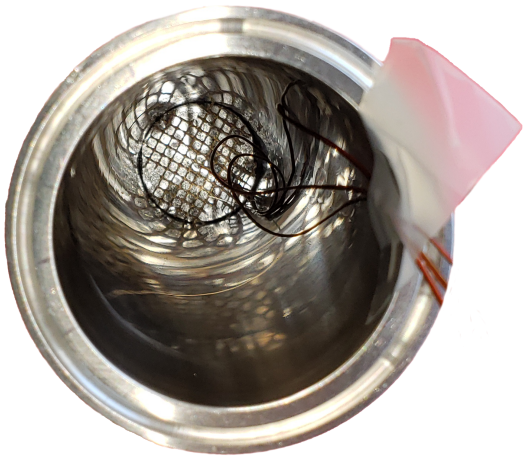

Figure 2.11: Placement of first thermocouple support in microfibrous media bed.

the disk roughly placed, a combination of the smaller push rod and the thin metal rod was used to align the piece of media properly into its position.

It was decided to pack the MFM bed in sections so as to more evenly compress the bed to a constant volume fraction of solid throughout its length. $10\,\mathrm{mm}$ per section was chosen as the target compressed length. At a target of 5% solid by volume, the target mass of microfibrous material per section was approximately $12.7\,\mathrm{g}$. The actual measurements of the 28 sections of the bed can be seen in Table 2.4. Uncompressed disks of microfibrous media are shown in Figure 2.12, and an example of a compressed section of microfibrous media is shown in Figure 2.14; this compressed section of media was not used in the final bed and is just for demonstration purposes. The MFM bed is shown after one of the sections has been compressed in Figure 2.15.

Media was loaded in sections until the bed length was reached to place another thermocouple support. The next thermocouple support was placed and the media compressed to the target length as shown in Figure 2.16. This process was repeated until the bed packing was completed.

It is noted that the microfibrous media sprang back after being compressed, so the recorded lengths are not correct in reality but rather target lengths that the media was

Table 2.4: Microfibrous media bed packing

Section	Mass (g)	Length (mm)	Volume Percent
1	12.68	10.0	5.00
2	12.36	9.8	5.0
3	13.42	10.6	5.00
4	15.35	12.1	5.01
5	13.36	10.5	5.02
6	11.95	9.4	5.0
7	17.57	13.9	4.99
8	11.42	9.0	5.0
9	13.56	10.7	5.00
10	11.76	9.3	5.0
11	15.75	12.4	5.01
12	14.06	11.1	5.00
13	15.82	12.5	4.99
14	13.75	10.9	4.98
15	14.15	11.2	4.99
16	13.11	10.3	5.02
17	14.26	11.3	4.98
18	15.10	11.9	5.01
19	13.61	10.7	5.02
20	18.84	14.9	4.99
21	8.44	6.7	5.0
22	14.68	11.6	4.99
23	15.62	12.3	5.01
24	12.43	9.8	5.0
25	12.90	10.2	4.99
26	17.35	13.7	5.00
27	11.04	8.7	5.0
28	12.08	9.2	5.2

The lengths and volume percents presented in this table are where the target values. Due to the fact the microfibrous media springs back partially after being compressed, these are not the actual values within the bed.

Figure 2.12: Microfibrous media that has been cut but not compressed stored in a plastic tub.

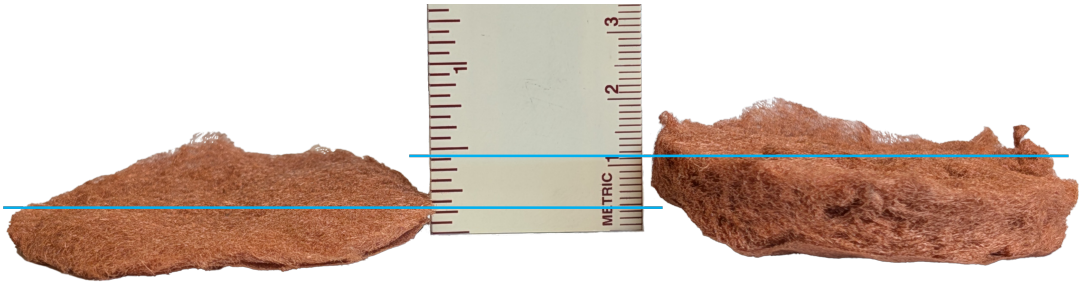

Figure 2.13: Two pieces of microfibrous media (MFM) shown to depict variance in the media used. The pieces are as cut from sheets of MFM and have not been compressed. The two pieces shown are extreme examples, and the lines drawn are approximately how thick the pieces are as there is variance within each piece.

Figure 2.14: Microfibrous media that was compressed in the same tube used for microfibrous media beds in this work.

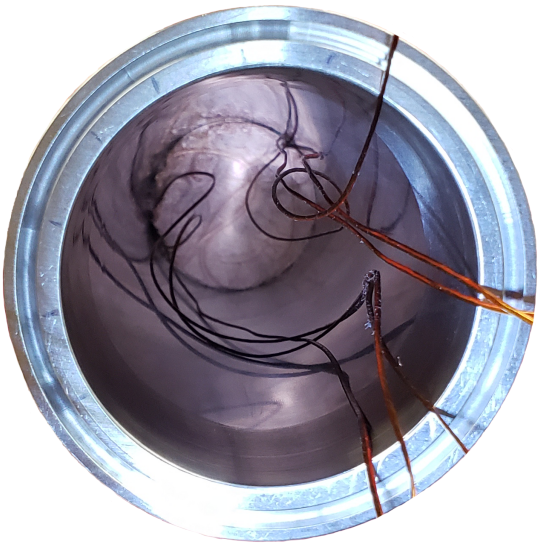

Figure 2.15: Microfibrous media bed being loaded.

Figure 2.16: Thermocouple support C inside of the microfibrous media bed.

compressed to before spring back. The spring back was only measured once and was approximately ten millimeters. Also because of this, the final solid percent was 4.8% solid by volume instead of the target 5%, and the final length of the MFM bed was $315.8\,\mathrm{mm}$ (12.43 in) instead of the target $304.8\,\mathrm{mm}$ (12 in).

The thermocouple supports target locations where the beginning of the bed, $\frac{1}{4}$ the length of the bed, $\frac{1}{2}$ the length of the bed, $\frac{3}{4}$ the length of the bed, and the end of the bed. The target distances were calculated from the target bed length of 304.8 mm (12 in), so they were 0 mm, 76.2 mm, 152.4 mm, 228.6 mm, and 304.8 mm. However, due to the spring back of the media they cannot be said to be exactly in their target locations. The thermocouple support positions are assumed to be at the target bed length fractions of the actual bed length. These positions being approximately 0 mm, 79 mm, 158 mm, 237 mm, and 316 mm.

The method used to complete the packing of the MFM bed is the same as the packed beds and is repeated here. After the bed was packed and the final thermocouple support was placed, 8 - $15\,\mu\mathrm{m}$ quartz wool was packed into the tube around the thermocouple wires. This was done to both insulate the bed and hold the bed in place. The remaining length of thermocouples was then pushed into the tube outside of the quartz wool, and the bed was sealed on that end. The sanitary tube was then flipped so that the stop rod was facing upward and the sealed end of the tube was facing downward. The stop rod was then removed and then end of the tube packed with quartz wool. This end was then also sealed completing the packing process.

2.1.5 Microfibrous Media Used for Packing

The microfibrous media (MFM) used in this work consisted of two layers, a top layer and a bottom (barrier) layer. The purpose of this is so that materials, such as catalysts or sorbents, can be entrapped in the MFM without falling completely through the material.

The top layer of the media was composed of $17\,\mu\mathrm{m}$ diameter fibers that were $6\,\mathrm{mm}$ long. The barrier layer of the media was composed of $6\,\mu\mathrm{m}$ diameter fibers that were $3\,\mathrm{mm}$ long.

It was necessary to determine the fraction of the media made up of each fiber size. To accomplish this disks of media were taken and the top and barrier layers separated by hand. Each layer of each disk was then massed and that mass recorded in tables Tables 2.5 to 2.7.

Three sets of five disks were used for this purpose. One set each of 0.25-in diameter disks, 0.5-in diameter disks, and 2.4-in diameter disks. The 0.25-in diameter disks and 0.5-in diameter disks were punched from the media using hammer-driven arch punches, and the 2.4-in diameter disks were cut on a computer numerical control (CNC) machine with a spinning cutter. The 2.4-in were the same diameter as the media used for packing the MFM bed, as they were cut using the same cutter.

Table 2.5: MFM fiber fractions measured from 0.25-inch disks.

Sample	Top Layer (g)	Bottom Layer (g)	Mass % Top Layer	Mass % Bottom Layer
1	0.02278	0.00280	89.1	10.9
2	0.01052	0.00365	74.2	25.8
3	0.01179	0.00278	80.9	19.1
4	0.01164	0.00313	78.8	21.2
5	0.01053	0.00265	79.9	20.1
Average	0.01345	0.00300	81.8	18.2

Microfibrous media used was composed of copper fibers and cut into disks using a 0.25-inch arch punch. The media consisted of a top layer and a bottom barrier layer. The top layer was composed of copper fibers $17\,\mu\mathrm{m}$ in diameter and $6\,\mathrm{mm}$ long. The bottom barrier layer was composed of copper fibers $6\,\mu\mathrm{m}$ in diameter and $3\,\mathrm{mm}$ long.

Table 2.6: MFM fiber fractions measured from 0.5-inch disks.

Sample	Top Layer (g)	Bottom Layer (g)	Mass % Top Layer	Mass % Bottom Layer
1	0.10697	0.01041	91.1	8.9
2	0.05782	0.01088	84.2	15.8
3	0.05273	0.01165	81.9	18.1
4	0.12874	0.01168	91.7	8.3
5	0.06129	0.01145	84.3	15.7
Average	0.08151	0.01121	87.9	12.1

Microfibrous media used was composed of copper fibers and cut into disks using a 0.5-inch arch punch. The media consisted of a top layer and a bottom barrier layer. The top layer was composed of copper fibers $17\,\mu\mathrm{m}$ in diameter and $6\,\mathrm{mm}$ long. The bottom barrier layer was composed of copper fibers $6\,\mu\mathrm{m}$ in diameter and $3\,\mathrm{mm}$ long.

Table 2.7: MFM fiber fractions measured from 2.400-inch disks.

Sample	Top Layer (g)	Bottom Layer (g)	Mass % Top Layer	Mass % Bottom Layer
1	1.88776	0.19231	90.8	9.2
2	1.63202	0.24870	86.8	13.2
3	1.49450	0.21656	87.3	12.7
4	1.88801	0.21928	89.6	10.4
5	1.50747	0.33855	81.7	18.3
Average	1.68195	0.24308	87.4	12.6

Microfibrous media used was composed of copper fibers and cut into disks using a 2.400-inch die cutter. The media consisted of a top layer and a bottom barrier layer. The top layer was composed of copper fibers $17\,\mu\mathrm{m}$ in diameter and $6\,\mathrm{mm}$ long. The bottom barrier layer was composed of copper fibers $6\,\mu\mathrm{m}$ in diameter and $3\,\mathrm{mm}$ long.

2.2 Alumina Packed Bed Experimental Results

Two sets of transient experiments were conducted using various gases in the the alumina packed bed. Experiments using argon, helium, hydrogen, nitrogen, and oxygen were conducted by submerging the bed at approximately 20 °C into an ice-water bath at approximately 0 °C and submerging the bed at approximately 0 °C into a water bath at approximately 20 °C.

Multiple experiments with the same gas were often conducted in series without stopping data logging in between. This was accomplished via the use of a binary switch used to trigger an event state in the data logger corresponding to the time when the switch was changed. The different experiments were then separated for analysis.

The experimental apparatus was pressurized with the corresponding gas to 40 pounds per square inch (psi) as read on an analog pressure gauge. The pressure of 40 psi for each experiment was measured at the current room temperature for the experiments. This would correspond to 40 psi at the time zero for the first experiment in a set with constant data recording.

Data was collected using a Grant 2040-4F16 data logger. Temperature data was collected from fifteen type-T thermocouples within the bed and from two type-T thermocouples measuring the environment temperature. The temperature was recorded once per second for the duration of the experiments. The temperatures recorded at the point at the axial and radial center of the bed for each experiment are shown in Figures 2.17 and 2.18. Figures 2.17 and 2.18 each have two parts that show the same temperature profiles in two different ways. Figures 2.17a and 2.18a show the temperature profiles in degrees Celsius,

and Figures 2.17b and 2.18b show the temperature normalized as

$$\theta \equiv \text{Normalized temperature}$$

$$T \equiv \text{Temperature in kelvin}$$

$$T_\infty \equiv \text{Average environmental temperature}$$

$$\theta = \frac{T}{T_\infty}$$

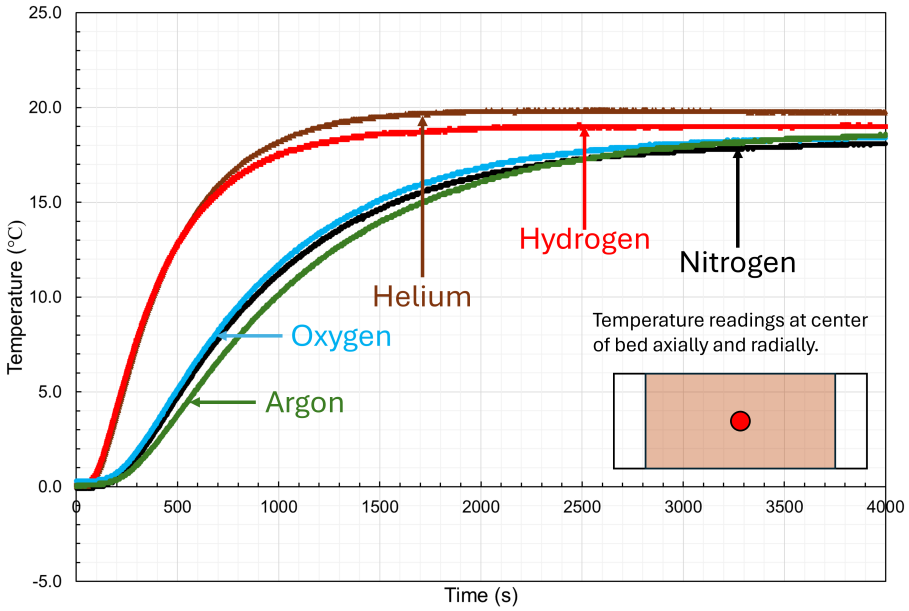

(a) Temperature profiles in degrees Celsius.

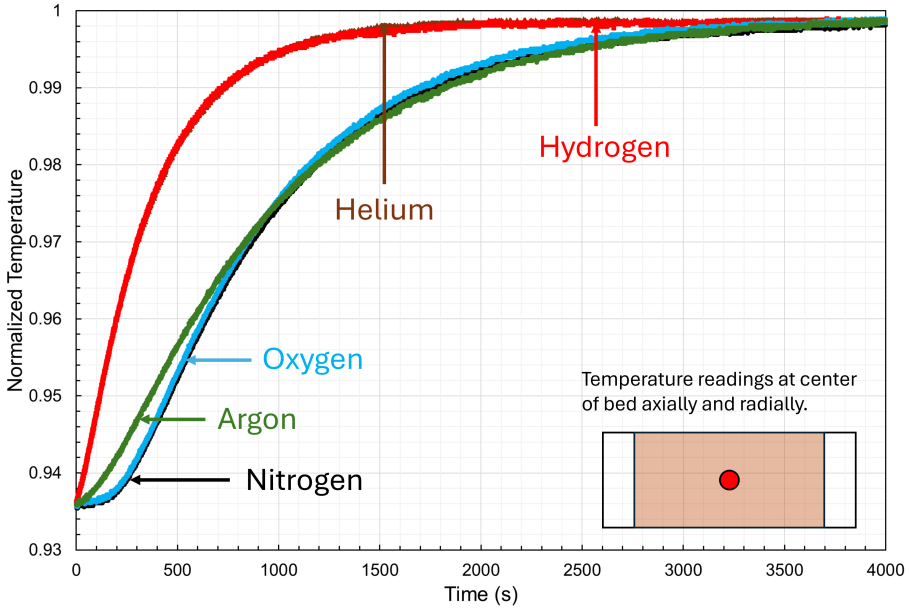

(b) Normalized temperature profiles in θ, where $\theta = \frac{\text{Temperature}}{\text{Temperature}_{\text{Environment}}}$.

Figure 2.17: Temperature readings at the center radially and center axially of an $\frac{1}{8}$-inch alumina pellet packed bed that begins at 0 °C and is submerged in a room-temperature-water bath of approximately 20 °C. The bed is approximately $304.8\,\text{mm}$ (12 inches) in length and $61.5\,\text{mm}$ (2.42 inches) in diameter. Data is recorded from the bed filled with various gases at 40 psi gauge. This data is truncated to all begin at 20.0 °C. The bed is packed at 11.7% alumina by volume.

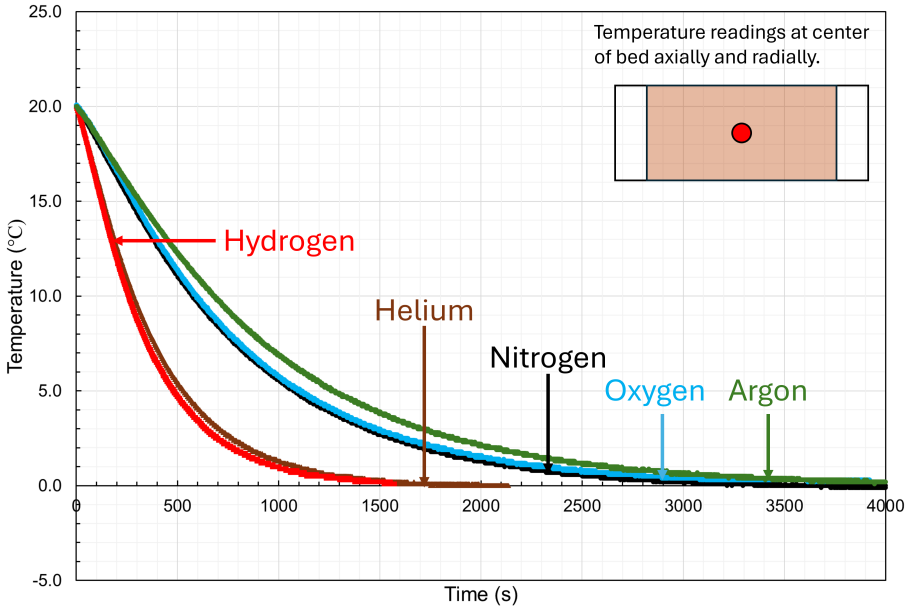

(a) Temperature profiles in degrees Celsius.

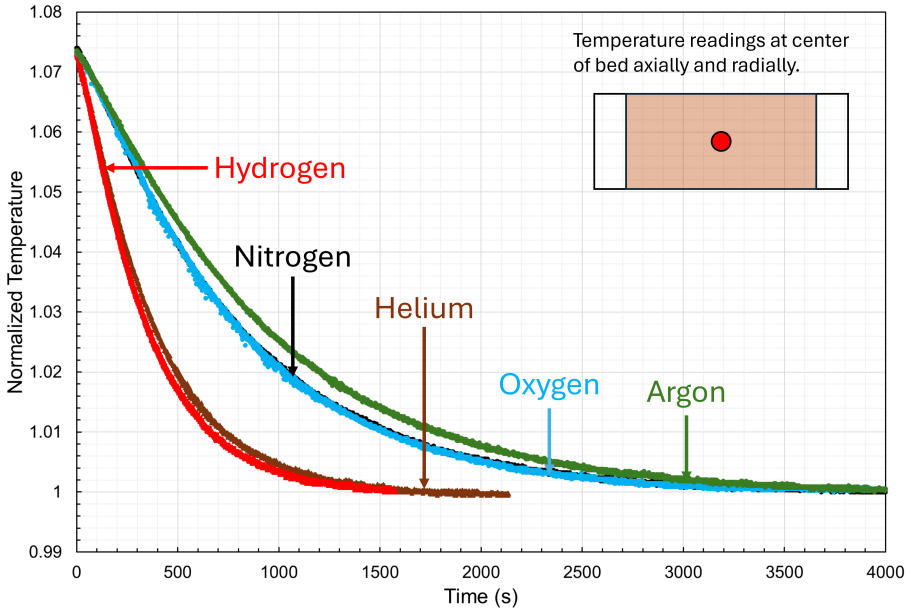

(b) Normalized temperature profiles in θ, where $\theta = \frac{\text{Temperature}}{\text{Temperature}_{\text{Environment}}}$.

Figure 2.18: Temperature readings at the center radially and center axially of an $\frac{1}{8}$-inch alumina pellet packed bed that begins at near 20.0 °C and is submerged in an ice-water bath of approximately 0.0 °C. The bed is approximately $304.8\,\text{mm}$ (12 inches) in length and $61.5\,\text{mm}$ (2.42 inches) in diameter. Data is recorded from the bed filled with various gases at 40 psi gauge. This data is truncated to all begin at 20.0 °C before it was normalized. The bed is packed at 11.7% alumina by volume.

2.3 Microfibrous Media Bed Experimental Results

Four sets of experiments were conducted using various gases in the the Cu-MFM bed. In addition, the same four experiments were performed with the same Cu-MFM bed under vacuum. Experiments using argon, carbon dioxide, helium, hydrogen, and oxygen were conducted by submerging the bed at approximately 20 °C into an ice-water bath at approximately 0 °C, submerging the bed at approximately 20 °C into a heated-water bath at approximately 70 °C, and submerging the bed at approximately 70 °C into a water bath at approximately 20 °C. Further experiments with carbon dioxide, helium, hydrogen, and oxygen were conducted by submerging the bed at approximately 0 °C into a water bath at approximately 20 °C.

Multiple experiments with the same gas were often conducted in series without stopping data logging in between. This was accomplished via the use of a binary switch used to trigger an event state in the data logger corresponding to the time when the switch was changed. The different experiments were then separated for analysis.

For the experiments involving gases, the experimental apparatus was pressurized with the corresponding gas to 50 pounds per square inch (psi) as read on an analog pressure gauge. The pressure of 50 psi for each experiment was measured at the current room temperature for the experiments. This would correspond to 50 psi at the time zero for the first experiment in a set with constant data recording.

For the experiments involving vacuum, a Pfeiffer Adixen Pascal 2005 SD pump was used to continuously pull vacuum on the apparatus throughout the experiments. The vacuum pressure was measured at the start of the first experiment in the set but not measured during the experiments to avoid damaging the digital vacuum gauge. A ball valve was used in line before the vacuum gauge to allow for the valve to be closed and the gauge removed without affecting the vacuum. The vacuum gauge was reattached at the end of a set of

experiments to measure the pressure again; however, a small amount of air was introduced in the fitting attached to the gauge making this measurement not meaningful.

Data was collected using a Grant 2040-4F16 data logger. Temperature data was collected from fifteen type-T thermocouples within the bed and from two type-T thermocouples measuring the environment temperature. The temperature was recorded once per second for the duration of the experiments. The temperatures recorded at the point at the axial and radial center of the bed for each experiment are shown in Figures 2.19 to 2.22. Figures 2.19 to 2.22 each have two parts that show the same temperature profiles in two different ways. Figures 2.19a, 2.20a, 2.21a and 2.22a show the temperature profiles in degrees Celsius, and Figures 2.19b, 2.20b, 2.21b and 2.22b show the temperature normalized as

$$\theta \equiv \text{Normalized temperature}$$

$$T \equiv \text{Temperature in kelvin}$$

$$T_\infty \equiv \text{Average environmental temperature}$$

$$\theta = \frac{T}{T_\infty}$$

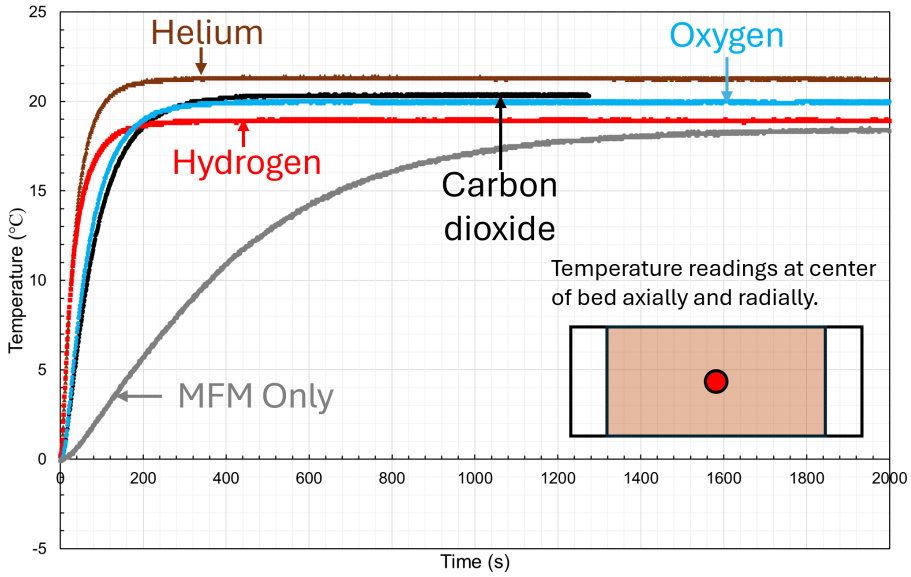

(a) Temperature profiles in degrees Celsius.

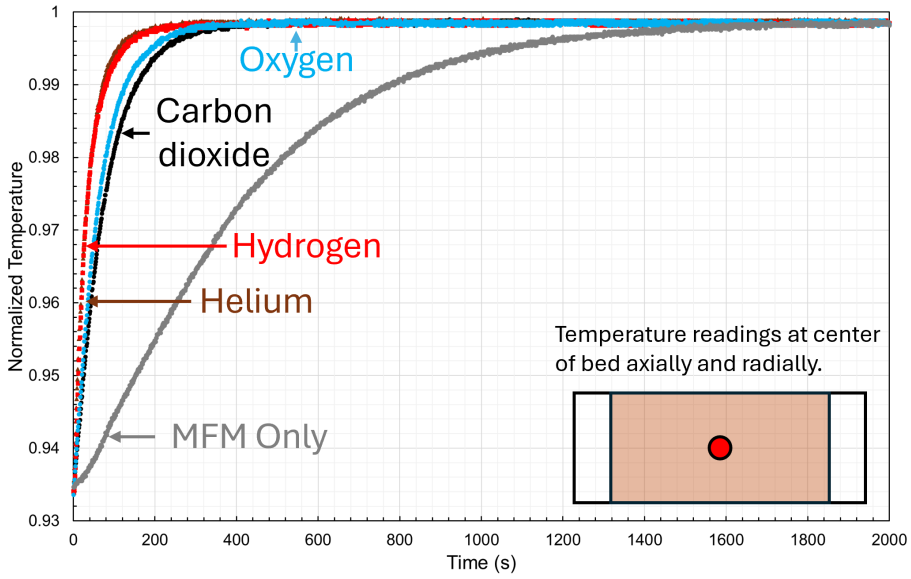

(b) Normalized temperature profiles in θ, where $\theta = \frac{\text{Temperature}}{\text{Temperature}_{\text{Environment}}}$.

Figure 2.19: Temperature readings at the center radially and center axially of a microfibrous media bed reaching a steady state temperature when the bed at approximately 0 °C is submerged in an room-temperature-water bath of approximately 20 °C. MFM only data was recorded at $0.029\,\text{mbar}$ vacuum.

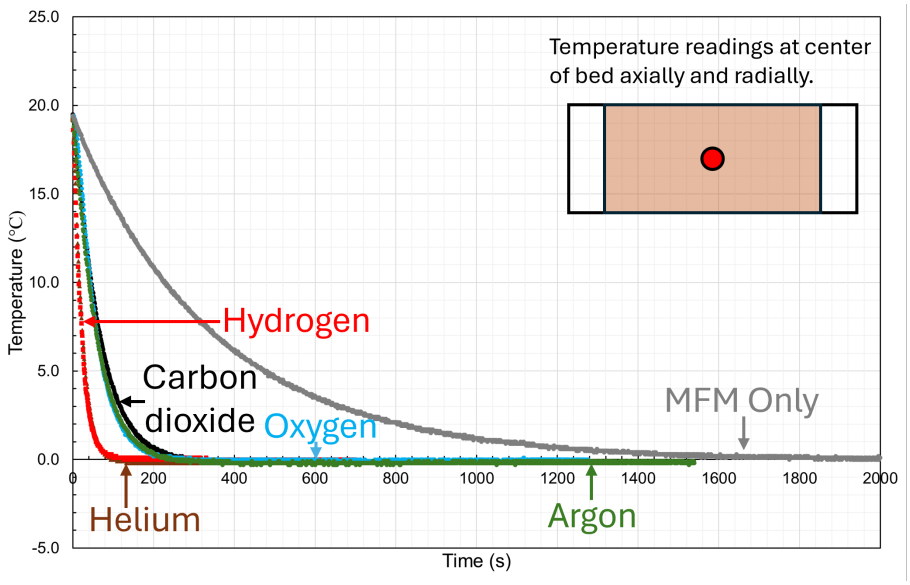

(a) Temperature profiles in degrees Celsius.

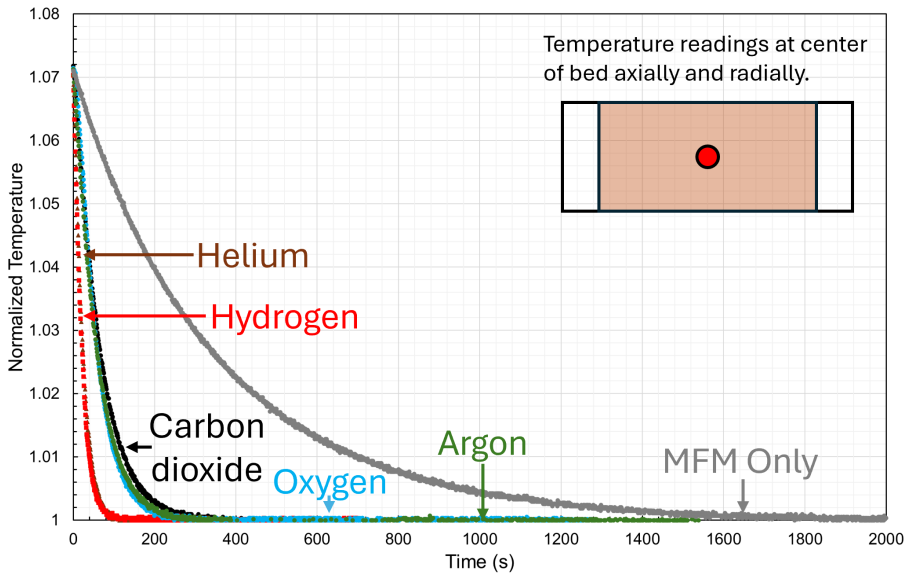

(b) Normalized temperature profiles in θ, where $\theta = \frac{\text{Temperature}}{\text{Temperature}_{\text{Environment}}}$.

Figure 2.20: Temperature readings at the center radially and center axially of a microfibrous media bed reaching a steady state temperature when the bed at approximately 20 °C is submerged in an ice-water bath at approximately 0 °C. MFM only data was recorded at $0.029\,\text{mbar}$ vacuum.

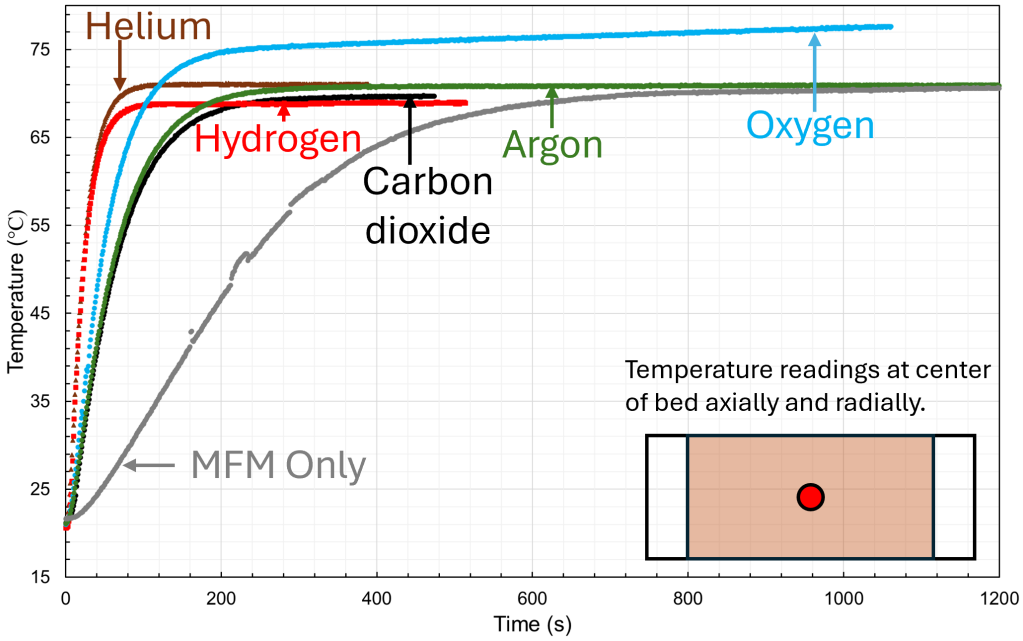

(a) Temperature profiles in degrees Celsius.

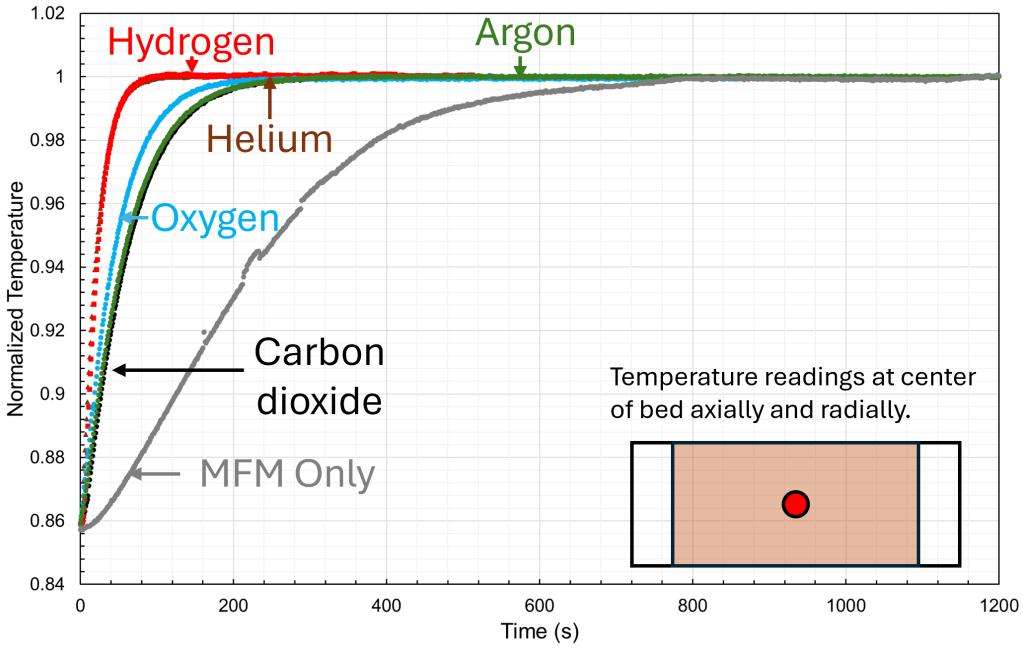

(b) Normalized temperature profiles in θ, where $\theta = \frac{\text{Temperature}}{\text{Temperature}_{\text{Environment}}}$.

Figure 2.21: Temperature readings at the center radially and center axially of a microfibrous media bed reaching a steady state temperature when the bed at approximately 20 °C is submerged in an heated-water bath of approximately 70 °C. MFM only data was recorded at $0.033\,\text{mbar}$ vacuum.

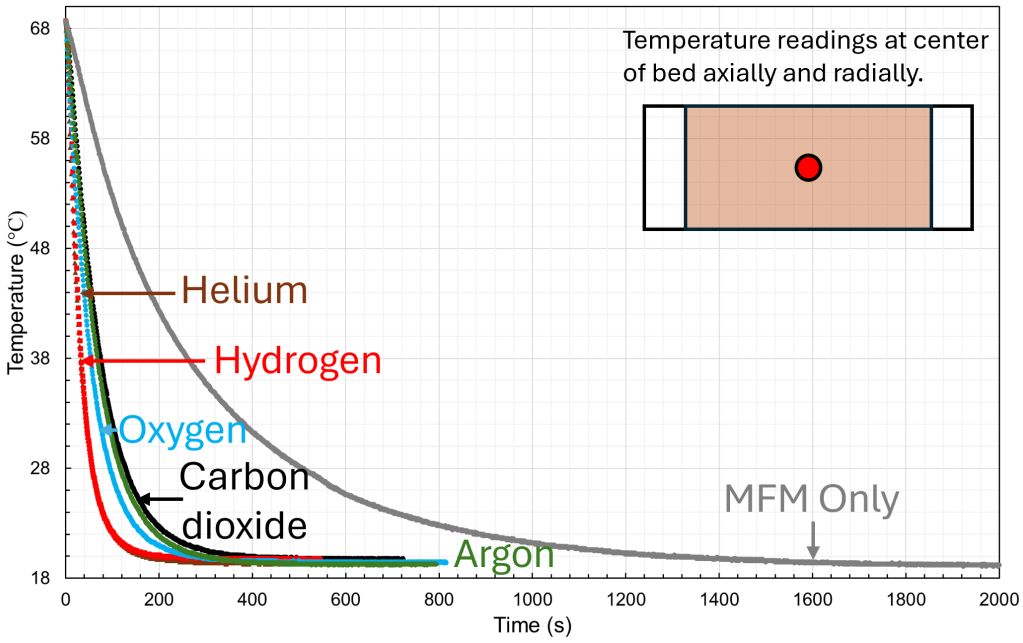

(a) Temperature profiles in degrees Celsius.

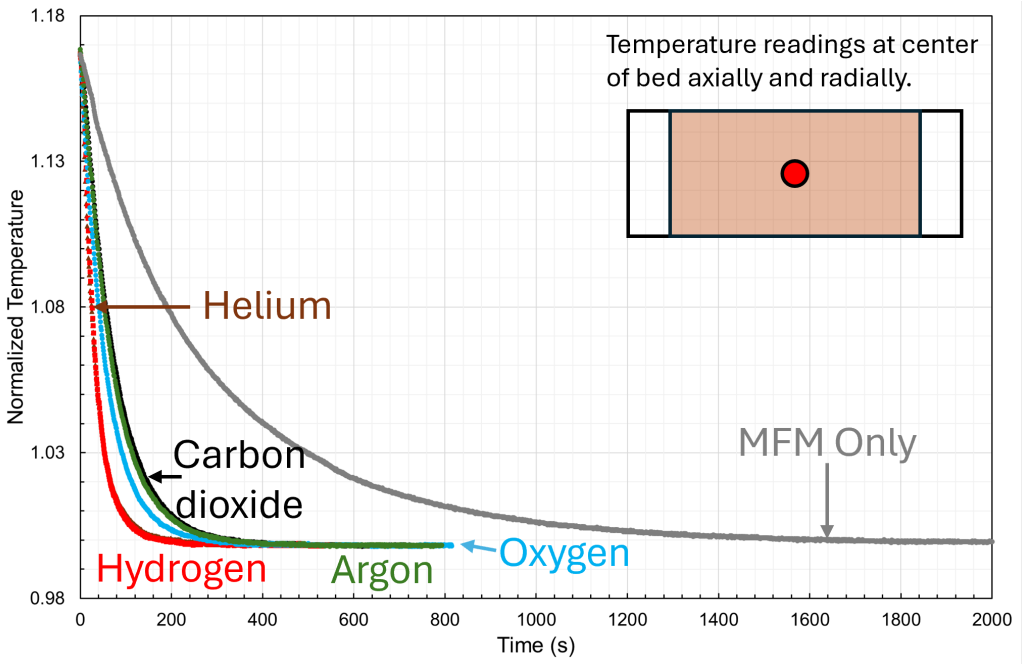

(b) Normalized temperature profiles in θ, where $\theta = \frac{\text{Temperature}}{\text{Temperature}_{\text{Environment}}}$.

Figure 2.22: Temperature readings at the center radially and center axially of a microfibrous media bed reaching a steady state temperature when the bed at approximately 70 °C is submerged in a room-temperature-water bath of approximately 70 °C. MFM only data was recorded at $0.033\,\text{mbar}$ vacuum.

2.4 Computational Model of Experiments with stagnant Gas

To compare the alumina packed bed and the microfibrous media bed, it was desired to estimate the effective thermal conductivity, k_{er}, and overall heat transfer coefficient, U_{id}. The effective thermal conductivity is a lumped parameter that is treated as the thermal conductivity but contains other modes of energy transport, such as radiation and dispersion. The overall heat transfer coefficient is defined in Equation 2.27 [20]. These definitions appear multiple times within this work; the purpose of this is so that these definitions appear in each of their relevant sections.

$$\frac{1}{r_{\text{id}}U_{\text{id}}} = \left(\frac{1}{r_{\text{id}}h_{\text{id}}} + \frac{\ln\left(\frac{r_{\text{od}}}{r_{\text{id}}}\right)}{k_{\text{wall}}} + \frac{1}{r_{\text{od}}h_{\text{od}}} \right) \qquad \text{[20]} \tag{2.1}$$

Where

$U_{\text{id}} =$ Overall heat transfer coefficient based on the inside wall

$r_{\text{id}} =$ Inside wall radius

$r_{\text{od}} =$ Outside wall radius

$h_{\text{id}} =$ Inside wall heat transfer coefficient

$h_{\text{od}} =$ Outside wall heat transfer coefficient

$k_{\text{wall}} =$ Thermal conductivity of the tube wall

To estimate these parameters, a computational model was developed for the energy equation in one dimension in radial coordinates. A program was written in Python to implement this model. This is further discussed in section 2.5.

2.4.1 Energy Equation in One Dimensions

The energy equation in radial coordinates is taken from Transport Phenomena [20] and simplified to one dimension (radial).

$$\rho \hat{C}_p \frac{\partial T}{\partial t} = k \left[\frac{1}{r} \frac{\partial T}{\partial r} + \frac{\partial^2 T}{\partial r^2} \right] \tag{2.2}$$

This equation is nondimensionalized as

$$\frac{\partial \theta}{\partial \tau} = \frac{1}{\xi} \frac{\partial \theta}{\partial \xi} + \frac{\partial^2 \theta}{\partial \xi^2} \tag{2.3}$$

Nondimensional variable definitions

$$\tau = \frac{\alpha_r}{R_{\text{id}}^2} t \qquad \theta = \frac{T}{T_0} \qquad \xi = \frac{r}{R_{\text{id}}} \tag{2.4}$$

The boundary conditions are

$$\text{at } \xi = 0 \,,\, \frac{\partial \theta}{\partial \xi} = 0 \qquad \text{at } \xi = 1 \,,\, \frac{\partial \theta}{\partial \xi} = \text{Bi}(\theta_\infty - \theta_b) \qquad \text{at } \tau = 0 \,,\, \theta = \theta_0 \tag{2.5}$$

where

$$\text{Bi} = \frac{U_{\text{id}} R}{k_{\text{er}}}$$

$\theta_\infty \equiv$ temperature of the environment surrounding the outside wall

$\theta_b \equiv$ bulk temperature inside the bed ; taken as $\theta_b = \theta_{\xi - \Delta\xi, j}^{n+1}$

$\theta_0 = \theta_{\xi=0}$ from the experimental data being fit

The derivatives in Equation 2.3 are approximated using the Taylor series. The time derivative is a forward first order approximation. The space derivatives are centered second order approximations.

$$\frac{\partial \theta}{\partial \tau} \approx \frac{\theta_{i,j}^{n+1} - \theta_{i,j}^{n}}{\Delta \tau} + \mathcal{O}[\Delta \tau] \tag{2.6}$$

$$\frac{\partial \theta}{\partial \xi} \approx \frac{\theta_{i+1,j}^{n+1} - \theta_{i-1,j}^{n+1}}{2(\Delta \xi)} + \mathcal{O}[(\Delta \xi)^2] \tag{2.7}$$

$$\frac{\partial^2 \theta}{\partial \xi^2} \approx \frac{\theta_{i+1,j}^{n+1} - 2\theta_{i,j}^{n+1} + \theta_{i-1,j}^{n+1}}{(\Delta \xi)^2} + \mathcal{O}[(\Delta \xi)^2] \tag{2.8}$$

Combining Equations 2.3, 2.6, 2.7, and 2.8 results in an implicit finite difference equation for the energy equation in one dimension.

$$\frac{\theta_{i,j}^{n+1} - \theta_{i,j}^{n}}{\Delta \tau} = \frac{1}{\xi} \frac{\theta_{i+1,j}^{n+1} - \theta_{i-1,j}^{n+1}}{2(\Delta \xi)} + \frac{\theta_{i+1,j}^{n+1} - 2\theta_{i,j}^{n+1} + \theta_{i-1,j}^{n+1}}{(\Delta \xi)^2} + \mathcal{O}[\Delta \tau, (\Delta \xi)^2] \tag{2.9}$$

2.4.2 von Neumann Analysis of the Energy Equation in One Dimensions

A von Neumann stability analysis [21] was performed for the one-dimensional heat transfer model as implemented. *Fundamental Algorithms in Computational Fluid Dynamics* [22] was referenced for implementing this analysis.

θ is taken to be of the form

$$\theta(\xi, \tau) = \lambda^n e^{ik\xi} \qquad [22] \tag{2.10}$$

$$e^{\alpha \Delta \tau} = \lambda^n \qquad [22] \tag{2.11}$$

The von Neumann stability criteria is

$$|\lambda| \leq 1 \qquad [22] \tag{2.12}$$

$$\frac{\lambda^{n+1}e^{ik\xi} - \lambda^n e^{ik\xi}}{\Delta\tau} = \frac{1}{\xi}\frac{\lambda^{n+1}e^{ik(\xi+\Delta\xi)} - \lambda^{n+1}e^{ik(\xi-\Delta\xi)}}{2(\Delta\xi)} + \frac{\lambda^{n+1}e^{ik(\xi+\Delta\xi)} - 2\lambda^{n+1}e^{ik\xi} + \lambda^{n+1}e^{ik(\xi-\Delta\xi)}}{(\Delta\xi)^2} \tag{2.13}$$

$$\frac{\lambda^{n+1} - \lambda^n}{\lambda^{n+1}\Delta\tau} = \frac{1}{\xi}\frac{e^{ik(\Delta\xi)} - e^{-ik(\Delta\xi)}}{2(\Delta\xi)} + \frac{e^{ik(\Delta\xi)} - 2 + e^{-ik(\Delta\xi)}}{(\Delta\xi)^2} \tag{2.14}$$

$$\frac{1}{\Delta\tau}\left(1 - \frac{1}{\lambda}\right) = \frac{1}{\xi}\frac{e^{ik(\Delta\xi)} - e^{-ik(\Delta\xi)}}{2(\Delta\xi)} + \frac{e^{ik(\Delta\xi)} - 2 + e^{-ik(\Delta\xi)}}{(\Delta\xi)^2} \tag{2.15}$$

$$\frac{1}{\lambda} = 1 - \frac{\Delta\tau}{2\xi(\Delta\xi)}\left(e^{ik(\Delta\xi)} - e^{-ik(\Delta\xi)}\right) - \frac{\Delta\tau}{(\Delta\xi)^2}\left(e^{ik(\Delta\xi)} - 2 + e^{-ik(\Delta\xi)}\right) \tag{2.16}$$

$$\sin(x) = \frac{e^{ix} - e^{-ix}}{2i} \qquad \cos(x) = \frac{e^{ix} + e^{-ix}}{2}$$

$$\frac{1}{\lambda} = 1 - \frac{\Delta\tau}{\xi(\Delta\xi)}\sin(k(\Delta\xi))i - \frac{2\Delta\tau}{(\Delta\xi)^2}\left(\cos(k(\Delta\xi)) - 1\right) \tag{2.17}$$

For convenience, the following is defined.

$$C_1 = \frac{2(\Delta\tau)}{(\Delta\xi)^2} \qquad C_2 = \frac{\Delta\tau}{\xi(\Delta\xi)}$$

$$\frac{1}{\lambda} = 1 - C_1\left(\cos(k(\Delta\xi)) - 1\right) - C_2\sin(k(\Delta\xi))i \tag{2.18}$$

$$c = a + bi \tag{2.19}$$

$$|c| = \sqrt{a^2 + b^2} \tag{2.20}$$

Let $\gamma = \frac{1}{\lambda}$.

For $|\lambda| \leq 1$ it must be true that $|\gamma| \geq 1$.

To satisfy $|c| \leq 1$, $a^2 + b^2 \leq 1$. Applying this to [add ref],

$$|\gamma|^2 = \left[1 - C_1\left(\cos(k(\Delta\xi)) - 1\right)\right]^2 + \left[-C_2\sin(k(\Delta\xi))\right]^2 \tag{2.21}$$

Breaking this into the parts

$$a^2 = [1 - C_1 (\cos(k(\Delta\xi)) - 1)]^2$$
$$b^2 = [-C_2 \sin(k(\Delta\xi))]^2$$

To satisfy $|\gamma| \geq 1$, it must be true that $a^2 + b^2 \geq 1$.

Sine and cosine are bound as

$$-1 \leq \sin(x) \leq 1$$
$$0 \leq \cos(x) \leq 1$$

Using this, it is known $1 \leq a^2 \leq (1 + C_1)^2$.

Since C_1 is positive, it is always true that $a^2 \geq 1$.

$b^2 \geq 0$.

Combining this, it is always true that $a^2 + b^2 \geq 1$.

This means it is always true that $\gamma \geq 1$.

Which further leads to it always being true that $\lambda \leq 1$.

Meaning this scheme is unconditionally stable by von Neumman analysis.

2.4.3 Virial Coefficients

The virial equation of state was used in this work to calculate moles of gas from pressure. The virial equation of state used is truncated after the second coefficient and is taken from *Molecular Thermodynamics of Fluid-Phase Equilibria Third Edition* [23].

$$\frac{Pv}{RT} = 1 + \frac{B}{v} \qquad \text{[23]} \tag{2.22}$$

Where

$$P = \text{Pressure; used as Pa}$$
$$v = \text{Molar volume; used as } \frac{\text{m}^3}{\text{mol}}$$
$$R = \text{Gas constant; used as } 8.31451 \ \frac{\text{Pa} \cdot \text{m}^3}{\text{mol} \cdot \text{K}}$$
$$T = \text{Absolute temperature; used as K}$$
$$B = \text{Second virial coefficient; used as } \frac{\text{m}^3}{\text{mol}}$$

Parameters for the calculation of the second virial coefficient were estimated for a variety of gases. The equation for the second virial coefficient is from *Molecular Thermodynamics of Fluid-Phase Equilibria Third Edition* and is based upon the square-well model of potential [23].

$$B = b_0 R^3 \left(1 - \frac{R^3 - 1}{R^3} \exp\left(\frac{\varepsilon}{kT}\right)\right) \qquad \text{[23]} \tag{2.23}$$

Where

$$B = \text{Second virial coefficient}$$
$$b_0 = \frac{2}{3}\pi N_A \sigma^3$$
$$\sigma = \text{Collision diameter}$$
$$N_A = \text{Avogadro's number}$$
$$R = \text{Reduced well width}$$
$$\frac{\varepsilon}{k} = \text{Well depth divided by Boltzmann's constant}$$
$$T = \text{Temperature in kelvin}$$

The parameters estimated were b_0, R, and $\frac{\varepsilon}{k}$. To estimate these parameters, second virial coefficient and temperature data was taken from *The Virial Coefficients of Pure Gases*

and Mixtures A Critical Compilation [24]. Trial values for the parameters were used to calculate second virial coefficients at each temperature used.

The sum of squared residuals was then calculated for the parameters as

$$\delta = \sum_{n=0}^{n=N} (B_n - B_n^*)^2 \tag{2.24}$$

Where

$\delta =$ Sum of squared residuals

$B_n =$ Second virial coefficient at temperature n as calculated

$B_n^* =$ Second virial coefficient at temperature n as presented in [24]

$n =$ Temperature the second virial coefficient is calculated at

$N =$ Number of temperatures second virial coefficient is calculated at

Microsoft Excel Solver was used to minimize the sum of squared residuals by varying the trial parameters. The result of this minimization was rounded to one decimal place and is reported.

Table 2.8: Parameters for the second virial coefficient and square-well potential.

	$b_0 \left(\frac{\text{cm}^3}{\text{mol}}\right)$	R	$\frac{\varepsilon}{k}\ (K)$	References	
Argon	35.2	1.7	98.9	[24]	*
Carbon dioxide	49.4	1.4	332.3	[24, 25]	*
Carbon monoxide	52.9	2.6	21.2	[24, 26]	
Helium	13.5	8.2	0.1	[24]	
Hydrogen	25.3	2.3	9.5	[24]	
Methane	49.2	1.7	126.7	[24]	*
Neon	18.1	1.8	25.3	[24]	
Nitrogen	45.1	1.6	84.1	[24]	*
Oxygen	33.8	1.6	114.6	[24]	
Xenon	61.6	1.7	181.9	[24]	*

[1] Data used to calculate parameters from *The Virial Coefficients of Pure Gases and Mixtures A Critical Compilation* [24].
[2] Values that only reference [24] are estimated from the suggested data in that text. Values with two references are estimated from data from [24] as taken from the other reference.
[3] Values rounded to one decimal place.
[*] Parameter values can be found in "Intermolecular potential functions and the second and third virial coefficients" [27]. The author would suggest deferring to that reference.

2.4.4 Properties of Select Gasses

Presented here are thermal properties for gasses used in experiments in this work. Argon, helium, hydrogen, nitrogen, and oxygen were used in packed bed experiments. Argon, carbon dioxide, helium, hydrogen, and oxygen were used in microfibrous media (MFM) bed experiments. In addition, experiments were also conducted for the MFM bed under vacuum to assess the heat transfer performance of the MFM alone.

Table 2.9: Properties of selected gases at 300 K [a]

	Thermal Conductivity $\frac{mW}{m \cdot K}$	Thermal Diffusivity[h] $\frac{cm^2}{s}$	Density[i] $\frac{kg}{m^3}$	Heat Capacity[j] $\frac{J}{kg \cdot K}$
Carbon dioxide	16.8	40.3	4.93	845.7
Argon	17.7	77	4.42	520.3
Nitrogen	26	80.7	3.1	1039.7
Oxygen	26.5	81.5	3.54	918.5
Helium	155.7	681.4	0.44	5193.1
Hydrogen	186.6	592.7	0.22	14311.1

[a] Density calculated at 40 °C.
[b] Carbon dioxide thermal conductivity referenced from [28, 29].
[c] Argon thermal conductivity referenced from [28, 30, 31].
[d] Nitrogen thermal conductivity referenced from [28, 32].
[e] Oxygen thermal conductivity referenced from [28, 32].
[r] Helium thermal conductivity referenced from [28, 33].
[g] Hydrogen thermal conductivity referenced from [28, 34].
[h] Calculated from the other thermophysical properties in this table.
[i] Calculated from data retrieved from [23, 24, 27, 35–41].
[j] Calculated from the Shomate equation [42] using parameters retrieved from the National Institute of Standards and Technology (NIST) [36–41].

2.5 Parameter Estimation

Parameter estimation was performed for both the alumina packed bed and microfibrous media (MFM) bed. The parameters estimated were the effective radial thermal conductivity, k_{er}, and the overall heat transfer coefficient based on the inside wall, U_{id}. Effective thermal conductivity is a lumped parameter that is treated as the thermal conductivity but contains other modes of energy transport, such as radiation and dispersion. The overall heat transfer coefficient is defined in Equation 2.25 [20].

$$\frac{1}{r_{\text{id}}U_{\text{id}}} = \left(\frac{1}{r_{\text{id}}h_{\text{id}}} + \frac{\ln\left(\frac{r_{\text{od}}}{r_{\text{id}}}\right)}{k_{\text{wall}}} + \frac{1}{r_{\text{od}}h_{\text{od}}} \right) \qquad \text{[20]} \tag{2.25}$$

Where

$U_{\text{id}} =$ Overall heat transfer coefficient based on the inside wall

$r_{\text{id}} =$ Inside wall radius

$r_{\text{od}} =$ Outside wall radius

$h_{\text{id}} =$ Inside wall heat transfer coefficient

$h_{\text{od}} =$ Outside wall heat transfer coefficient

$k_{\text{wall}} =$ Thermal conductivity of the tube wall

To perform the parameter estimation, a program was written in Python for the model shown in section 2.4.1. The Sherpa application was used for the actual parameter estimation and statistical analysis [43]. The values in Table 2.8 are included in the program within their own function. This is noted as this function could be exported to other programs where it is necessary to calculate temperature dependent virial coefficients.

The Levenberg-Marquardt (LM) algorithm was used for the parameter estimation and is shown in equation 2.26 [44]. It is noted that some of the variable definitions for the LM

algorithm are taken verbatim from *Scientific Computing An Introductory Survery Second Edition* [44].

$$\left(\boldsymbol{J}^T\left(\boldsymbol{x}_k\right)\boldsymbol{J}\left(\boldsymbol{x}_k\right)+\mu_k\boldsymbol{I}\right)\boldsymbol{s}_k=-\boldsymbol{J}^T\left(\boldsymbol{x}_k\right)\boldsymbol{r}\left(\boldsymbol{x}_k\right) \qquad [44] \tag{2.26}$$

Where

$$\begin{aligned}
\boldsymbol{J}\left(\boldsymbol{x}_k\right) &= \text{Jacobian matrix of } \boldsymbol{r}\left(\boldsymbol{x}_k\right)\\
\boldsymbol{J}^T\left(\boldsymbol{x}_k\right) &= \text{Transpose of the Jacobian matrix of } \boldsymbol{r}\left(\boldsymbol{x}_k\right)\\
\boldsymbol{I} &= \text{Identity matrix}\\
\boldsymbol{r}\left(\boldsymbol{x}_k\right) &= \text{Residual vector of } \boldsymbol{x}_k\\
\boldsymbol{s}_k &= \text{Step-size vector}\\
\boldsymbol{x}_k &= \text{Vector of current parameter guesses/solutions}\\
\mu &= \text{Nonnegative scalar parameter}\\
k &= \text{Number of current iteration}
\end{aligned}$$

To begin the LM algorithm, an initial guess for each parameter to be estimated is provided. The initial parameter guesses are vector $\boldsymbol{x}_0$. The model for which parameters is being estimated is then solved using $\boldsymbol{x}_0$ and the residual vector $\boldsymbol{r}\left(\boldsymbol{x}_0\right)$ calculated.

A statistic is then chosen and calculated for $\boldsymbol{r}\left(\boldsymbol{x}_0\right)$ [45]. This process is repeated until a set of parameter guesses satisfies the convergence criteria of $\boldsymbol{r}\left(\boldsymbol{x}_0\right)$ or the number of function iterations exceeds a set allowable number [46]. This process is repeated until a set of parameters guesses satisfies the convergence criteria or the number of iterations exceeds a set allowable number of iterations.

The convergence criteria used was $\boldsymbol{r}\left(\boldsymbol{x}_{\text{k}}\right)-\boldsymbol{r}\left(\boldsymbol{x}_{\text{k-1}}\right)\leq xtol$, where $xtol$ is the largest difference between iteration residuals accepted for convergence [46]. The default value of $xtol$ in the Sherpa application was used.

2.6 Alumina Packed Bed Parameter Estimates

Parameter estimation was performed for each of the alumina packed bed heat-transfer experiments presented. That is, one set of experiments each for an alumina packed bed pressurized to 40 pounds per square inch (psi) with argon, helium, hydrogen, and oxygen. In addition, three sets of experiments were performed with the same alumina packed bed pressurized to 40 psi with nitrogen. The purpose of repeating the set of experiments with nitrogen was to test repeatability.

The parameters estimated were the effective radial thermal conductivity, k_{er}, and the overall heat transfer coefficient based on the inside wall, U_{id}. Effective thermal conductivity is a lumped parameter that is treated as the thermal conductivity but contains other modes of energy transport, such as radiation and dispersion. The overall heat transfer coefficient is defined in Equation 2.27 [20].

$$\frac{1}{r_{\text{id}}U_{\text{id}}} = \left(\frac{1}{r_{\text{id}}h_{\text{id}}} + \frac{\ln\left(\frac{r_{\text{od}}}{r_{\text{id}}}\right)}{k_{\text{wall}}} + \frac{1}{r_{\text{od}}h_{\text{od}}} \right) \qquad \text{[20]} \tag{2.27}$$

Where

$$U_{\text{id}} = \text{Overall heat transfer coefficient based on the inside wall}$$

$$r_{\text{id}} = \text{Inside wall radius}$$

$$r_{\text{od}} = \text{Outside wall radius}$$

$$h_{\text{id}} = \text{Inside wall heat transfer coefficient}$$

$$h_{\text{od}} = \text{Outside wall heat transfer coefficient}$$

$$k_{\text{wall}} = \text{Thermal conductivity of the tube wall}$$

A separate parameter estimation was performed for each thermocouple couple support, A - E, within the bed except support B. Support B was not used as the temperatures

read by thermocouples B2 and B3 appeared to be reversed. Originally, it was thought that these thermocouples were mistakenly inserted backwards. However, when the bed was unpacked and the thermocouples were inspected, it was found that the thermocouples were not mistakenly reversed as originally thought. It is unknown what caused the unexpected readings, so thermocouple support B was excluded from analysis.

Furthermore, thermocouple supports A and E are not considered to offer useful information. This is because these supports are at the ends of the bed and only have the bed material on one side of the support with quartz wool being on the other side. The information from these supports is included here only for completeness, as these thermocouples were included in the bed for other experiments.

Table 2.10: Estimated thermal parameters for a packed bed of 11.7% aluminum oxide by volume and pressurized to 40 psi gauge with argon.

	Effective radial thermal conductivity $\frac{W}{m \cdot K}$			Effective Overall heat transfer coefficient $\frac{W}{m^2 \cdot K}$		
Bed taken from approximately 0 °C and submerged in an approximately 19 °C water bath						
	Best Fit	Lower Bound	Upper Bound	Best Fit	Lower Bound	Upper Bound
Support A	Failed to fit.					
Support B	Not reported due to poor temperature data from support B.					
Support C	0.0945	- 0.00177	+ 0.00184	24.3	- 0.598	+ 0.627
Support D	0.105	- 0.00114	+ 0.00115	32.1	- 0.535	+ 0.556
Support E	0.101	- 0.00103	+ 0.00105	40.2	- 0.804	+ 0.837
Bed taken from approximately 22 °C and submerged in an approximately 0 °C ice-water bath						
	Best Fit	Lower Bound	Upper Bound	Best Fit	Lower Bound	Upper Bound
Support A	0.573	- 0.0162	+ 0.0170	18.9	- 0.105	+ 0.106
Support B	Not reported due to poor temperature data from support B.					
Support C	0.0874	- 0.000625	+ 0.000635	21.2	- 0.186	+ 0.189
Support D	0.103	- 0.000823	+ 0.000828	24.5	- 0.236	+ 0.242
Support E	0.0965	- 0.000695	+ 0.000704	29.1	- 0.312	+ 0.319

[1] The bed is approximately 11.7% by volume aluminum oxide (gamma phase).
[2] The aluminum oxide is $\frac{1}{8}$-in diameter pellets.
[3] Overall heat transfer coefficient is based on the inside tube diameter.
[4] Values are rounded to two significant figures.
[5] Confidence is 2-sigma.

Table 2.11: Estimated thermal parameters for a packed bed of 11.7% aluminum oxide by volume and pressurized to 40 psi gauge with helium.

	Effective radial thermal conductivity $\frac{W}{m \cdot K}$			Effective Overall heat transfer coefficient $\frac{W}{m^2 \cdot K}$		
Bed taken from approximately 0 °C and submerged in an approximately 21 °C water bath						
	Best Fit	Lower Bound	Upper Bound	Best Fit	Lower Bound	Upper Bound
Support A	2.55	- 0.212	+ 0.255	65.4	- 0.879	+ 0.896
Support B	Not reported due to poor temperature data from support B.					
Support C	0.199	- 0.00241	+ 0.00247	83.2	- 2.08	+ 2.18
Support D	0.189	- 0.00224	+ 0.00228	114	- 3.91	+ 4.20
Support E	0.267	- 0.00437	+ 0.00446	178	- 9.15	+ 10.3
Bed taken from approximately 21 °C and submerged in an approximately 0 °C ice-water bath						
	Best Fit	Lower Bound	Upper Bound	Best Fit	Lower Bound	Upper Bound
Support A	2.61	- 0.216	+ 0.257	63.6	- 0.785	+ 0.803
Support B	Not reported due to poor temperature data from support B.					
Support C	0.197	- 0.00216	+ 0.00221	98.3	- 2.61	+ 2.75
Support D	0.192	- 0.00206	+ 0.00210	138	- 5.04	+ 5.43
Support E	0.295	- 0.00474	+ 0.00489	163	- 6.98	+ 7.60

[1] The bed is approximately 11.7% by volume aluminum oxide (gamma phase).
[2] The aluminum oxide is $\frac{1}{8}$-in diameter pellets.
[3] Overall heat transfer coefficient is based on the inside tube diameter.
[4] Values are rounded to two significant figures.
[5] Confidence is 2-sigma.

Table 2.12: Estimated thermal parameters for a packed bed of 11.7% aluminum oxide by volume and pressurized to 40 psi gauge with hydrogen.

	Effective radial thermal conductivity $\frac{W}{m \cdot K}$			Effective Overall heat transfer coefficient $\frac{W}{m^2 \cdot K}$		
Bed taken from approximately 0 °C and submerged in an approximately 19 °C water bath						
	Best Fit	Lower Bound	Upper Bound	Best Fit	Lower Bound	Upper Bound
Support A	2.46	- 0.211	+ 0.254	68.5	- 1.02	+ 1.04
Support B	Not reported due to poor temperature data from support B.					
Support C	0.227	- 0.00328	+ 0.00337	72.1	- 1.67	+ 1.75
Support D	0.216	- 0.00310	+ 0.00318	88.0	- 2.54	+ 2.70
Support E	0.320	- 0.00712	+ 0.00751	127	- 5.61	+ 6.06
Bed taken from approximately 21 °C and submerged in an approximately 0 °C ice-water bath						
	Best Fit	Lower Bound	Upper Bound	Best Fit	Lower Bound	Upper Bound
Support A	3.47	- 0.350	+ 0.437	66.1	- 0.801	+ 0.818
Support B	Not reported due to poor temperature data from support B.					
Support C	0.222	- 0.00258	+ 0.00264	106	- 2.89	+ 3.04
Support D	0.218	- 0.00247	+ 0.00252	150	- 5.53	+ 5.97
Support E	0.325	- 0.00533	+ 0.00546	236	- 13.2	+ 14.9

[1] The bed is approximately 11.7% by volume aluminum oxide (gamma phase).
[2] The aluminum oxide is $\frac{1}{8}$-in diameter pellets.
[3] Overall heat transfer coefficient is based on the inside tube diameter.
[4] Values are rounded to two significant figures.
[5] Confidence is 2-sigma.

Table 2.13: Estimated thermal parameters for experiment 1 for a packed bed of 11.7% aluminum oxide by volume and pressurized to 40 psi gauge with nitrogen.

	Effective radial thermal conductivity $\frac{W}{m \cdot K}$			Effective Overall heat transfer coefficient $\frac{W}{m^2 \cdot K}$		
Bed taken from approximately 0 °C and submerged in an approximately 19 °C water bath						
	Best Fit	Lower Bound	Upper Bound	Best Fit	Lower Bound	Upper Bound
Support A	4.34	- 0.825	+ 1.35	24.2	- 0.189	+ 0.189
Support B	Not reported due to poor temperature data from support B.					
Support C	0.106	- 0.00108	+ 0.00110	29.1	- 0.414	+ 0.425
Support D	0.113	- 0.00253	+ 0.00264	28.8	- 1.48	+ 1.60
Support E	0.114	- 0.00251	+ 0.00262	50.7	- 2.41	+ 2.65
Bed taken from approximately 21 °C and submerged in an approximately 0 °C ice-water bath						
	Best Fit	Lower Bound	Upper Bound	Best Fit	Lower Bound	Upper Bound
Support A	Failed to fit.					
Support B	Not reported due to poor temperature data from support B.					
Support C	0.103	- 0.00165	+ 0.00170	40.6	- 1.26	+ 1.34
Support D	0.110	- 0.00193	+ 0.00201	54.5	- 2.30	+ 2.49
Support E	0.107	- 0.00174	+ 0.00179	77.7	- 4.30	+ 4.83

[1] The bed is approximately 11.7% by volume aluminum oxide (gamma phase).
[2] The aluminum oxide is $\frac{1}{8}$-in diameter pellets.
[3] Overall heat transfer coefficient is based on the inside tube diameter.
[4] Values are rounded to two significant figures.
[5] Confidence is 2-sigma.

Table 2.14: Estimated thermal parameters for experiment 2 for a packed bed of 11.7% aluminum oxide by volume and pressurized to 40 psi gauge with nitrogen.

	Effective radial thermal conductivity $\frac{W}{m \cdot K}$			Effective Overall heat transfer coefficient $\frac{W}{m^2 \cdot K}$		
Bed taken from approximately 0 °C and submerged in an approximately 18 °C water bath						
	Best Fit	Lower Bound	Upper Bound	Best Fit	Lower Bound	Upper Bound
Support A	3.31	- 0.887	+ 1.91	25.0	- 0.404	+ 0.415
Support B	Not reported due to poor temperature data from support B.					
Support C	0.106	- 0.00213	+ 0.00221	30.9	- 0.923	+ 0.977
Support D	0.111	- 0.00247	+ 0.00258	40.9	- 1.66	+ 1.80
Support E	0.114	- 0.00252	+ 0.00264	53.3	- 2.67	+ 2.94
Bed taken from approximately 18 °C and submerged in an approximately 0 °C ice-water bath						
	Best Fit	Lower Bound	Upper Bound	Best Fit	Lower Bound	Upper Bound
Support A	Failed to fit.					
Support B	Not reported due to poor temperature data from support B.					
Support C	0.101	- 0.00195	+ 0.00202	36.7	- 1.27	+ 1.36
Support D	0.108	- 0.00226	+ 0.00235	51.8	- 2.51	+ 2.77
Support E	0.107	- 0.00219	+ 0.00227	65.7	- 3.90	+ 4.41

[1] The bed is approximately 11.7% by volume aluminum oxide (gamma phase).
[2] The aluminum oxide is $\frac{1}{8}$-in diameter pellets.
[3] Overall heat transfer coefficient is based on the inside tube diameter.
[4] Values are rounded to two significant figures.
[5] Confidence is 2-sigma.

Table 2.15: Estimated thermal parameters for experiment 3 for a packed bed of 11.7% aluminum oxide by volume and pressurized to 40 psi gauge with nitrogen.

	Effective radial thermal conductivity $\frac{W}{m \cdot K}$			Effective Overall heat transfer coefficient $\frac{W}{m^2 \cdot K}$		
Bed taken from approximately 0 °C and submerged in an approximately 18 °C water bath						
	Best Fit	Lower Bound	Upper Bound	Best Fit	Lower Bound	Upper Bound
Support A	4.03	- 1.24	+ 3.23	24.7	- 0.394	+ 0.404
Support B	Not reported due to poor temperature data from support B.					
Support C	0.106	- 0.00213	+ 0.00221	30.6	- 0.903	+ 0.955
Support D	0.111	- 0.00248	+ 0.00259	40.7	- 1.66	+ 1.80
Support E	0.111	- 0.00242	+ 0.00252	53.6	- 2.73	+ 3.03
Bed taken from approximately 18 °C and submerged in an approximately 0 °C ice-water bath						
	Best Fit	Lower Bound	Upper Bound	Best Fit	Lower Bound	Upper Bound
Support A	Failed to fit.					
Support B	Not reported due to poor temperature data from support B.					
Support C	0.101	- 0.00193	+ 0.00201	38.2	- 1.36	+ 1.45
Support D	0.108	- 0.00223	+ 0.00233	53.1	- 2.61	+ 2.87
Support E	0.109	- 0.00221	+ 0.00230	65.6	- 3.83	+ 4.31

[1] The bed is approximately 11.7% by volume aluminum oxide (gamma phase).
[2] The aluminum oxide is $\frac{1}{8}$-in diameter pellets.
[3] Overall heat transfer coefficient is based on the inside tube diameter.
[4] Values are rounded to two significant figures.
[5] Confidence is 2-sigma.

Table 2.16: Estimated thermal parameters for a packed bed of 11.7% aluminum oxide by volume and pressurized to 40 psi gauge with oxygen.

	Effective radial thermal conductivity $\frac{W}{m \cdot K}$			Effective Overall heat transfer coefficient $\frac{W}{m^2 \cdot K}$		
Bed taken from approximately 0 °C and submerged in an approximately 19 °C water bath						
	Best Fit	Lower Bound	Upper Bound	Best Fit	Lower Bound	Upper Bound
Support A	Failed to fit.					
Support B	Not reported due to poor temperature data from support B.					
Support C	0.106	- 0.00211	+ 0.00219	31.2	- 0.918	+ 0.971
Support D	0.111	- 0.00244	+ 0.00254	41.6	- 1.69	+ 1.84
Support E	0.115	- 0.00254	+ 0.00265		- 2.38	+ 2.62
Bed taken from approximately 21 °C and submerged in an approximately 0 °C ice-water bath						
	Best Fit	Lower Bound	Upper Bound	Best Fit	Lower Bound	Upper Bound
Support A	Failed to fit.					
Support B	Not reported due to poor temperature data from support B.					
Support C	0.103	- 0.00168	+ 0.00173	40.7	- 1.29	+ 1.38
Support D	0.111	- 0.00199	+ 0.00207	54.3	- 2.33	+ 2.52
Support E	0.107	- 0.00179	+ 0.00184	84.8	- 5.19	+ 5.91

[1] The bed is approximately 11.7% by volume aluminum oxide (gamma phase).
[2] The aluminum oxide is $\frac{1}{8}$-in diameter pellets.
[3] Overall heat transfer coefficient is based on the inside tube diameter.
[4] Values are rounded to two significant figures.
[5] Confidence is 2-sigma.

2.7 Comparison of Alumina Packed Bed Experimental Data and Model Fits

For each parameter estimation in section 2.6, a graph was produced comparing the temperature profiles used for the estimation and the temperature profiles generated at the corresponding positions using the estimated parameters (here called model fits). The experimental data is represented by markers, while the model fits are represented by continuous lines. It is noted that due to the number of data points and how close some temperature profiles are to one another, they can be difficult to distinguish.

Comparison graphs for the experimental data and model fits for each thermocouple couple support, A - E, within the bed are shown here, with the exception of support B. The exclusion of support B is discussed in section 2.6. Also, as mentioned in section 2.6 thermocouple supports A and E are not considered to offer useful information. This is because these supports are at the ends of the bed and only have the bed material on one side of the support with quartz wool being on the other side. The comparison graphs for these supports are included here only for completeness, as these thermocouples were included in the bed for other experiments.

2.8 Experimental and Model Comparisons for an Alumina Packed Bed Containing Stagnant Argon Taken from Approximately 0 °C and Submerged in a 19 °C Water Bath

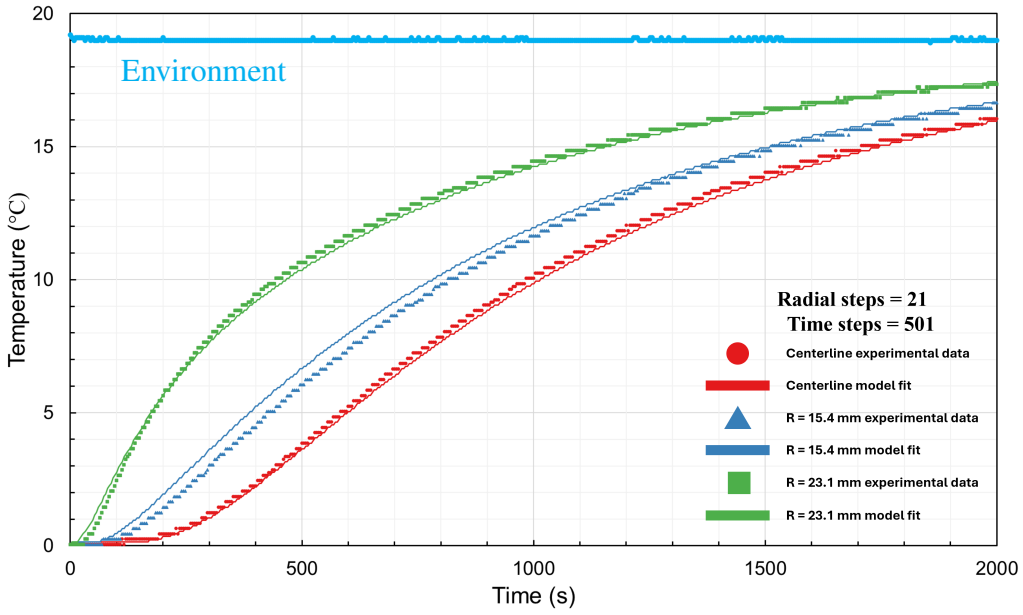

Figure 2.23: Experimental temperature data of support C of an alumina packed bed compared with a model fit of the data as the bed is taken from approximately 0 °C and submerged in an approximately 19 °C water bath. The bed was pressurized to 40 psi gauge with argon at room temperature.

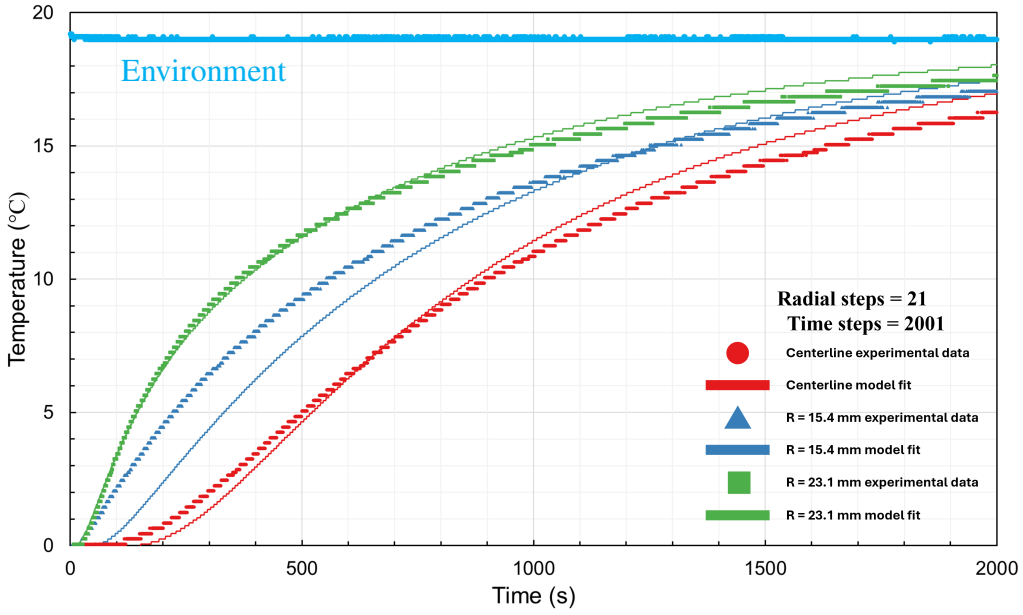

Figure 2.24: Experimental temperature data of support D of an alumina packed bed compared with a model fit of the data as the bed is taken from approximately 0 °C and submerged in an approximately 19 °C water bath. The bed was pressurized to 40 psi gauge with argon at room temperature.

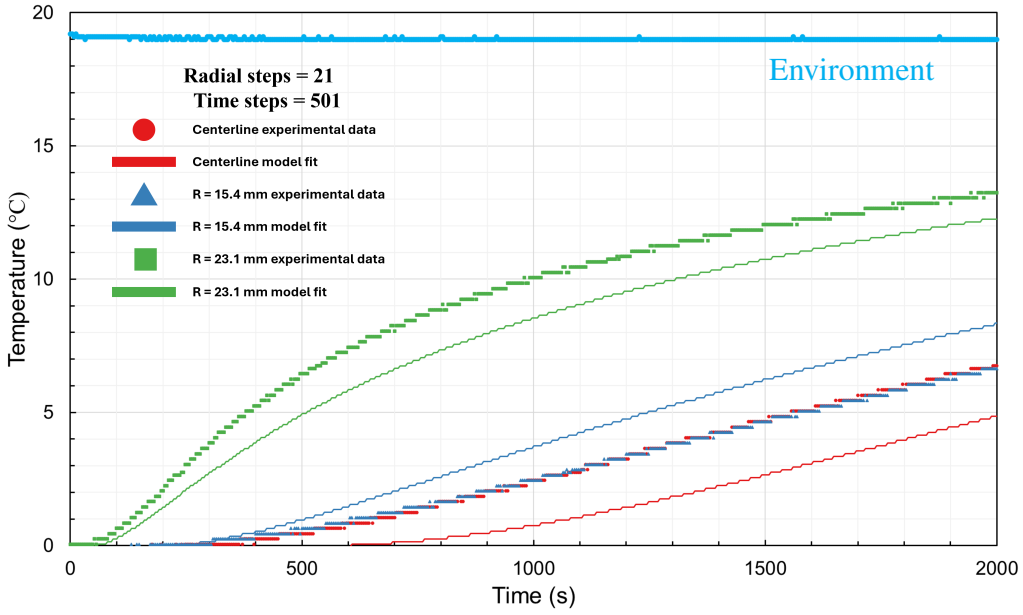

Figure 2.25: Experimental temperature data of support E of an alumina packed bed compared with a model fit of the data as the bed is taken from approximately 0 °C and submerged in an approximately 19 °C water bath. The bed was pressurized to 40 psi gauge with argon at room temperature.

2.9 Experimental and Model Comparisons for an Alumina Packed Bed Containing Stagnant Argon Taken from Approximately 22 °C and Submerged in a 0 °C Ice-Water Bath

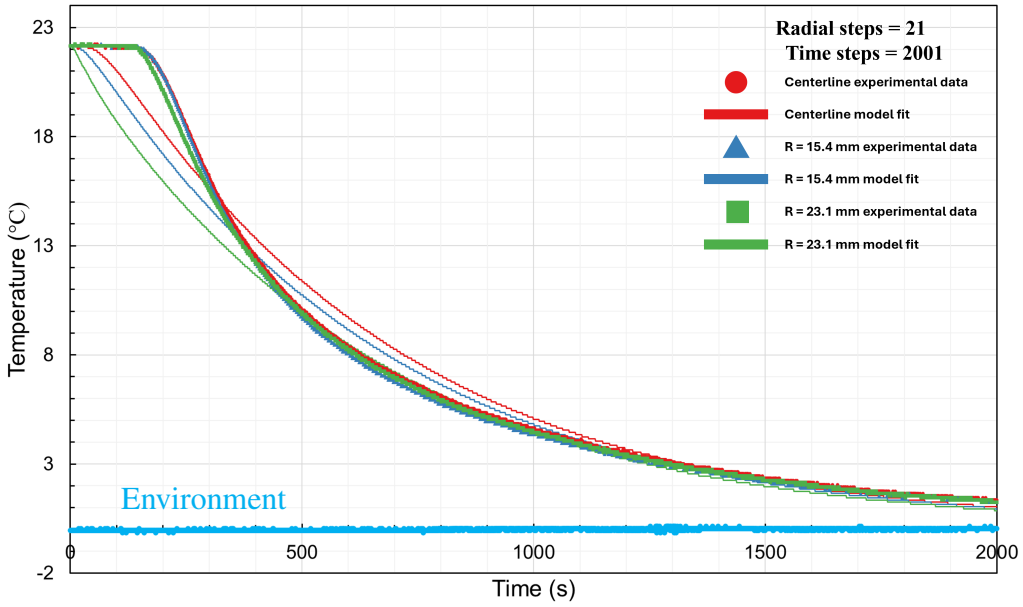

Figure 2.26: Experimental temperature data of support A of an alumina packed bed compared with a model fit of the data as the bed is taken from approximately 22 °C and submerged in an approximately 0 °C ice-water bath. The bed was pressurized to 40 psi gauge with argon at room temperature.

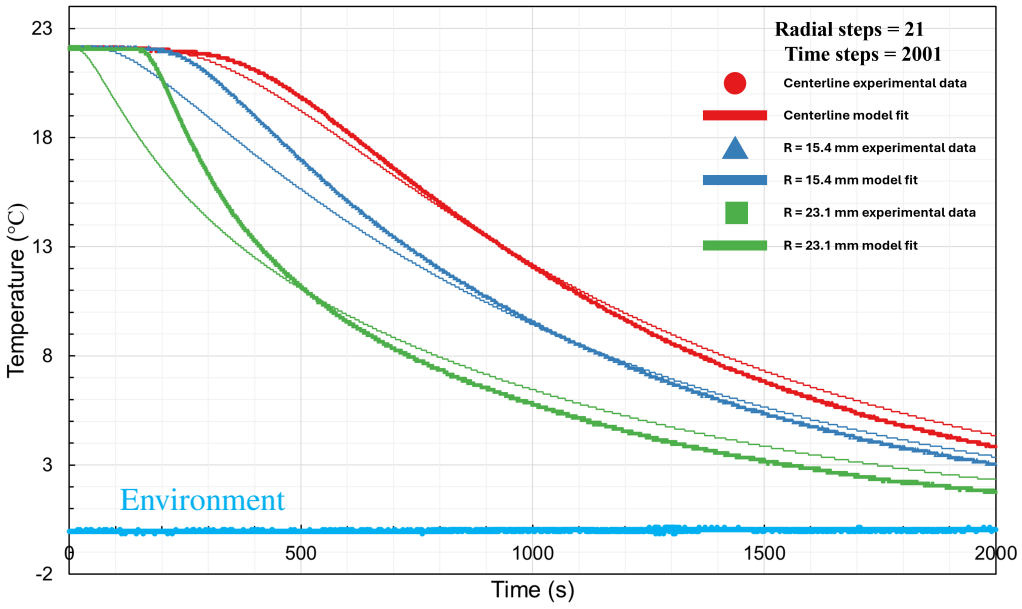

Figure 2.27: Experimental temperature data of support C of an alumina packed bed compared with a model fit of the data as the bed is taken from approximately 22 °C and submerged in an approximately 0 °C ice-water bath. The bed was pressurized to 40 psi gauge with argon at room temperature.

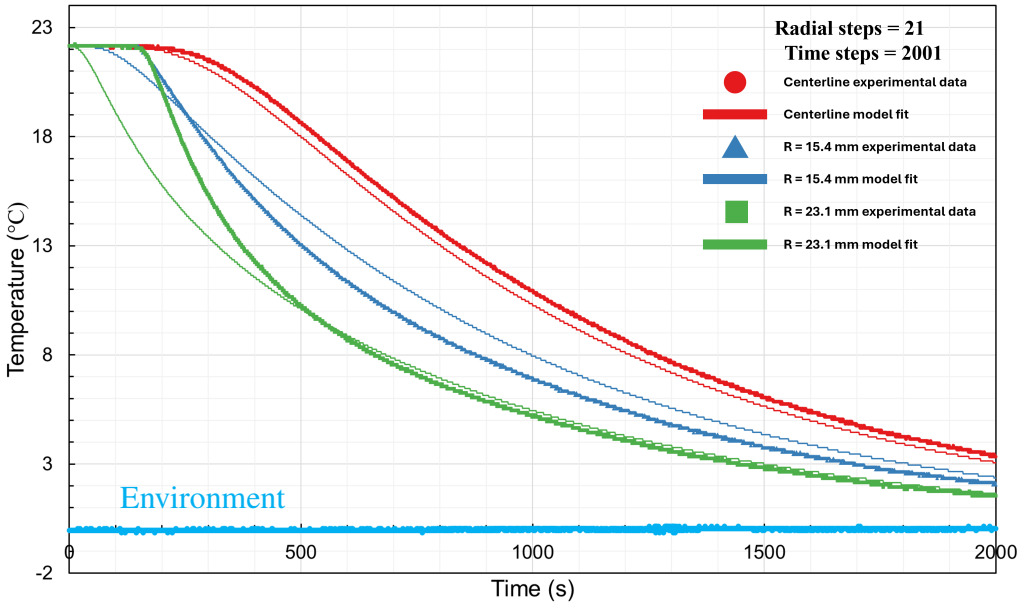

Figure 2.28: Experimental temperature data of support D of an alumina packed bed compared with a model fit of the data as the bed is taken from approximately 22 °C and submerged in an approximately 0 °C ice-water bath. The bed was pressurized to 40 psi gauge with argon at room temperature.

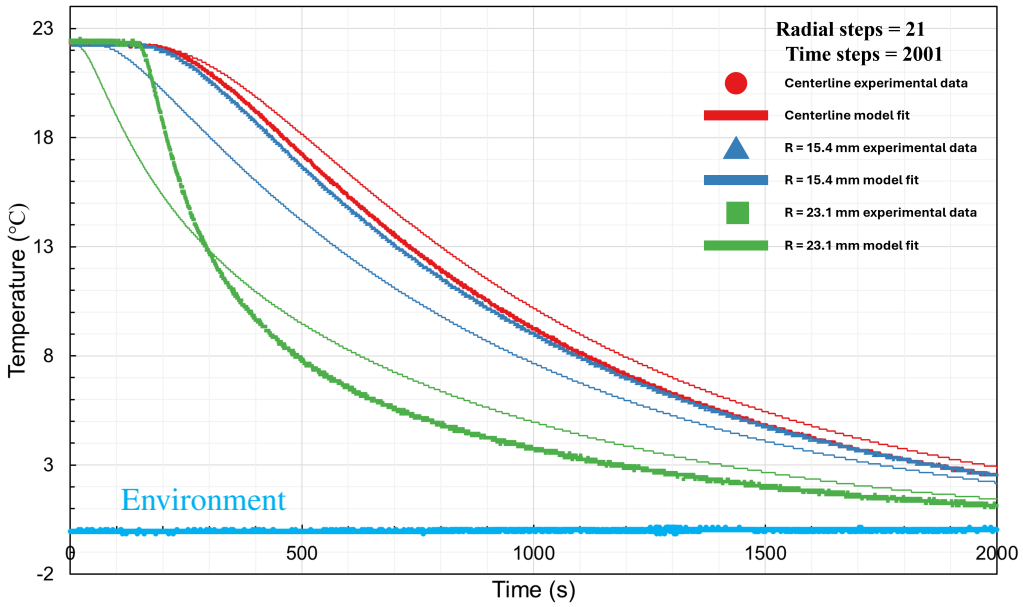

Figure 2.29: Experimental temperature data of support E of an alumina packed bed compared with a model fit of the data as the bed is taken from approximately 22 °C and submerged in an approximately 0 °C ice-water bath. The bed was pressurized to 40 psi gauge with argon at room temperature.

2.10 Experimental and Model Comparisons for an Alumina Packed Bed Containing Stagnant Helium Taken from Approximately 0 °C and Submerged in a 21 °C Water Bath

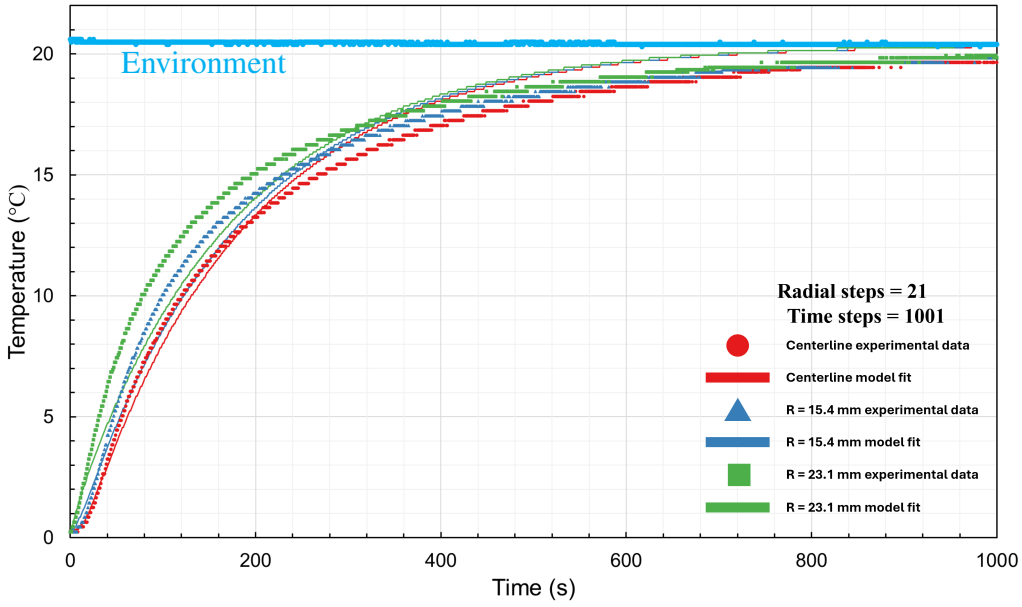

Figure 2.30: Experimental temperature data of support A of an alumina packed bed compared with a model fit of the data as the bed is taken from approximately 0 °C and submerged in an approximately 21 °C water bath. The bed was pressurized to 40 psi gauge with helium at room temperature.

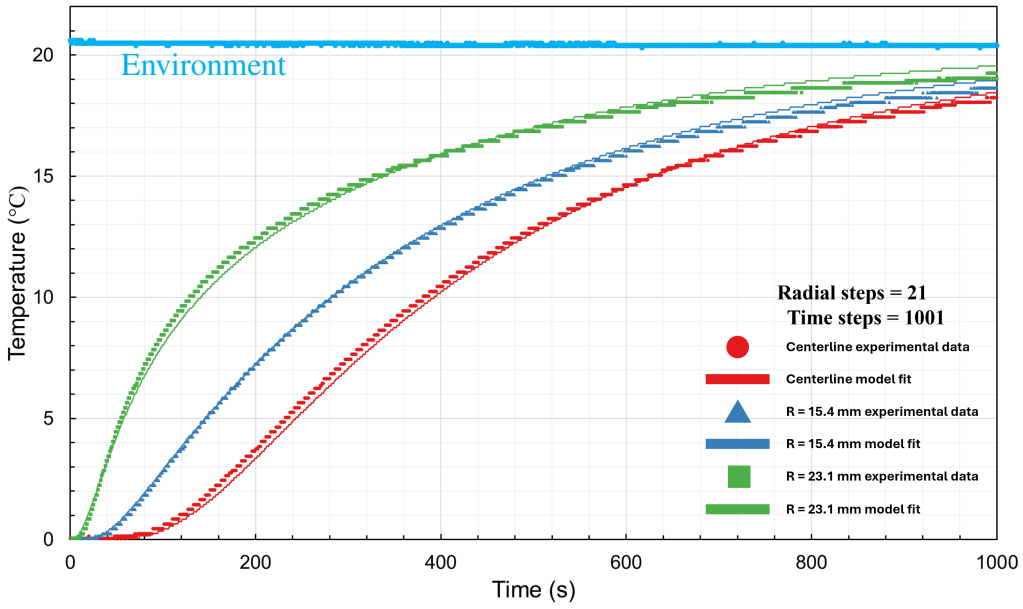

Figure 2.31: Experimental temperature data of support C of an alumina packed bed compared with a model fit of the data as the bed is taken from approximately 0 °C and submerged in an approximately 21 °C water bath. The bed was pressurized to 40 psi gauge with helium at room temperature.

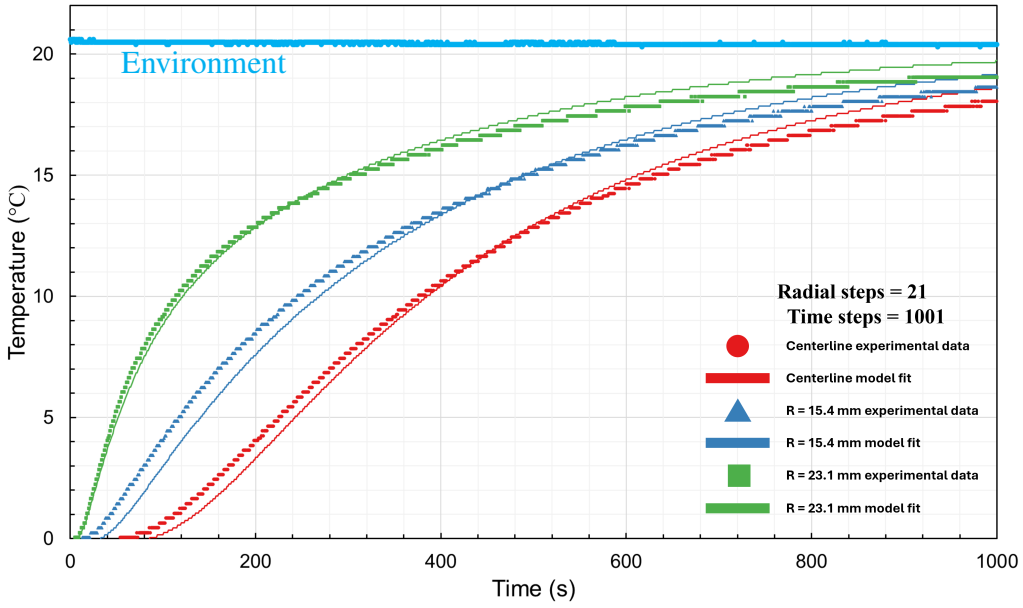

Figure 2.32: Experimental temperature data of support D of an alumina packed bed compared with a model fit of the data as the bed is taken from approximately 0 °C and submerged in an approximately 21 °C water bath. The bed was pressurized to 40 psi gauge with helium at room temperature.

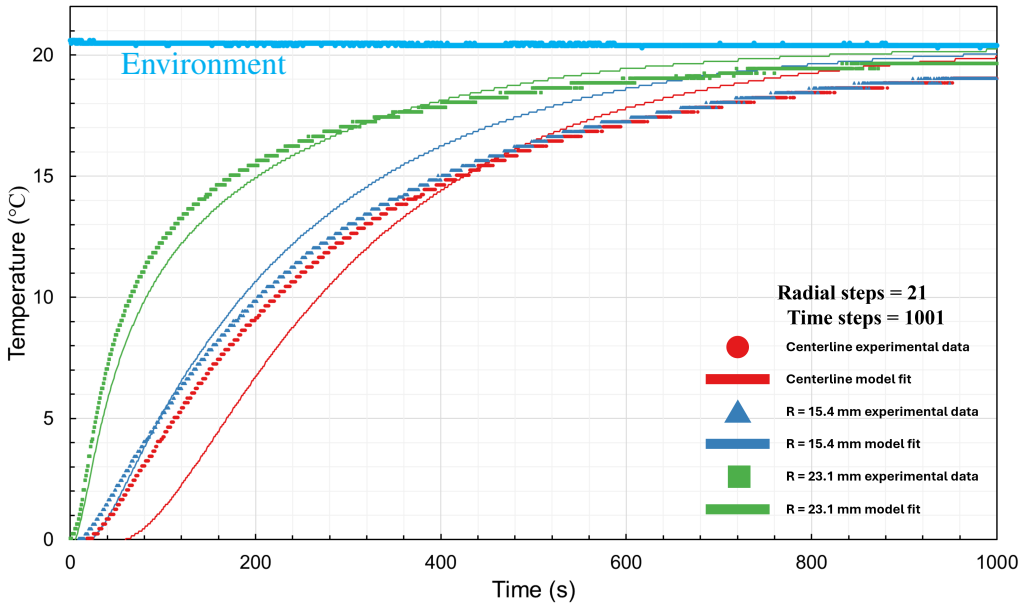

Figure 2.33: Experimental temperature data of support E of an alumina packed bed compared with a model fit of the data as the bed is taken from approximately 0 °C and submerged in an approximately 21 °C water bath. The bed was pressurized to 40 psi gauge with helium at room temperature.

2.11 Experimental and Model Comparisons for an Alumina Packed Bed Containing Stagnant Helium Taken from Approximately 21 °C and Submerged in a 0 °C Ice-Water Bath

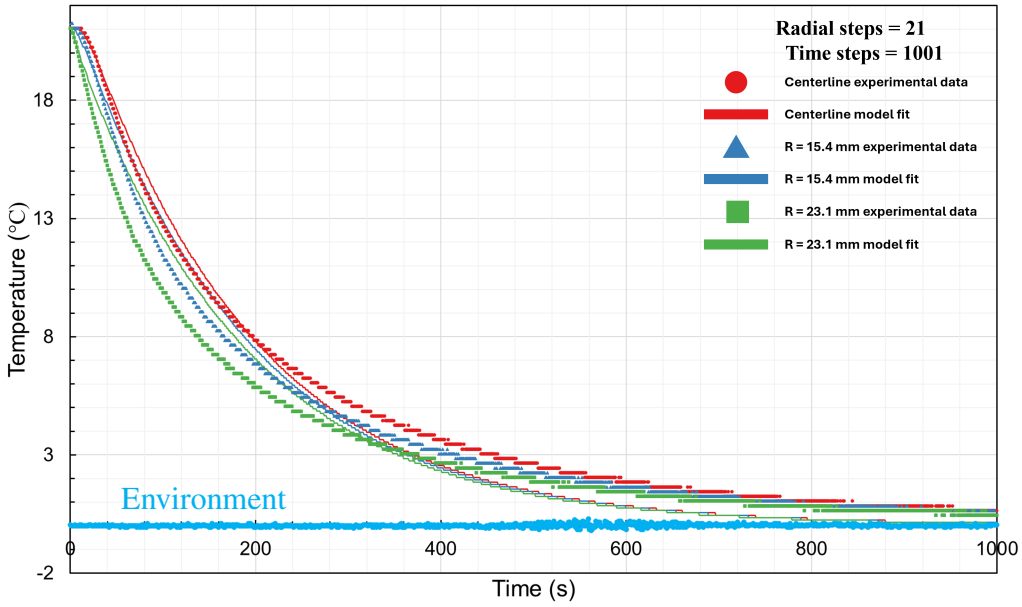

Figure 2.34: Experimental temperature data of support A of an alumina packed bed compared with a model fit of the data as the bed is taken from approximately 21 °C and submerged in an approximately 0 °C ice-water bath. The bed was pressurized to 40 psi gauge with helium at room temperature.

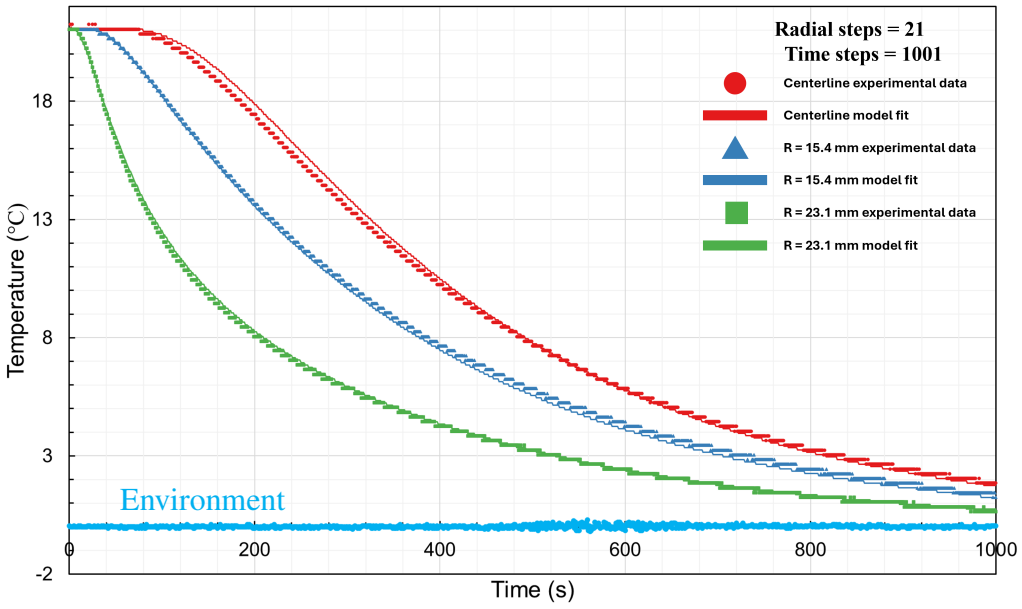

Figure 2.35: Experimental temperature data of support C of an alumina packed bed compared with a model fit of the data as the bed is taken from approximately 21 °C and submerged in an approximately 0 °C ice-water bath. The bed was pressurized to 40 psi gauge with helium at room temperature.

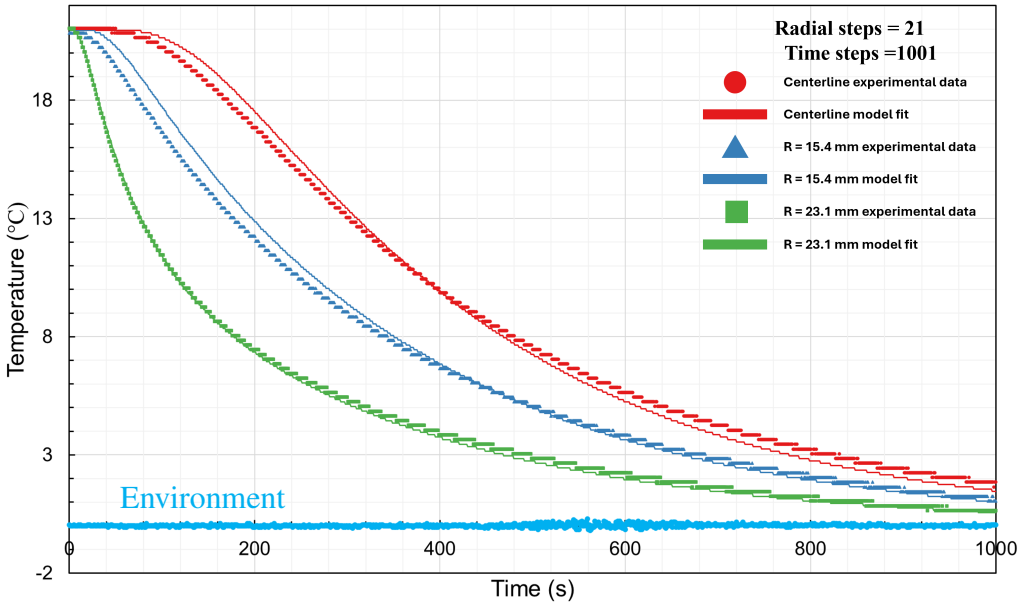

Figure 2.36: Experimental temperature data of support D of an alumina packed bed compared with a model fit of the data as the bed is taken from approximately 21 °C and submerged in an approximately 0 °C ice-water bath. The bed was pressurized to 40 psi gauge with helium at room temperature.

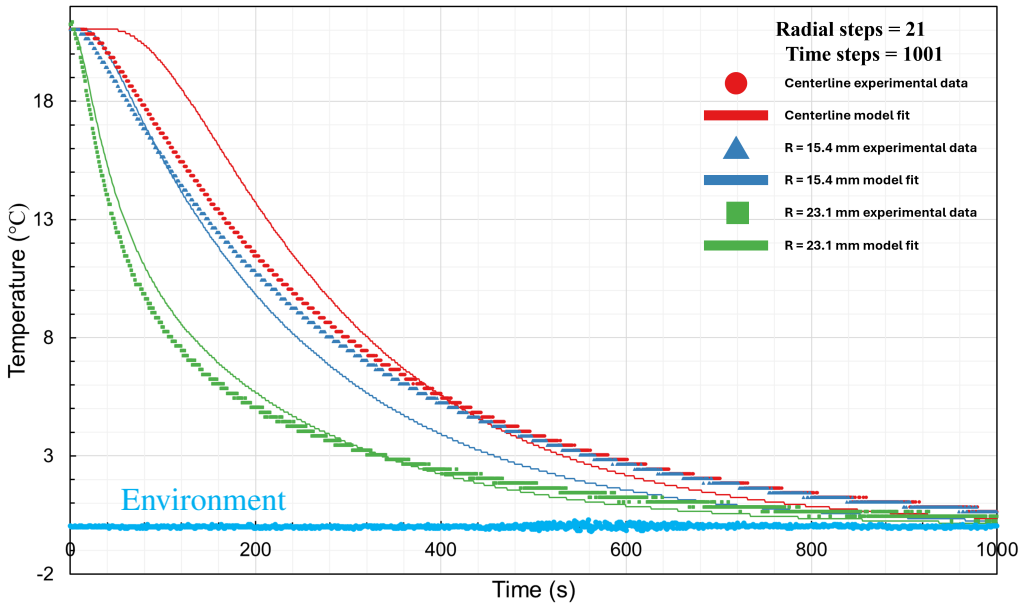

Figure 2.37: Experimental temperature data of support E of an alumina packed bed compared with a model fit of the data as the bed is taken from approximately 21 °C and submerged in an approximately 0 °C ice-water bath. The bed was pressurized to 40 psi gauge with helium at room temperature.

2.12 Experimental and Model Comparisons for an Alumina Packed Bed Containing Stagnant Hydrogen Taken from Approximately 0 °C and Submerged in a 19 °C Water Bath

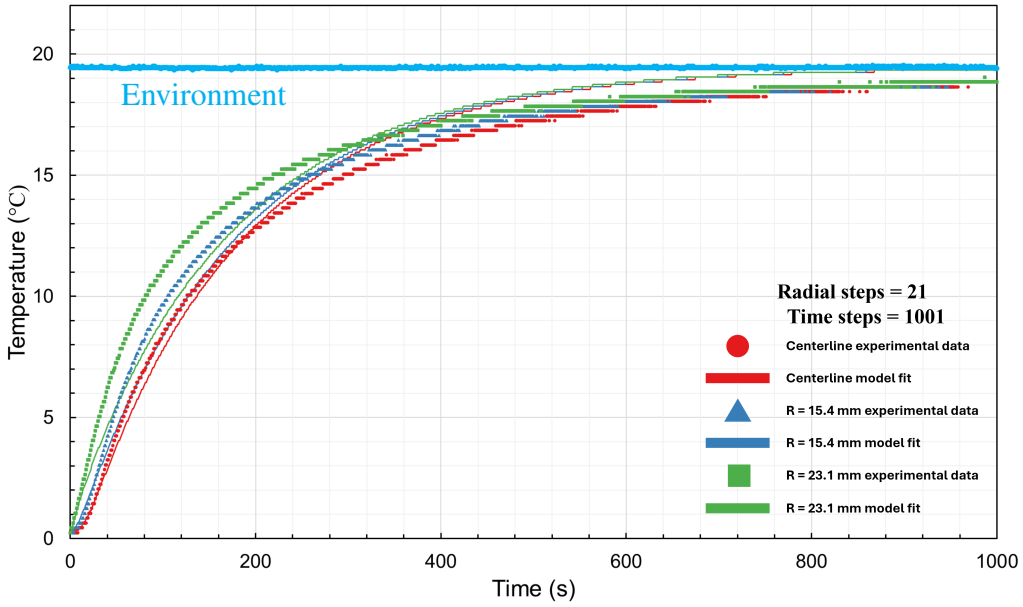

Figure 2.38: Experimental temperature data of support A of an alumina packed bed compared with a model fit of the data as the bed is taken from approximately 0 °C and submerged in an approximately 19 °C water bath. The bed was pressurized to 40 psi gauge with hydrogen at room temperature.

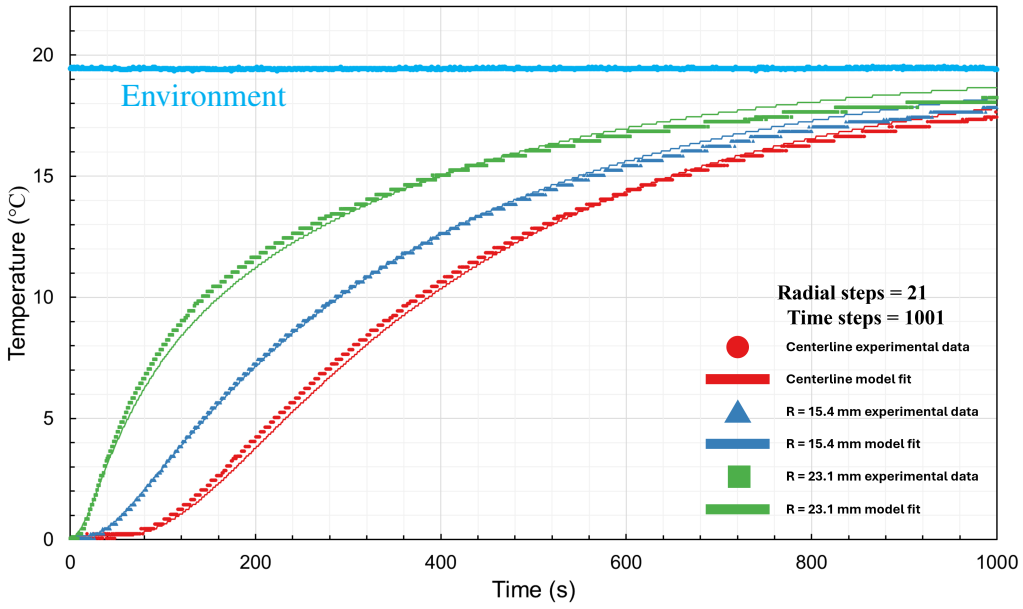

Figure 2.39: Experimental temperature data of support C of an alumina packed bed compared with a model fit of the data as the bed is taken from approximately 0 °C and submerged in an approximately 19 °C water bath. The bed was pressurized to 40 psi gauge with hydrogen at room temperature.

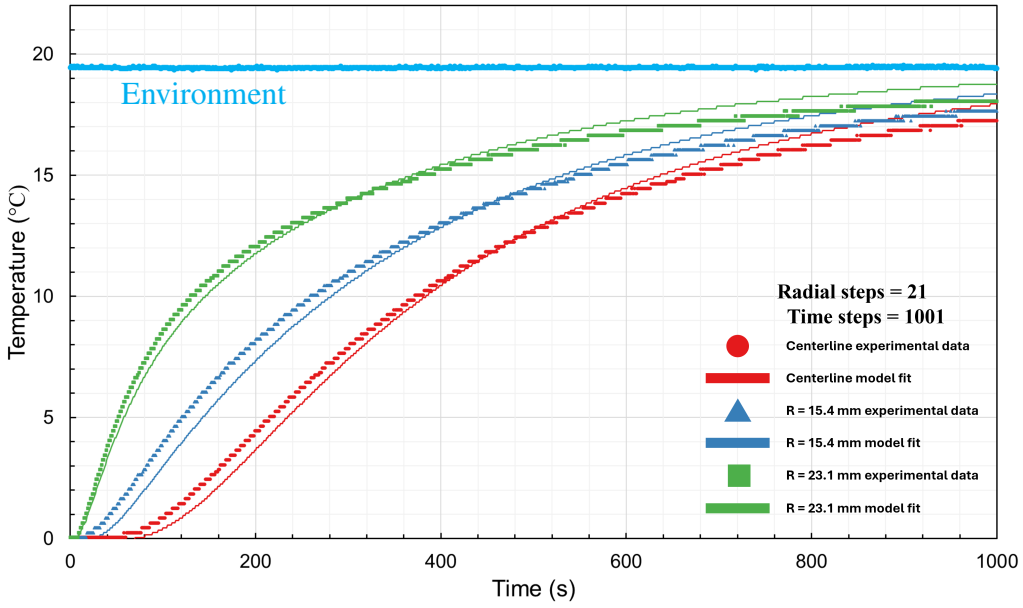

Figure 2.40: Experimental temperature data of support D of an alumina packed bed compared with a model fit of the data as the bed is taken from approximately 0 °C and submerged in an approximately 19 °C water bath. The bed was pressurized to 40 psi gauge with hydrogen at room temperature.

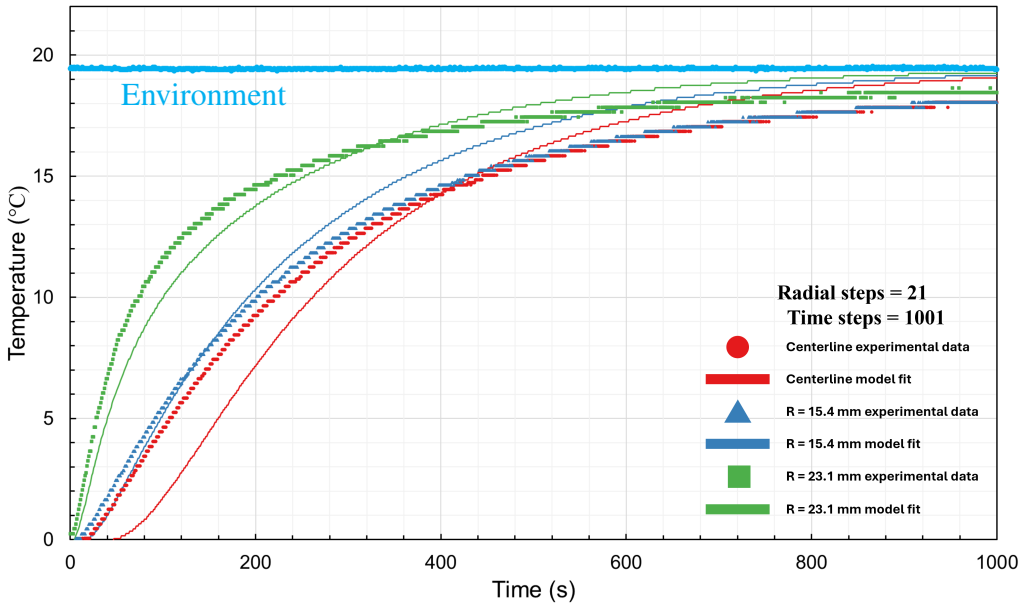

Figure 2.41: Experimental temperature data of support E of an alumina packed bed compared with a model fit of the data as the bed is taken from approximately 0 °C and submerged in an approximately 19 °C water bath. The bed was pressurized to 40 psi gauge with hydrogen at room temperature.

2.13 Experimental and Model Comparisons for an Alumina Packed Bed Containing Stagnant Hydrogen Taken from Approximately 21 °C and Submerged in a 0 °C Ice-Water Bath

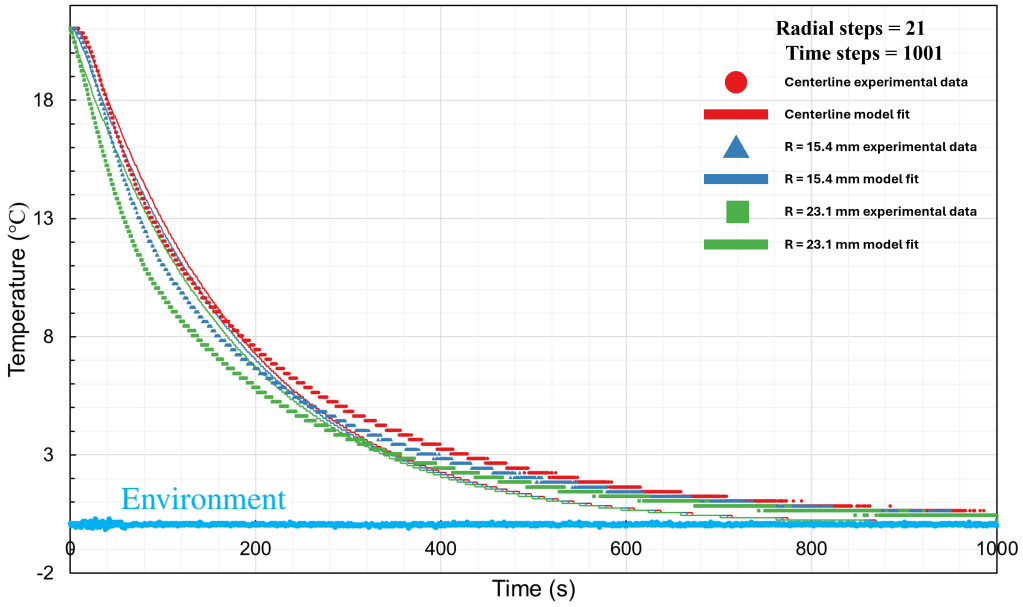

Figure 2.42: Experimental temperature data of support A of an alumina packed bed compared with a model fit of the data as the bed is taken from approximately 21 °C and submerged in an approximately 0 °C ice-water bath. The bed was pressurized to 40 psi gauge with hydrogen at room temperature.

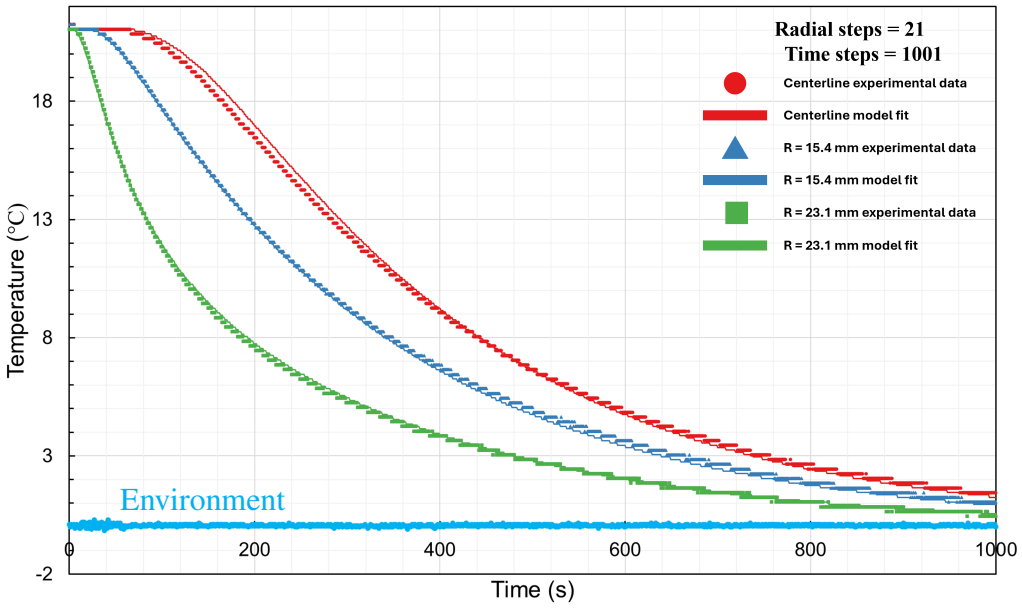

Figure 2.43: Experimental temperature data of support C of an alumina packed bed compared with a model fit of the data as the bed is taken from approximately 21 °C and submerged in an approximately 0 °C ice-water bath. The bed was pressurized to 40 psi gauge with hydrogen at room temperature.

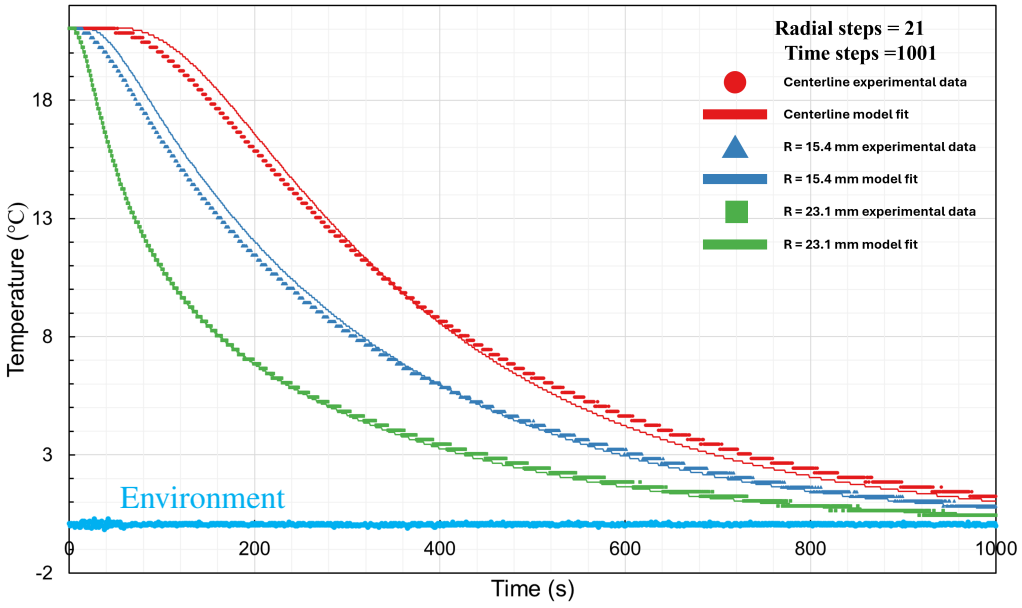

Figure 2.44: Experimental temperature data of support D of an alumina packed bed compared with a model fit of the data as the bed is taken from approximately 21 °C and submerged in an approximately 0 °C ice-water bath. The bed was pressurized to 40 psi gauge with hydrogen at room temperature.

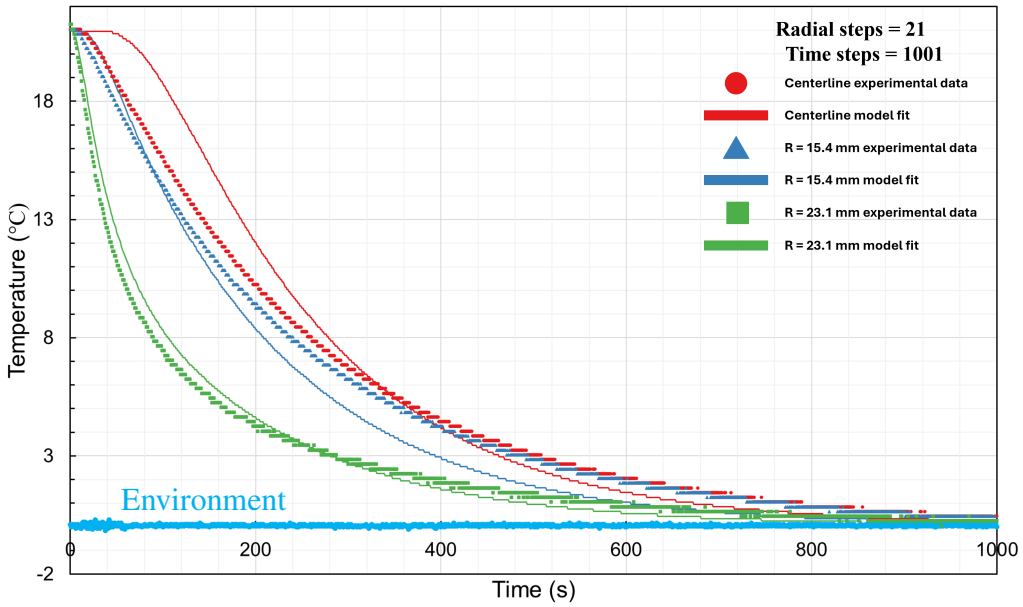

Figure 2.45: Experimental temperature data of support E of an alumina packed bed compared with a model fit of the data as the bed is taken from approximately 21 °C and submerged in an approximately 0 °C ice-water bath. The bed was pressurized to 40 psi gauge with hydrogen at room temperature.

2.14 Experimental and Model Comparisons for experiment 1 for an Alumina Packed Bed Containing Stagnant Nitrogen Taken from Approximately 0 °C and Submerged in a 19 °C Water Bath

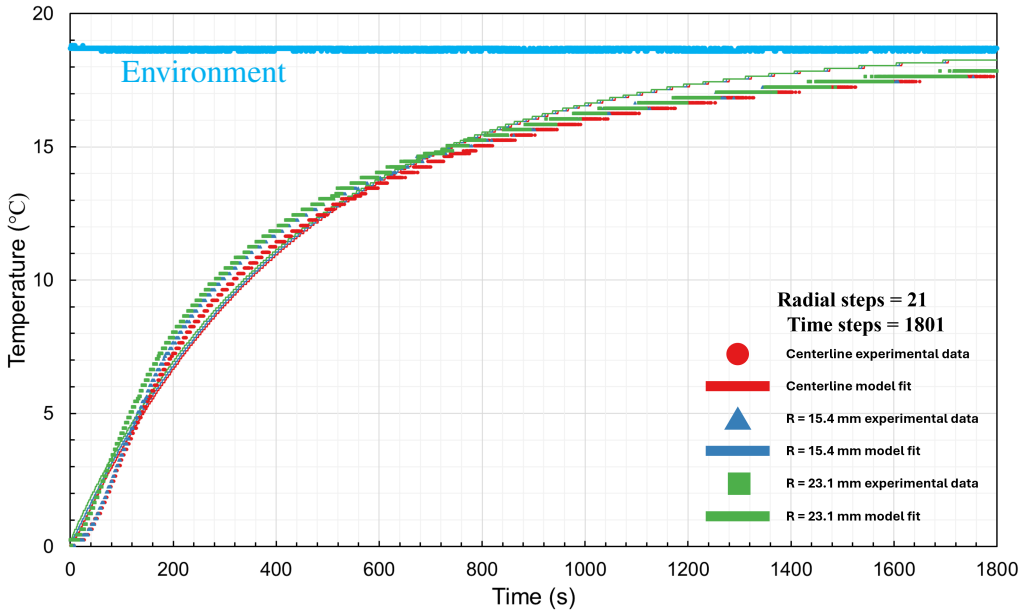

Figure 2.46: Experimental temperature data of support A of an alumina packed bed compared with a model fit of the data as the bed is taken from approximately 0 °C and submerged in an approximately 19 °C water bath. The bed was pressurized to 40 psi gauge with nitrogen at room temperature.

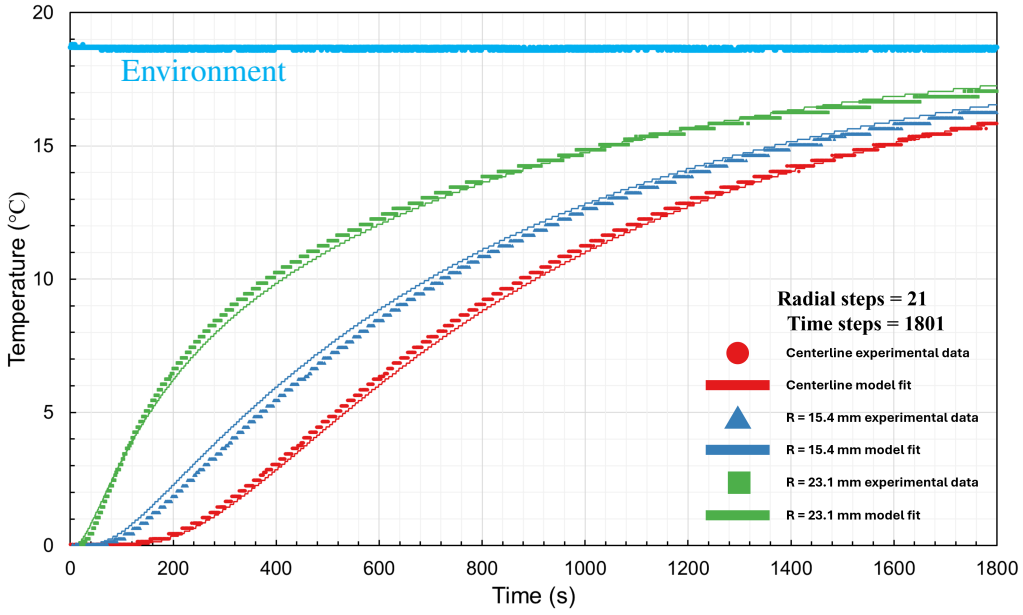

Figure 2.47: Experimental temperature data of support C of an alumina packed bed compared with a model fit of the data as the bed is taken from approximately 0 °C and submerged in an approximately 19 °C water bath. The bed was pressurized to 40 psi gauge with nitrogen at room temperature.

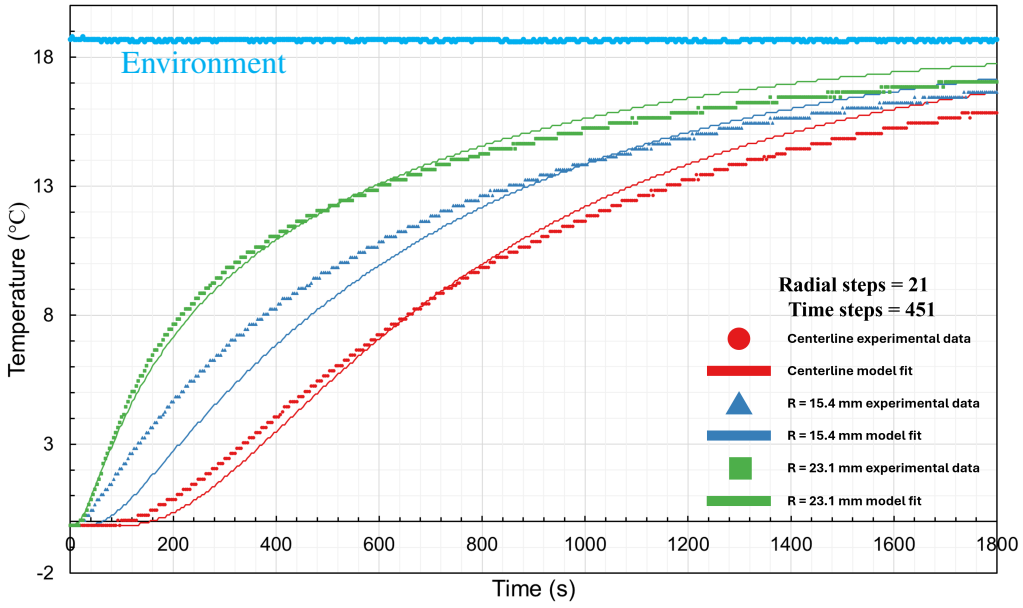

Figure 2.48: Experimental temperature data of support D of an alumina packed bed compared with a model fit of the data as the bed is taken from approximately 0 °C and submerged in an approximately 19 °C water bath. The bed was pressurized to 40 psi gauge with nitrogen at room temperature.

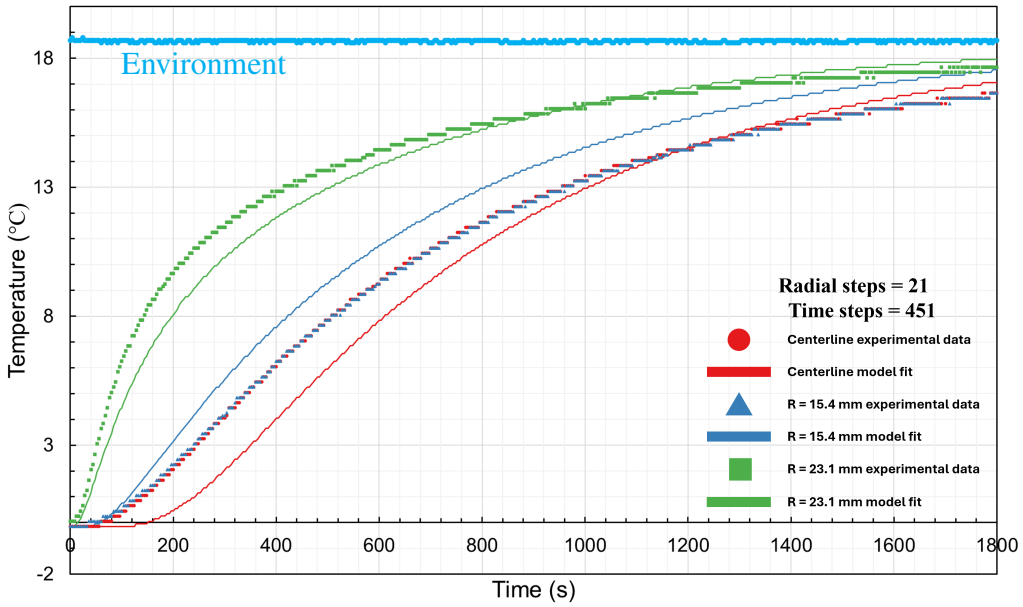

Figure 2.49: Experimental temperature data of support E of an alumina packed bed compared with a model fit of the data as the bed is taken from approximately 0 °C and submerged in an approximately 19 °C water bath. The bed was pressurized to 40 psi gauge with nitrogen at room temperature.

2.15 Experimental and Model Comparisons for experiment 1 for an Alumina Packed Bed Containing Stagnant Nitrogen Taken from Approximately 21 °C and Submerged in a 0 °C Ice-Water Bath

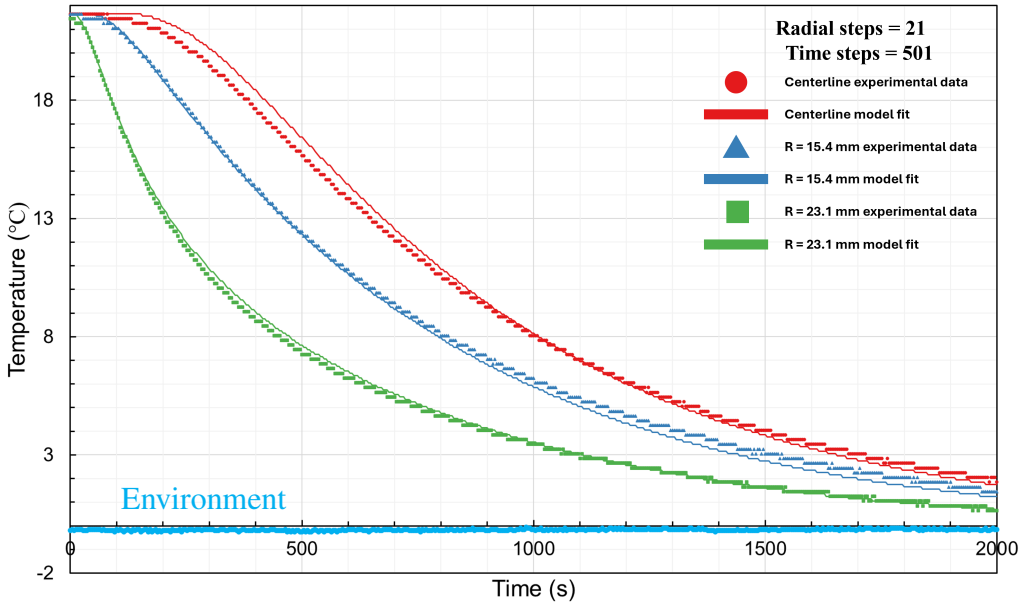

Figure 2.50: Experimental temperature data of support C of an alumina packed bed compared with a model fit of the data as the bed is taken from approximately 21 °C and submerged in an approximately 0 °C ice-water bath. The bed was pressurized to 40 psi gauge with nitrogen at room temperature.

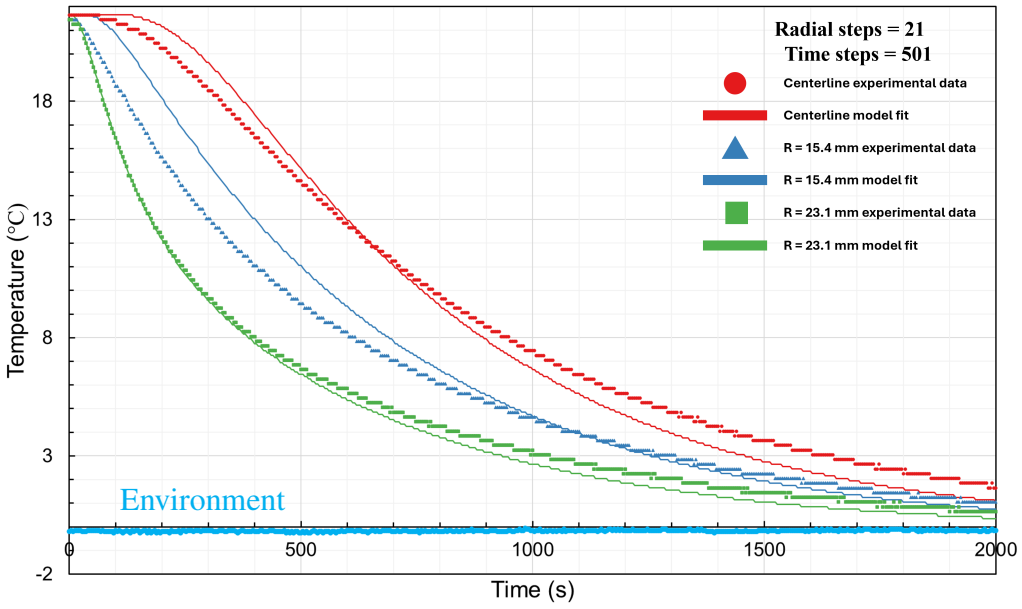

Figure 2.51: Experimental temperature data of support D of an alumina packed bed compared with a model fit of the data as the bed is taken from approximately 21 °C and submerged in an approximately 0 °C ice-water bath. The bed was pressurized to 40 psi gauge with nitrogen at room temperature.

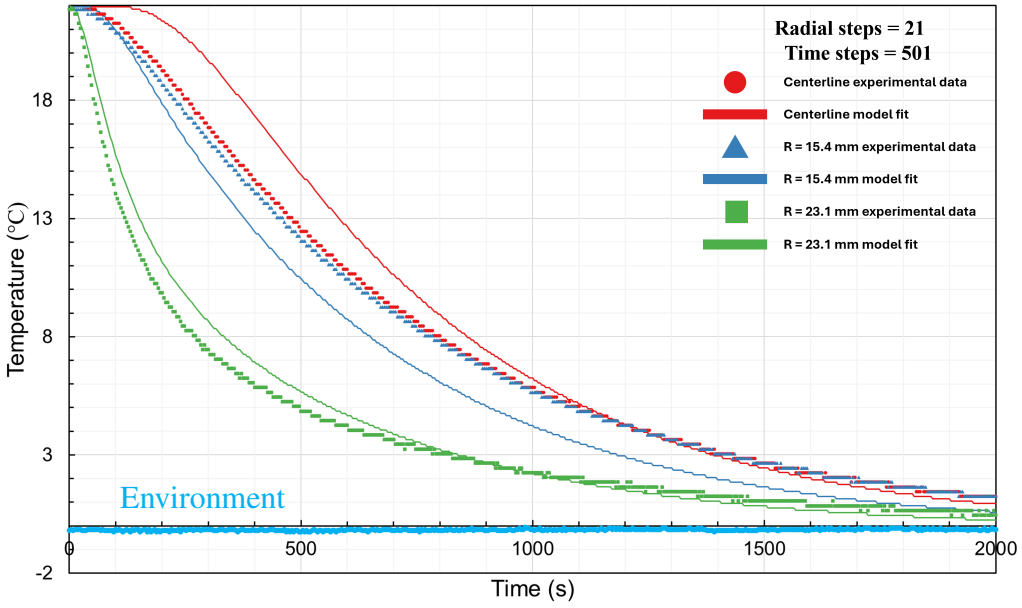

Figure 2.52: Experimental temperature data of support E of an alumina packed bed compared with a model fit of the data as the bed is taken from approximately 21 °C and submerged in an approximately 0 °C ice-water bath. The bed was pressurized to 40 psi gauge with nitrogen at room temperature.

2.16 Experimental and Model Comparisons for experiment 2 for an Alumina Packed Bed Containing Stagnant Nitrogen Taken from Approximately 0 °C and Submerged in a 19 °C Water Bath

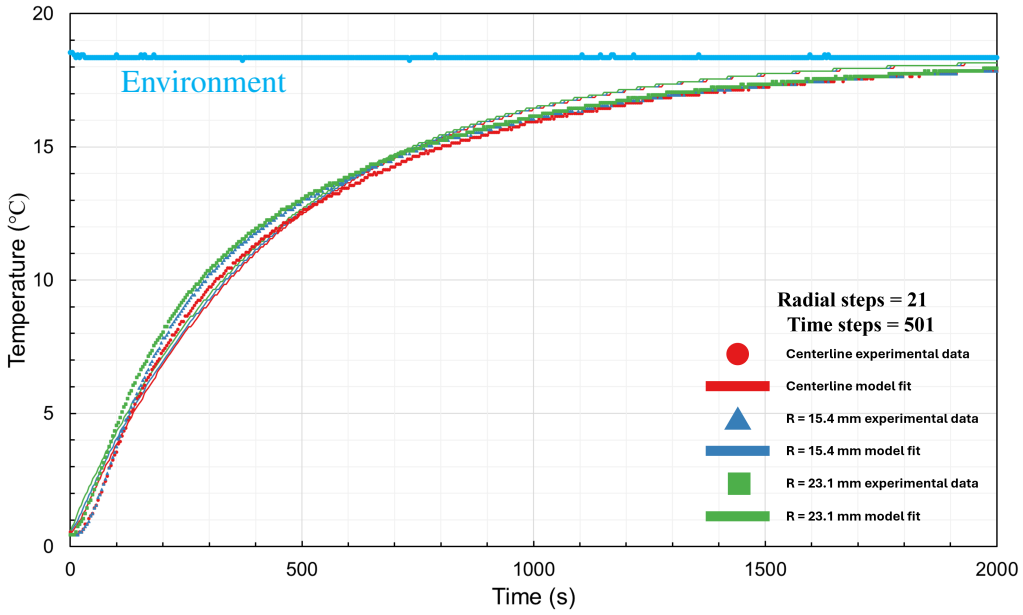

Figure 2.53: Experimental temperature data of support A of an alumina packed bed compared with a model fit of the data as the bed is taken from approximately 0 °C and submerged in an approximately 18 °C water bath. The bed was pressurized to 40 psi gauge with nitrogen at room temperature.

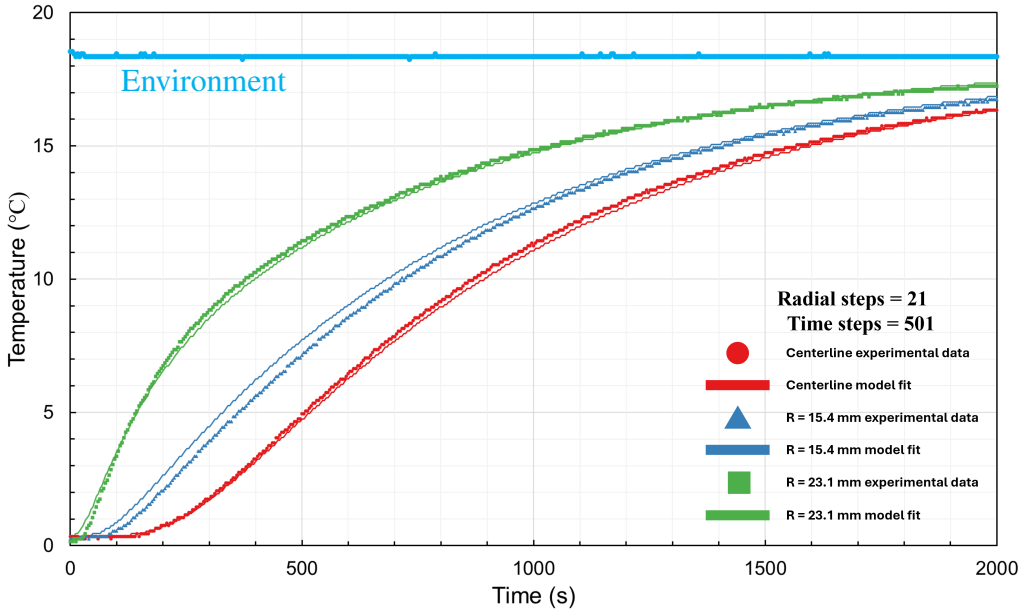

Figure 2.54: Experimental temperature data of support C of an alumina packed bed compared with a model fit of the data as the bed is taken from approximately 0 °C and submerged in an approximately 18 °C water bath. The bed was pressurized to 40 psi gauge with nitrogen at room temperature.

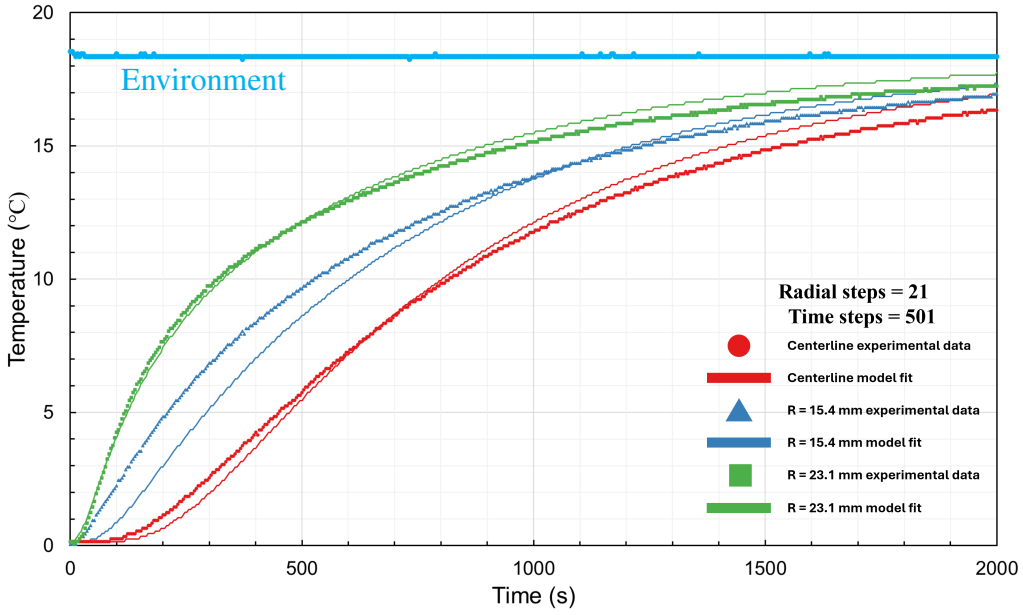

Figure 2.55: Experimental temperature data of support D of an alumina packed bed compared with a model fit of the data as the bed is taken from approximately 0 °C and submerged in an approximately 18 °C water bath. The bed was pressurized to 40 psi gauge with nitrogen at room temperature.

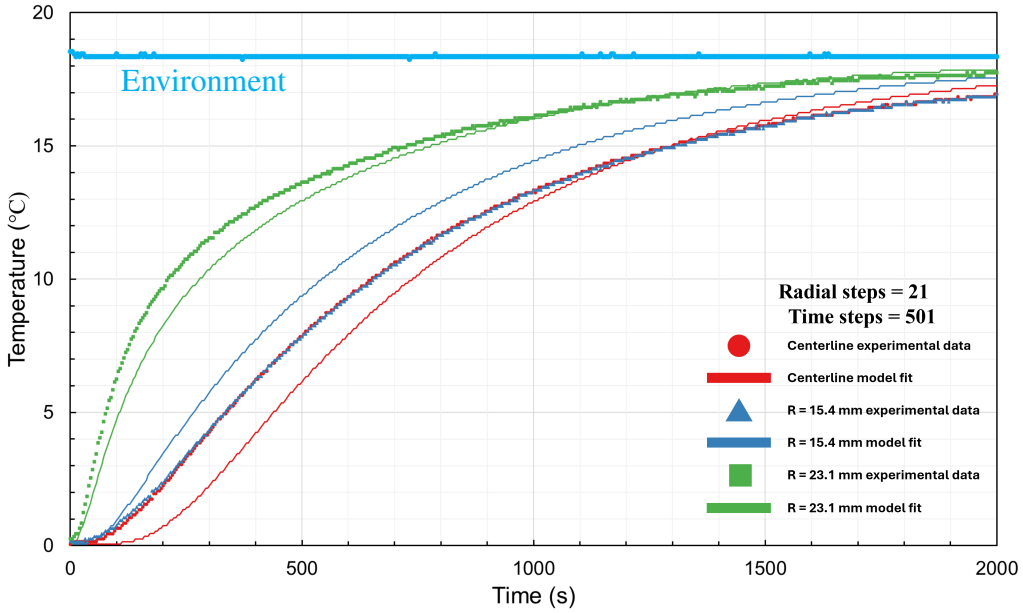

Figure 2.56: Experimental temperature data of support E of an alumina packed bed compared with a model fit of the data as the bed is taken from approximately 0 °C and submerged in an approximately 18 °C water bath. The bed was pressurized to 40 psi gauge with nitrogen at room temperature.

2.17 Experimental and Model Comparisons for experiment 2 for an Alumina Packed Bed Containing Stagnant Nitrogen Taken from Approximately 21 °C and Submerged in a 0 °C Ice-Water Bath

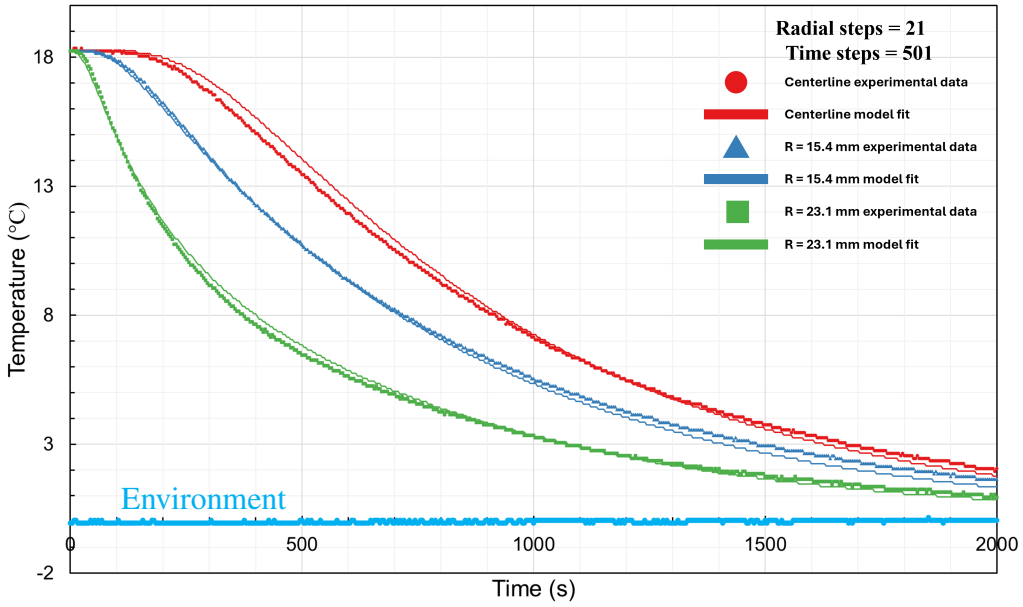

Figure 2.57: Experimental temperature data of support C of an alumina packed bed compared with a model fit of the data as the bed is taken from approximately 18 °C and submerged in an approximately 0 °C ice-water bath. The bed was pressurized to 40 psi gauge with nitrogen at room temperature.

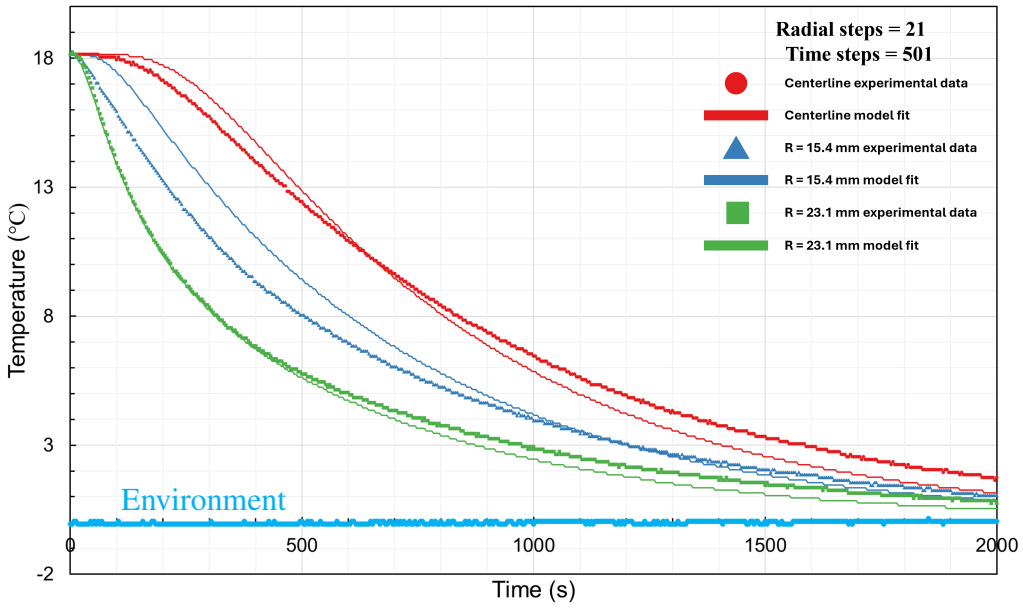

Figure 2.58: Experimental temperature data of support D of an alumina packed bed compared with a model fit of the data as the bed is taken from approximately 18 °C and submerged in an approximately 0 °C ice-water bath. The bed was pressurized to 40 psi gauge with nitrogen at room temperature.

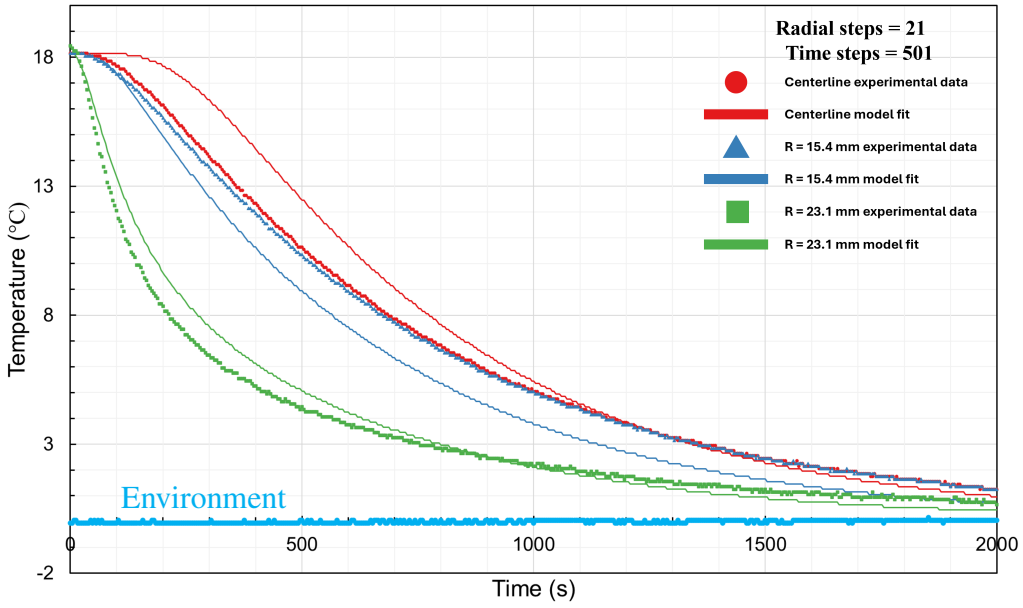

Figure 2.59: Experimental temperature data of support E of an alumina packed bed compared with a model fit of the data as the bed is taken from approximately 18 °C and submerged in an approximately 0 °C ice-water bath. The bed was pressurized to 40 psi gauge with nitrogen at room temperature.

2.18 Experimental and Model Comparisons for experiment 3 for an Alumina Packed Bed Containing Stagnant Nitrogen Taken from Approximately 0 °C and Submerged in a 19 °C Water Bath

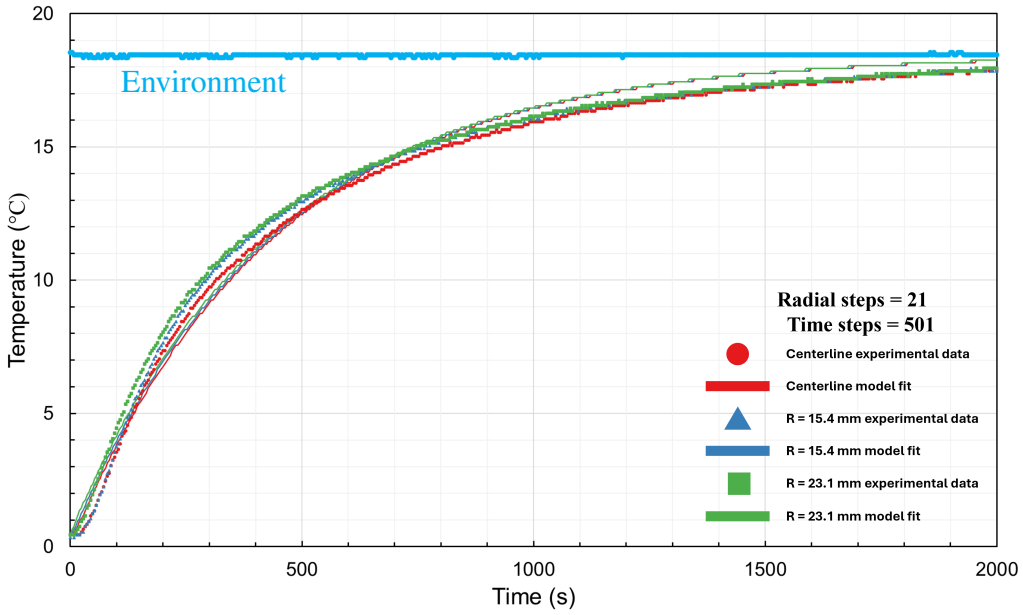

Figure 2.60: Experimental temperature data of support A of an alumina packed bed compared with a model fit of the data as the bed is taken from approximately 0 °C and submerged in an approximately 19 °C water bath. The bed was pressurized to 40 psi gauge with nitrogen at room temperature.

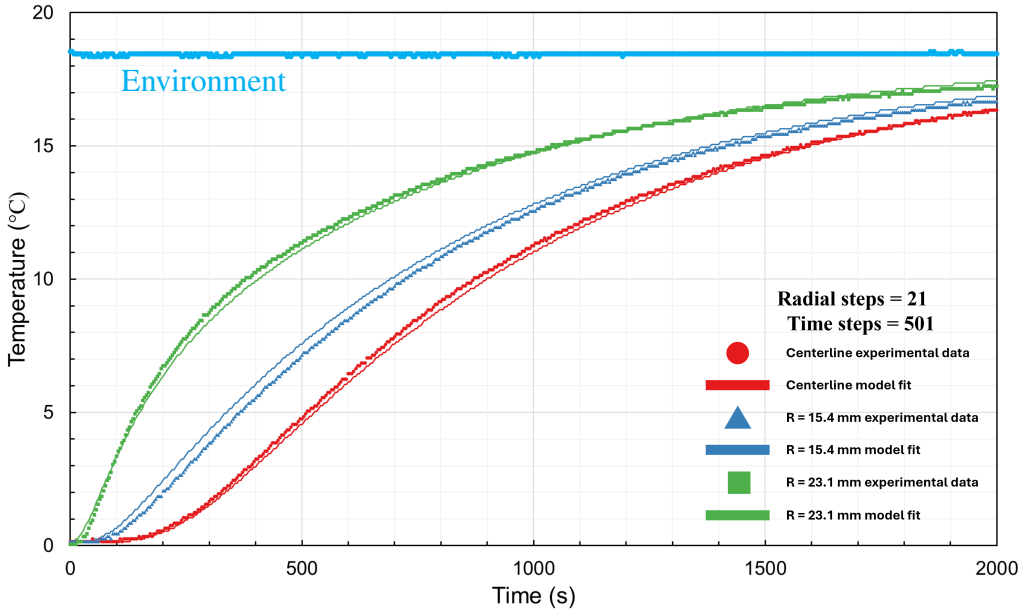

Figure 2.61: Experimental temperature data of support C of an alumina packed bed compared with a model fit of the data as the bed is taken from approximately 0 °C and submerged in an approximately 19 °C water bath. The bed was pressurized to 40 psi gauge with nitrogen at room temperature.

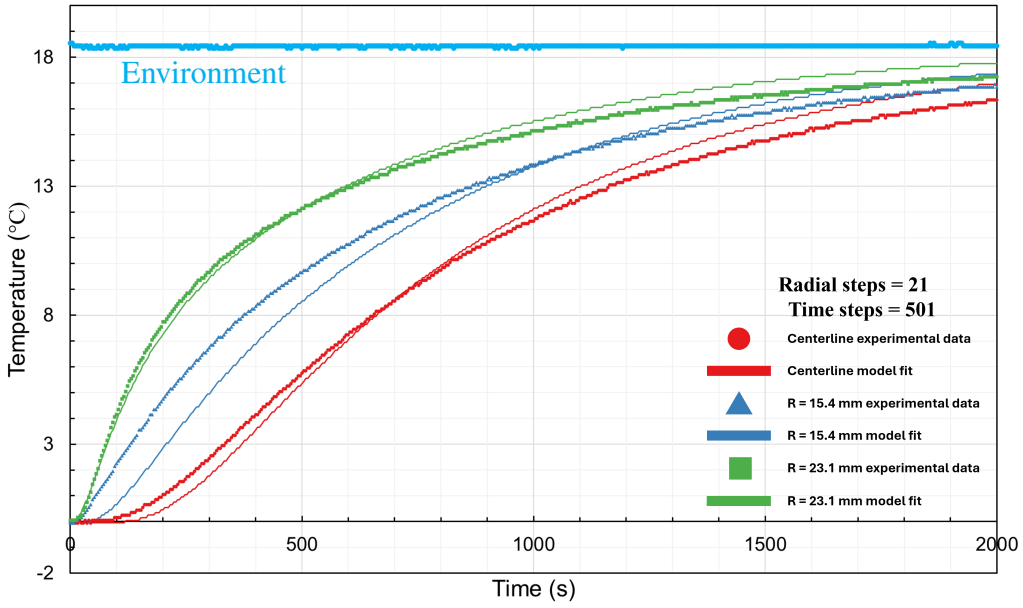

Figure 2.62: Experimental temperature data of support D of an alumina packed bed compared with a model fit of the data as the bed is taken from approximately 0 °C and submerged in an approximately 19 °C water bath. The bed was pressurized to 40 psi gauge with nitrogen at room temperature.

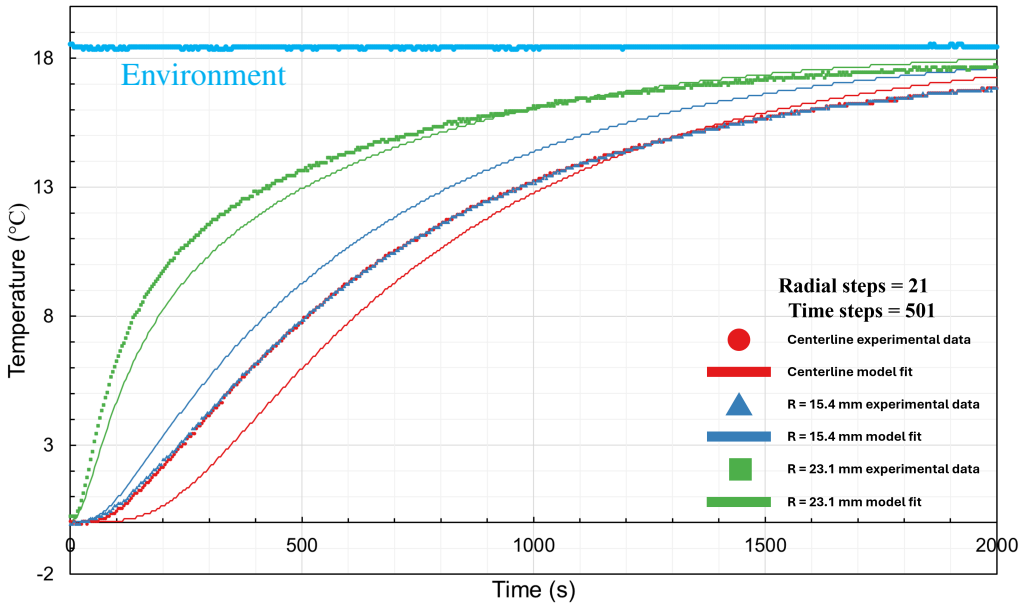

Figure 2.63: Experimental temperature data of support E of an alumina packed bed compared with a model fit of the data as the bed is taken from approximately 0 °C and submerged in an approximately 19 °C water bath. The bed was pressurized to 40 psi gauge with nitrogen at room temperature.

2.19 Experimental and Model Comparisons for experiment 3 for an Alumina Packed Bed Containing Stagnant Nitrogen Taken from Approximately 21 °C and Submerged in a 0 °C Ice-Water Bath

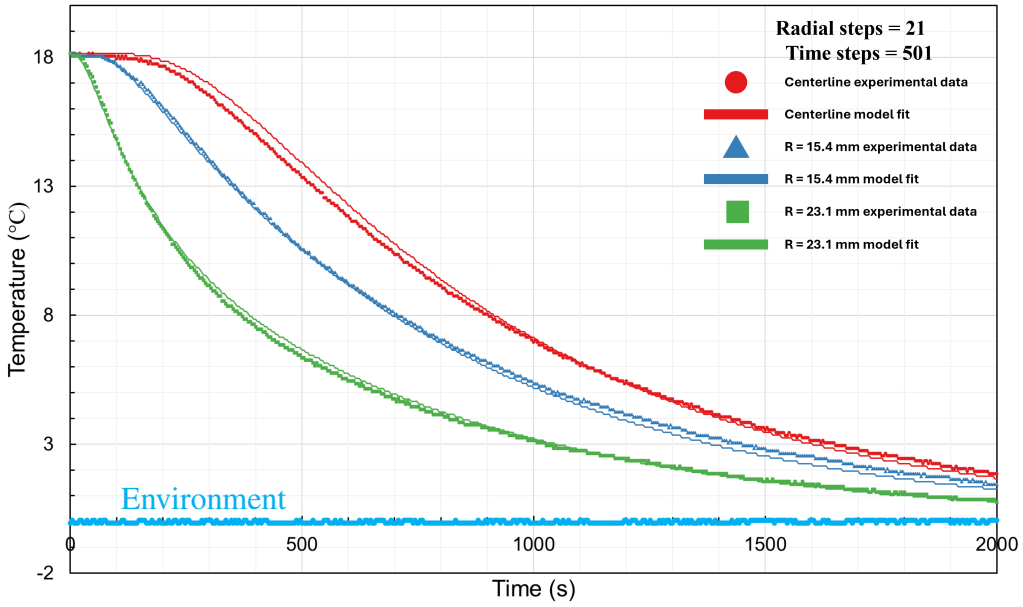

Figure 2.64: Experimental temperature data of support C of an alumina packed bed compared with a model fit of the data as the bed is taken from approximately 21 °C and submerged in an approximately 0 °C ice-water bath. The bed was pressurized to 40 psi gauge with nitrogen at room temperature.

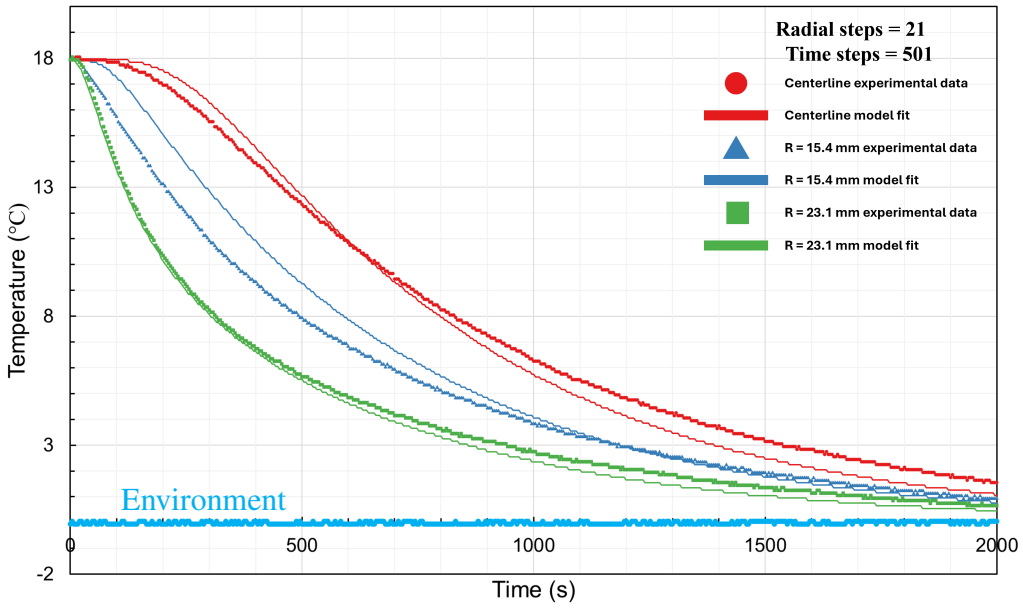

Figure 2.65: Experimental temperature data of support D of an alumina packed bed compared with a model fit of the data as the bed is taken from approximately 21 °C and submerged in an approximately 0 °C ice-water bath. The bed was pressurized to 40 psi gauge with nitrogen at room temperature.

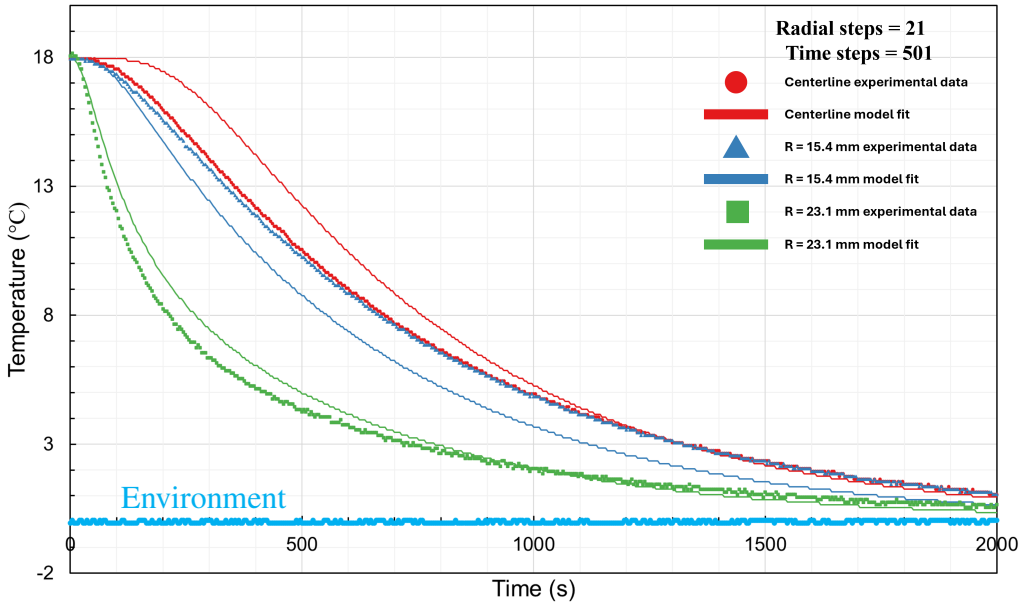

Figure 2.66: Experimental temperature data of support E of an alumina packed bed compared with a model fit of the data as the bed is taken from approximately 21 °C and submerged in an approximately 0 °C ice-water bath. The bed was pressurized to 40 psi gauge with nitrogen at room temperature.

2.20 Experimental and Model Comparisons for an Alumina Packed Bed Containing Stagnant Oxygen Taken from Approximately 0 °C and Submerged in a 19 °C Water Bath

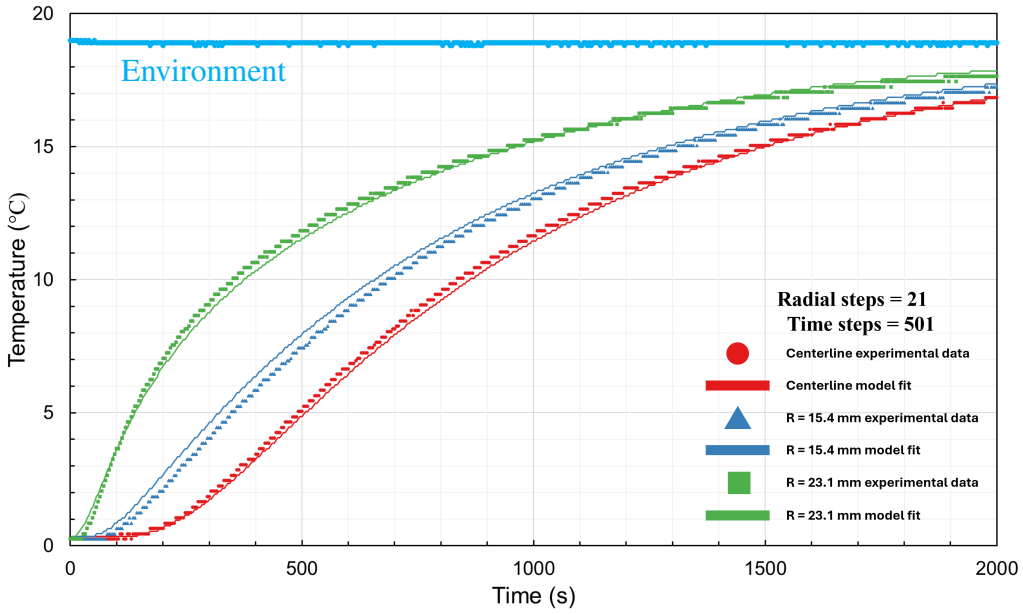

Figure 2.67: Experimental temperature data of support C of an alumina packed bed compared with a model fit of the data as the bed is taken from approximately 0 °C and submerged in an approximately 19 °C water bath. The bed was pressurized to 40 psi gauge with oxygen at room temperature.

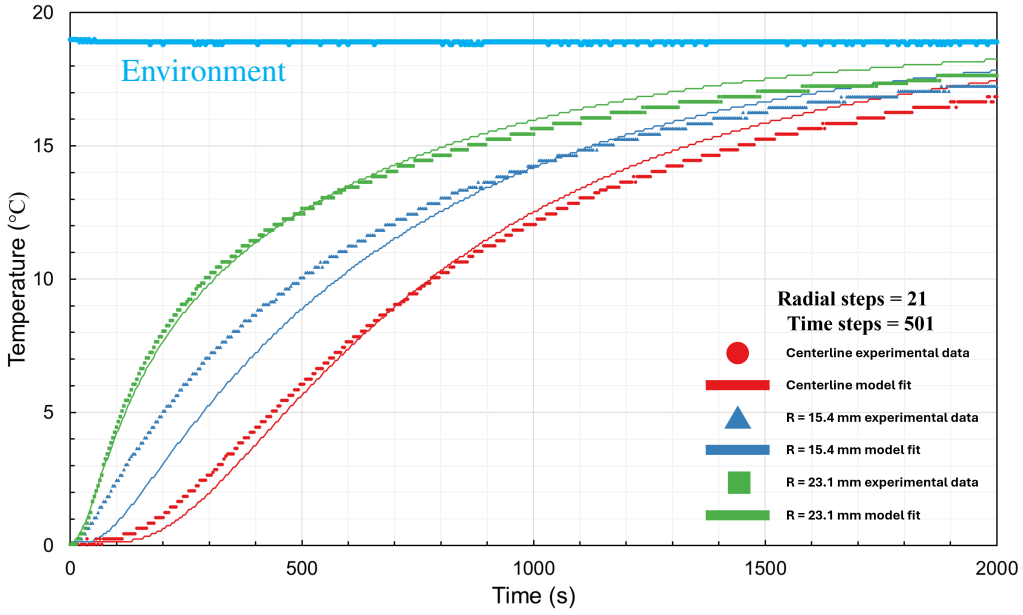

Figure 2.68: Experimental temperature data of support D of an alumina packed bed compared with a model fit of the data as the bed is taken from approximately 0 °C and submerged in an approximately 19 °C water bath. The bed was pressurized to 40 psi gauge with oxygen at room temperature.

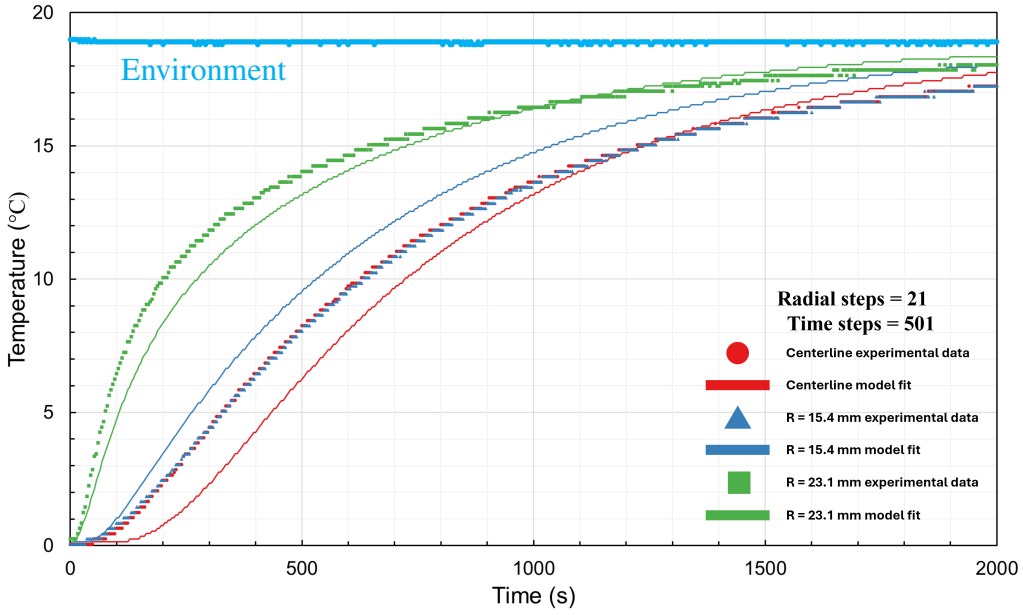

Figure 2.69: Experimental temperature data of support E of an alumina packed bed compared with a model fit of the data as the bed is taken from approximately 0 °C and submerged in an approximately 19 °C water bath. The bed was pressurized to 40 psi gauge with oxygen at room temperature.

2.21 Experimental and Model Comparisons for an Alumina Packed Bed Containing Stagnant Oxygen Taken from Approximately 0 °C and Submerged in a 19 °C Water Bath

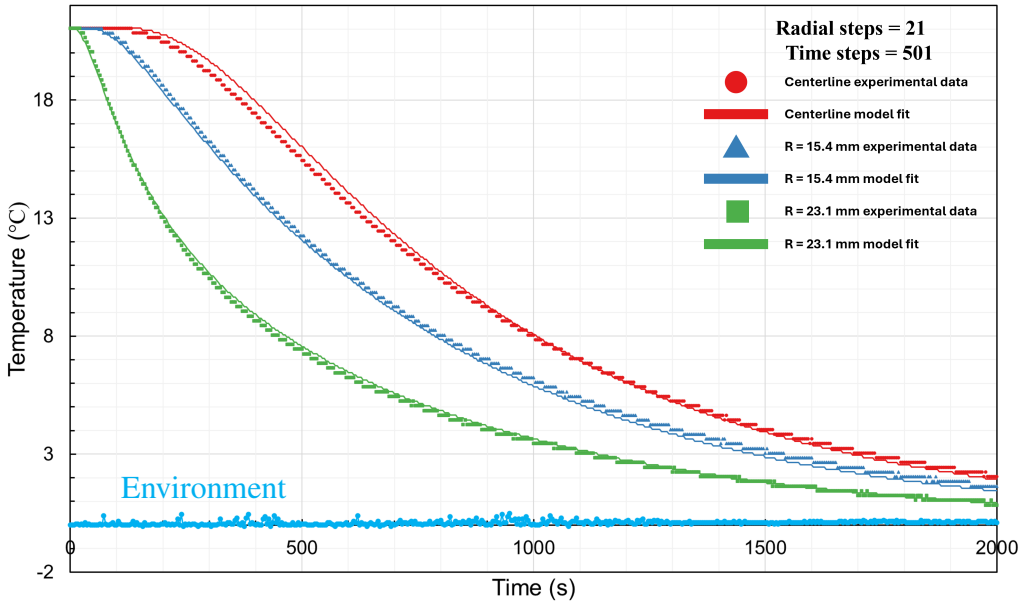

Figure 2.70: Experimental temperature data of support C of an alumina packed bed compared with a model fit of the data as the bed is taken from approximately 21 °C and submerged in an approximately 0 °C ice-water bath. The bed was pressurized to 40 psi gauge with oxygen at room temperature.

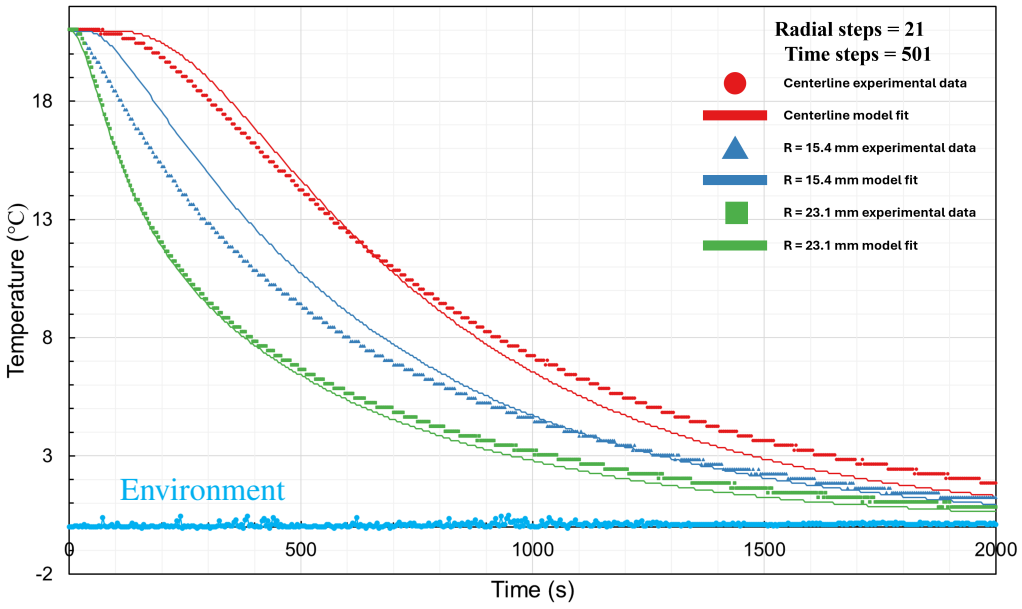

Figure 2.71: Experimental temperature data of support D of an alumina packed bed compared with a model fit of the data as the bed is taken from approximately 21 °C and submerged in an approximately 0 °C ice-water bath. The bed was pressurized to 40 psi gauge with oxygen at room temperature.

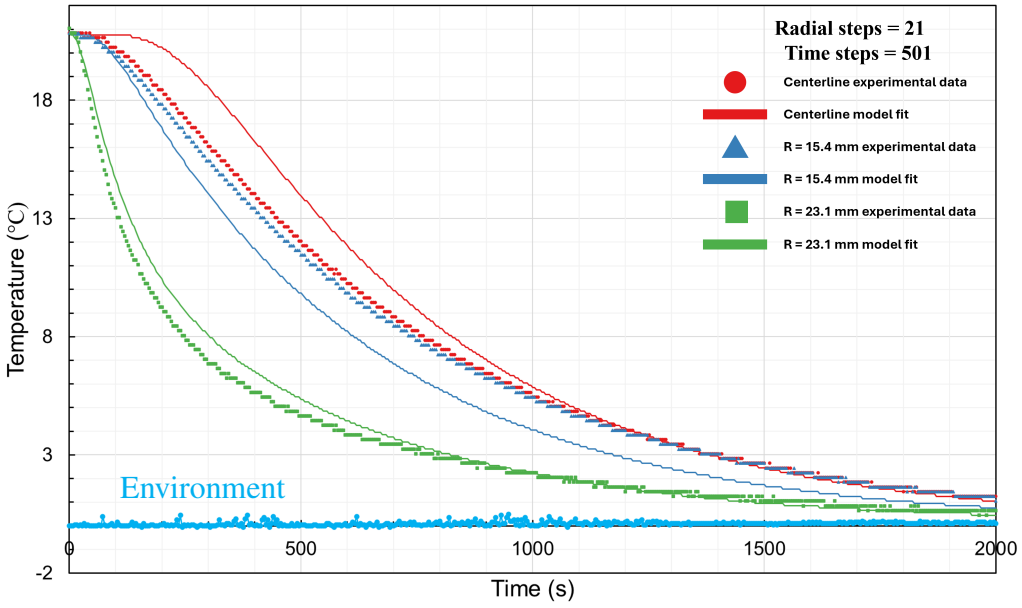

Figure 2.72: Experimental temperature data of support E of an alumina packed bed compared with a model fit of the data as the bed is taken from approximately 21 °C and submerged in an approximately 0 °C ice-water bath. The bed was pressurized to 40 psi gauge with oxygen at room temperature.

2.22 Microfibrous Media Bed Parameter Estimates

Parameter estimation was performed for each of the microfibrous media (MFM) bed experiments presented. The parameters estimated were the effective radial thermal conductivity, k_{er}, and the overall heat transfer coefficient based on the inside wall, U_{id}. Effective thermal conductivity is a lumped parameter that is treated as the thermal conductivity but contains other modes of energy transport, such as radiation and dispersion. The overall heat transfer coefficient is defined in Equation 2.28 [20].

$$\frac{1}{r_{\text{id}}U_{\text{id}}} = \left(\frac{1}{r_{\text{id}}h_{\text{id}}} + \frac{\ln\left(\frac{r_{\text{od}}}{r_{\text{id}}}\right)}{k_{\text{wall}}} + \frac{1}{r_{\text{od}}h_{\text{od}}} \right) \qquad \text{[20]} \tag{2.28}$$

Where

$U_{\text{id}} =$ Overall heat transfer coefficient based on the inside wall

$r_{\text{id}} =$ Inside wall radius

$r_{\text{od}} =$ Outside wall radius

$h_{\text{id}} =$ Inside wall heat transfer coefficient

$h_{\text{od}} =$ Outside wall heat transfer coefficient

$k_{\text{wall}} =$ Thermal conductivity of the tube wall

A separate parameter estimation was performed for each thermocouple couple support, A - E. However, thermocouple supports A and E are not considered to offer useful information. This is because these supports are at the ends of the bed and only have the bed material on one side of the support with quartz wool being on the other side. The information from these supports is included here only for completeness, as these thermocouples were included in the bed for other experiments.

Table 2.17: Estimated thermal parameters for a microfibrous media bed of 4.8% copper by volume and pressurized to 50 psi gauge with argon.

	Effective radial thermal conductivity $\frac{W}{m \cdot K}$			Effective Overall heat transfer coefficient $\frac{W}{m^2 \cdot K}$		
Bed taken from approximately 21 °C and submerged in an approximately 71 °C water bath						
	Best Fit	Lower Bound	Upper Bound	Best Fit	Lower Bound	Upper Bound
Support A	1.1	- 0.028	+ 0.029	100	- 1.2	+ 1.3
Support B	2.4	- 0.097	+ 0.10	95	- 0.85	+ 0.88
Support C	2.8	- 0.13	+ 0.15	89	- 0.73	+ 0.75
Support D	2.7	- 0.11	+ 0.12	120	- 1.2	+ 1.3
Support E	0.92	- 0.017	+ 0.018	170	- 2.8	+ 2.9
Bed taken from approximately 71 °C and submerged in an approximately 20 °C water bath						
	Best Fit	Lower Bound	Upper Bound	Best Fit	Lower Bound	Upper Bound
Support A	1.4	- 0.041	+ 0.043	75	- 0.63	+ 0.64
Support B	2.4	- 0.10	+ 0.11	77	- 0.59	+ 0.60
Support C	2.2	- 0.086	+ 0.092	78	- 0.58	+ 0.60
Support D	2.9	- 0.13	+ 0.14	98	- 0.83	+ 0.85
Support E	0.91	- 0.017	+ 0.017	140	- 1.9	+ 2.0
Bed taken from approximately 0 °C and submerged in an approximately 30 °C water bath						
	Best Fit	Lower Bound	Upper Bound	Best Fit	Lower Bound	Upper Bound
Support A	1.6	- 0.096	+ 0.11	64	- 0.85	+ 0.87
Support B	2.4	- 0.18	+ 0.21	73	- 0.95	+ 0.98
Support C	3.2	- 0.29	+ 0.36	69	- 0.81	+ 0.83
Support D	3.4	- 0.30	+ 0.36	88	- 1.2	+ 1.2
Support E	1.6	- 0.082	+ 0.091	96	- 1.6	+ 1.7
Bed taken from approximately 21 °C and submerged in an approximately 0 °C ice-water bath						
	Best Fit	Lower Bound	Upper Bound	Best Fit	Lower Bound	Upper Bound
Support A	1.6	- 0.12	+ 0.13	74	- 1.5	+ 1.5
Support B	2.1	- 0.18	+ 0.21	86	- 1.7	+ 1.8
Support C	2.6	- 0.25	+ 0.30	86	- 1.6	+ 1.7
Support D	2.8	- 0.25	+ 0.30	120	- 2.8	+ 3.0
Support E	1.6	- 0.098	+ 0.11	120	- 3.3	+ 3.5

[1] The bed is approximately 4.8% by volume copper MFM (Cu-MFM).
[2] The Cu-MFM is approximately 87.5% fibers that are 17 μm in diameter and 6 mm in length and 12.5% fibers that are 6 μm and 3 mm in length.
[3] Overall heat transfer coefficient is based on the inside tube diameter.
[4] Values are rounded to two significant figures.
[5] Confidence is 2-sigma.

Table 2.18: Estimated thermal parameters for a microfibrous media bed of 4.8% copper by volume and pressurized to 50 psi gauge with carbon dioxide.

	Effective radial thermal conductivity $\frac{W}{m \cdot K}$			Effective Overall heat transfer coefficient $\frac{W}{m^2 \cdot K}$		
Bed taken from approximately 21 °C and submerged in an approximately 70 °C water bath						
	Best Fit	Lower Bound	Upper Bound	Best Fit	Lower Bound	Upper Bound
Support A	1.1	- 0.026	+ 0.027	110	- 1.4	+ 1.4
Support B	2.7	- 0.12	+ 0.13	94	- 0.84	+ 0.86
Support C	2.6	- 0.11	+ 0.12	90	- 0.77	+ 0.79
Support D	2.6	- 0.10	+ 0.11	120	- 1.3	+ 1.3
Support E	0.93	- 0.018	+ 0.018	160	- 2.7	+ 2.8
Bed taken from approximately 70 °C and submerged in an approximately 20 °C water bath						
	Best Fit	Lower Bound	Upper Bound	Best Fit	Lower Bound	Upper Bound
Support A	1.4	- 0.043	+ 0.046	71	- 0.59	+ 0.60
Support B	2.4	- 0.10	+ 0.11	75	- 0.58	+ 0.59
Support C	2.2	- 0.086	+ 0.093	75	- 0.57	+ 0.58
Support D	2.7	- 0.11	+ 0.12	95	- 0.81	+ 0.83
Support E	0.91	- 0.017	+ 0.018	130	- 1.8	+ 1.8
Bed taken from approximately 0 °C and submerged in an approximately 21 °C water bath						
	Best Fit	Lower Bound	Upper Bound	Best Fit	Lower Bound	Upper Bound
Support A	1.7	- 0.14	+ 0.17	56	- 0.98	+ 1.0
Support B	2.3	- 0.23	+ 0.28	64	- 1.1	+ 1.1
Support C	2.6	- 0.29	+ 0.36	60	- 0.94	+ 0.98
Support D	2.9	- 0.32	+ 0.41	77	- 1.4	+ 1.4
Support E	0.88	- 0.040	+ 0.044	94	- 2.5	+ 2.6
Bed taken from approximately 21 °C and submerged in an approximately 0 °C ice-water bath						
	Best Fit	Lower Bound	Upper Bound	Best Fit	Lower Bound	Upper Bound
Support A	1.8	- 0.15	+ 0.18	67	- 1.3	+ 1.3
Support B	2.5	- 0.24	+ 0.30	78	- 1.4	+ 1.5
Support C	2.4	- 0.23	+ 0.27	77	- 1.3	+ 1.4
Support D	2.6	- 0.22	+ 0.27	107	- 2.2	+ 2.3
Support E	0.97	- 0.044	+ 0.048	130	- 4.1	+ 4.3

[1] The bed is approximately 4.8% by volume copper MFM (Cu-MFM).
[2] The Cu-MFM is approximately 87.5% fibers that are 17 μm in diameter and 6 mm in length and 12.5% fibers that are 6 μm and 3 mm in length.
[3] Overall heat transfer coefficient is based on the inside tube diameter.
[4] Values are rounded to two significant figures.
[5] Confidence is 2-sigma.

Table 2.19: Estimated thermal parameters for a microfibrous media bed of 4.8% copper by volume and pressurized to 50 psi gauge with helium.

	Effective radial thermal conductivity $\frac{W}{m \cdot K}$			Effective Overall heat transfer coefficient $\frac{W}{m^2 \cdot K}$		
Bed taken from approximately 21 °C and submerged in an approximately 71 °C water bath						
	Best Fit	Lower Bound	Upper Bound	Best Fit	Lower Bound	Upper Bound
Support A	2.3	- 0.066	+ 0.070	300	- 5.8	+ 6.0
Support B	5.0	- 0.26	+ 0.29	250	- 3.5	+ 3.6
Support C	6.1	- 0.36	+ 0.40	260	- 3.6	+ 3.7
Support D	4.0	- 0.15	+ 0.16	390	- 7.6	+ 7.9
Support E	2.4	- 0.062	+ 0.065	450	- 11	+ 11
Bed taken from approximately 71 °C and submerged in an approximately 20 °C water bath						
	Best Fit	Lower Bound	Upper Bound	Best Fit	Lower Bound	Upper Bound
Support A	2.1	- 0.068	+ 0.073	180	- 2.7	+ 2.8
Support B	6.2	- 0.46	+ 0.53	160	- 1.7	+ 1.7
Support C	7.2	- 0.59	+ 0.70	160	- 1.7	+ 1.8
Support D	4.7	- 0.26	+ 0.29	210	- 3.1	+ 3.1
Support E	2.6	- 0.085	+ 0.091	240	- 3.9	+ 4.0
Bed taken from approximately 0 °C and submerged in an approximately 22 °C water bath						
	Best Fit	Lower Bound	Upper Bound	Best Fit	Lower Bound	Upper Bound
Support A	4.1	- 0.53	+ 0.72	120	- 3.0	+ 3.2
Support B	6.4	- 1.1	+ 1.6	140	- 3.2	+ 3.3
Support C	9.7	- 2.2	+ 4.1	130	- 1.7	+ 2.9
Support D	7.9	- 1.5	+ 2.3	160	- 4.0	+ 4.2
Support E	3.5	- 0.35	+ 0.43	180	- 5.5	+ 5.9
Bed taken from approximately 21 °C and submerged in an approximately 0 °C ice-water bath						
	Best Fit	Lower Bound	Upper Bound	Best Fit	Lower Bound	Upper Bound
Support A	2.7	- 0.23	+ 0.27	200	- 7.1	+ 7.7
Support B	5.1	- 0.65	+ 0.86	200	- 6.0	+ 6.3
Support C	6.4	- 0.90	+ 1.3	220	- 6.5	+ 6.9
Support D	4.1	- 0.38	+ 0.46	330	- 13	+ 14
Support E	2.9	- 0.22	+ 0.25	330	- 15	+ 16

[1] The bed is approximately 4.8% by volume copper MFM (Cu-MFM).
[2] The Cu-MFM is approximately 87.5% fibers that are 17 μm in diameter and 6 mm in length and 12.5% fibers that are 6 μm and 3 mm in length.
[3] Overall heat transfer coefficient is based on the inside tube diameter.
[4] Values are rounded to two significant figures.
[5] Confidence is 2-sigma.

Table 2.20: Estimated thermal parameters for a microfibrous media bed of 4.8% copper by volume and pressurized to 50 psi gauge with hydrogen.

	Effective radial thermal conductivity $\frac{W}{m \cdot K}$			Effective Overall heat transfer coefficient $\frac{W}{m^2 \cdot K}$		
Bed taken from approximately 21 °C and submerged in an approximately 69 °C water bath						
	Best Fit	Lower Bound	Upper Bound	Best Fit	Lower Bound	Upper Bound
Support A	2.2	- 0.060	+ 0.063	340	- 7.7	+ 8.0
Support B	5.5	- 0.30	+ 0.34	260	- 3.9	+ 4.1
Support C	5.3	- 0.27	+ 0.30	280	- 4.3	+ 4.4
Support D	4.2	- 0.17	+ 0.19	390	- 8.0	+ 8.3
Support E	2.6	- 0.071	+ 0.075	440	- 11	+ 11
Bed taken from approximately 69 °C and submerged in an approximately 20 °C water bath						
	Best Fit	Lower Bound	Upper Bound	Best Fit	Lower Bound	Upper Bound
Support A	2.3	- 0.079	+ 0.085	190	- 3.0	+ 3.1
Support B	6.7	- 0.54	+ 0.64	170	- 2.0	+ 2.0
Support C	4.5	- 0.25	+ 0.28	190	- 2.5	+ 2.6
Support D	5.6	- 0.36	+ 0.42	210	- 3.1	+ 3.2
Support E	2.8	- 0.10	+ 0.11	260	- 4.6	+ 4.7
Bed taken from approximately 0 °C and submerged in an approximately 19 °C water bath						
	Best Fit	Lower Bound	Upper Bound	Best Fit	Lower Bound	Upper Bound
Support A	2.5	- 0.26	+ 0.33	150	- 5.5	+ 6.0
Support B	9.8	- 2.5	+ 5.0	130	- 1.9	+ 3.5
Support C	Failed to fit.					
Support D	9.6	- 2.3	+ 4.5	150	- 2.6	+ 4.4
Support E	3.4	- 0.39	+ 0.49	180	- 6.2	+ 6.7
Bed taken from approximately 21 °C and submerged in an approximately 0 °C ice-water bath						
	Best Fit	Lower Bound	Upper Bound	Best Fit	Lower Bound	Upper Bound
Support A	2.0	- 0.12	+ 0.14	280	- 13	+ 14
Support B	5.4	- 0.68	+ 0.89	220	- 6.6	+ 7.0
Support C	5.6	- 0.69	+ 0.90	240	- 7.7	+ 8.2
Support D	3.7	- 0.31	+ 0.36	340	- 14	+ 15
Support E	2.7	- 0.18	+ 0.20	360	- 17	+ 18

[1] The bed is approximately 4.8% by volume copper MFM (Cu-MFM).
[2] The Cu-MFM is approximately 87.5% fibers that are 17 μm in diameter and 6 mm in length and 12.5% fibers that are 6 μm and 3 mm in length.
[3] Overall heat transfer coefficient is based on the inside tube diameter.
[4] Values are rounded to two significant figures.
[5] Confidence is 2-sigma.

Table 2.21: Estimated thermal parameters for a microfibrous media bed of 4.8% copper by volume and pressurized to 50 psi gauge with oxygen.

	Effective radial thermal conductivity $\frac{W}{m \cdot K}$			Effective Overall heat transfer coefficient $\frac{W}{m^2 \cdot K}$		
Bed taken from approximately 21 °C and submerged in an approximately 75 °C water bath						
	Best Fit	Lower Bound	Upper Bound	Best Fit	Lower Bound	Upper Bound
Support A	1.2	- 0.027	+ 0.028	140	- 1.8	+ 1.8
Support B	2.9	- 0.11	+ 0.12	120	- 1.1	+ 1.1
Support C	3.1	- 0.13	+ 0.14	110	- 0.97	+ 1.0
Support D	2.9	- 0.10	+ 0.11	160	- 1.6	+ 1.7
Support E	1.1	- 0.019	+ 0.019	200	- 3.4	+ 3.5
Bed taken from approximately 78 °C and submerged in an approximately 20 °C water bath						
	Best Fit	Lower Bound	Upper Bound	Best Fit	Lower Bound	Upper Bound
Support A	1.4	- 0.035	+ 0.037	95	- 0.85	+ 0.86
Support B	2.9	- 0.12	+ 0.13	92	- 0.68	+ 0.69
Support C	2.9	- 0.12	+ 0.13	93	- 0.67	+ 0.68
Support D	3.4	- 0.14	+ 0.15	120	- 1.0	+ 1.0
Support E	1.1	- 0.019	+ 0.019	160	- 2.0	+ 2.1
Bed taken from approximately 0 °C and submerged in an approximately 20 °C water bath						
	Best Fit	Lower Bound	Upper Bound	Best Fit	Lower Bound	Upper Bound
Support A	1.9	- 0.18	+ 0.22	67	- 1.3	+ 1.4
Support B	2.8	- 0.31	+ 0.40	76	- 1.4	+ 1.5
Support C	2.5	- 0.25	+ 0.31	74	- 1.3	+ 1.4
Support D	3.6	- 0.45	+ 0.60	89	- 1.8	+ 1.9
Support E	1.0	- 0.053	+ 0.058	110	- 3.3	+ 3.5
Bed taken from approximately 20 °C and submerged in an approximately 0 °C ice-water bath						
	Best Fit	Lower Bound	Upper Bound	Best Fit	Lower Bound	Upper Bound
Support A	1.7	- 0.14	+ 0.16	89	- 2.2	+ 2.3
Support B	2.9	- 0.31	+ 0.39	98	- 2.1	+ 2.2
Support C	2.7	- 0.27	+ 0.33	100	- 2.2	+ 2.3
Support D	2.9	- 0.27	+ 0.33	140	- 3.7	+ 3.9
Support E	1.1	- 0.055	+ 0.060	170	- 6.6	+ 7.1

[1] The bed is approximately 4.8% by volume copper MFM (Cu-MFM).
[2] The Cu-MFM is approximately 87.5% fibers that are 17 μm in diameter and 6 mm in length and 12.5% fibers that are 6 μm and 3 mm in length.
[3] Overall heat transfer coefficient is based on the inside tube diameter.
[4] Values are rounded to two significant figures.
[5] Confidence is 2-sigma.

Table 2.22: Estimated thermal parameters for a microfibrous media bed of 4.8% copper by volume and reduced to vacuum.

	Effective radial thermal conductivity $\frac{W}{m \cdot K}$			Effective Overall heat transfer coefficient $\frac{W}{m^2 \cdot K}$		
Bed taken from approximately 22 °C and submerged in an approximately 70 °C water bath						
	Best Fit	Lower Bound	Upper Bound	Best Fit	Lower Bound	Upper Bound
Support A	0.73	- 0.019	+ 0.020	24	- 0.13	+ 0.13
Support B	0.58	- 0.016	+ 0.017	27	- 0.19	+ 0.19
Support C	0.46	- 0.010	+ 0.010	28	- 0.20	+ 0.20
Support D	0.58	- 0.014	+ 0.015	31	- 0.23	+ 0.23
Support E	0.41	- 0.0078	+ 0.0080	37	- 0.33	+ 0.34
Bed taken from approximately 70 °C and submerged in an approximately 19 °C water bath						
	Best Fit	Lower Bound	Upper Bound	Best Fit	Lower Bound	Upper Bound
Support A	Failed to fit.					
Support B	Failed to fit.					
Support C	2.1	- 0.29	+ 0.40	18	- 0.14	+ 0.14
Support D	Thermocouple D1 did not record data, so no fit was performed.					
Support E	0.63	- 0.015	+ 0.016	29	- 0.18	+ 0.18
Bed taken from approximately 0 °C and submerged in an approximately 19 °C water bath						
	Best Fit	Lower Bound	Upper Bound	Best Fit	Lower Bound	Upper Bound
Support A	1.7	- 0.27	+ 0.39	12	- 0.096	+ 0.098
Support B	0.62	- 0.043	+ 0.050	13	- 0.11	+ 0.11
Support C	0.45	- 0.024	+ 0.027	12	- 0.10	+ 0.11
Support D	0.90	- 0.082	+ 0.099	13	- 0.11	+ 0.11
Support E	0.28	- 0.0096	+ 0.10	17	- 0.18	+ 0.19
Bed taken from approximately 22 °C and submerged in an approximately 0 °C ice-water bath						
	Best Fit	Lower Bound	Upper Bound	Best Fit	Lower Bound	Upper Bound
Support A	Failed to fit.					
Support B	Failed to fit.					
Support C	1.6	- 0.38	+ 0.72	14	- 0.19	+ 0.19
Support D	2.0	- 0.52	+ 1.1	16	- 0.25	+ 0.26
Support E	0.40	- 0.031	+ 0.037	20	- 0.42	+ 0.44

[1] The bed is approximately 4.8% by volume copper MFM (Cu-MFM).
[2] The Cu-MFM is approximately 87.5% fibers that are 17 µm in diameter and 6 mm in length and 12.5% fibers that are 6 µm and 3 mm in length.
[3] Overall heat transfer coefficient is based on the inside tube diameter.
[4] Values are rounded to two significant figures.
[5] Confidence is 2-sigma.

2.23 Comparison of Microfibrous Media Bed Experimental Data and Model Fits

For each parameter estimation in section 2.22, a graph was produced comparing the temperature profiles used for the estimation and the temperature profiles generated at the corresponding positions using the estimated parameters (here called model fits). The experimental data is represented by markers, while the model fits are represented by continuous lines. It is noted that due to the number of data points and how close some temperature profiles are to one another, they can be difficult to distinguish.

Comparison graphs for the experimental data and model fits for each thermocouple couple support, A - E, within the bed are shown here. Also, as mentioned in section 2.22 thermocouple supports A and E are not considered to offer useful information. This is because these supports are at the ends of the bed and only have the bed material on one side of the support with quartz wool being on the other side. The comparison graphs for these supports are included here only for completeness, as these thermocouples were included in the bed for other experiments.

2.24 Experimental and Model Comparisons for a Microfibrous Media (MFM) Bed Containing Stagnant Argon Taken from Approximately 21 °C and Submerged in a 71 °C Water Bath

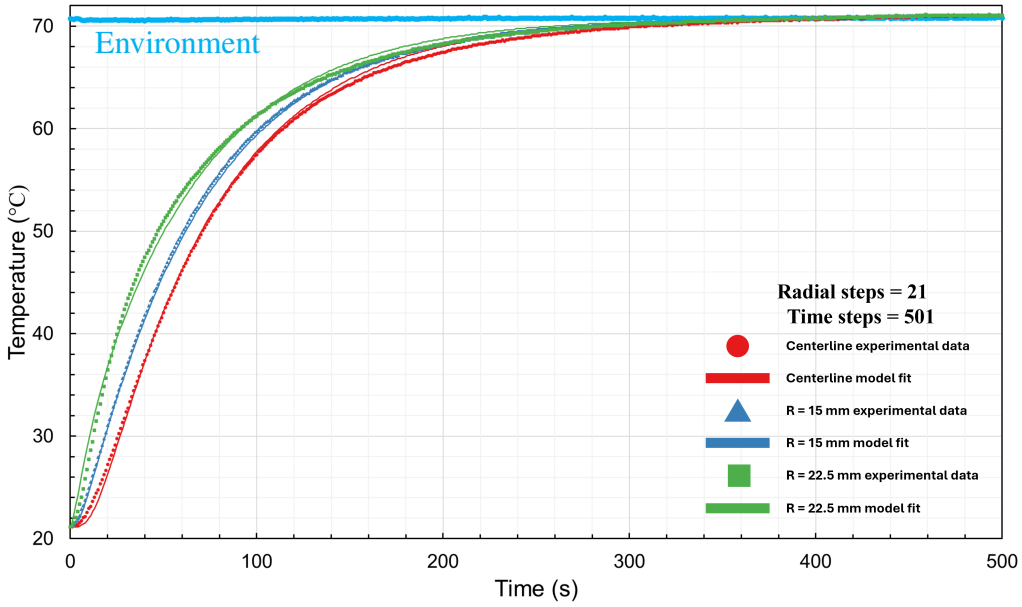

Figure 2.73: Experimental temperature data of support A of a microfibrous media bed compared with a model fit of the data as the bed is taken from approximately 21 °C and submerged in an approximately 71 °C water bath. The bed was pressurized to 50 psi gauge with argon at room temperature.

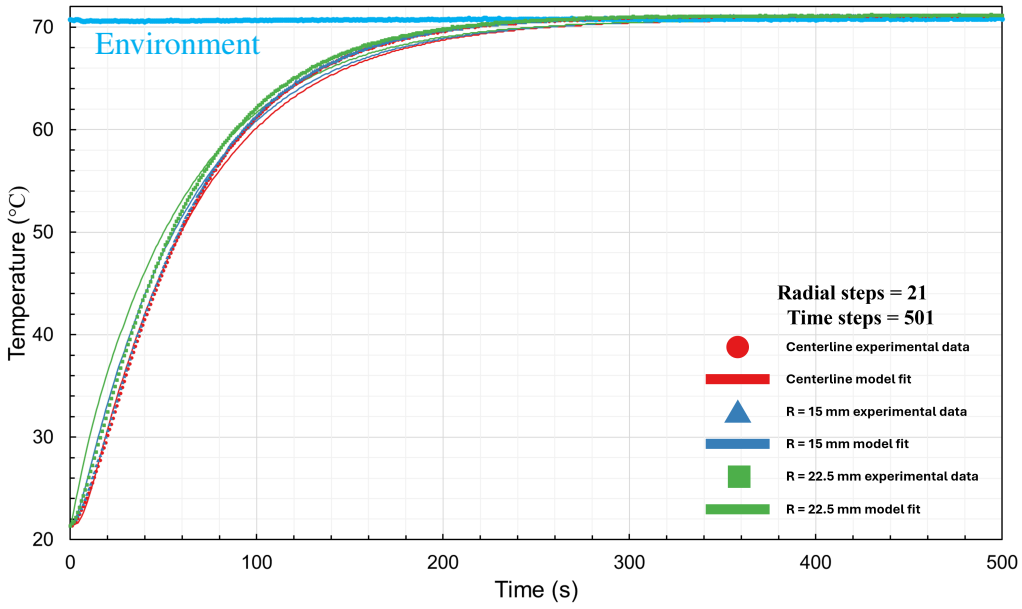

Figure 2.74: Experimental temperature data of support B of a microfibrous media bed compared with a model fit of the data as the bed is taken from approximately 21 °C and submerged in an approximately 71 °C water bath. The bed was pressurized to 50 psi gauge with argon at room temperature.

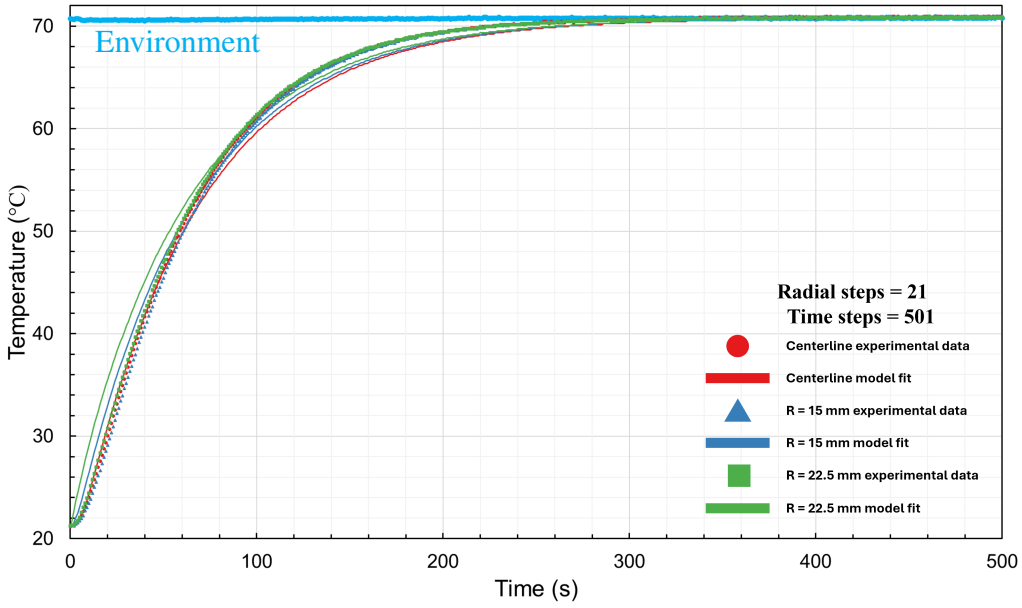

Figure 2.75: Experimental temperature data of support C of a microfibrous media bed compared with a model fit of the data as the bed is taken from approximately 21 °C and submerged in an approximately 71 °C water bath. The bed was pressurized to 50 psi gauge with argon at room temperature.

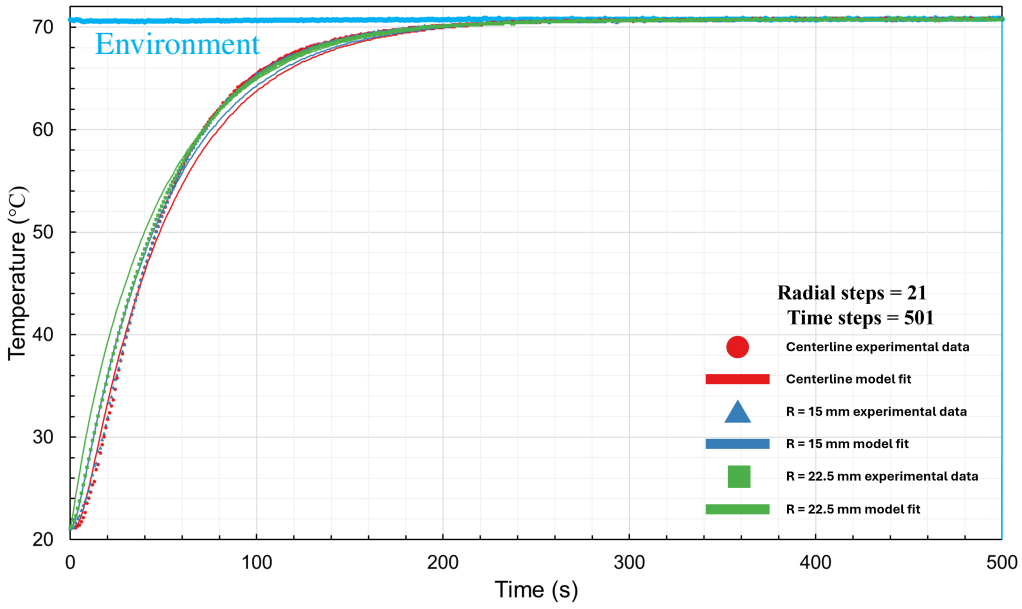

Figure 2.76: Experimental temperature data of support D of a microfibrous media bed compared with a model fit of the data as the bed is taken from approximately 21 °C and submerged in an approximately 71 °C water bath. The bed was pressurized to 50 psi gauge with argon at room temperature.

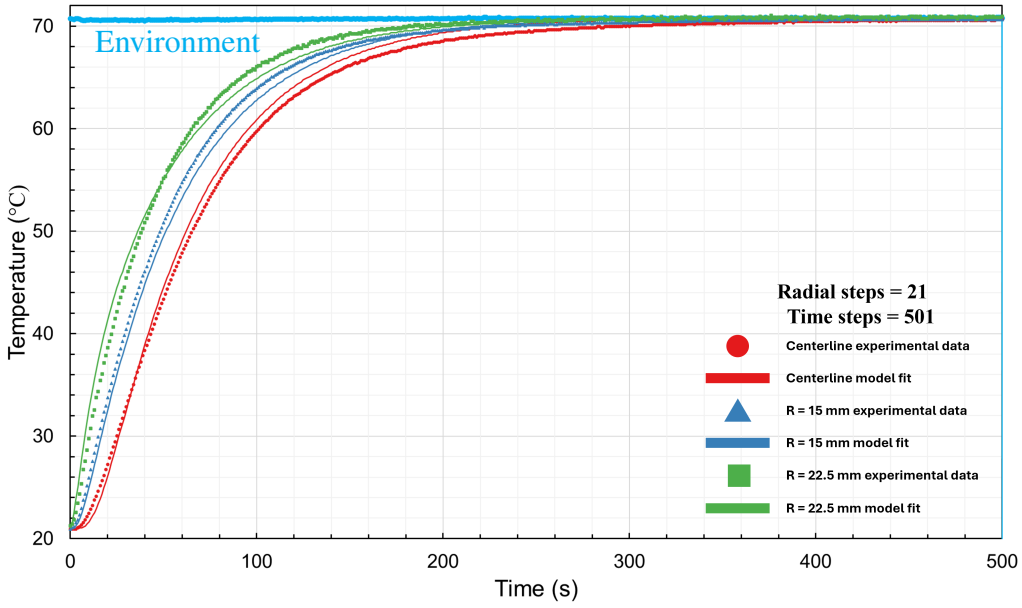

Figure 2.77: Experimental temperature data of support E of a microfibrous media bed compared with a model fit of the data as the bed is taken from approximately 21 °C and submerged in an approximately 71 °C water bath. The bed was pressurized to 50 psi gauge with argon at room temperature.

2.25 Experimental and Model Comparisons for a Microfibrous Media (MFM) Bed Containing Stagnant Argon Taken from Approximately 71 °C and Submerged in a 20 °C Water Bath

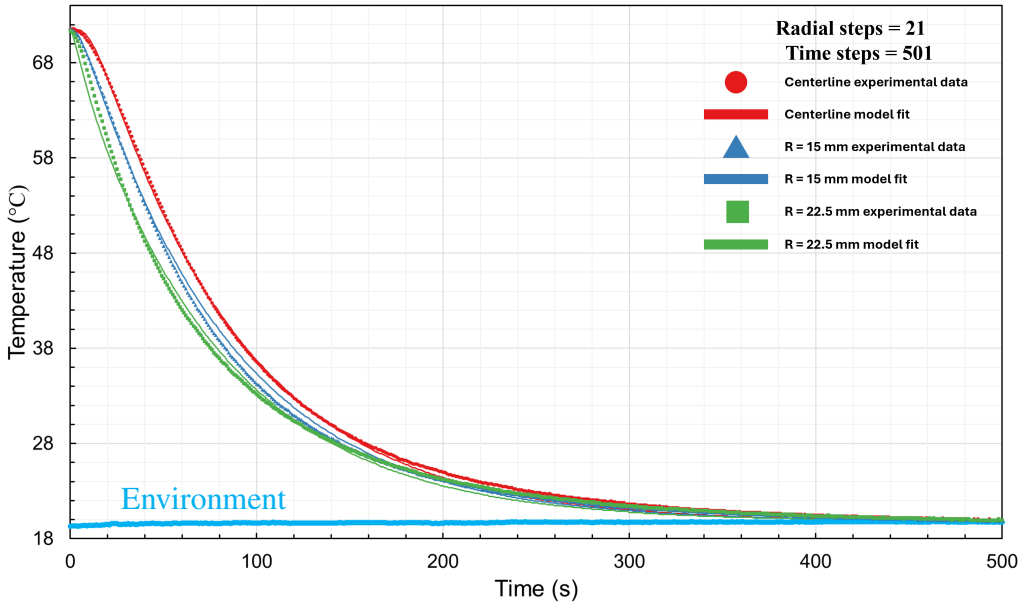

Figure 2.78: Experimental temperature data of support A of a microfibrous media bed compared with a model fit of the data as the bed is taken from approximately 71 °C and submerged in an approximately 20 °C water bath. The bed was pressurized to 50 psi gauge with argon at room temperature.

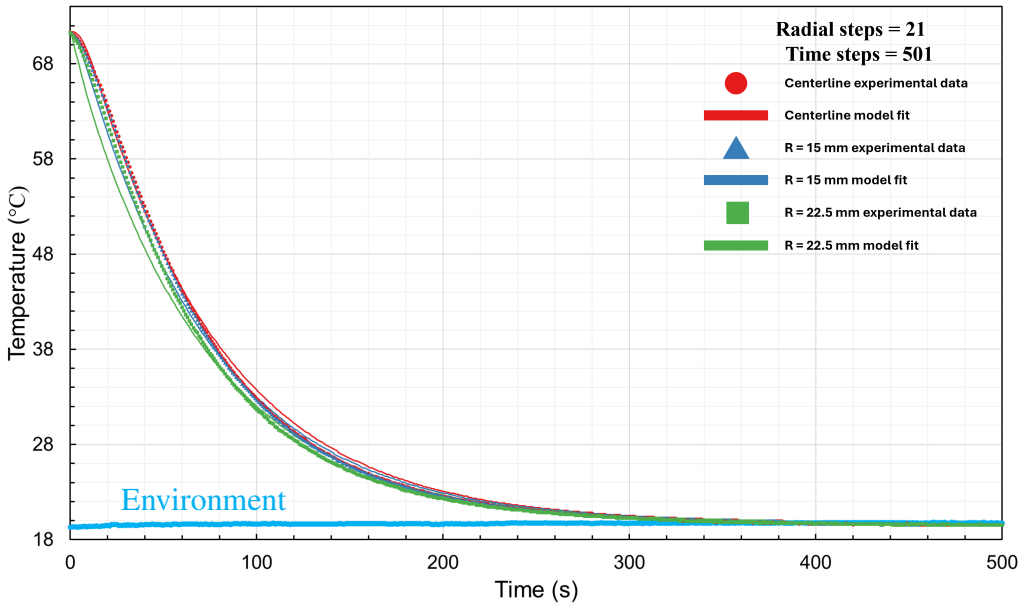

Figure 2.79: Experimental temperature data of support B of a microfibrous media bed compared with a model fit of the data as the bed is taken from approximately 71 °C and submerged in an approximately 20 °C water bath. The bed was pressurized to 50 psi gauge with argon at room temperature.

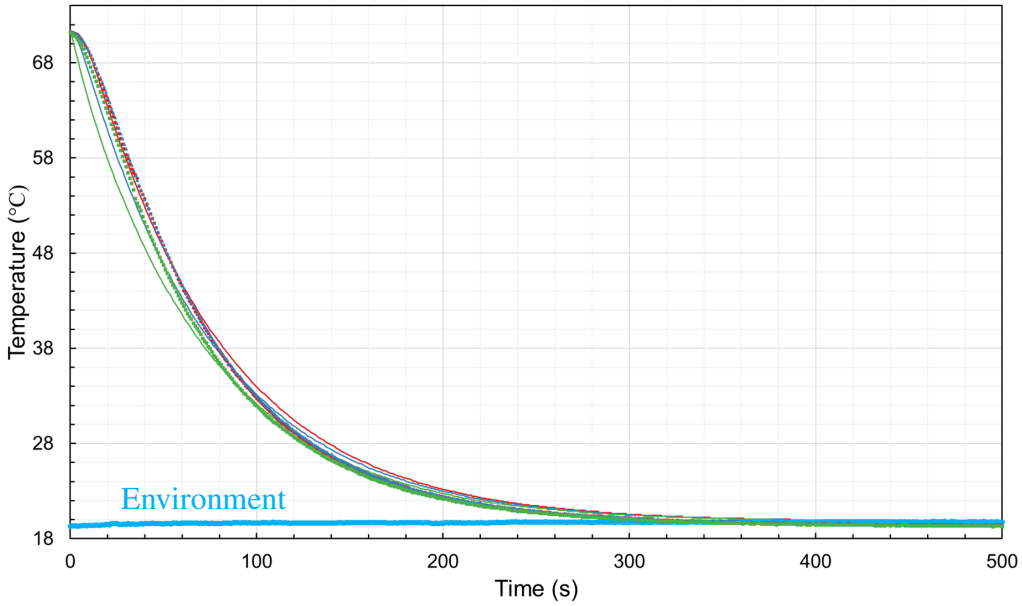

Figure 2.80: Experimental temperature data of support C of a microfibrous media bed compared with a model fit of the data as the bed is taken from approximately 71 °C and submerged in an approximately 20 °C water bath. The bed was pressurized to 50 psi gauge with argon at room temperature.

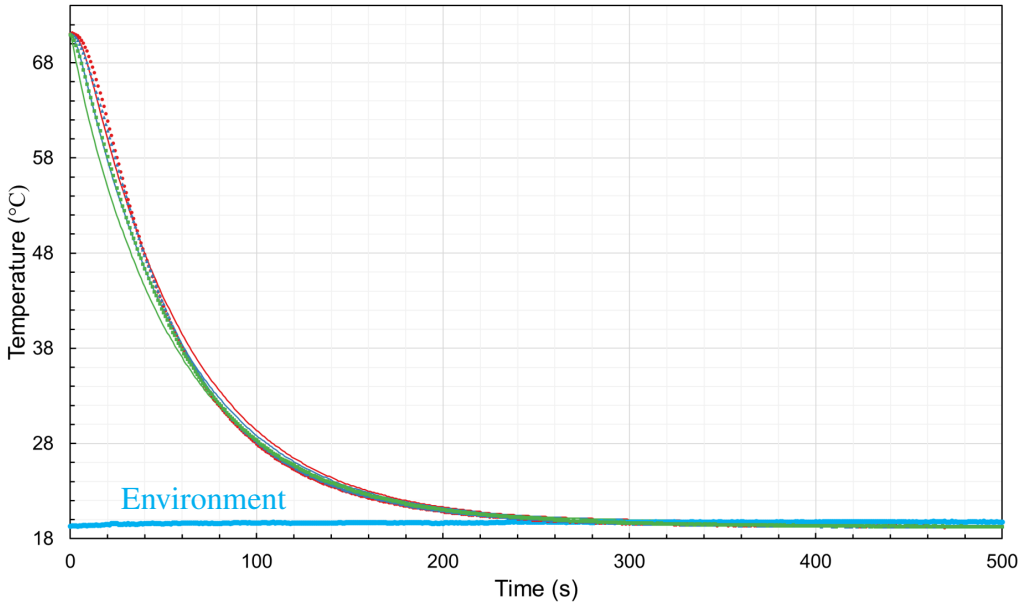

Figure 2.81: Experimental temperature data of support D of a microfibrous media bed compared with a model fit of the data as the bed is taken from approximately 71 °C and submerged in an approximately 20 °C water bath. The bed was pressurized to 50 psi gauge with argon at room temperature.

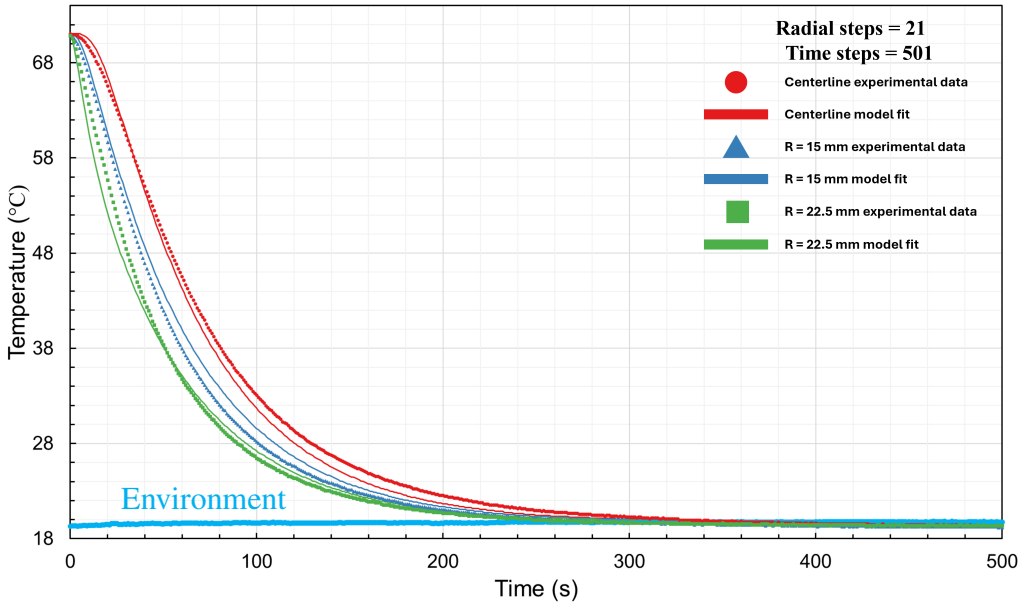

Figure 2.82: Experimental temperature data of support E of a microfibrous media bed compared with a model fit of the data as the bed is taken from approximately 71 °C and submerged in an approximately 20 °C water bath. The bed was pressurized to 50 psi gauge with argon at room temperature.

2.26 Experimental and Model Comparisons for a Microfibrous Media (MFM) Bed Containing Stagnant Argon Taken from Approximately 0 °C and Submerged in a 30 °C Water Bath

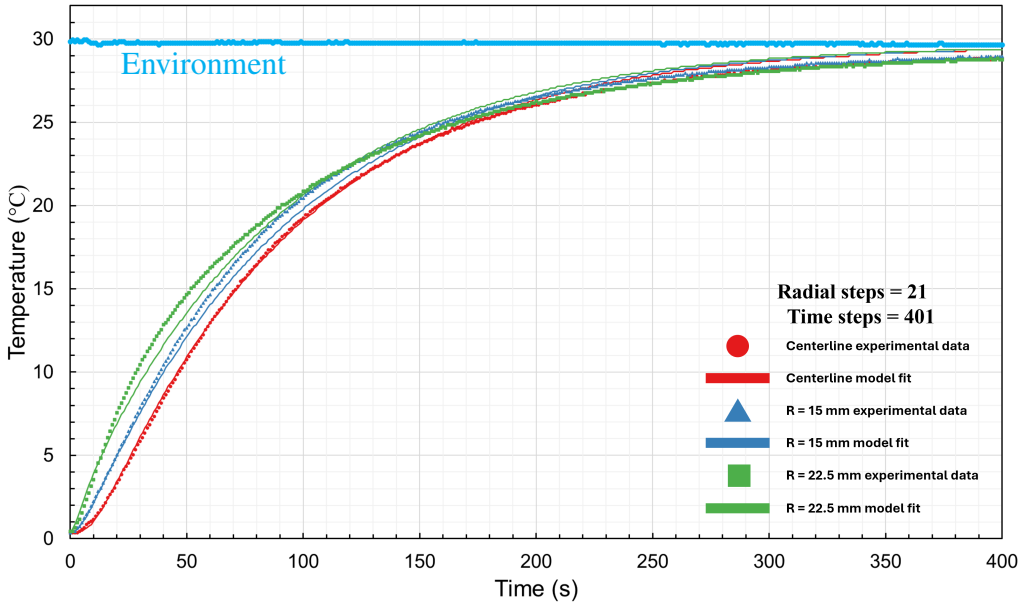

Figure 2.83: Experimental temperature data of support A of a microfibrous media bed compared with a model fit of the data as the bed is taken from approximately 0 °C and submerged in an approximately 20 °C water bath. The bed was pressurized to 50 psi gauge with argon at room temperature.

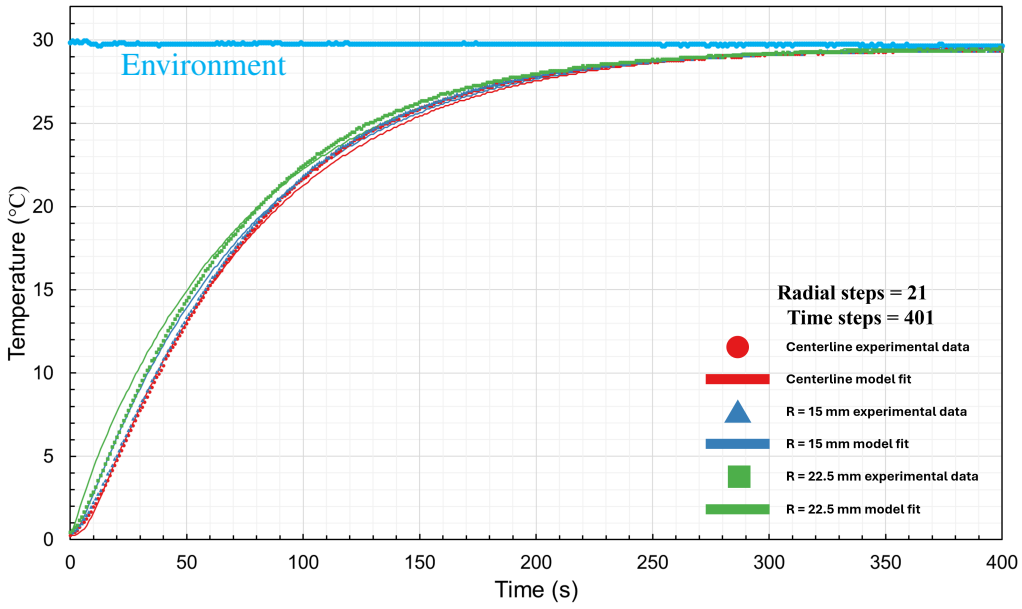

Figure 2.84: Experimental temperature data of support B of a microfibrous media bed compared with a model fit of the data as the bed is taken from approximately 0 °C and submerged in an approximately 20 °C water bath. The bed was pressurized to 50 psi gauge with argon at room temperature.

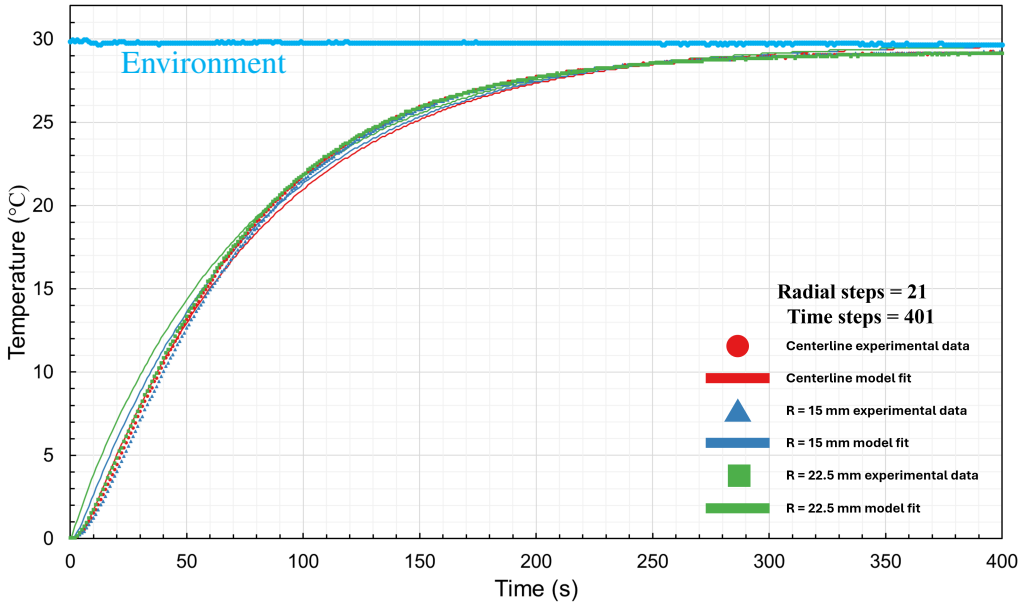

Figure 2.85: Experimental temperature data of support C of a microfibrous media bed compared with a model fit of the data as the bed is taken from approximately 0 °C and submerged in an approximately 20 °C water bath. The bed was pressurized to 50 psi gauge with argon at room temperature.

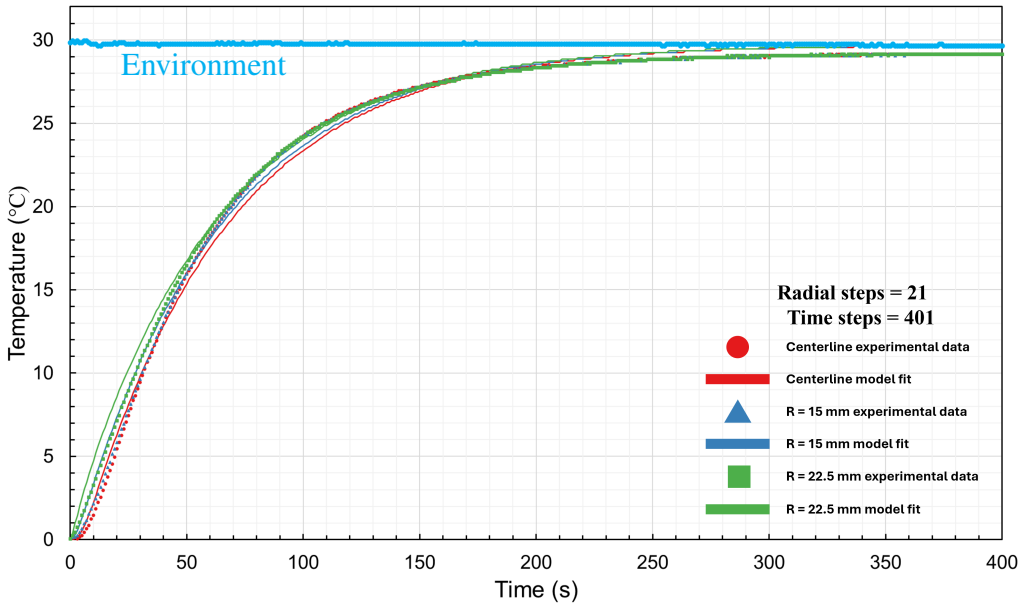

Figure 2.86: Experimental temperature data of support D of a microfibrous media bed compared with a model fit of the data as the bed is taken from approximately 0 °C and submerged in an approximately 20 °C water bath. The bed was pressurized to 50 psi gauge with argon at room temperature.

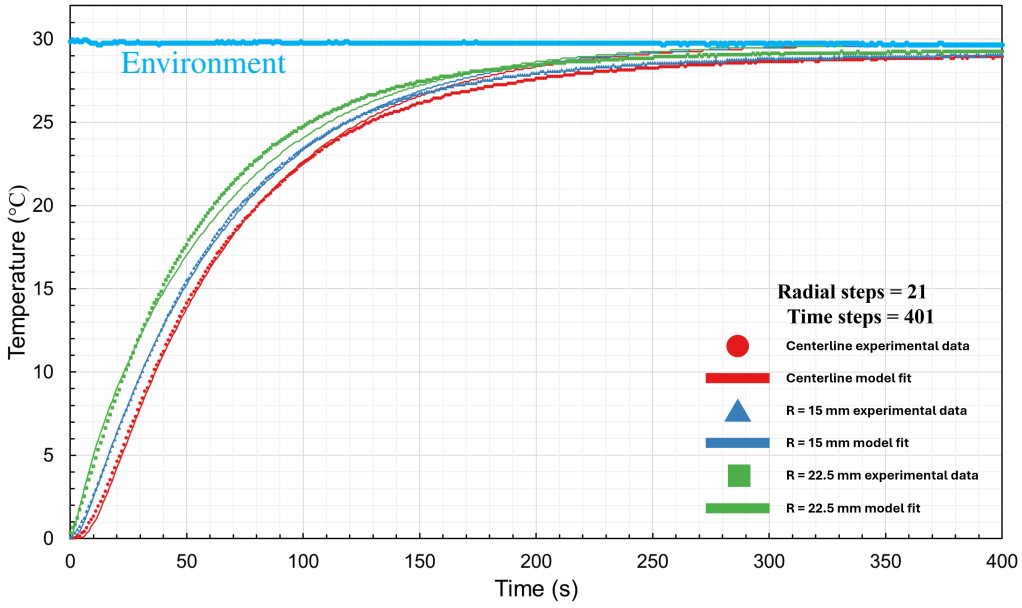

Figure 2.87: Experimental temperature data of support E of a microfibrous media bed compared with a model fit of the data as the bed is taken from approximately 0 °C and submerged in an approximately 20 °C water bath. The bed was pressurized to 50 psi gauge with argon at room temperature.

2.27 Experimental and Model Comparisons for a Microfibrous Media (MFM) Bed Containing Stagnant Argon Taken from Approximately 21 °C and Submerged in a 0 °C Ice-Water Bath

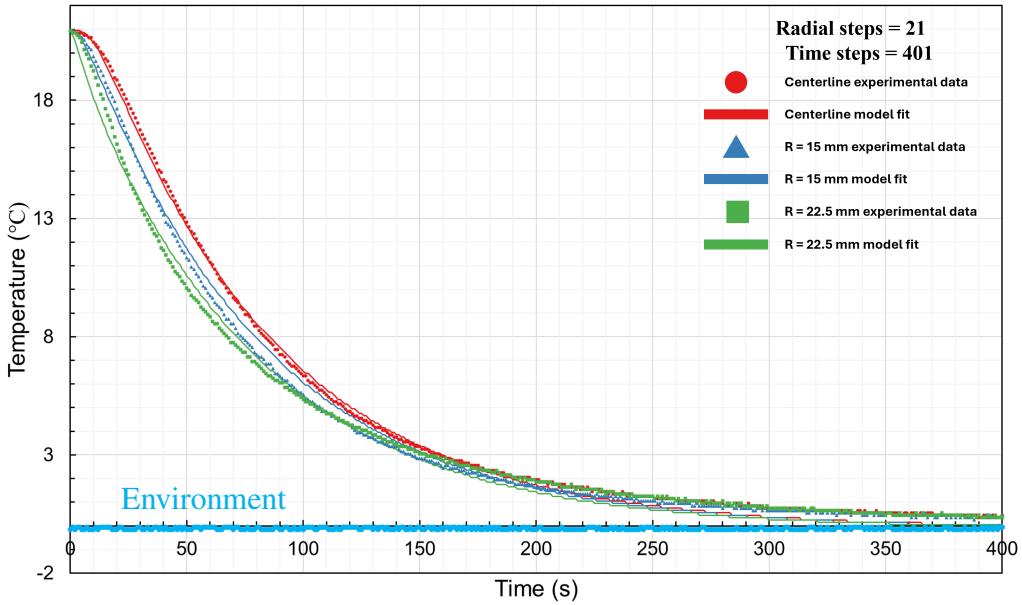

Figure 2.88: Experimental temperature data of support A of a microfibrous media bed compared with a model fit of the data as the bed is taken from approximately 21 °C and submerged in an approximately 0 °C ice-water bath. The bed was pressurized to 50 psi gauge with argon at room temperature.

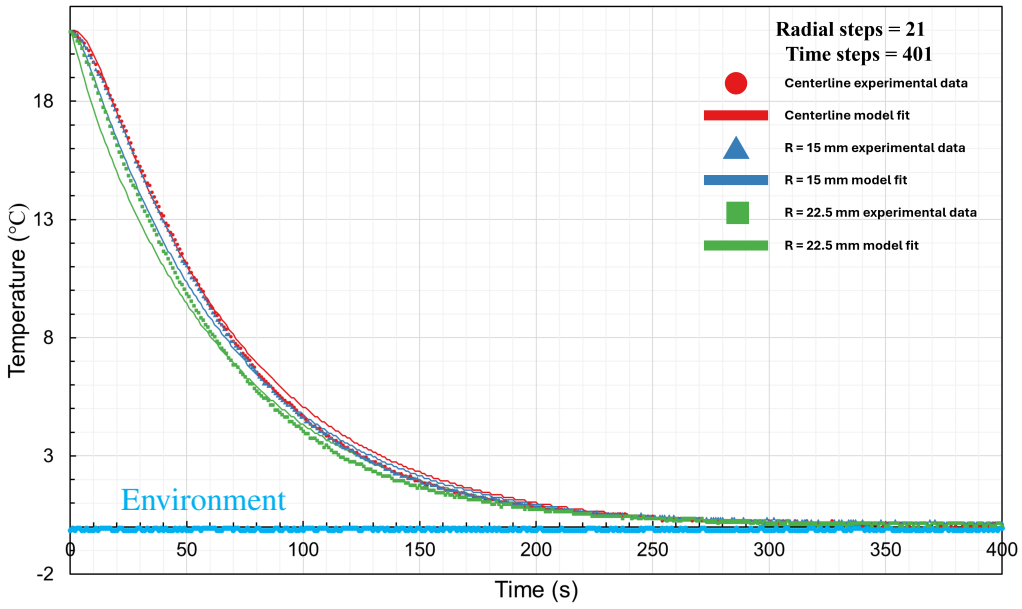

Figure 2.89: Experimental temperature data of support B of a microfibrous media bed compared with a model fit of the data as the bed is taken from approximately 21 °C and submerged in an approximately 0 °C ice-water bath. The bed was pressurized to 50 psi gauge with argon at room temperature.

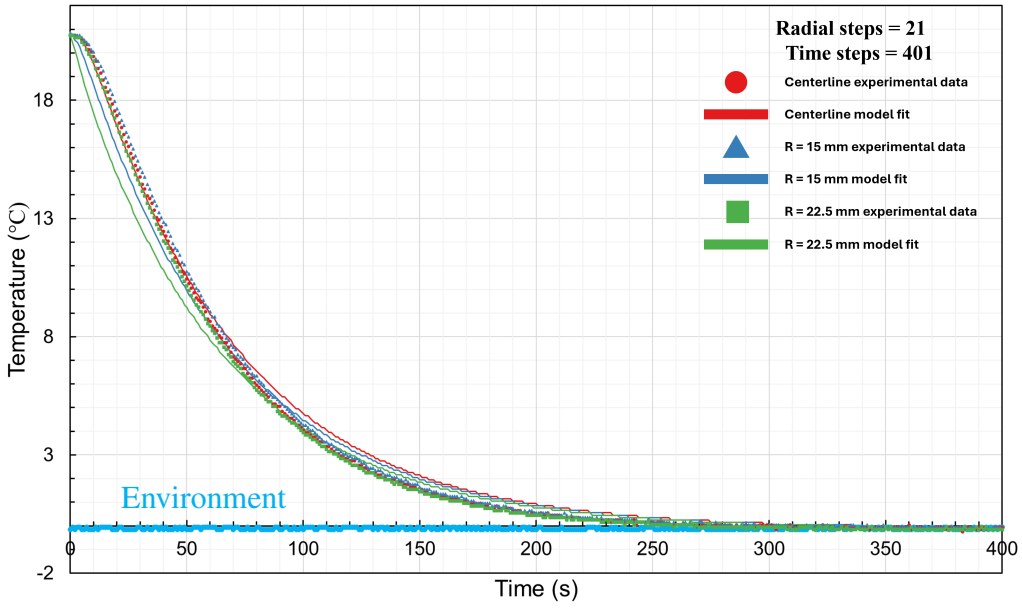

Figure 2.90: Experimental temperature data of support C of a microfibrous media bed compared with a model fit of the data as the bed is taken from approximately 21 °C and submerged in an approximately 0 °C ice-water bath. The bed was pressurized to 50 psi gauge with argon at room temperature.

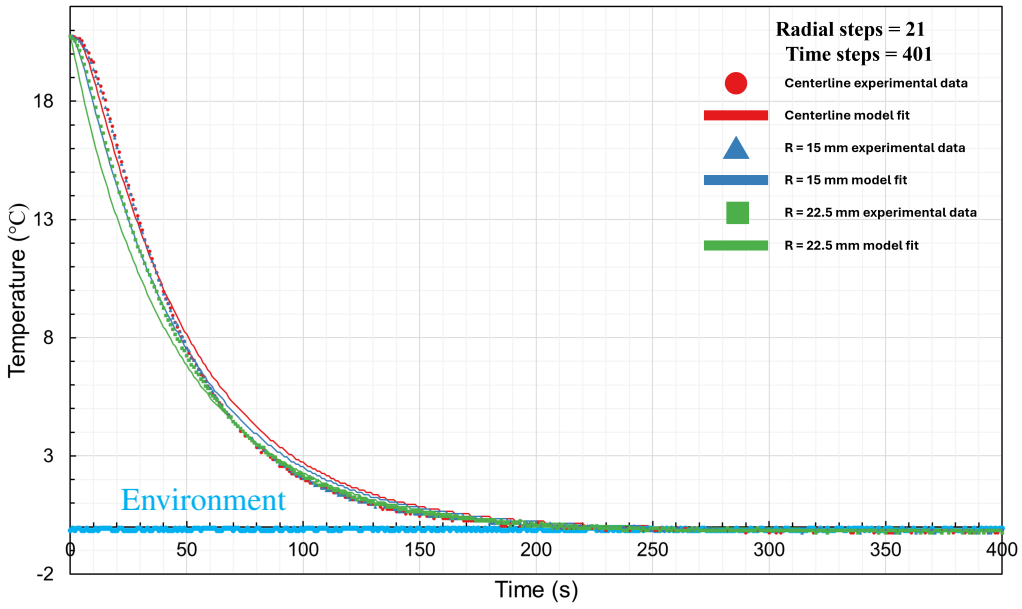

Figure 2.91: Experimental temperature data of support D of a microfibrous media bed compared with a model fit of the data as the bed is taken from approximately 21 °C and submerged in an approximately 0 °C ice-water bath. The bed was pressurized to 50 psi gauge with argon at room temperature.

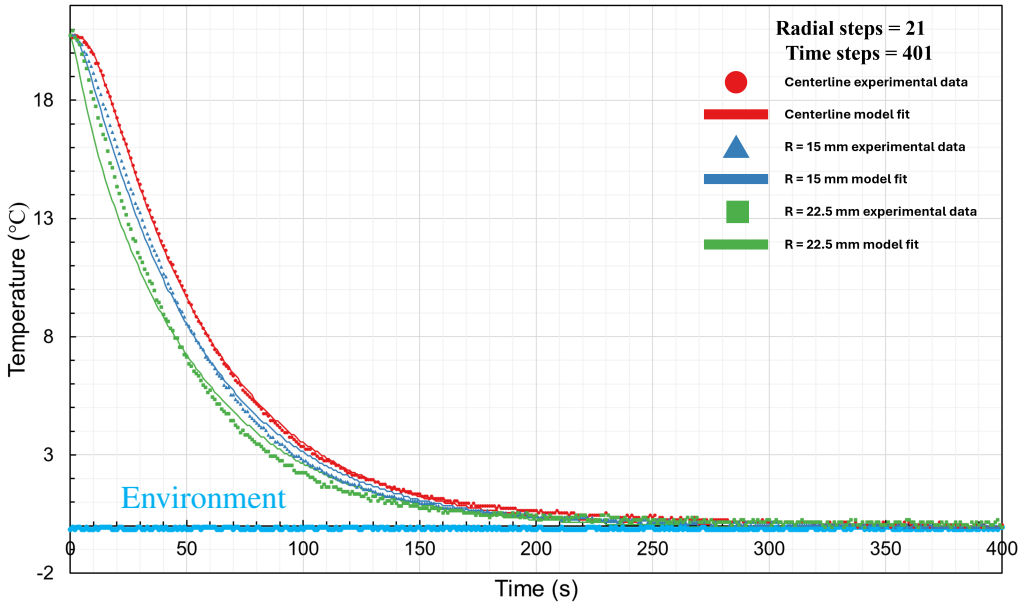

Figure 2.92: Experimental temperature data of support E of a microfibrous media bed compared with a model fit of the data as the bed is taken from approximately 21 °C and submerged in an approximately 0 °C ice-water bath. The bed was pressurized to 50 psi gauge with argon at room temperature.

2.28 Experimental and Model comparisons for a Microfibrous Media (MFM) Bed Containing Stagnant Carbon Dioxide Taken from Approximately 21 °C and Submerged in a 71 °C Water Bath

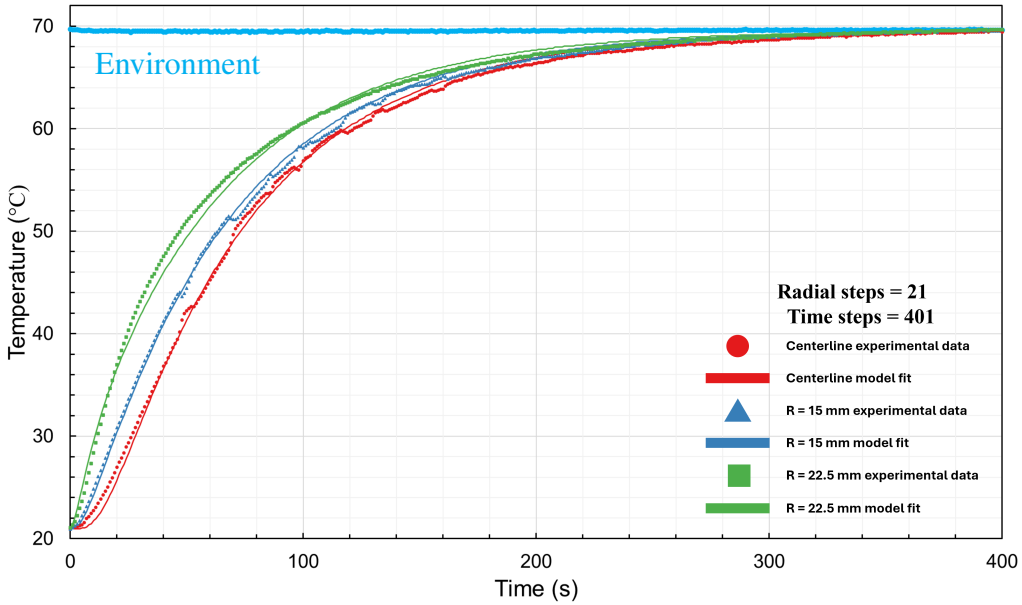

Figure 2.93: Experimental temperature data of support A of a microfibrous media bed compared with a model fit of the data as the bed is taken from approximately 21 °C and submerged in an approximately 70 °C water bath. The bed was pressurized to 50 psi gauge with carbon dioxide at room temperature.

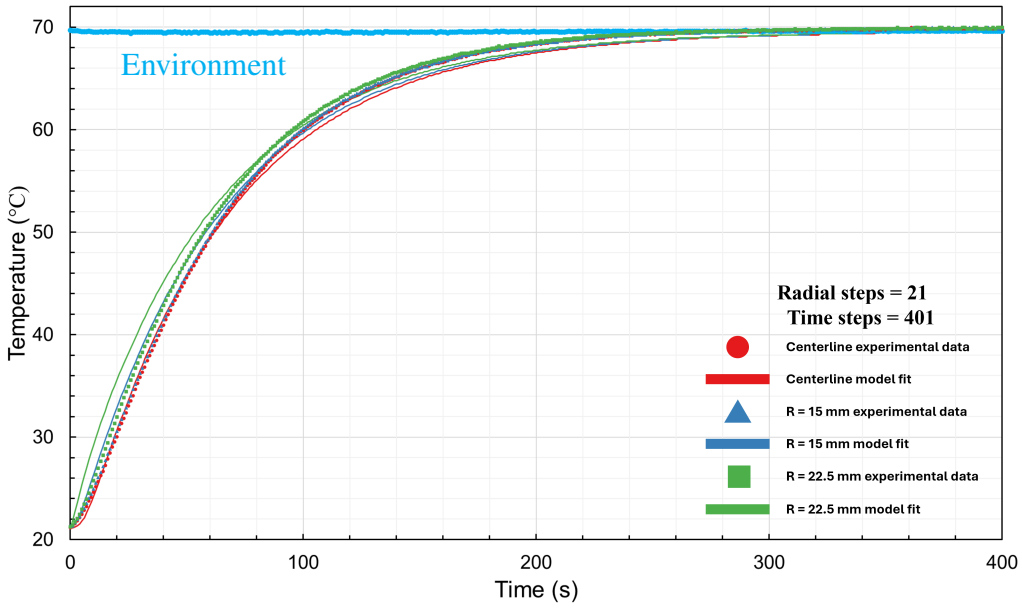

Figure 2.94: Experimental temperature data of support B of a microfibrous media bed compared with a model fit of the data as the bed is taken from approximately 21 °C and submerged in an approximately 70 °C water bath. The bed was pressurized to 50 psi gauge with carbon dioxide at room temperature.

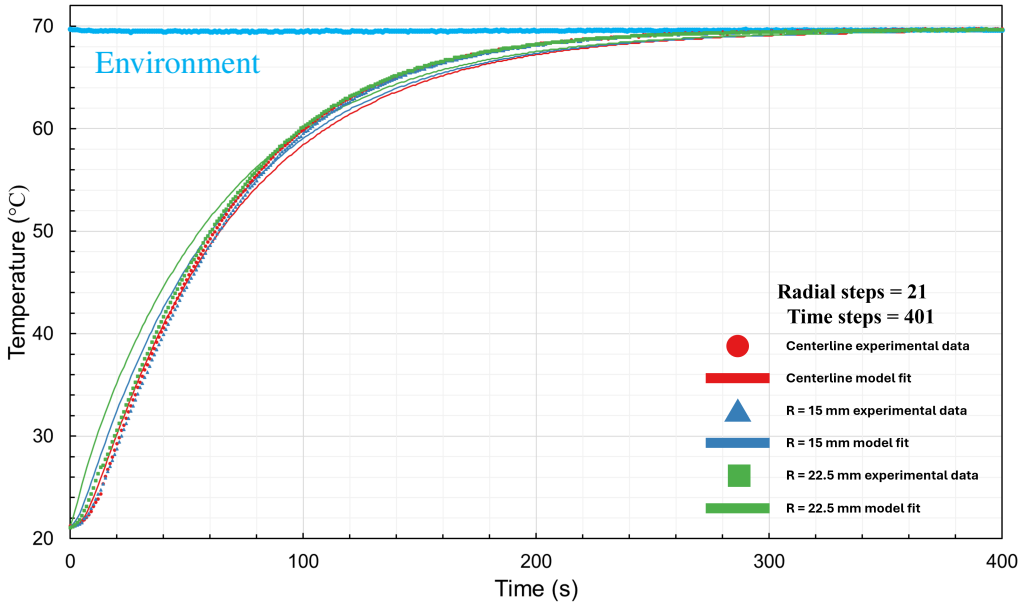

Figure 2.95: Experimental temperature data of support C of a microfibrous media bed compared with a model fit of the data as the bed is taken from approximately 21 °C and submerged in an approximately 70 °C water bath. The bed was pressurized to 50 psi gauge with carbon dioxide at room temperature.

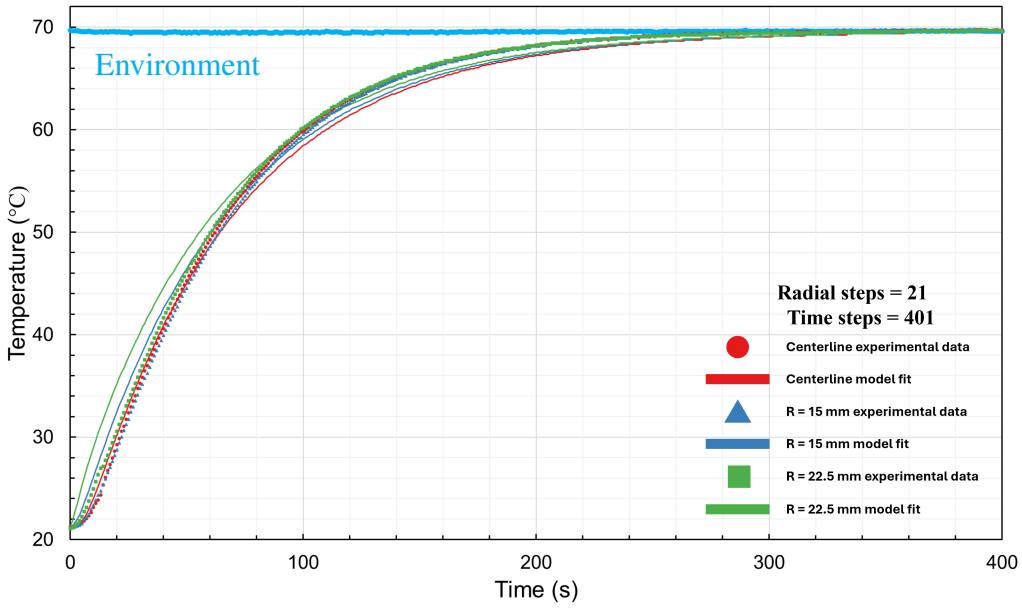

Figure 2.96: Experimental temperature data of support D of a microfibrous media bed compared with a model fit of the data as the bed is taken from approximately 21 °C and submerged in an approximately 70 °C water bath. The bed was pressurized to 50 psi gauge with carbon dioxide at room temperature.

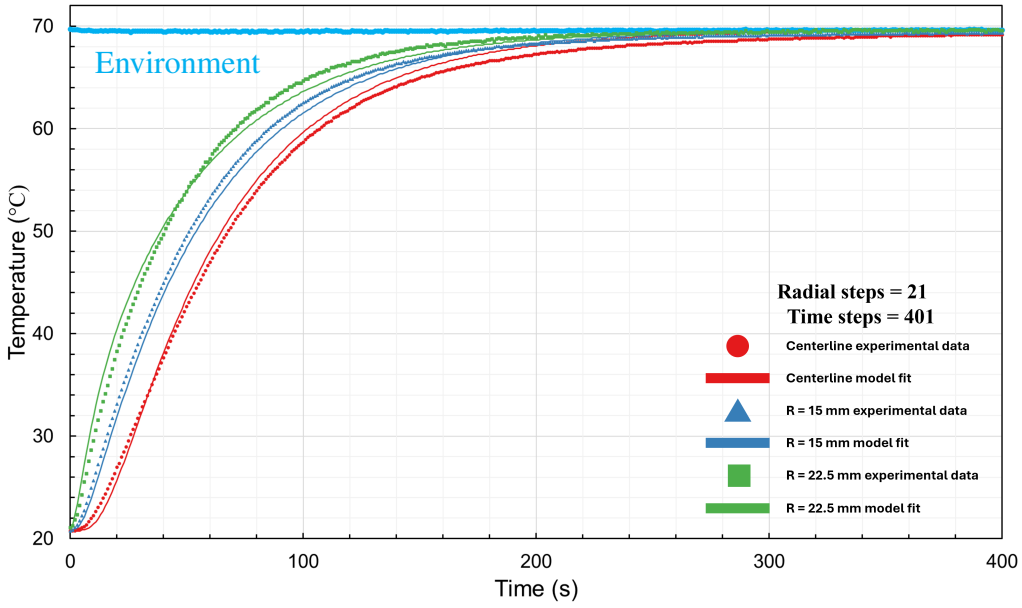

Figure 2.97: Experimental temperature data of support E of a microfibrous media bed compared with a model fit of the data as the bed is taken from approximately 21 °C and submerged in an approximately 70 °C water bath. The bed was pressurized to 50 psi gauge with carbon dioxide at room temperature.

2.29 Experimental and Model comparisons for a Microfibrous Media (MFM) Bed Containing Stagnant Carbon Dioxide Taken from Approximately 70 °C and Submerged in a 20 °C Water Bath

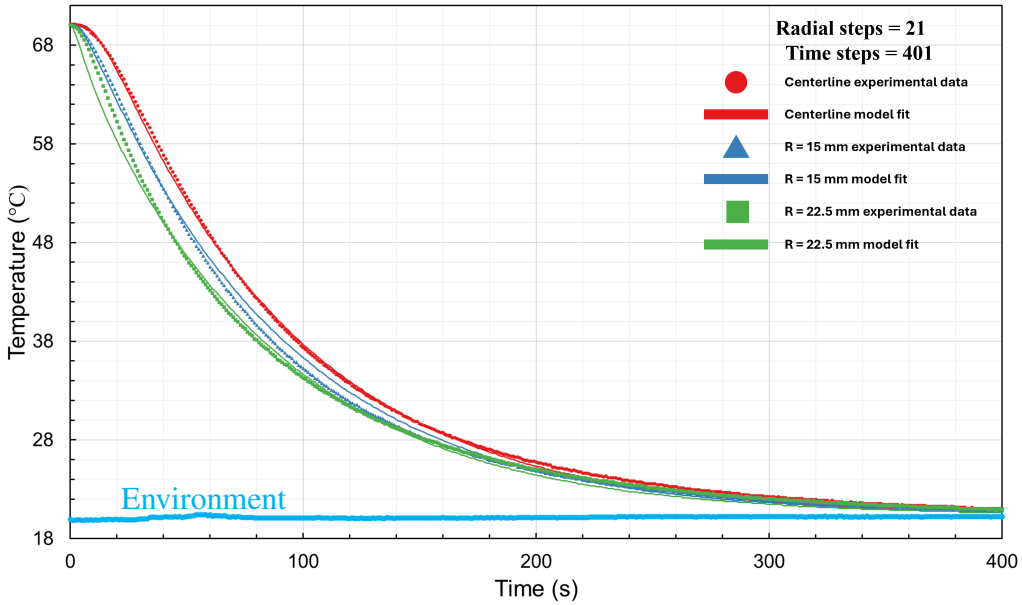

Figure 2.98: Experimental temperature data of support A of a microfibrous media bed compared with a model fit of the data as the bed is taken from approximately 70 °C and submerged in an approximately 20 °C water bath. The bed was pressurized to 50 psi gauge with carbon dioxide at room temperature.

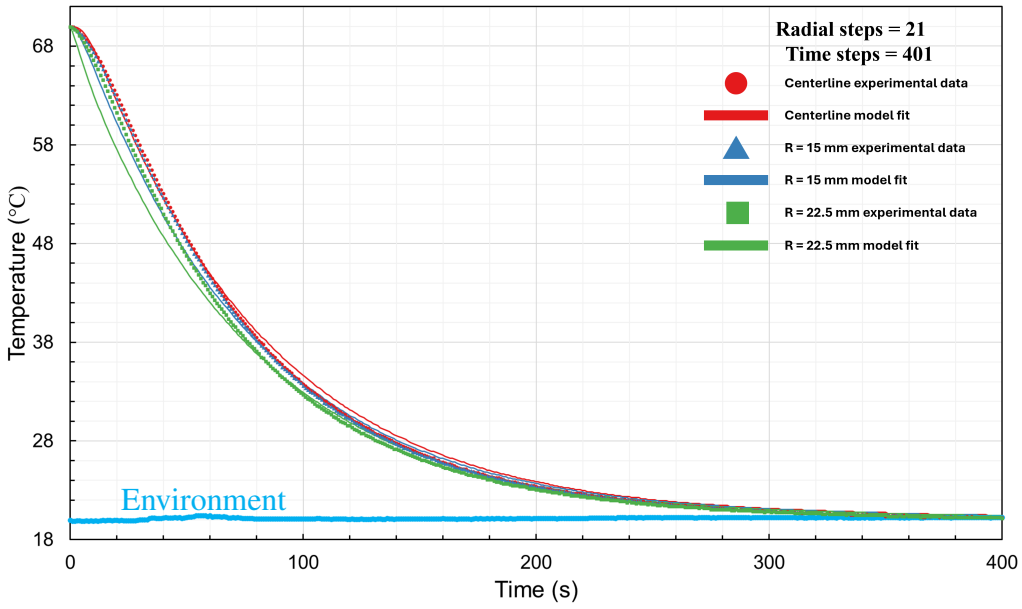

Figure 2.99: Experimental temperature data of support B of a microfibrous media bed compared with a model fit of the data as the bed is taken from approximately 70 °C and submerged in an approximately 20 °C water bath. The bed was pressurized to 50 psi gauge with carbon dioxide at room temperature.

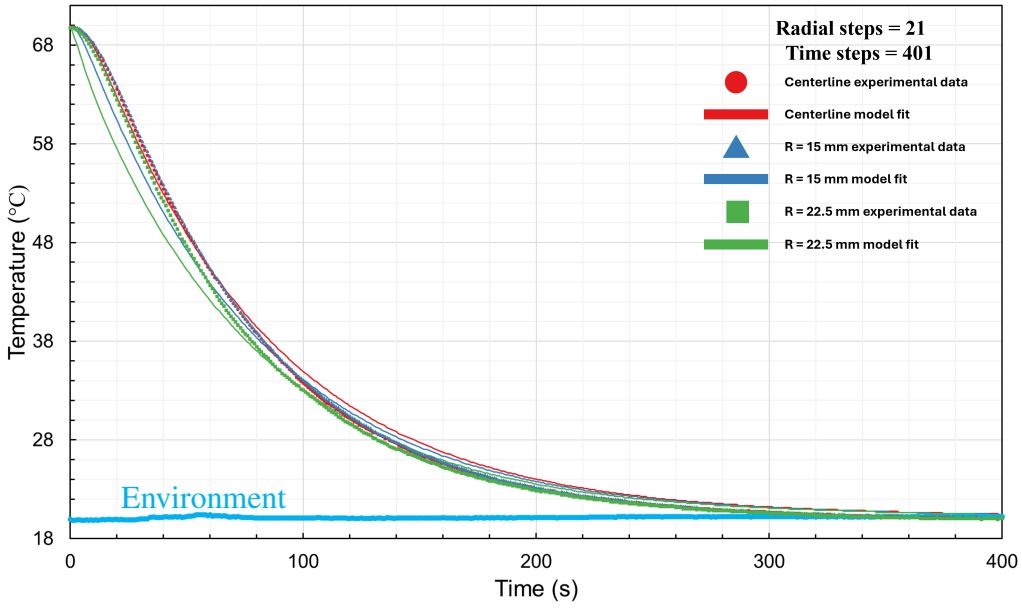

Figure 2.100: Experimental temperature data of support C of a microfibrous media bed compared with a model fit of the data as the bed is taken from approximately 70 °C and submerged in an approximately 20 °C water bath. The bed was pressurized to 50 psi gauge with carbon dioxide at room temperature.

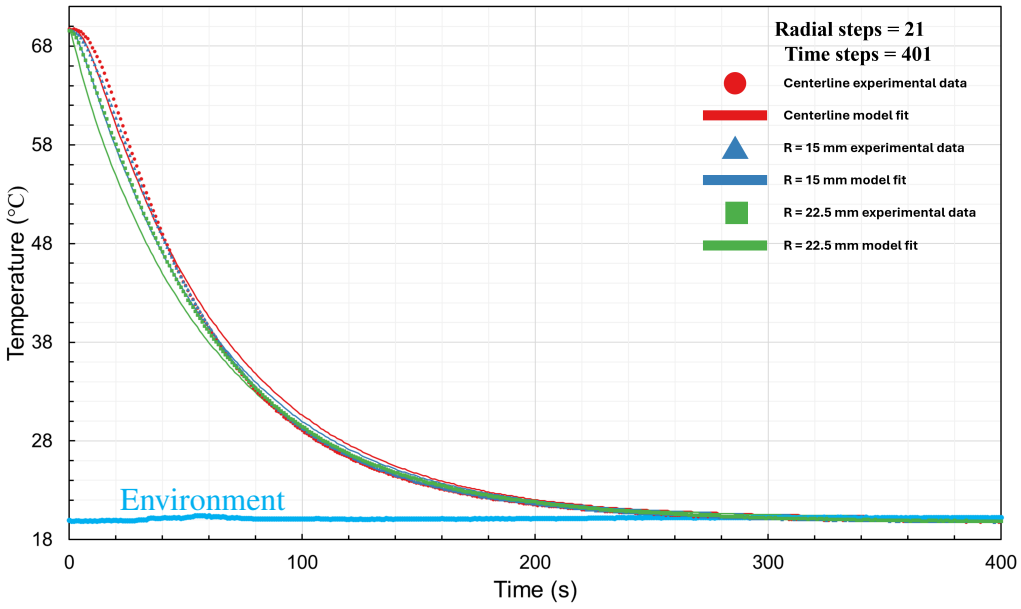

Figure 2.101: Experimental temperature data of support D of a microfibrous media bed compared with a model fit of the data as the bed is taken from approximately 70 °C and submerged in an approximately 20 °C water bath. The bed was pressurized to 50 psi gauge with carbon dioxide at room temperature.

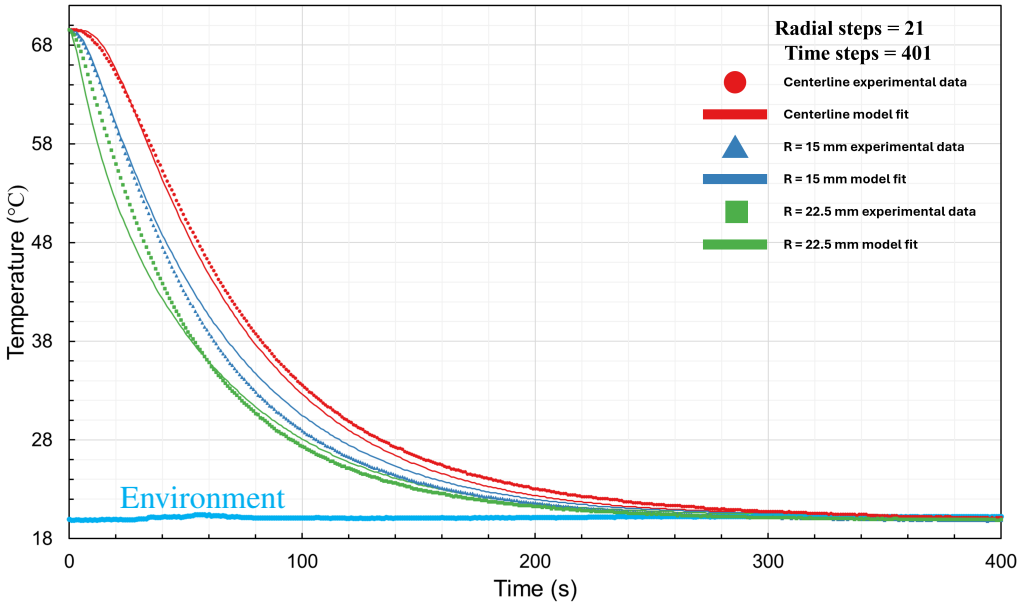

Figure 2.102: Experimental temperature data of support E of a microfibrous media bed compared with a model fit of the data as the bed is taken from approximately 70 °C and submerged in an approximately 20 °C water bath. The bed was pressurized to 50 psi gauge with carbon dioxide at room temperature.

2.30 Experimental and Model comparisons for a Microfibrous Media (MFM) Bed Containing Stagnant Carbon Dioxide Taken from Approximately 0 °C and Submerged in a 21 °C Water Bath

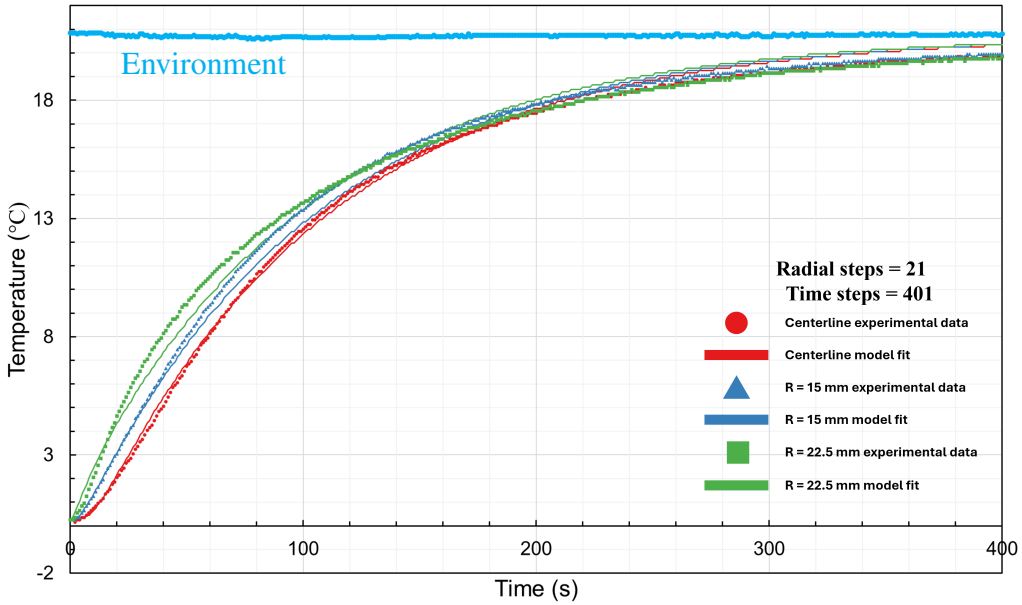

Figure 2.103: Experimental temperature data of support A of a microfibrous media bed compared with a model fit of the data as the bed is taken from approximately 0 °C and submerged in an approximately 21 °C water bath. The bed was pressurized to 50 psi gauge with carbon dioxide at room temperature.

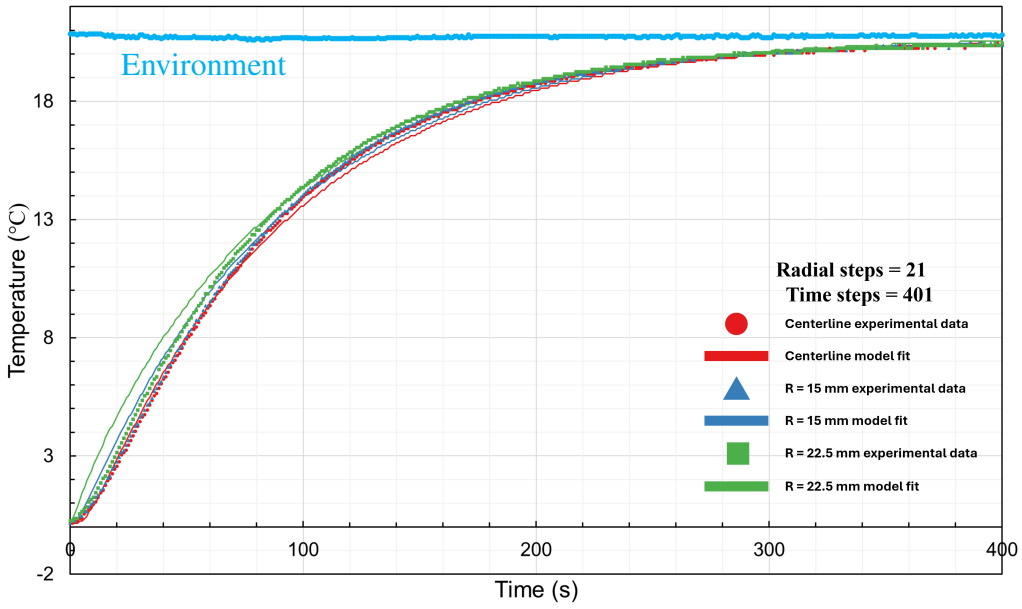

Figure 2.104: Experimental temperature data of support B of a microfibrous media bed compared with a model fit of the data as the bed is taken from approximately 0 °C and submerged in an approximately 21 °C water bath. The bed was pressurized to 50 psi gauge with carbon dioxide at room temperature.

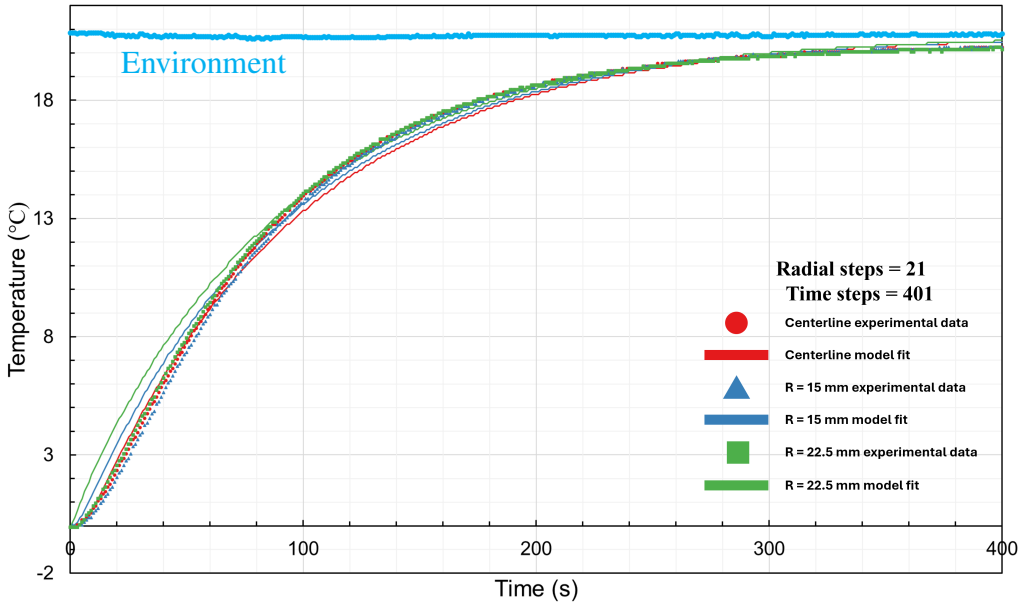

Figure 2.105: Experimental temperature data of support C of a microfibrous media bed compared with a model fit of the data as the bed is taken from approximately 0 °C and submerged in an approximately 21 °C water bath. The bed was pressurized to 50 psi gauge with carbon dioxide at room temperature.

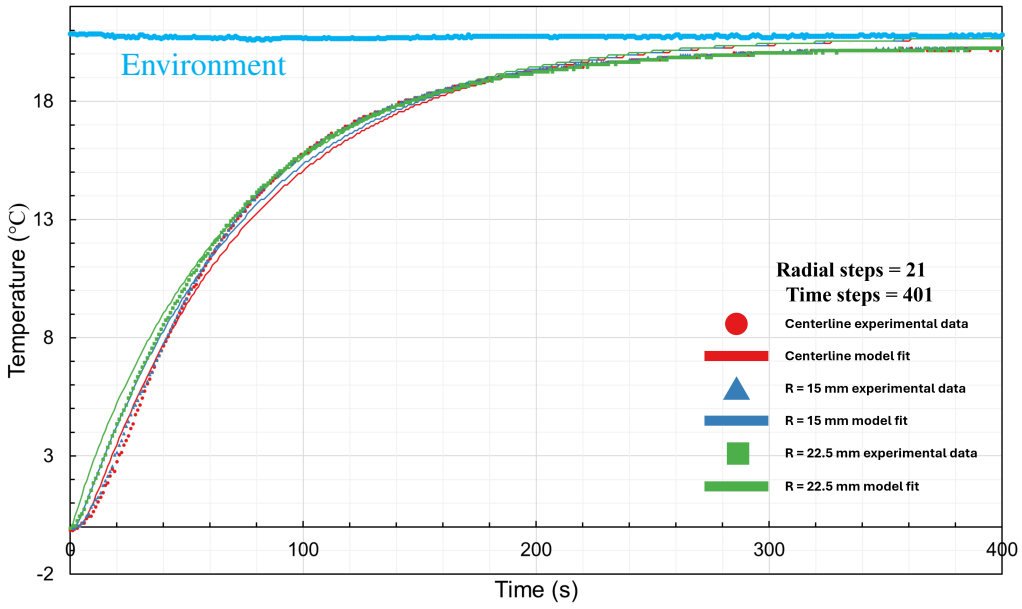

Figure 2.106: Experimental temperature data of support D of a microfibrous media bed compared with a model fit of the data as the bed is taken from approximately 0 °C and submerged in an approximately 21 °C water bath. The bed was pressurized to 50 psi gauge with carbon dioxide at room temperature.

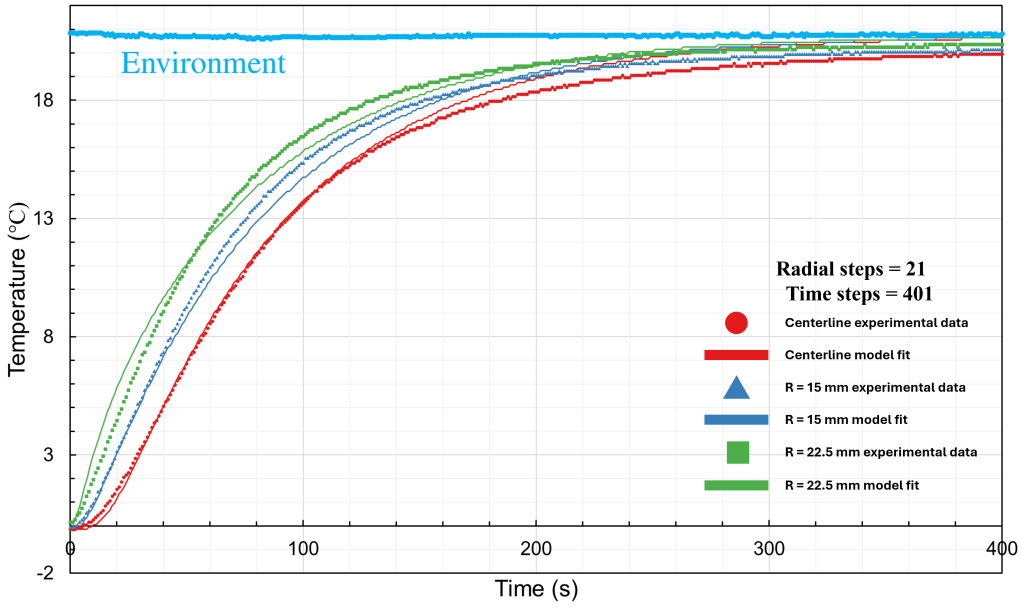

Figure 2.107: Experimental temperature data of support E of a microfibrous media bed compared with a model fit of the data as the bed is taken from approximately 0 °C and submerged in an approximately 21 °C water bath. The bed was pressurized to 50 psi gauge with carbon dioxide at room temperature.

2.31 Experimental and Model comparisons for a Microfibrous Media (MFM) Bed Containing Stagnant Carbon Dioxide Taken from Approximately 21 °C and Submerged in a 0 °C Ice-Water Bath

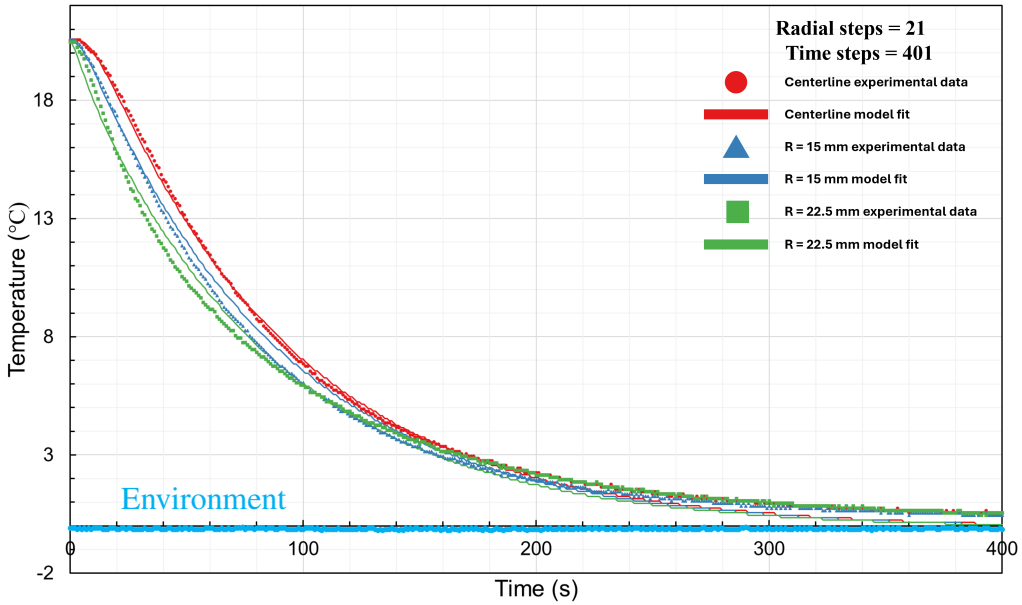

Figure 2.108: Experimental temperature data of support A of a microfibrous media bed compared with a model fit of the data as the bed is taken from approximately 21 °C and submerged in an approximately 0 °C ice-water bath. The bed was pressurized to 50 psi gauge with carbon dioxide at room temperature.

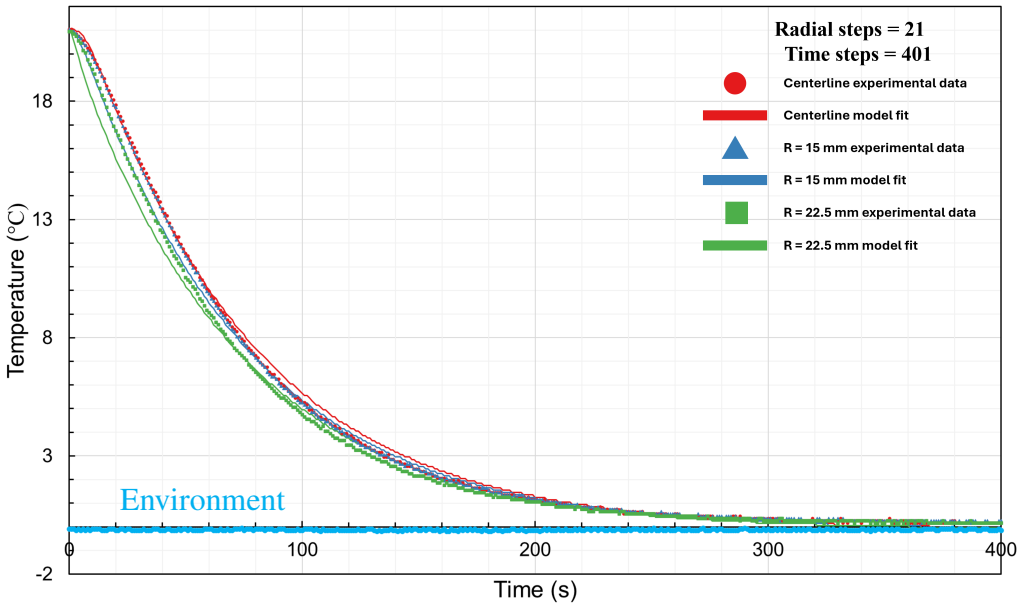

Figure 2.109: Experimental temperature data of support B of a microfibrous media bed compared with a model fit of the data as the bed is taken from approximately 21 °C and submerged in an approximately 0 °C ice-water bath. The bed was pressurized to 50 psi gauge with carbon dioxide at room temperature.

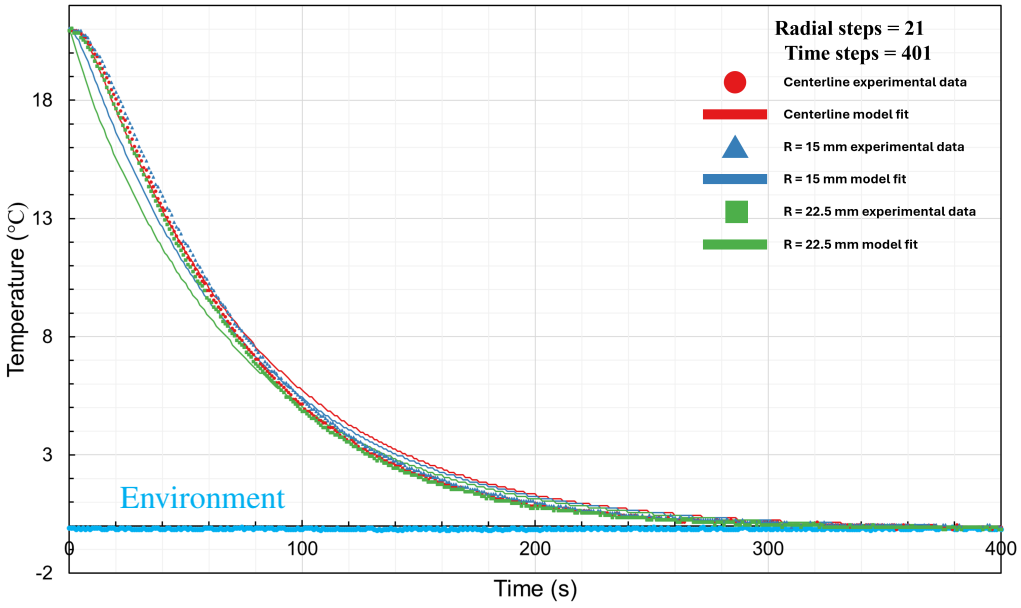

Figure 2.110: Experimental temperature data of support C of a microfibrous media bed compared with a model fit of the data as the bed is taken from approximately 21 °C and submerged in an approximately 0 °C ice-water bath. The bed was pressurized to 50 psi gauge with carbon dioxide at room temperature.

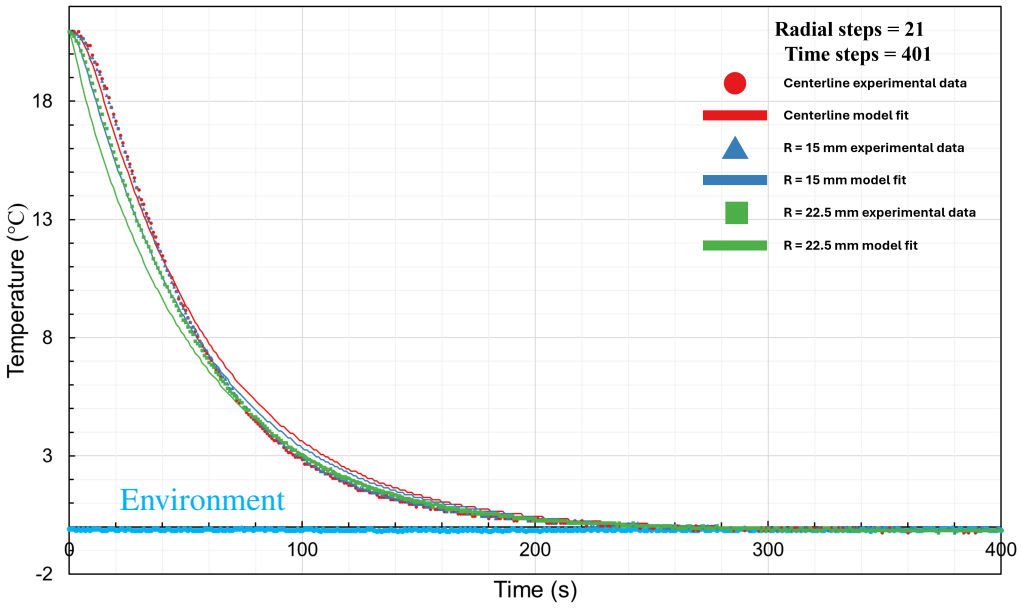

Figure 2.111: Experimental temperature data of support D of a microfibrous media bed compared with a model fit of the data as the bed is taken from approximately 21 °C and submerged in an approximately 0 °C ice-water bath. The bed was pressurized to 50 psi gauge with carbon dioxide at room temperature.

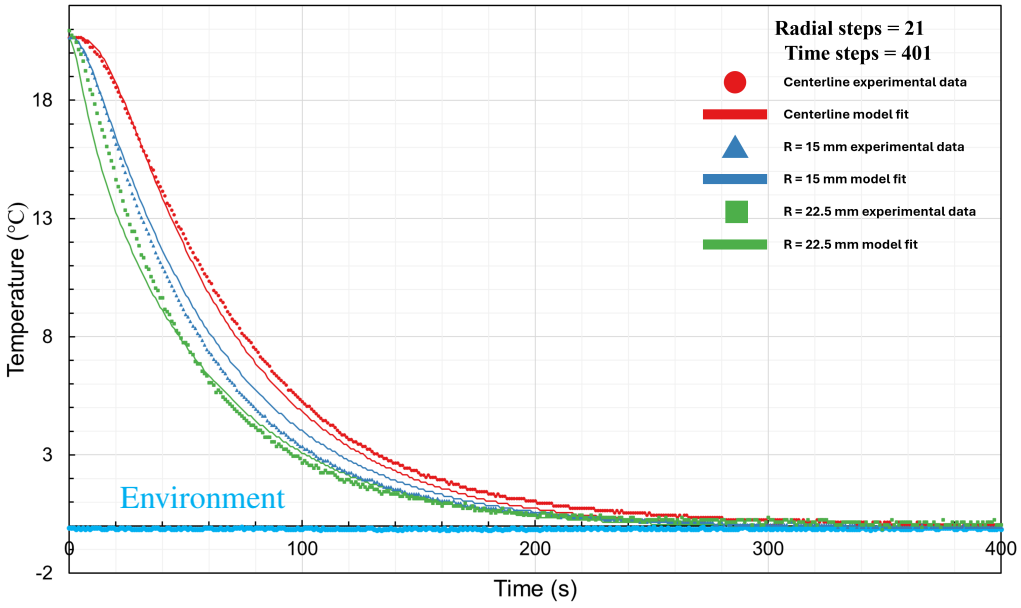

Figure 2.112: Experimental temperature data of support E of a microfibrous media bed compared with a model fit of the data as the bed is taken from approximately 21 °C and submerged in an approximately 0 °C ice-water bath. The bed was pressurized to 50 psi gauge with carbon dioxide at room temperature.

2.32 Experimental and Model Comparisons for a Microfibrous Media (MFM) Bed Containing Stagnant Helium Taken from Approximately 21 °C and Submerged in a 71 °C Water Bath

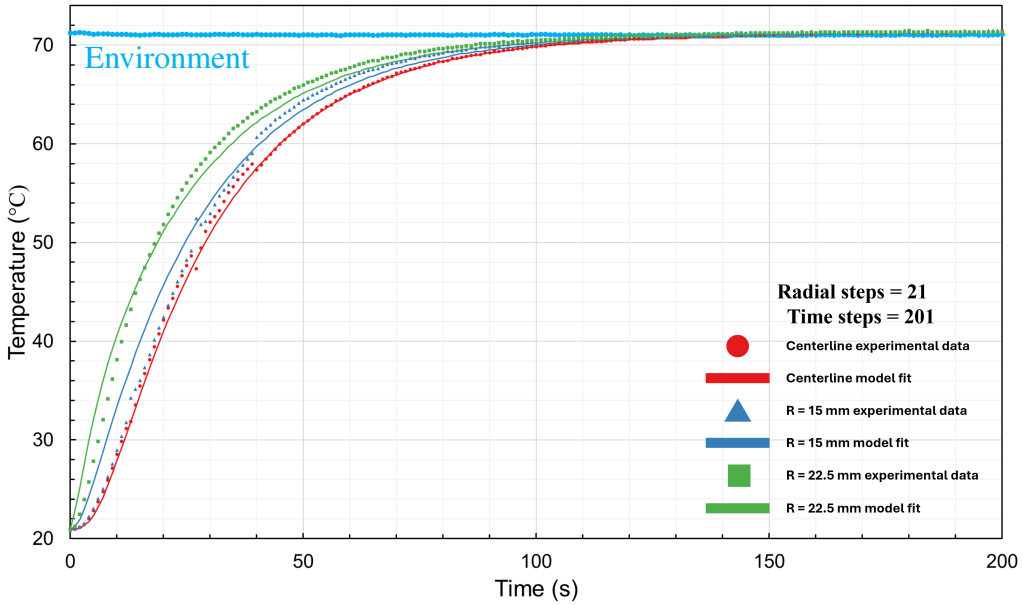

Figure 2.113: Experimental temperature data of support A of a microfibrous media bed compared with a model fit of the data as the bed is taken from approximately 21 °C and submerged in an approximately 71 °C water bath. The bed was pressurized to 50 psi gauge with helium at room temperature.

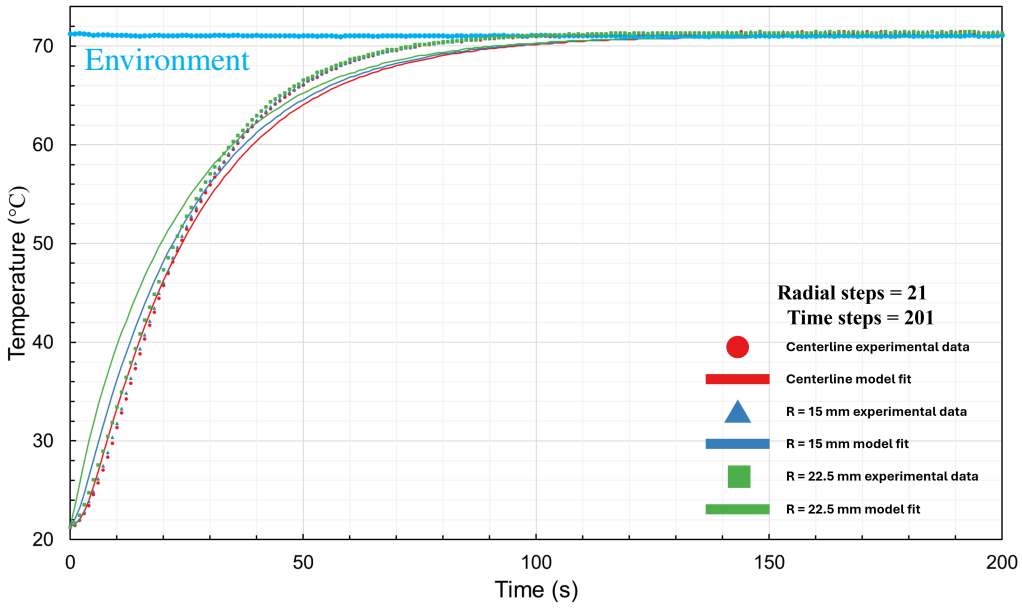

Figure 2.114: Experimental temperature data of support B of a microfibrous media bed compared with a model fit of the data as the bed is taken from approximately 21 °C and submerged in an approximately 71 °C water bath. The bed was pressurized to 50 psi gauge with helium at room temperature.

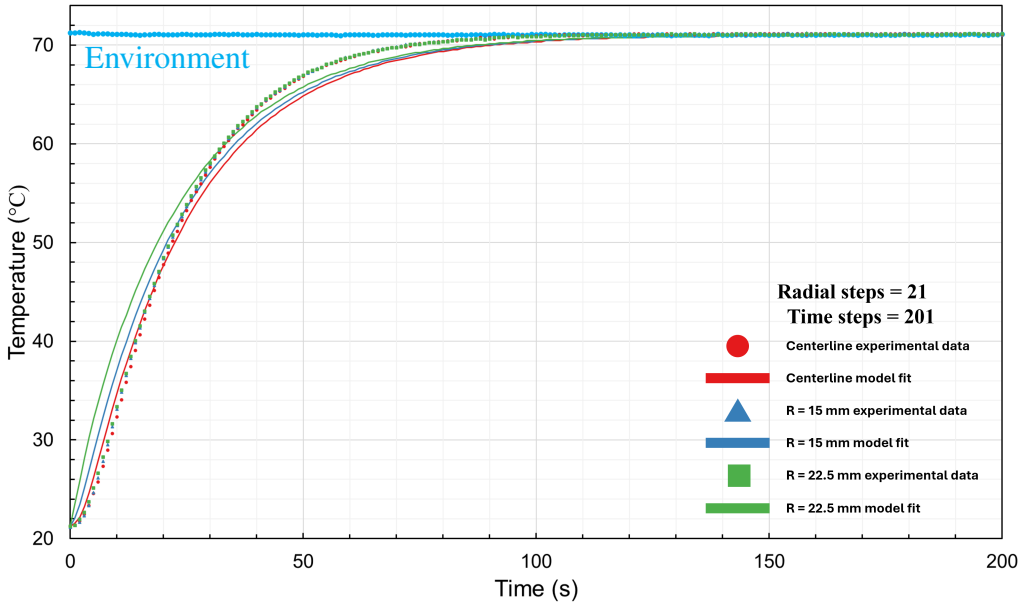

Figure 2.115: Experimental temperature data of support C of a microfibrous media bed compared with a model fit of the data as the bed is taken from approximately 21 °C and submerged in an approximately 71 °C water bath. The bed was pressurized to 50 psi gauge with helium at room temperature.

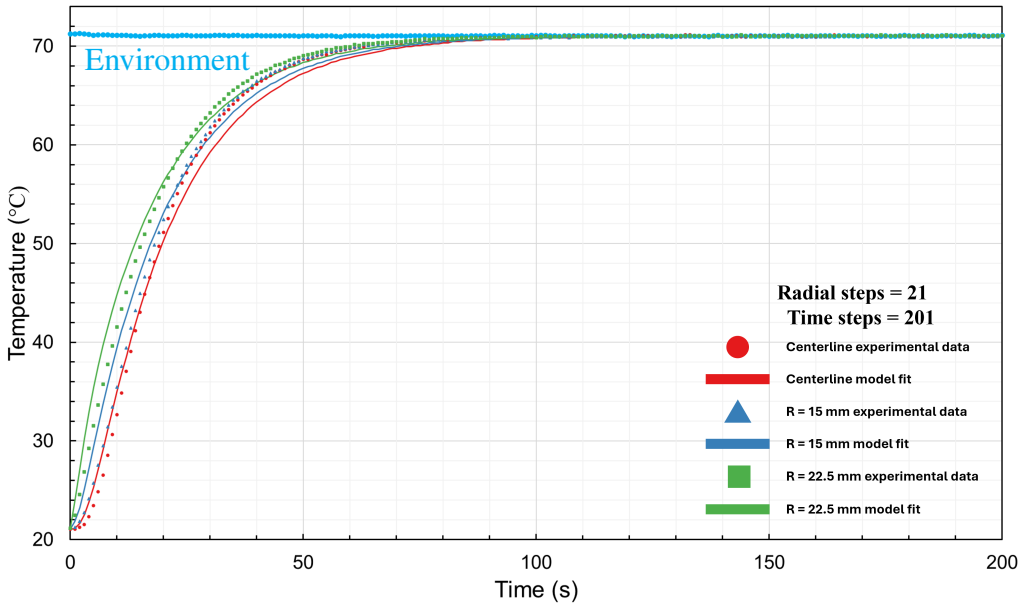

Figure 2.116: Experimental temperature data of support D of a microfibrous media bed compared with a model fit of the data as the bed is taken from approximately 21 °C and submerged in an approximately 71 °C water bath. The bed was pressurized to 50 psi gauge with helium at room temperature.

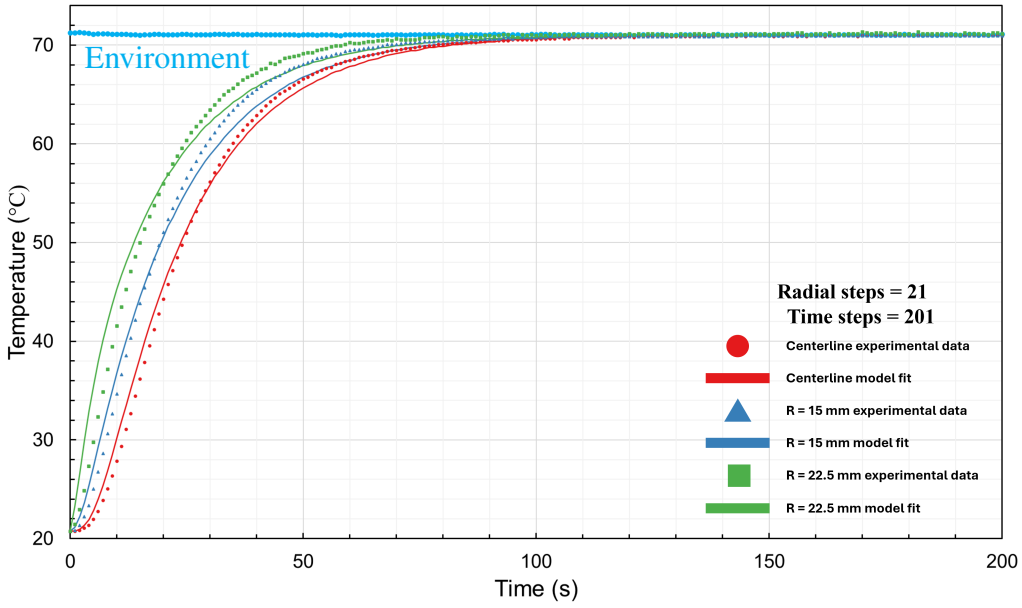

Figure 2.117: Experimental temperature data of support E of a microfibrous media bed compared with a model fit of the data as the bed is taken from approximately 21 °C and submerged in an approximately 71 °C water bath. The bed was pressurized to 50 psi gauge with helium at room temperature.

2.33 Experimental and Model Comparisons for a Microfibrous Media (MFM) Bed Containing Stagnant Helium Taken from Approximately 71 °C and Submerged in a 20 °C Water Bath

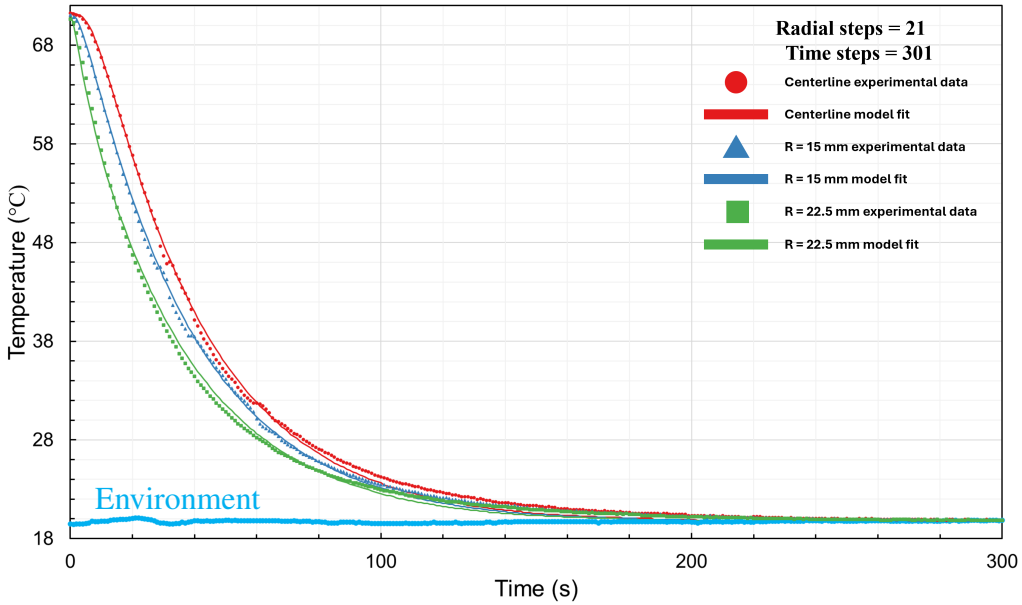

Figure 2.118: Experimental temperature data of support A of a microfibrous media bed compared with a model fit of the data as the bed is taken from approximately 71 °C and submerged in an approximately 20 °C water bath. The bed was pressurized to 50 psi gauge with helium at room temperature.

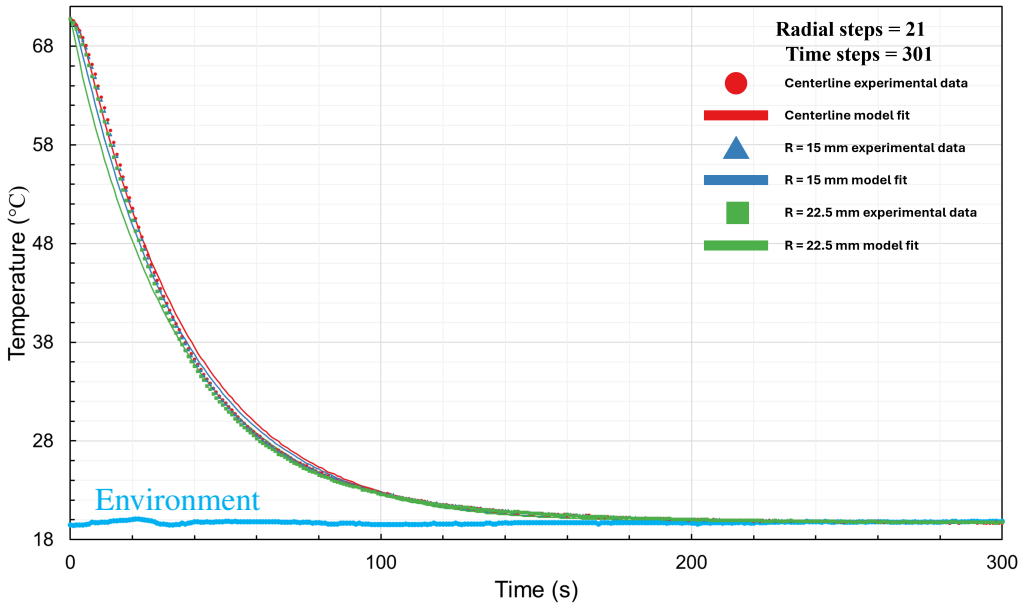

Figure 2.119: Experimental temperature data of support B of a microfibrous media bed compared with a model fit of the data as the bed is taken from approximately 71 °C and submerged in an approximately 20 °C water bath. The bed was pressurized to 50 psi gauge with helium at room temperature.

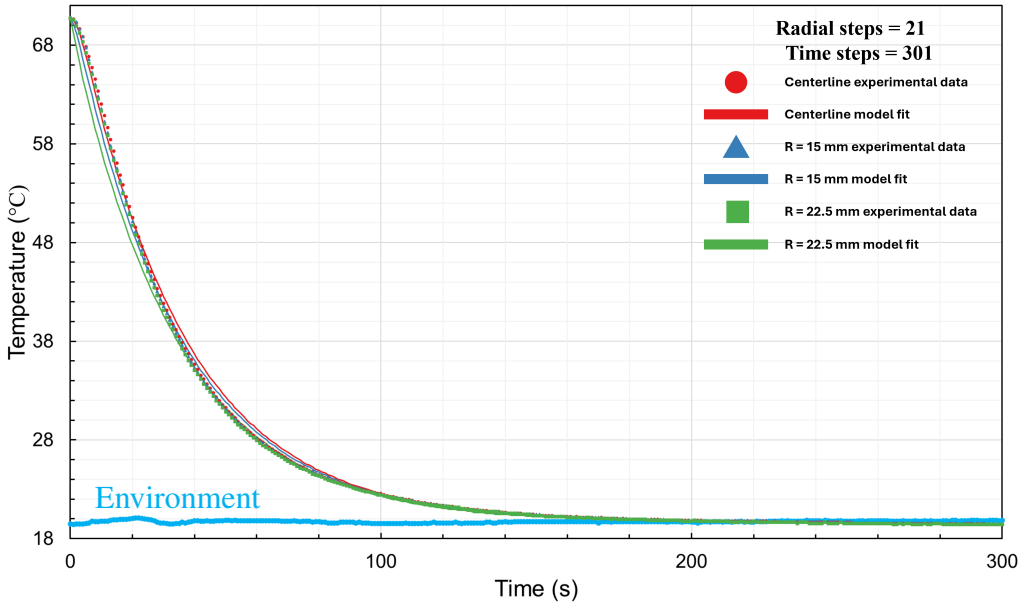

Figure 2.120: Experimental temperature data of support C of a microfibrous media bed compared with a model fit of the data as the bed is taken from approximately 71 °C and submerged in an approximately 20 °C water bath. The bed was pressurized to 50 psi gauge with helium at room temperature.

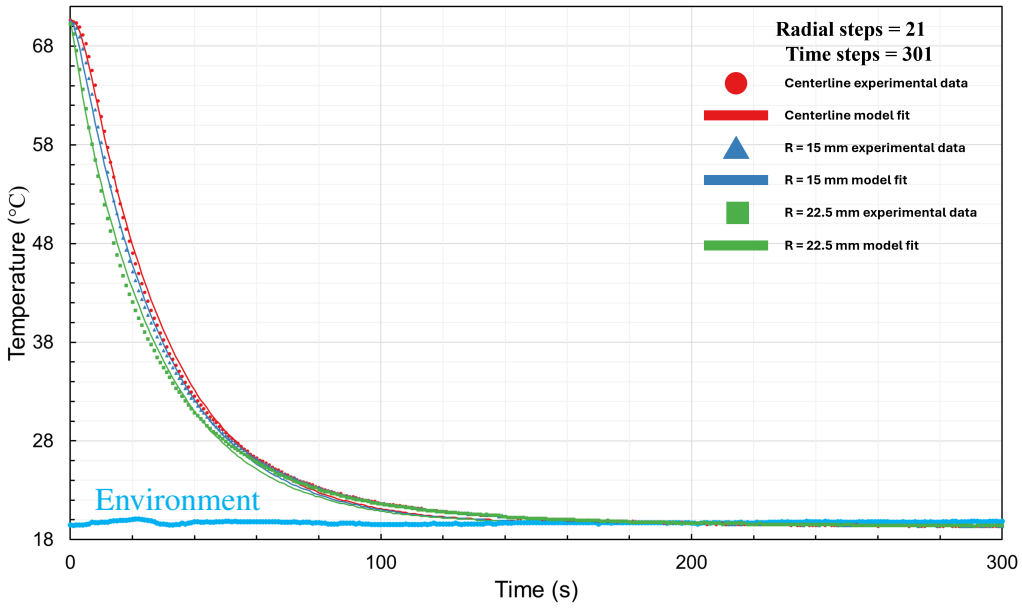

Figure 2.121: Experimental temperature data of support D of a microfibrous media bed compared with a model fit of the data as the bed is taken from approximately 71 °C and submerged in an approximately 20 °C water bath. The bed was pressurized to 50 psi gauge with helium at room temperature.

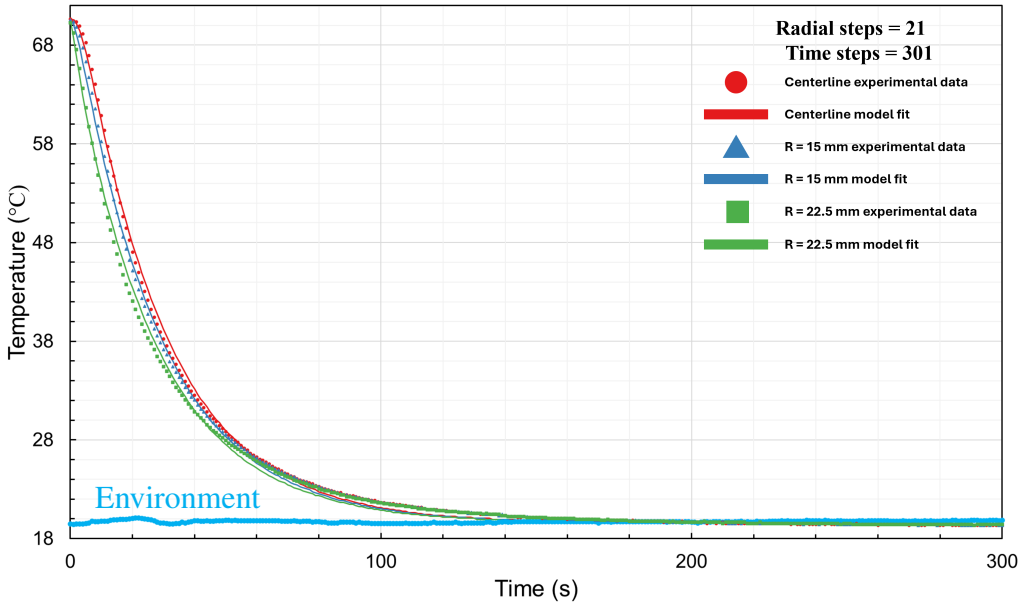

Figure 2.122: Experimental temperature data of support E of a microfibrous media bed compared with a model fit of the data as the bed is taken from approximately 71 °C and submerged in an approximately 20 °C water bath. The bed was pressurized to 50 psi gauge with helium at room temperature.

2.34 Experimental and Model Comparisons for a Microfibrous Media (MFM) Bed Containing Stagnant Helium Taken from Approximately 0 °C and Submerged in a 22 °C Water Bath

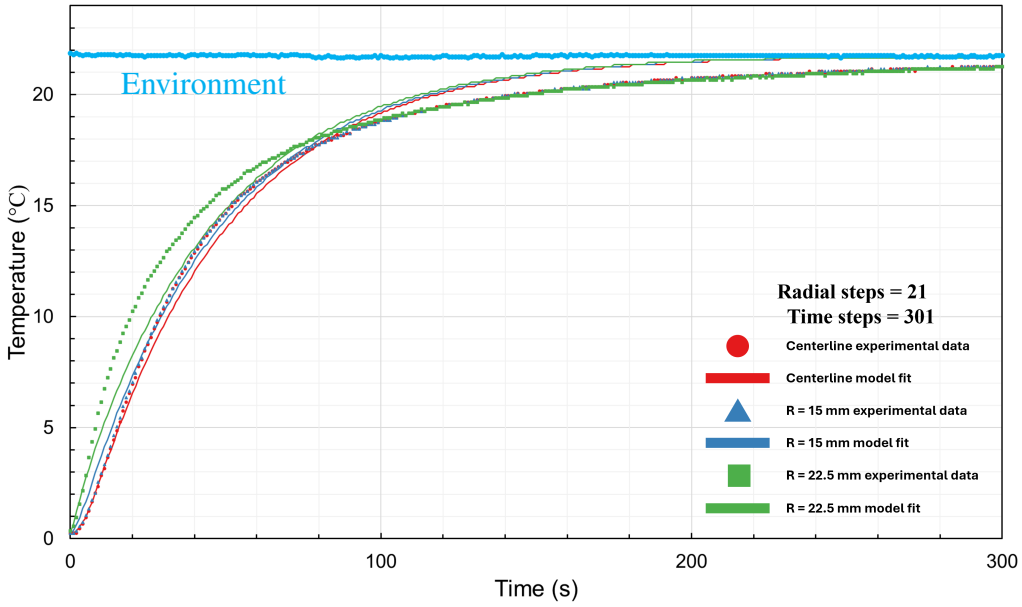

Figure 2.123: Experimental temperature data of support A of a microfibrous media bed compared with a model fit of the data as the bed is taken from approximately 0 °C and submerged in an approximately 22 °C water bath. The bed was pressurized to 50 psi gauge with helium at room temperature.

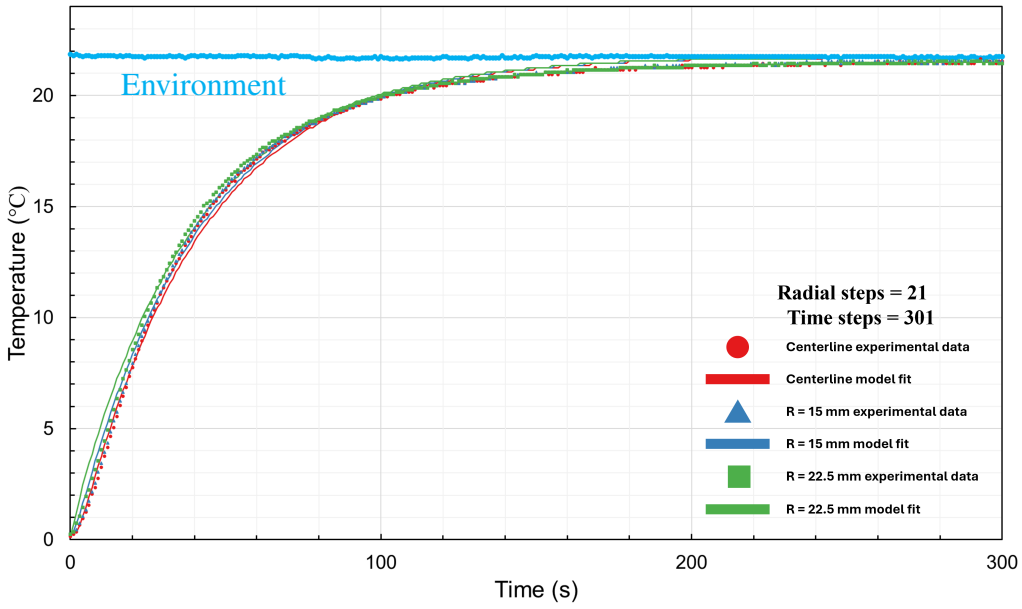

Figure 2.124: Experimental temperature data of support B of a microfibrous media bed compared with a model fit of the data as the bed is taken from approximately 0 °C and submerged in an approximately 22 °C water bath. The bed was pressurized to 50 psi gauge with helium at room temperature.

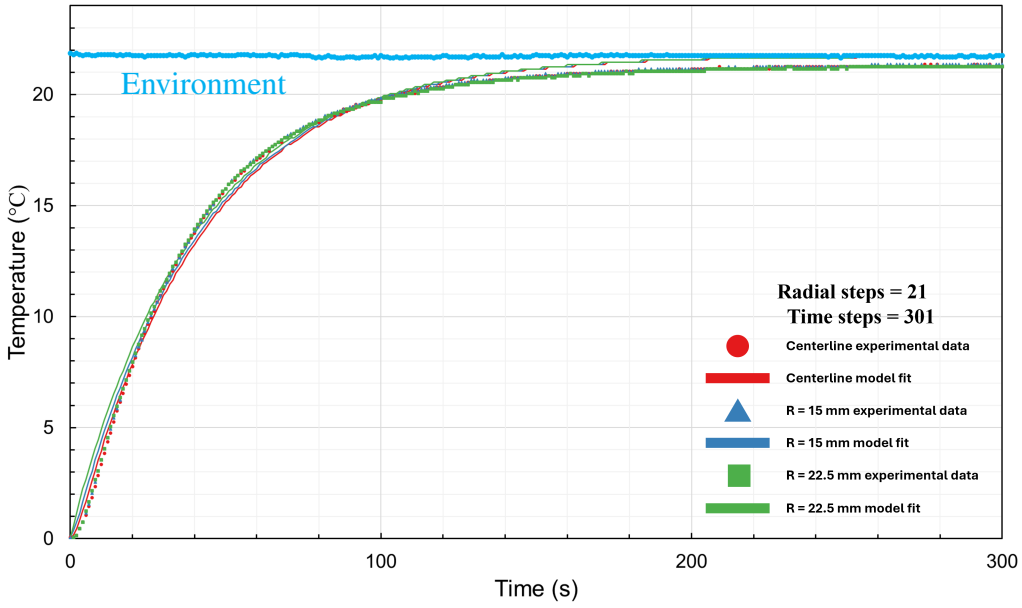

Figure 2.125: Experimental temperature data of support C of a microfibrous media bed compared with a model fit of the data as the bed is taken from approximately 0 °C and submerged in an approximately 22 °C water bath. The bed was pressurized to 50 psi gauge with helium at room temperature.

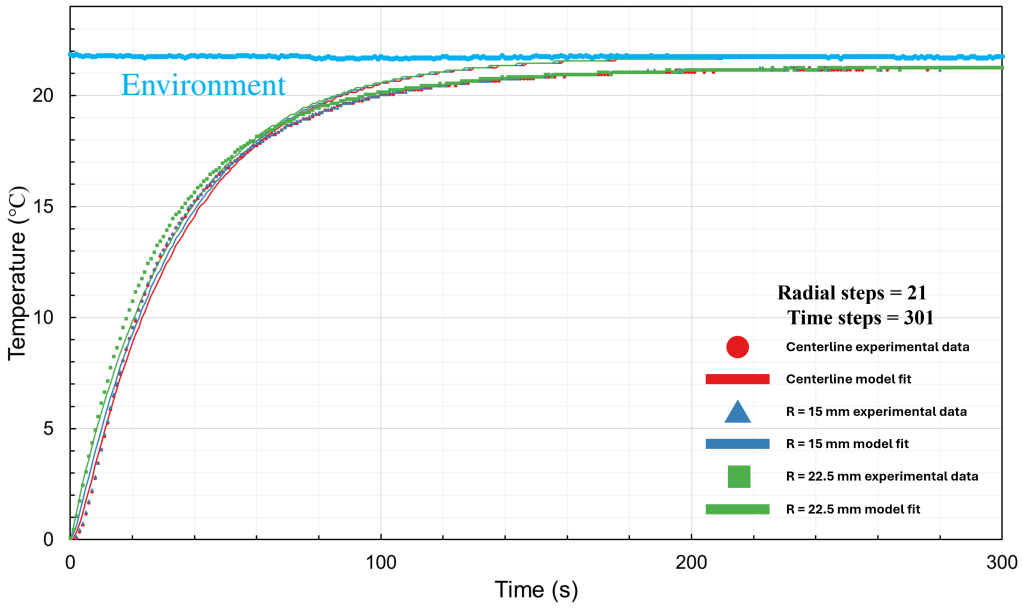

Figure 2.126: Experimental temperature data of support D of a microfibrous media bed compared with a model fit of the data as the bed is taken from approximately 0 °C and submerged in an approximately 22 °C water bath. The bed was pressurized to 50 psi gauge with helium at room temperature.

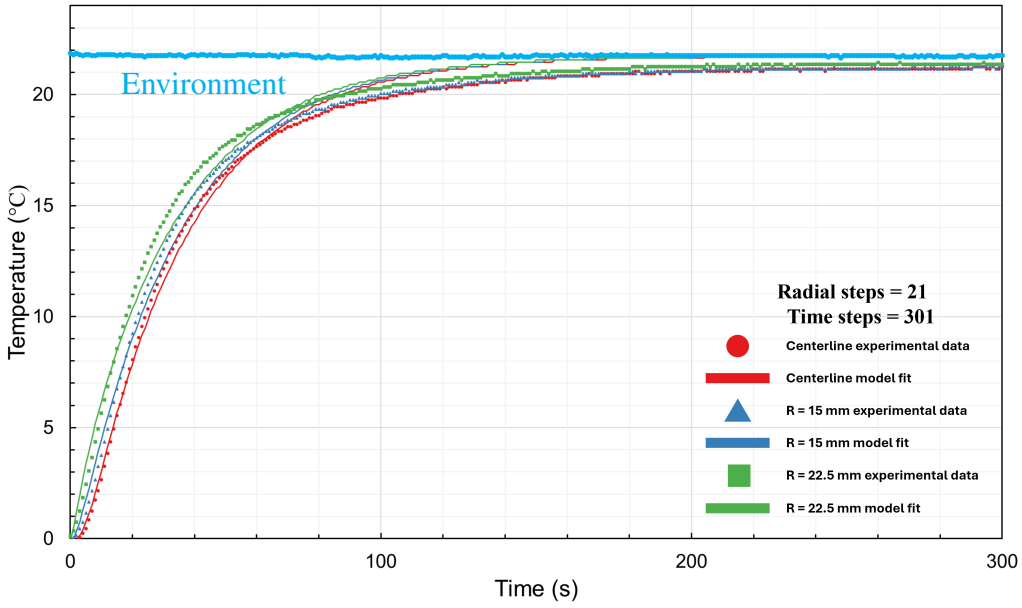

Figure 2.127: Experimental temperature data of support E of a microfibrous media bed compared with a model fit of the data as the bed is taken from approximately 0 °C and submerged in an approximately 22 °C water bath. The bed was pressurized to 50 psi gauge with helium at room temperature.

2.35 Experimental and Model Comparisons for a Microfibrous Media (MFM) Bed Containing Stagnant Helium Taken from Approximately 21 °C and Submerged in a 0 °C Ice-Water Bath

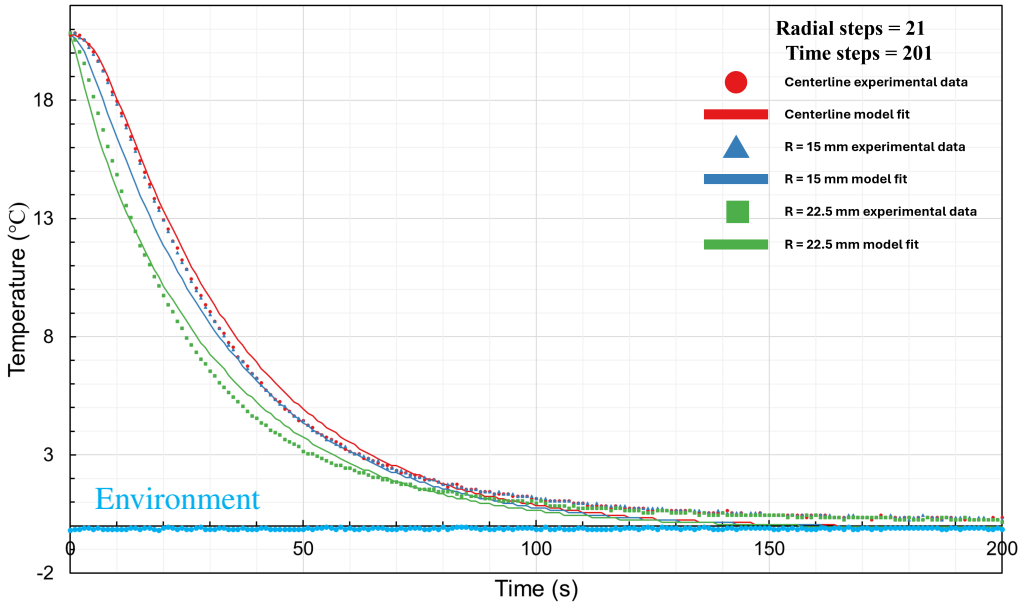

Figure 2.128: Experimental temperature data of support A of a microfibrous media bed compared with a model fit of the data as the bed is taken from approximately 21 °C and submerged in an approximately 0 °C ice-water bath. The bed was pressurized to 50 psi gauge with helium at room temperature.

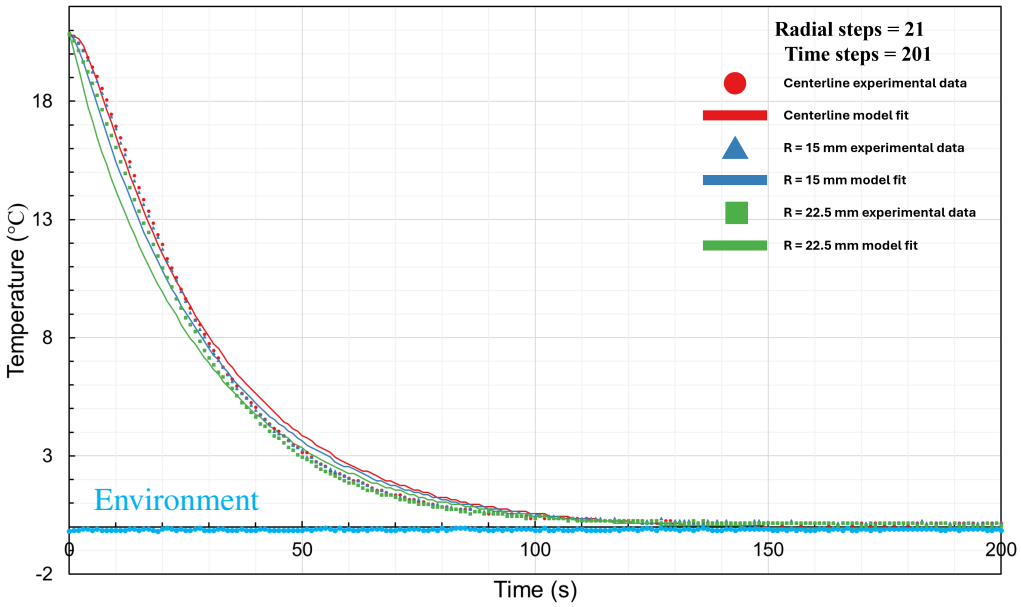

Figure 2.129: Experimental temperature data of support B of a microfibrous media bed compared with a model fit of the data as the bed is taken from approximately 21 °C and submerged in an approximately 0 °C ice-water bath. The bed was pressurized to 50 psi gauge with helium at room temperature.

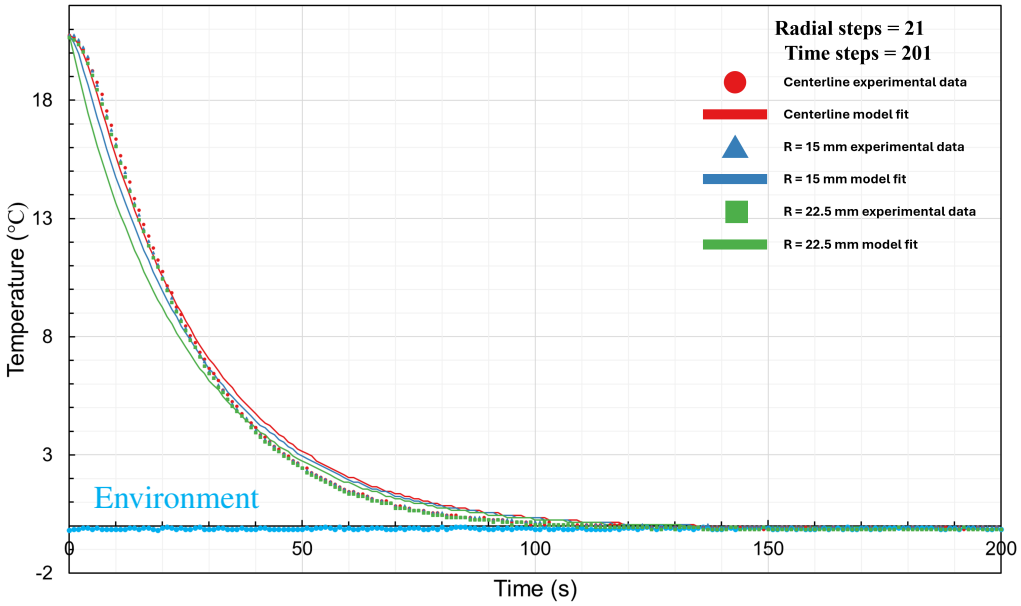

Figure 2.130: Experimental temperature data of support C of a microfibrous media bed compared with a model fit of the data as the bed is taken from approximately 21 °C and submerged in an approximately 0 °C ice-water bath. The bed was pressurized to 50 psi gauge with helium at room temperature.

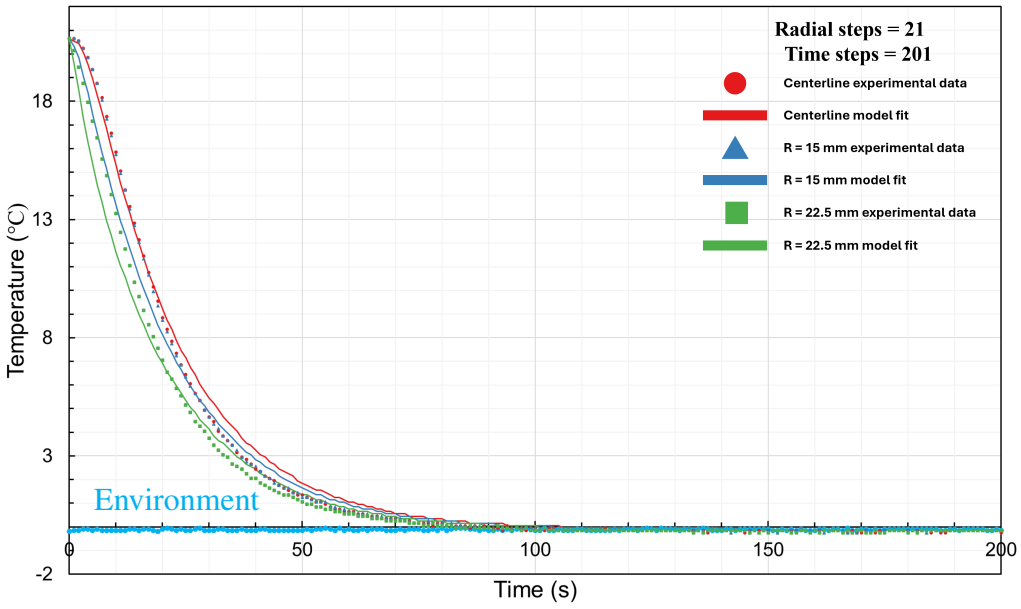

Figure 2.131: Experimental temperature data of support D of a microfibrous media bed compared with a model fit of the data as the bed is taken from approximately 21 °C and submerged in an approximately 0 °C ice-water bath. The bed was pressurized to 50 psi gauge with helium at room temperature.

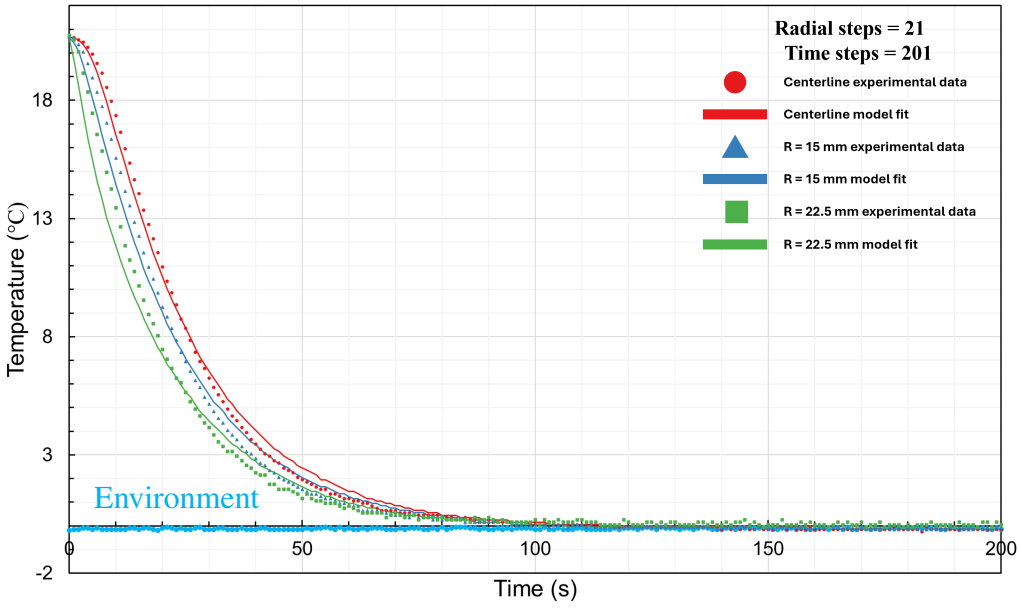

Figure 2.132: Experimental temperature data of support E of a microfibrous media bed compared with a model fit of the data as the bed is taken from approximately 21 °C and submerged in an approximately 0 °C ice-water bath. The bed was pressurized to 50 psi gauge with helium at room temperature.

2.36 Experimental and Model Comparisons for a Microfibrous Media (MFM) Bed Containing Stagnant Hydrogen Taken from Approximately 21 °C and Submerged in a 69 °C Water Bath

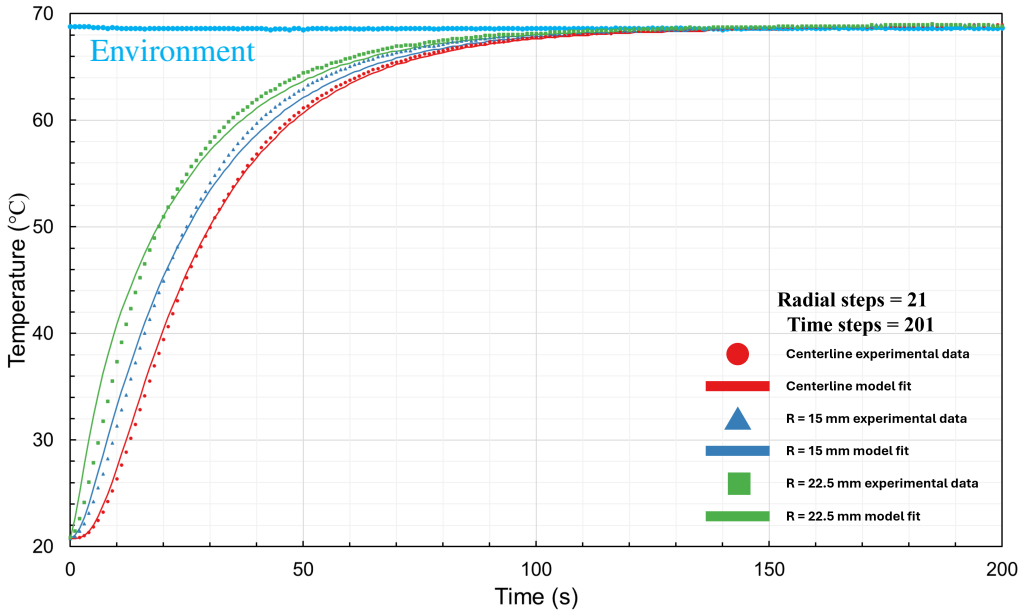

Figure 2.133: Experimental temperature data of support A of a microfibrous media bed compared with a model fit of the data as the bed is taken from approximately 69 °C and submerged in an approximately 20 °C water bath. The bed was pressurized to 50 psi gauge with hydrogen at room temperature.

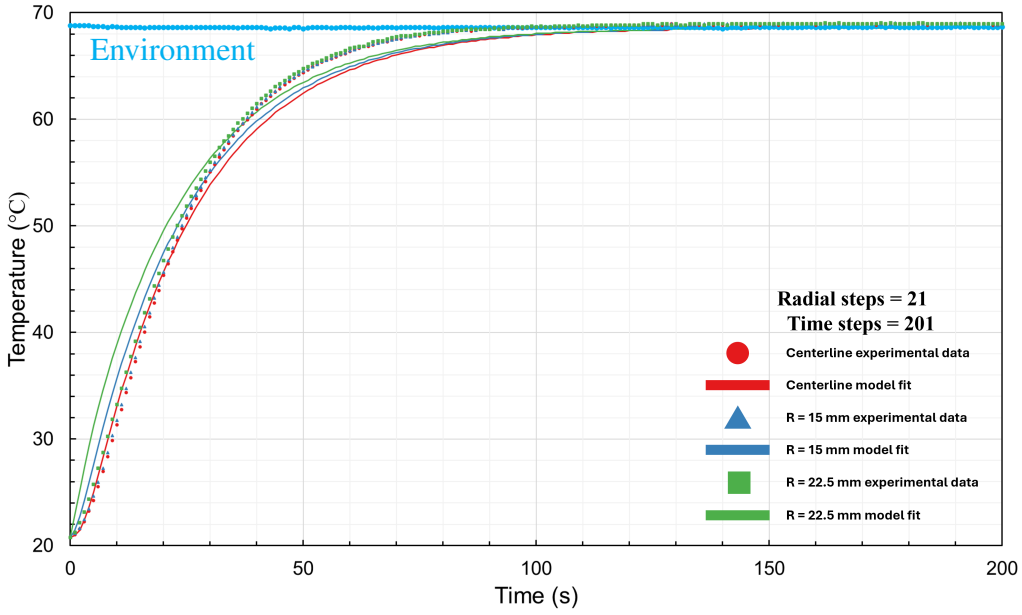

Figure 2.134: Experimental temperature data of support B of a microfibrous media bed compared with a model fit of the data as the bed is taken from approximately 69 °C and submerged in an approximately 20 °C water bath. The bed was pressurized to 50 psi gauge with hydrogen at room temperature.

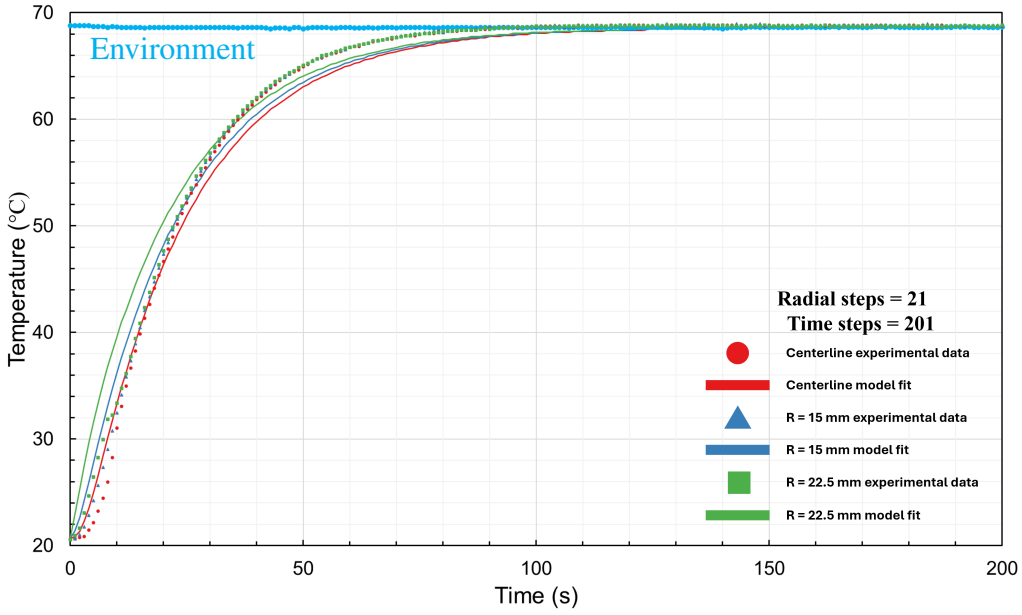

Figure 2.135: Experimental temperature data of support C of a microfibrous media bed compared with a model fit of the data as the bed is taken from approximately 69 °C and submerged in an approximately 20 °C water bath. The bed was pressurized to 50 psi gauge with hydrogen at room temperature.

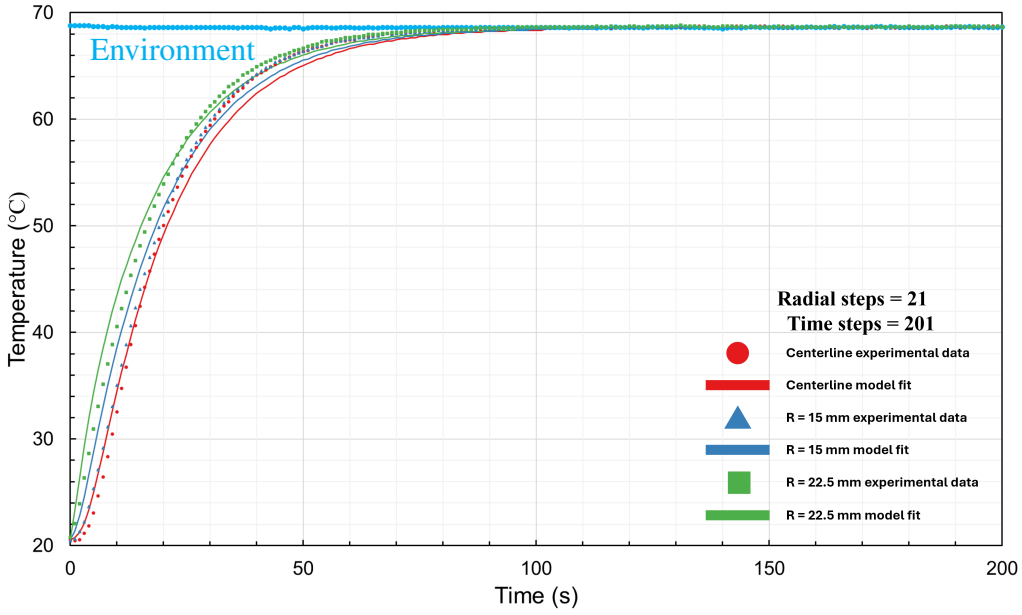

Figure 2.136: Experimental temperature data of support D of a microfibrous media bed compared with a model fit of the data as the bed is taken from approximately 69 °C and submerged in an approximately 20 °C water bath. The bed was pressurized to 50 psi gauge with hydrogen at room temperature.

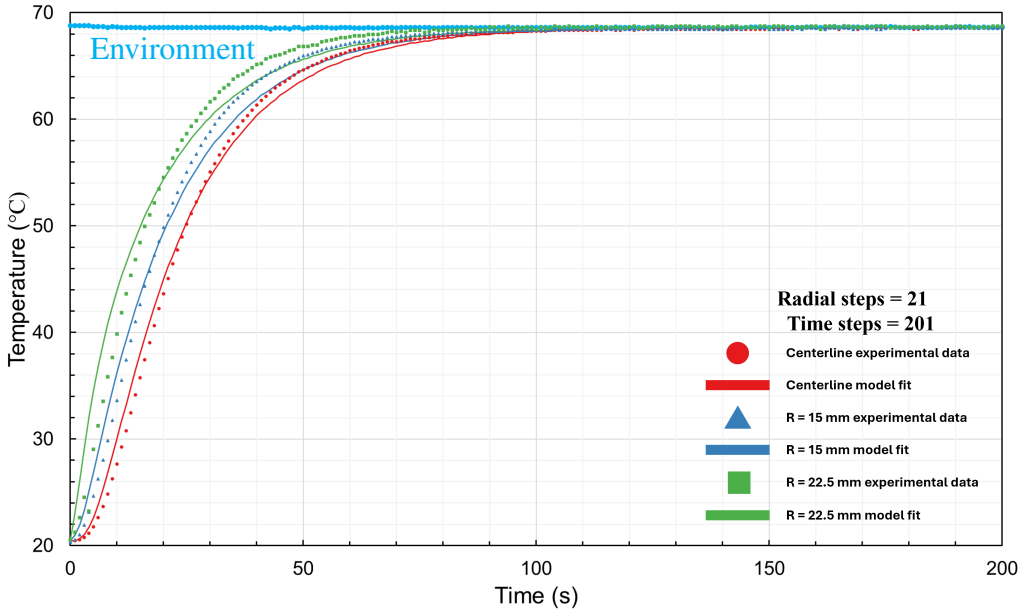

Figure 2.137: Experimental temperature data of support E of a microfibrous media bed compared with a model fit of the data as the bed is taken from approximately 69 °C and submerged in an approximately 20 °C water bath. The bed was pressurized to 50 psi gauge with hydrogen at room temperature.

2.37 Experimental and Model Comparisons for a Microfibrous Media (MFM) Bed Containing Stagnant Hydrogen Taken from Approximately 69 °C and Submerged in a 20 °C Water Bath

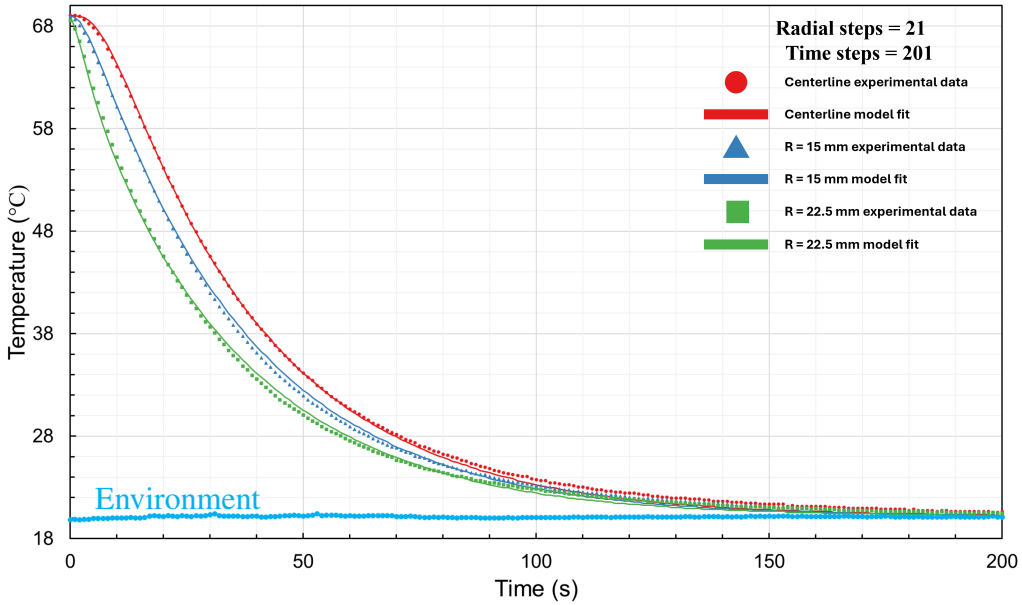

Figure 2.138: Experimental temperature data of support A of a microfibrous media bed compared with a model fit of the data as the bed is taken from approximately 69 °C and submerged in an approximately 20 °C water bath. The bed was pressurized to 50 psi gauge with hydrogen at room temperature.

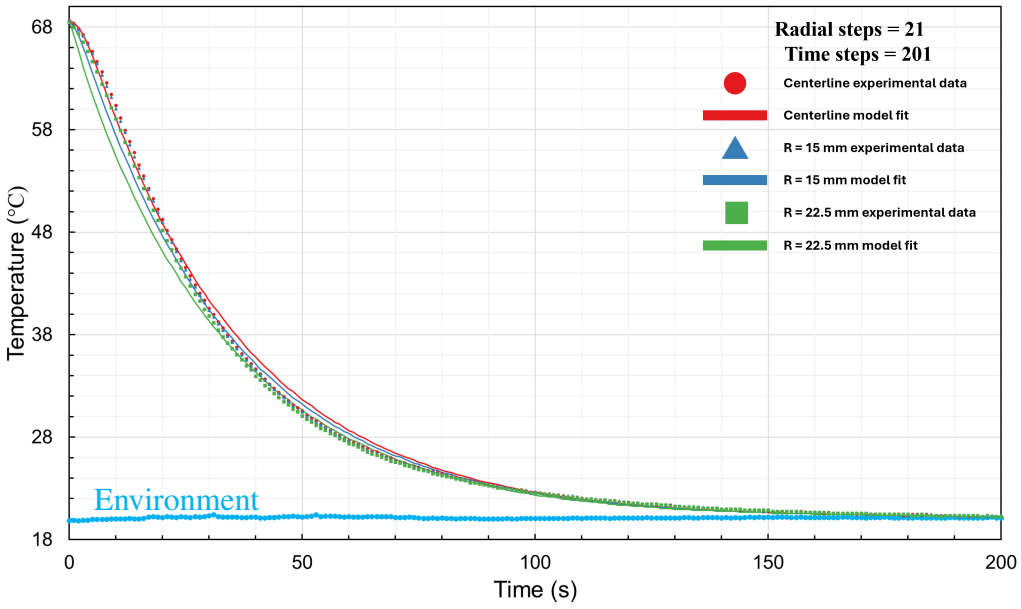

Figure 2.139: Experimental temperature data of support B of a microfibrous media bed compared with a model fit of the data as the bed is taken from approximately 69 °C and submerged in an approximately 20 °C water bath. The bed was pressurized to 50 psi gauge with hydrogen at room temperature.

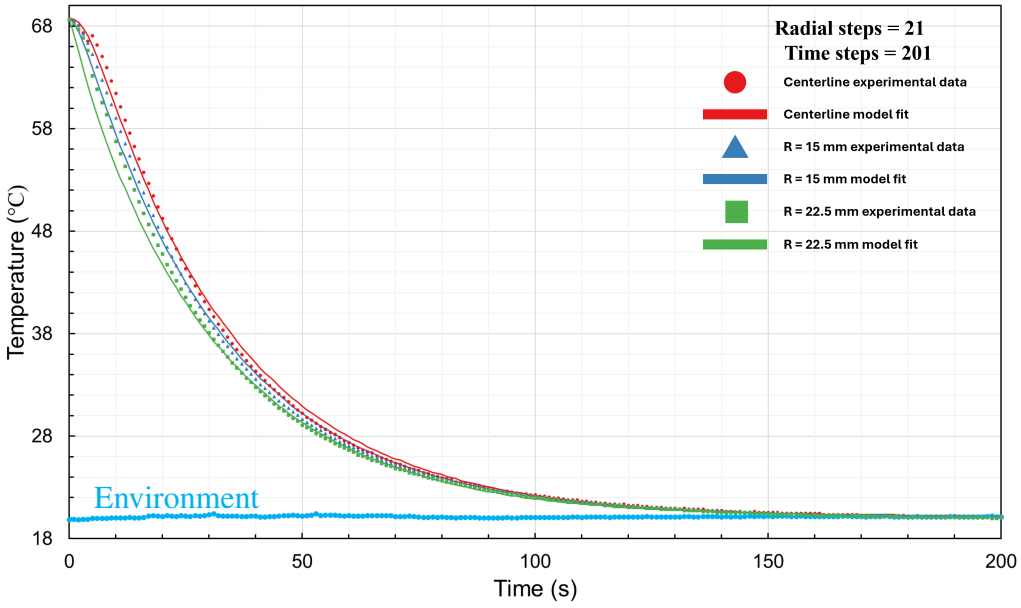

Figure 2.140: Experimental temperature data of support C of a microfibrous media bed compared with a model fit of the data as the bed is taken from approximately 69 °C and submerged in an approximately 20 °C water bath. The bed was pressurized to 50 psi gauge with hydrogen at room temperature.

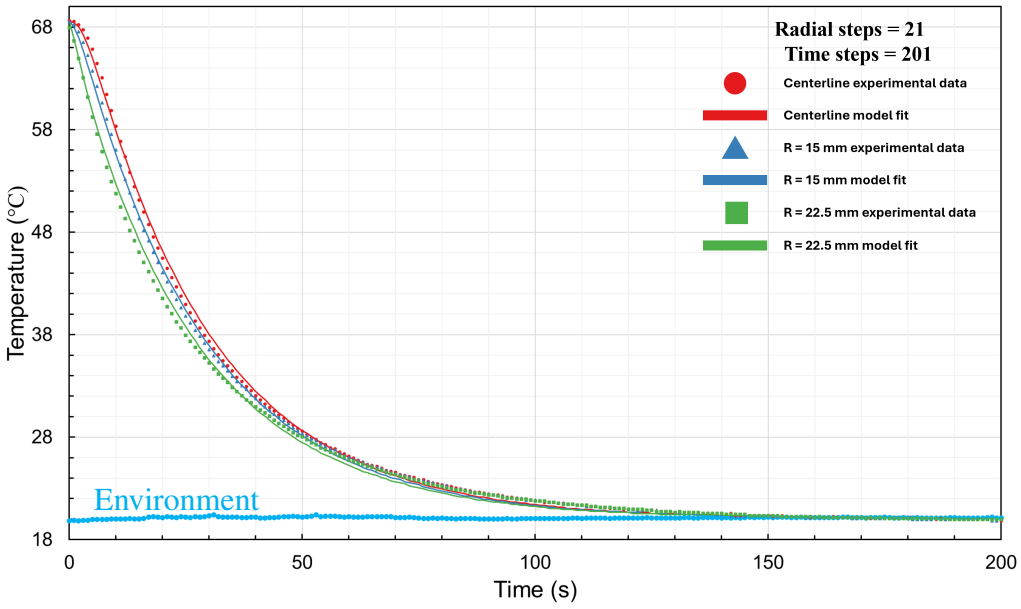

Figure 2.141: Experimental temperature data of support D of a microfibrous media bed compared with a model fit of the data as the bed is taken from approximately 69 °C and submerged in an approximately 20 °C water bath. The bed was pressurized to 50 psi gauge with hydrogen at room temperature.

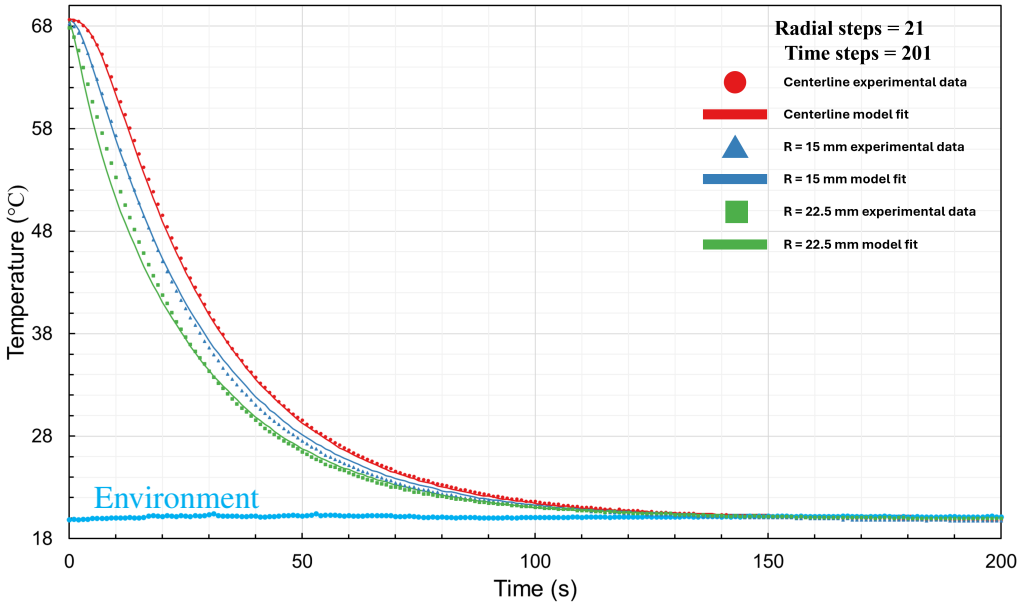

Figure 2.142: Experimental temperature data of support E of a microfibrous media bed compared with a model fit of the data as the bed is taken from approximately 69 °C and submerged in an approximately 20 °C water bath. The bed was pressurized to 50 psi gauge with hydrogen at room temperature.

2.38 Experimental and Model Comparisons for a Microfibrous Media (MFM) Bed Containing Stagnant Hydrogen Taken from Approximately 0 °C and Submerged in a 19 °C Water Bath

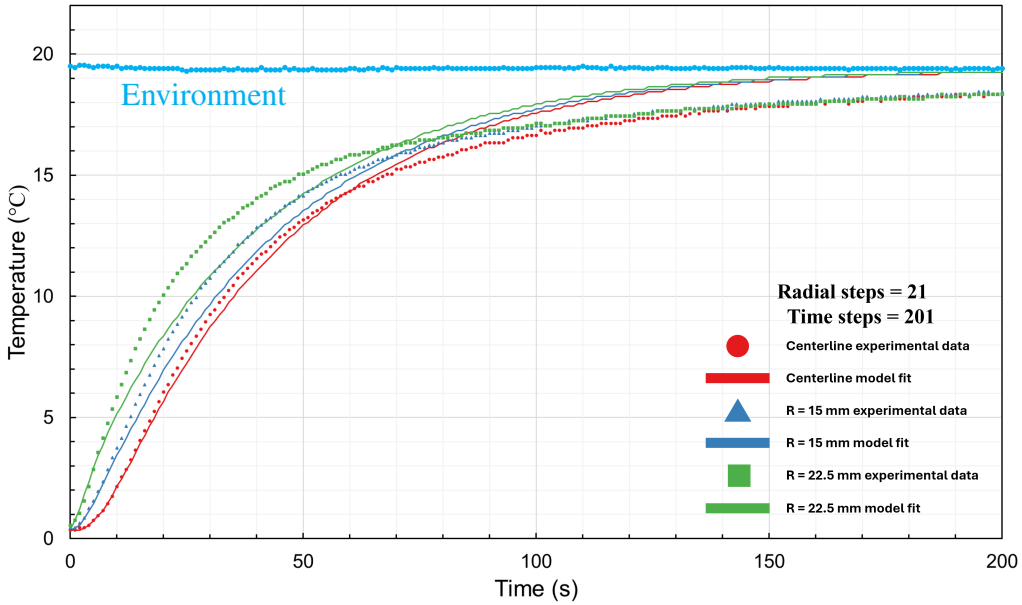

Figure 2.143: Experimental temperature data of support A of a microfibrous media bed compared with a model fit of the data as the bed is taken from approximately 0 °C and submerged in an approximately 19 °C water bath. The bed was pressurized to 50 psi gauge with hydrogen at room temperature.

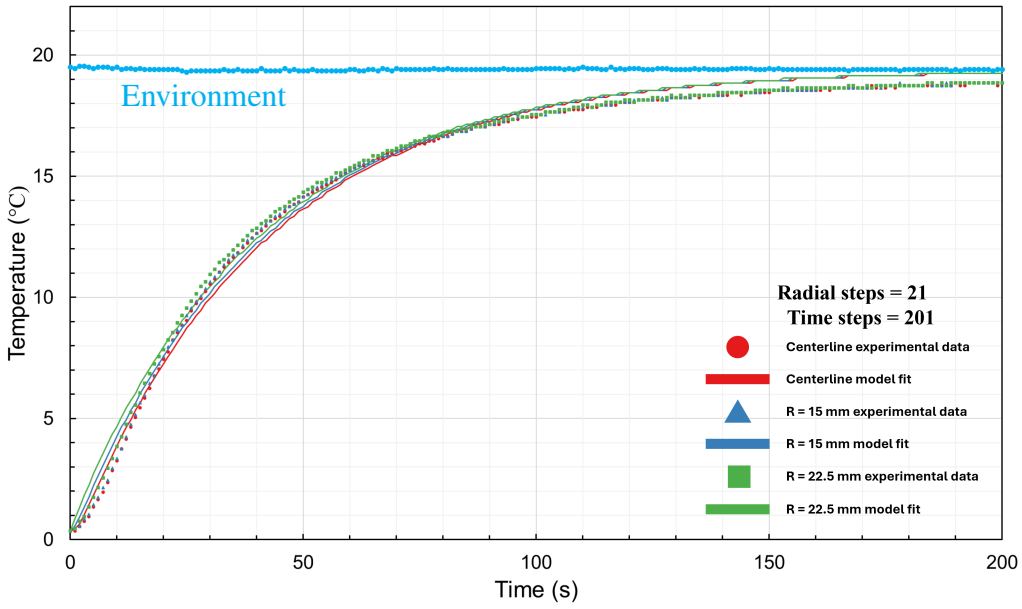

Figure 2.144: Experimental temperature data of support B of a microfibrous media bed compared with a model fit of the data as the bed is taken from approximately 0 °C and submerged in an approximately 19 °C water bath. The bed was pressurized to 50 psi gauge with hydrogen at room temperature.

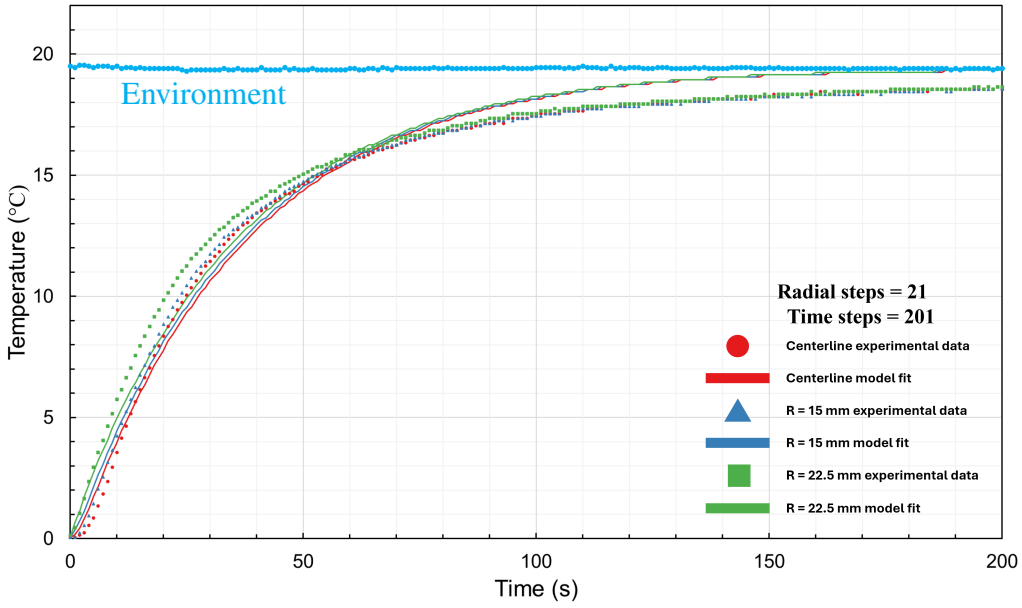

Figure 2.145: Experimental temperature data of support D of a microfibrous media bed compared with a model fit of the data as the bed is taken from approximately 0 °C and submerged in an approximately 19 °C water bath. The bed was pressurized to 50 psi gauge with hydrogen at room temperature.

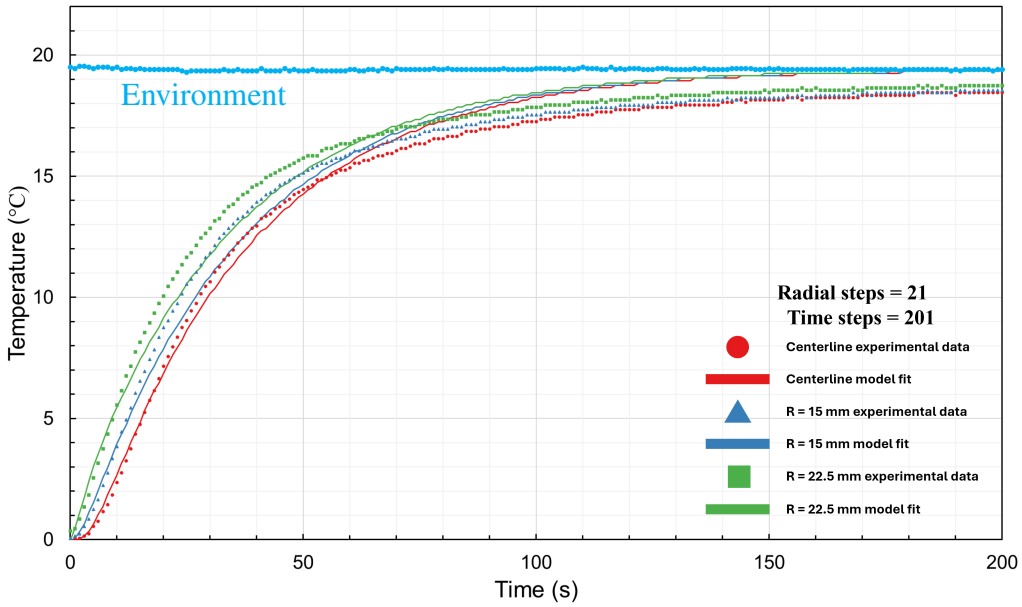

Figure 2.146: Experimental temperature data of support E of a microfibrous media bed compared with a model fit of the data as the bed is taken from approximately 0 °C and submerged in an approximately 19 °C water bath. The bed was pressurized to 50 psi gauge with hydrogen at room temperature.

2.39 Experimental and Model Comparisons for a Microfibrous Media (MFM) Bed Containing Stagnant Hydrogen Taken from Approximately 21 °C and Submerged in a 0 °C Ice-Water Bath

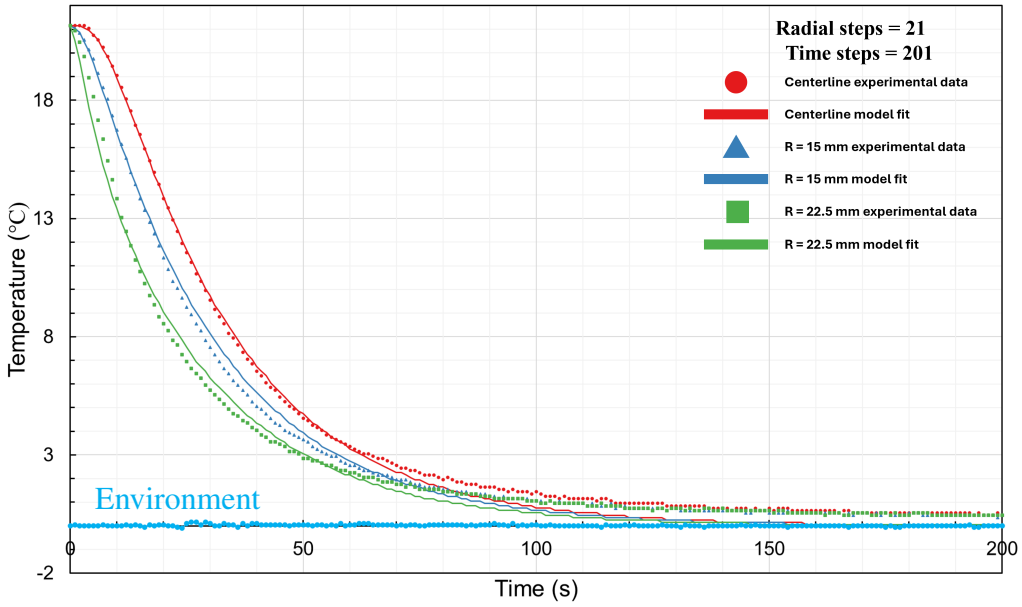

Figure 2.147: Experimental temperature data of support A of a microfibrous media bed compared with a model fit of the data as the bed is taken from approximately 21 °C and submerged in an approximately 0 °C ice-water bath. The bed was pressurized to 50 psi gauge with hydrogen at room temperature.

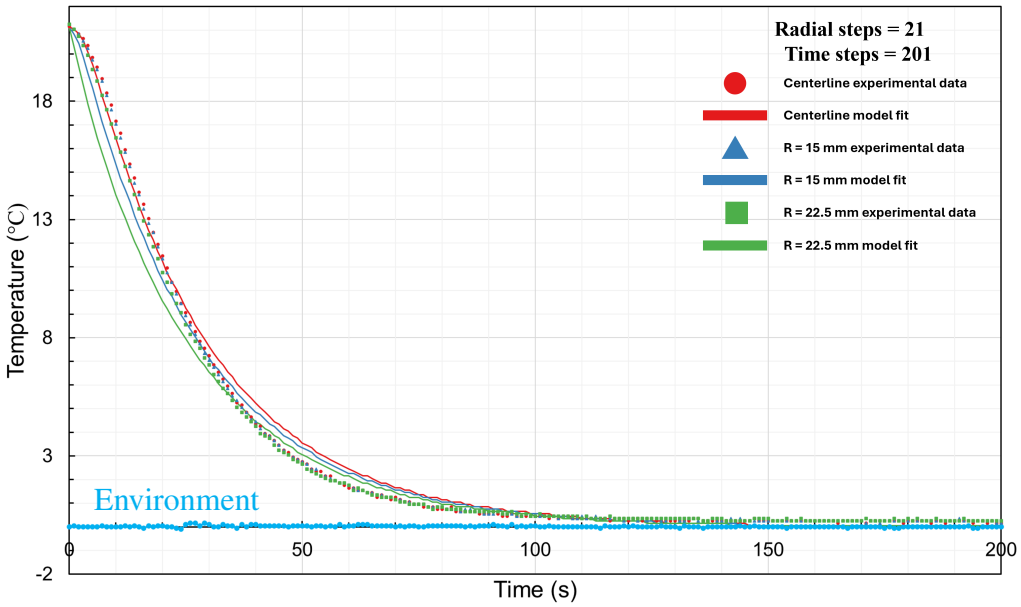

Figure 2.148: Experimental temperature data of support B of a microfibrous media bed compared with a model fit of the data as the bed is taken from approximately 21 °C and submerged in an approximately 0 °C ice-water bath. The bed was pressurized to 50 psi gauge with hydrogen at room temperature.

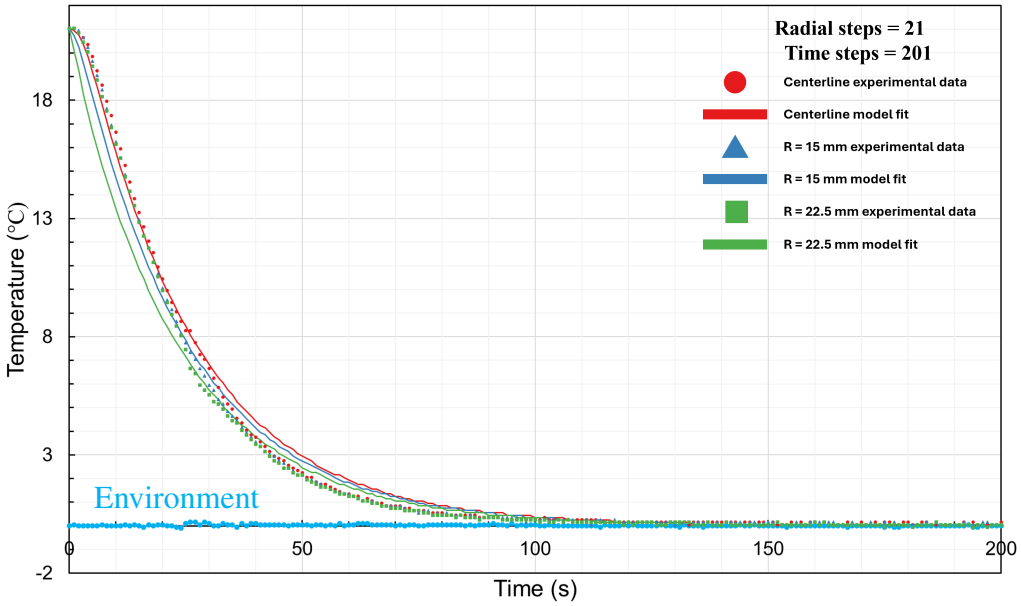

Figure 2.149: Experimental temperature data of support C of a microfibrous media bed compared with a model fit of the data as the bed is taken from approximately 21 °C and submerged in an approximately 0 °C ice-water bath. The bed was pressurized to 50 psi gauge with hydrogen at room temperature.

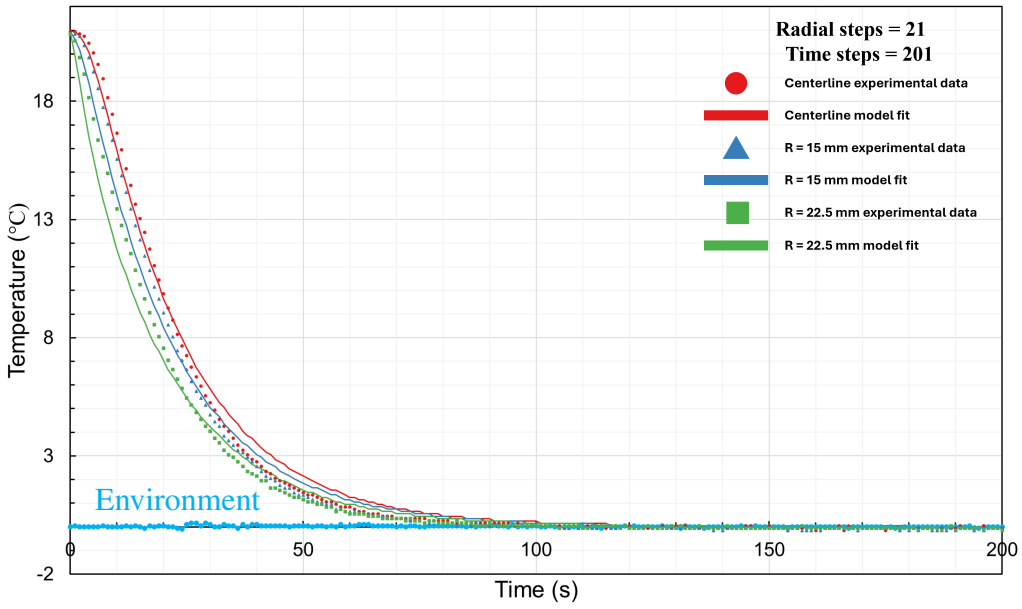

Figure 2.150: Experimental temperature data of support D of a microfibrous media bed compared with a model fit of the data as the bed is taken from approximately 21 °C and submerged in an approximately 0 °C ice-water bath. The bed was pressurized to 50 psi gauge with hydrogen at room temperature.

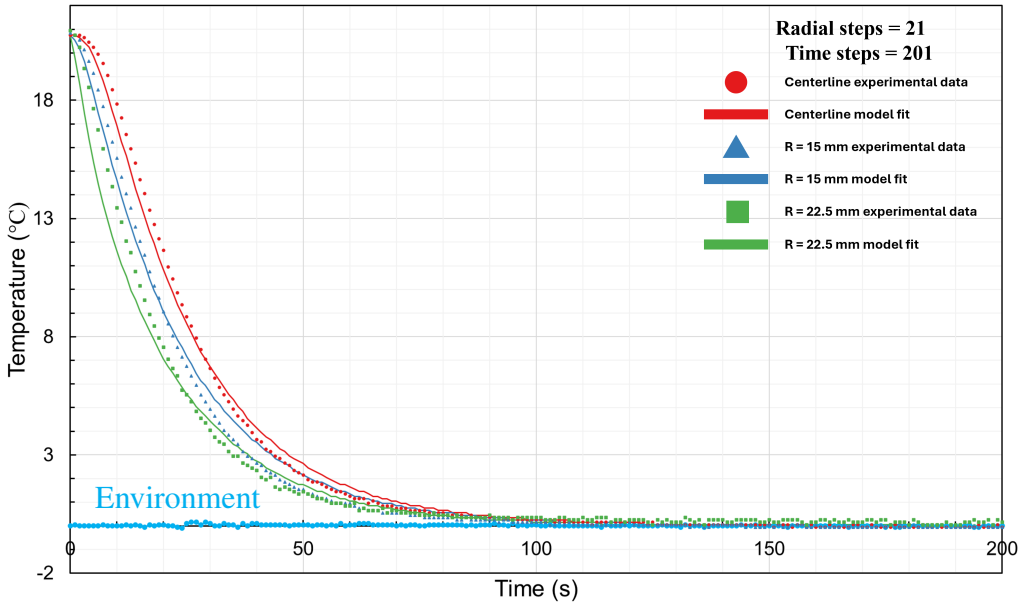

Figure 2.151: Experimental temperature data of support E of a microfibrous media bed compared with a model fit of the data as the bed is taken from approximately 21 °C and submerged in an approximately 0 °C ice-water bath. The bed was pressurized to 50 psi gauge with hydrogen at room temperature.

2.40 Experimental and Model Comparisons for a Microfibrous Media (MFM) Bed Containing Stagnant Oxygen Taken from Approximately 21 °C and Submerged in a 75 °C Water Bath

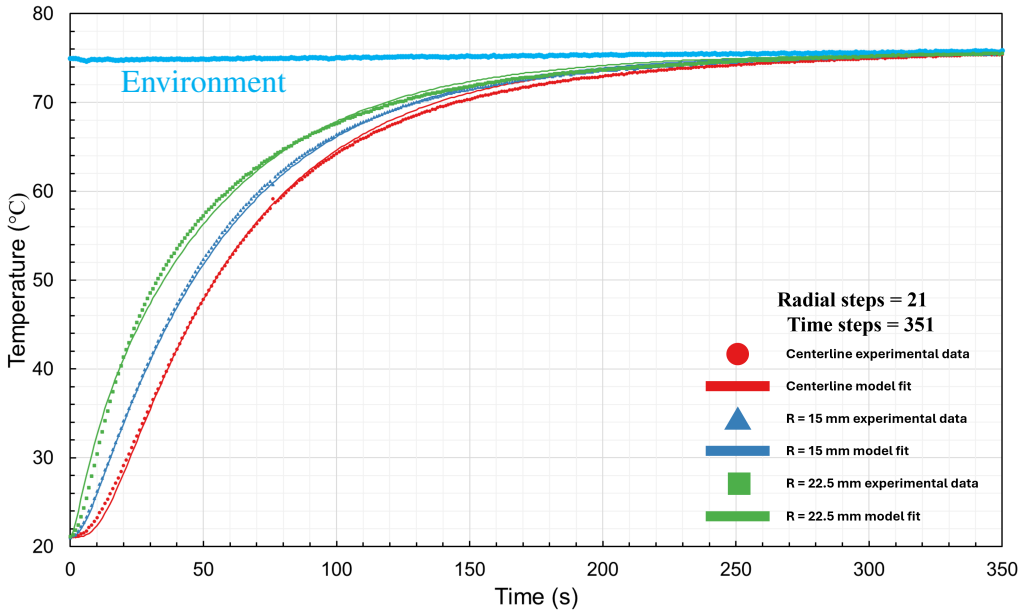

Figure 2.152: Experimental temperature data of support A of a microfibrous media bed compared with a model fit of the data as the bed is taken from approximately 21 °C and submerged in an approximately 75 °C water bath. The bed was pressurized to 50 psi gauge with oxygen at room temperature.

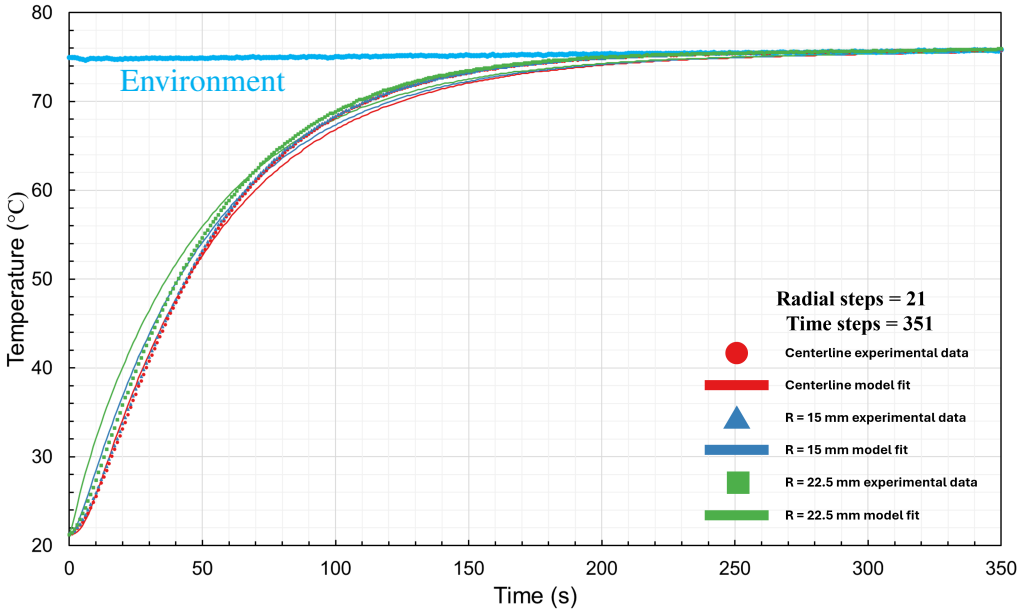

Figure 2.153: Experimental temperature data of support B of a microfibrous media bed compared with a model fit of the data as the bed is taken from approximately 21 °C and submerged in an approximately 75 °C water bath. The bed was pressurized to 50 psi gauge with oxygen at room temperature.

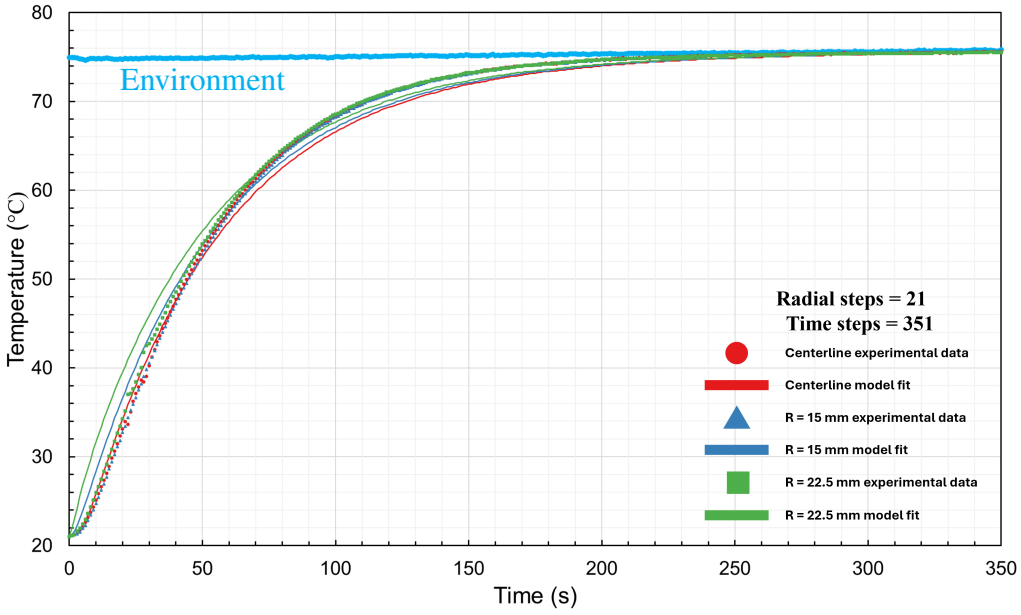

Figure 2.154: Experimental temperature data of support C of a microfibrous media bed compared with a model fit of the data as the bed is taken from approximately 21 °C and submerged in an approximately 75 °C water bath. The bed was pressurized to 50 psi gauge with oxygen at room temperature.

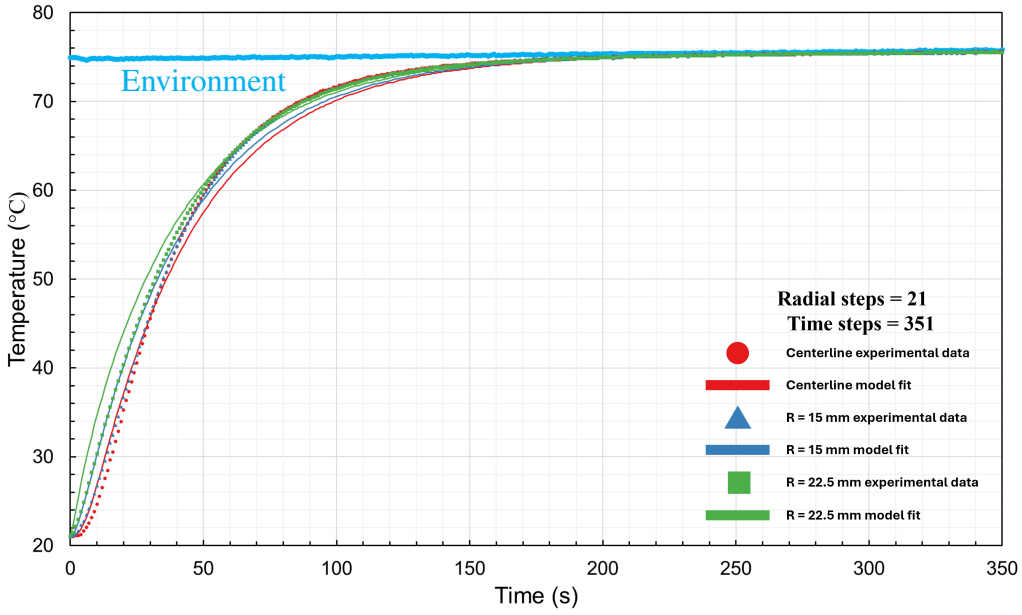

Figure 2.155: Experimental temperature data of support D of a microfibrous media bed compared with a model fit of the data as the bed is taken from approximately 21 °C and submerged in an approximately 75 °C water bath. The bed was pressurized to 50 psi gauge with oxygen at room temperature.

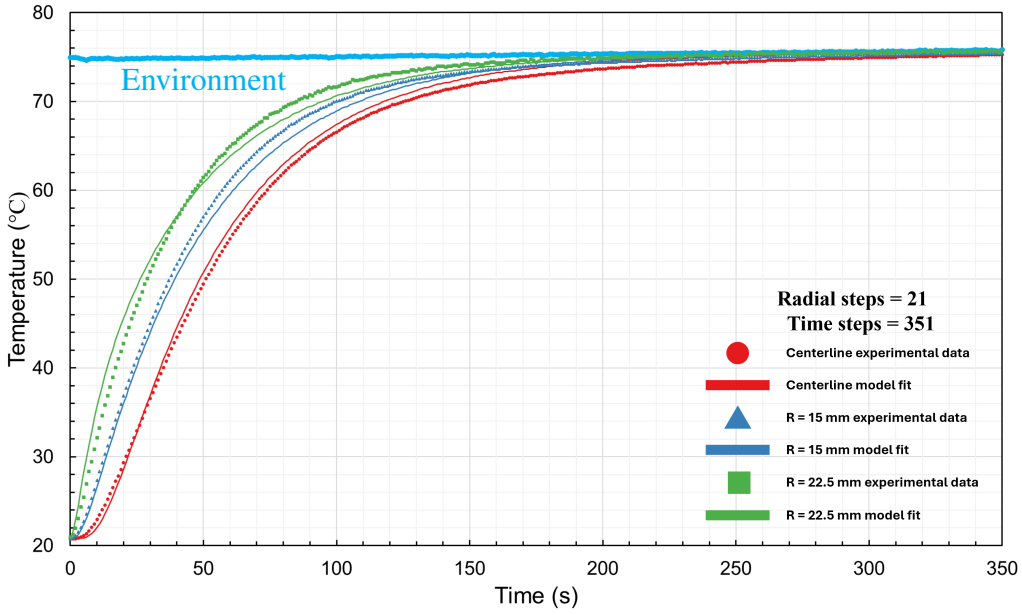

Figure 2.156: Experimental temperature data of support E of a microfibrous media bed compared with a model fit of the data as the bed is taken from approximately 21 °C and submerged in an approximately 75 °C water bath. The bed was pressurized to 50 psi gauge with oxygen at room temperature.

2.41 Experimental and Model Comparisons for a Microfibrous Media (MFM) Bed Containing Stagnant Oxygen Taken from Approximately 78 °C and Submerged in a 20 °C Water Bath

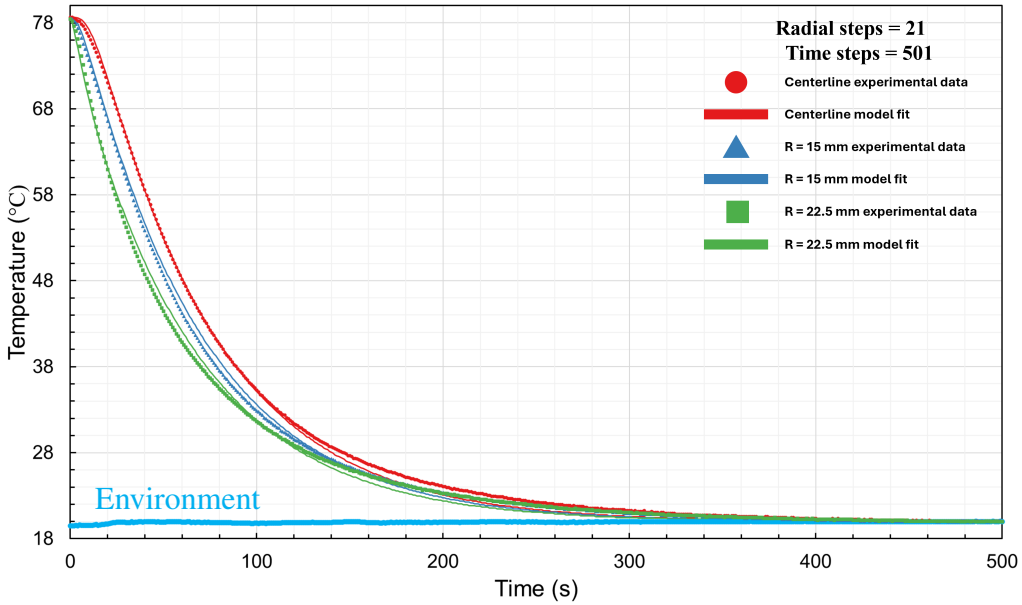

Figure 2.157: Experimental temperature data of support A of a microfibrous media bed compared with a model fit of the data as the bed is taken from approximately 78 °C and submerged in an approximately 20 °C water bath. The bed was pressurized to 50 psi gauge with oxygen at room temperature.

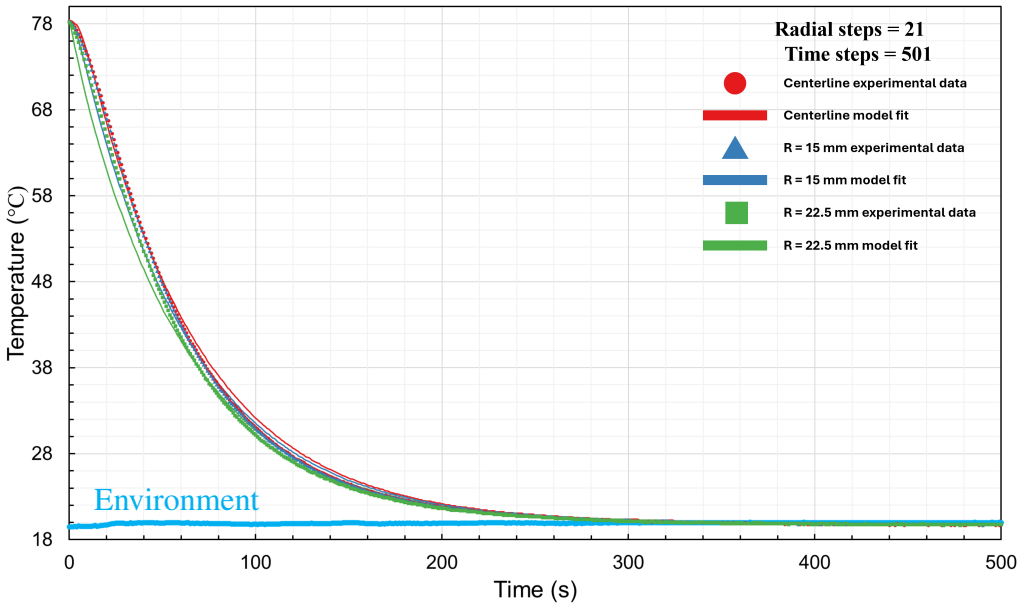

Figure 2.158: Experimental temperature data of support B of a microfibrous media bed compared with a model fit of the data as the bed is taken from approximately 78 °C and submerged in an approximately 20 °C water bath. The bed was pressurized to 50 psi gauge with oxygen at room temperature.

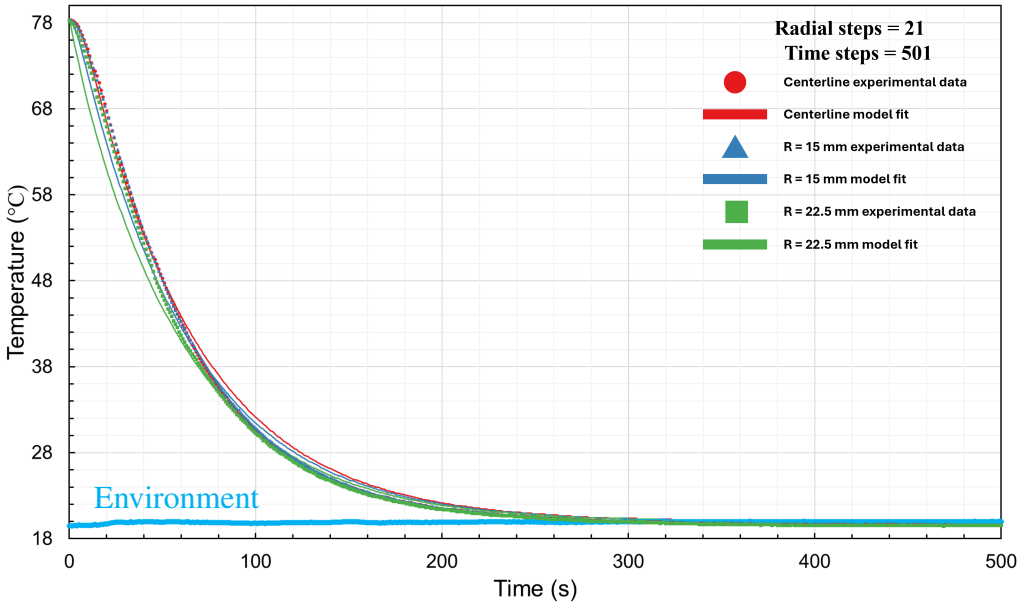

Figure 2.159: Experimental temperature data of support C of a microfibrous media bed compared with a model fit of the data as the bed is taken from approximately 78 °C and submerged in an approximately 20 °C water bath. The bed was pressurized to 50 psi gauge with oxygen at room temperature.

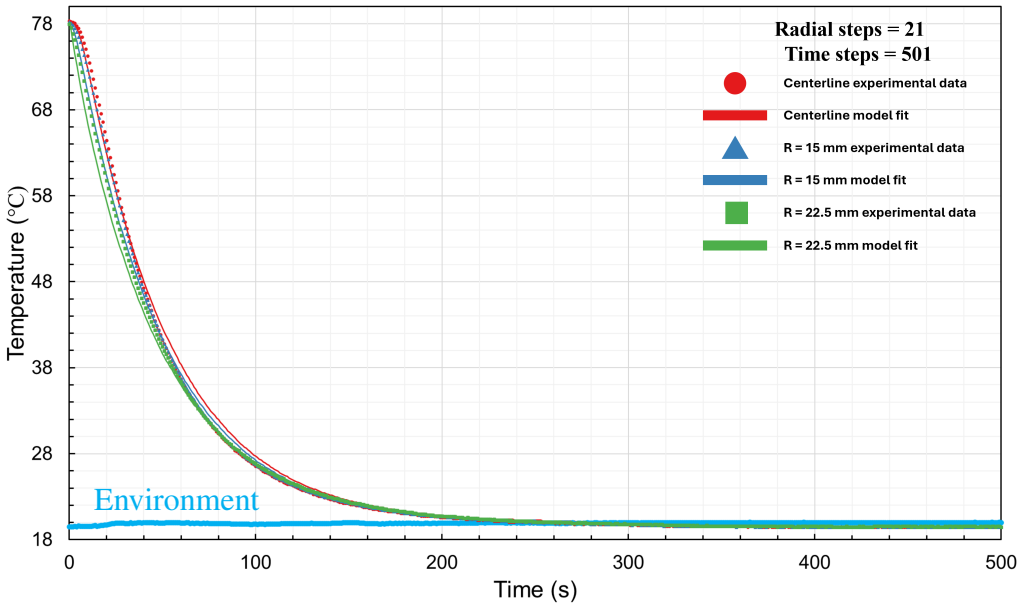

Figure 2.160: Experimental temperature data of support D of a microfibrous media bed compared with a model fit of the data as the bed is taken from approximately 78 °C and submerged in an approximately 20 °C water bath. The bed was pressurized to 50 psi gauge with oxygen at room temperature.

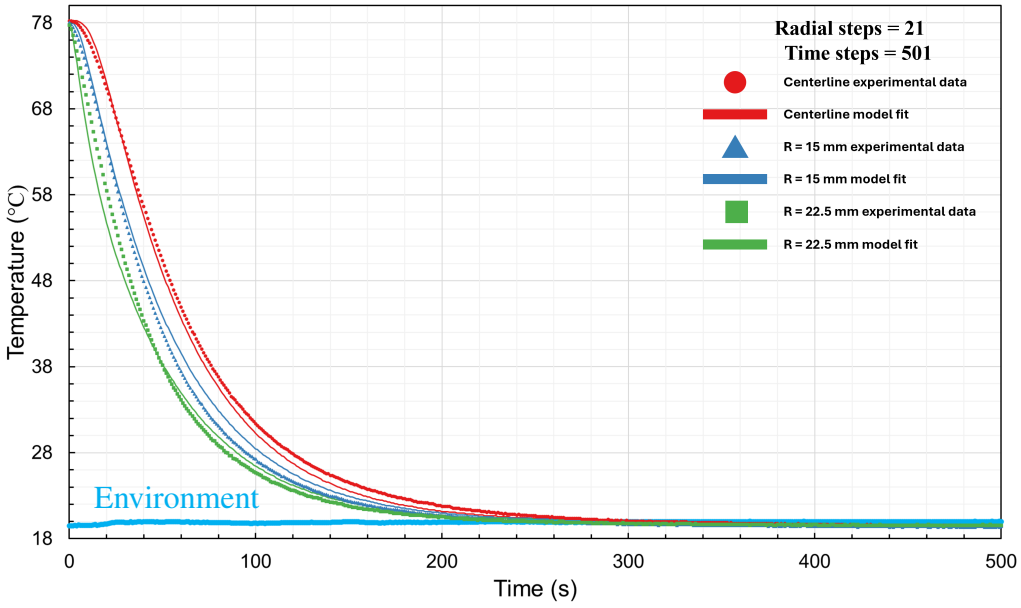

Figure 2.161: Experimental temperature data of support E of a microfibrous media bed compared with a model fit of the data as the bed is taken from approximately 78 °C and submerged in an approximately 20 °C water bath. The bed was pressurized to 50 psi gauge with oxygen at room temperature.

2.42 Experimental and Model Comparisons for a Microfibrous Media (MFM) Bed Containing Stagnant Oxygen Taken from Approximately 0 °C and Submerged in a 20 °C Water Bath

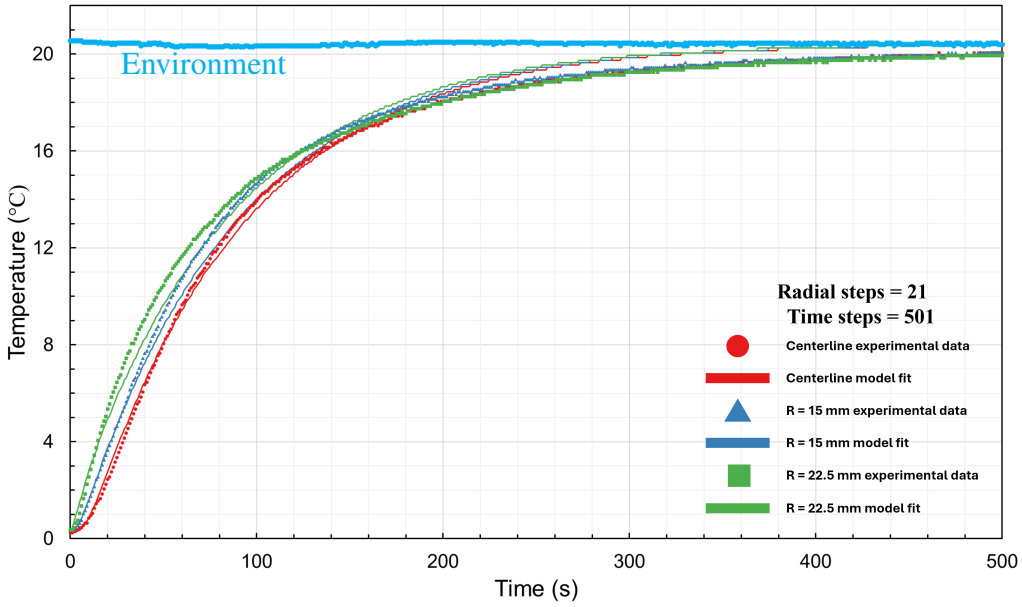

Figure 2.162: Experimental temperature data of support A of a microfibrous media bed compared with a model fit of the data as the bed is taken from approximately 0 °C and submerged in an approximately 20 °C water bath. The bed was pressurized to 50 psi gauge with oxygen at room temperature.

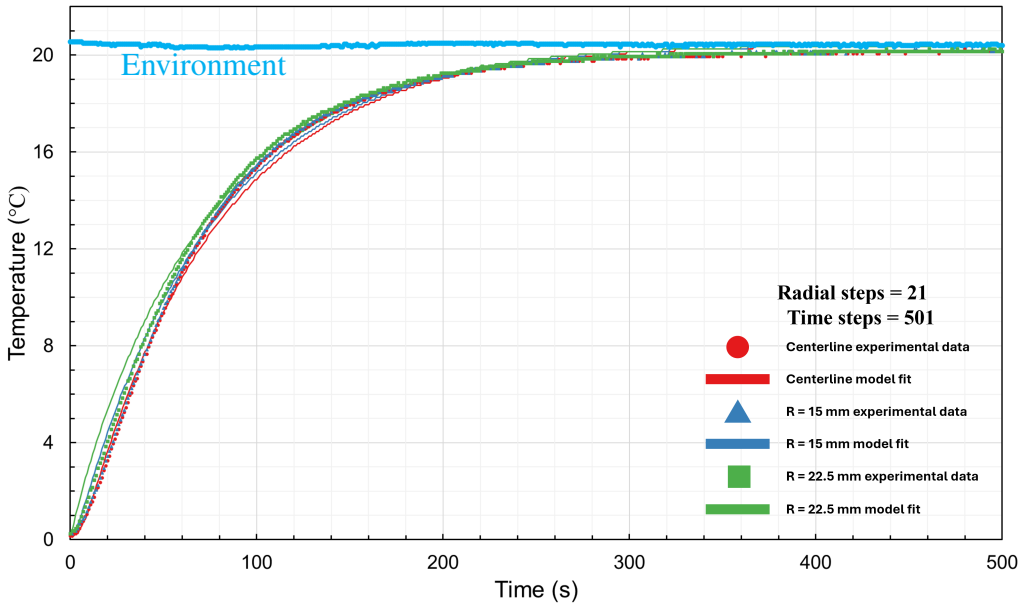

Figure 2.163: Experimental temperature data of support B of a microfibrous media bed compared with a model fit of the data as the bed is taken from approximately 0 °C and submerged in an approximately 20 °C water bath. The bed was pressurized to 50 psi gauge with oxygen at room temperature.

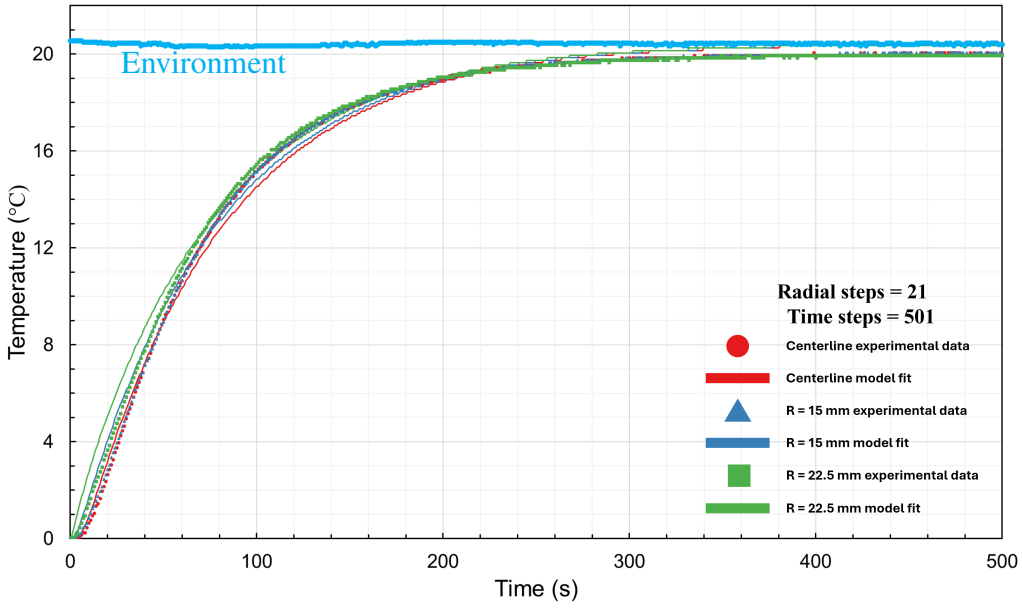

Figure 2.164: Experimental temperature data of support C of a microfibrous media bed compared with a model fit of the data as the bed is taken from approximately 0 °C and submerged in an approximately 20 °C water bath. The bed was pressurized to 50 psi gauge with oxygen at room temperature.

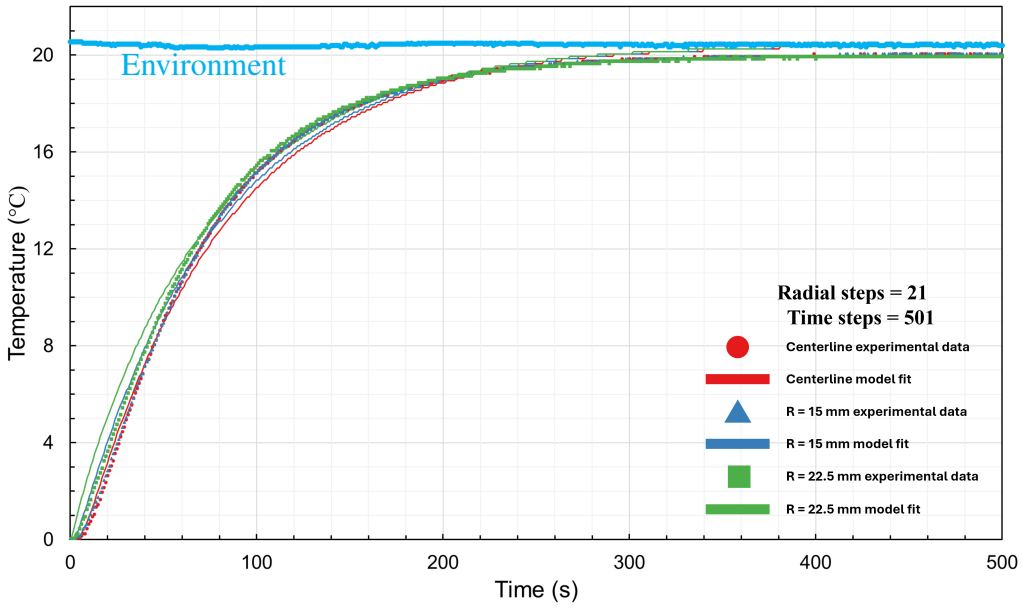

Figure 2.165: Experimental temperature data of support D of a microfibrous media bed compared with a model fit of the data as the bed is taken from approximately 0 °C and submerged in an approximately 20 °C water bath. The bed was pressurized to 50 psi gauge with oxygen at room temperature.

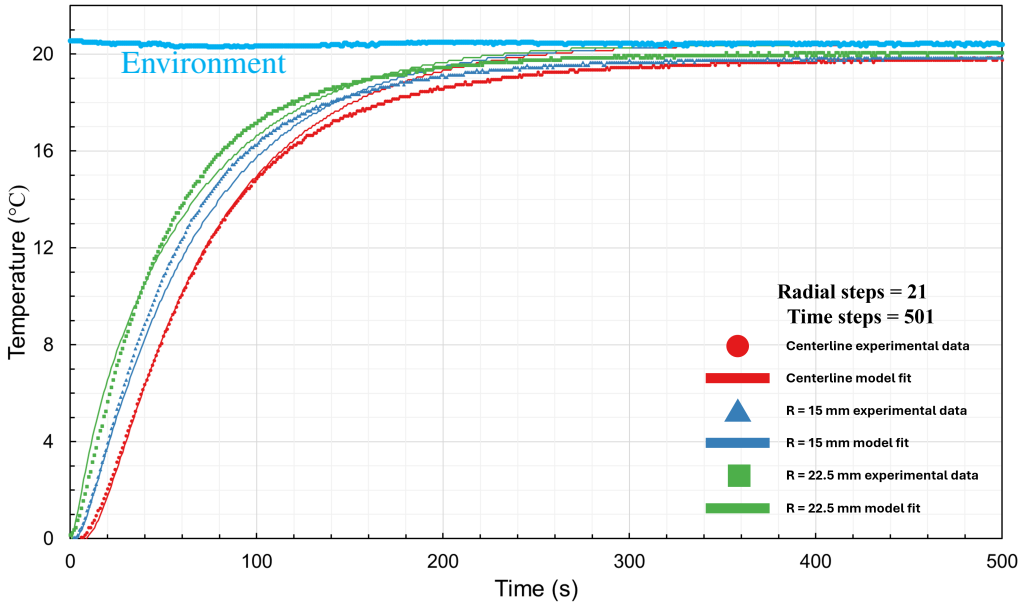

Figure 2.166: Experimental temperature data of support E of a microfibrous media bed compared with a model fit of the data as the bed is taken from approximately 0 °C and submerged in an approximately 20 °C water bath. The bed was pressurized to 50 psi gauge with oxygen at room temperature.

2.43 Experimental and Model Comparisons for a Microfibrous Media (MFM) Bed Containing Stagnant Oxygen Taken from Approximately 20 °C and Submerged in a 0 °C Ice-Water Bath

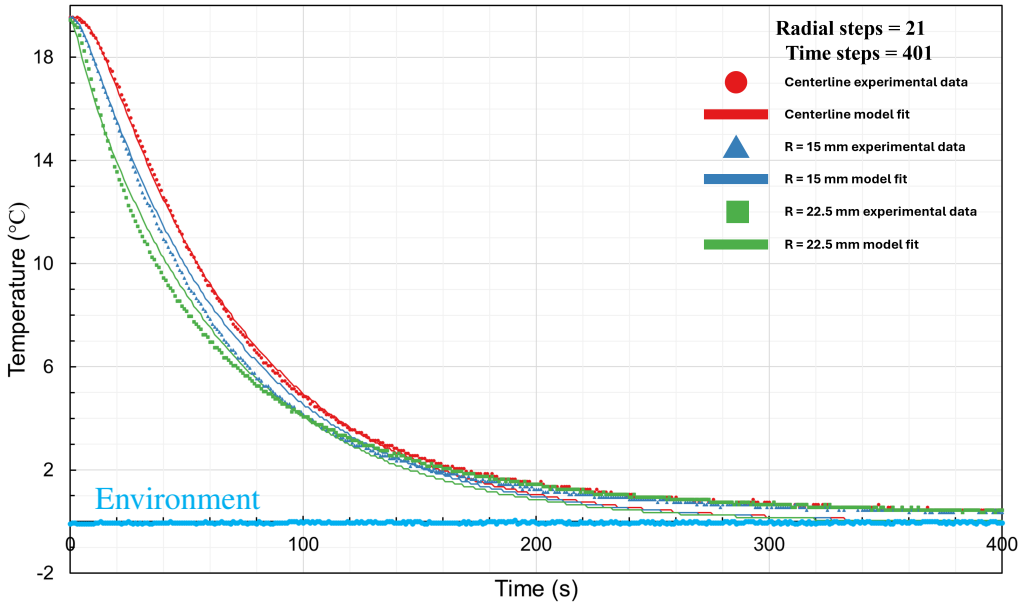

Figure 2.167: Experimental temperature data of support A of a microfibrous media bed compared with a model fit of the data as the bed is taken from approximately 20 °C and submerged in an approximately 0 °C ice-water bath. The bed was pressurized to 50 psi gauge with oxygen at room temperature.

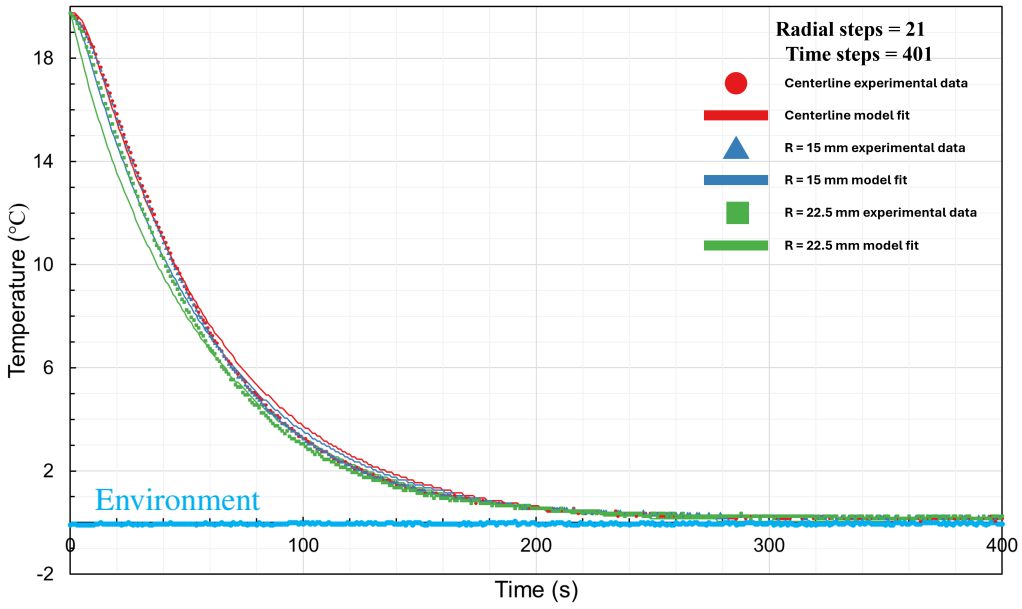

Figure 2.168: Experimental temperature data of support B of a microfibrous media bed compared with a model fit of the data as the bed is taken from approximately 20 °C and submerged in an approximately 0 °C ice-water bath. The bed was pressurized to 50 psi gauge with oxygen at room temperature.

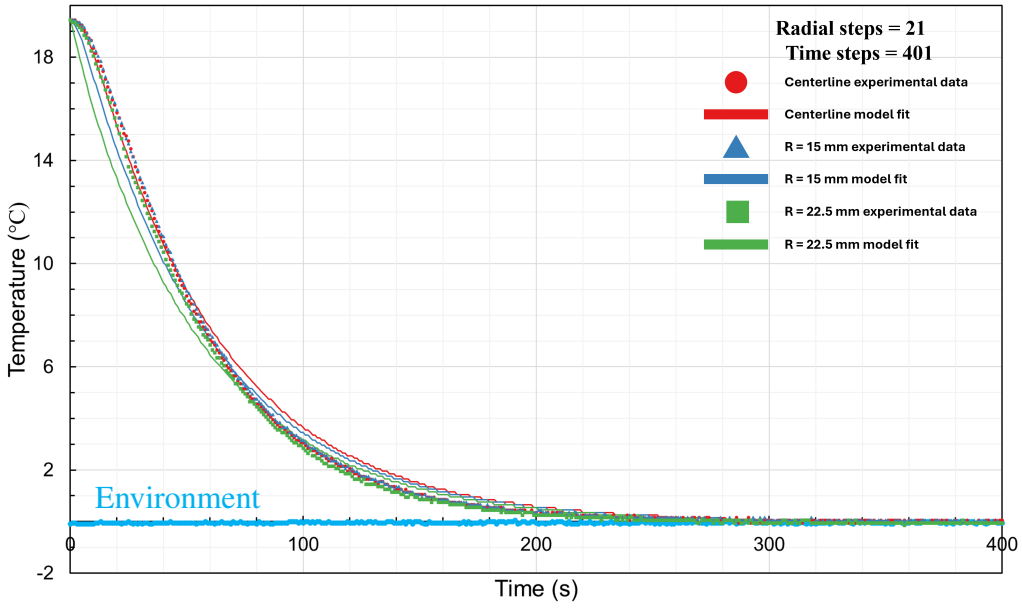

Figure 2.169: Experimental temperature data of support C of a microfibrous media bed compared with a model fit of the data as the bed is taken from approximately 20 °C and submerged in an approximately 0 °C ice-water bath. The bed was pressurized to 50 psi gauge with oxygen at room temperature.

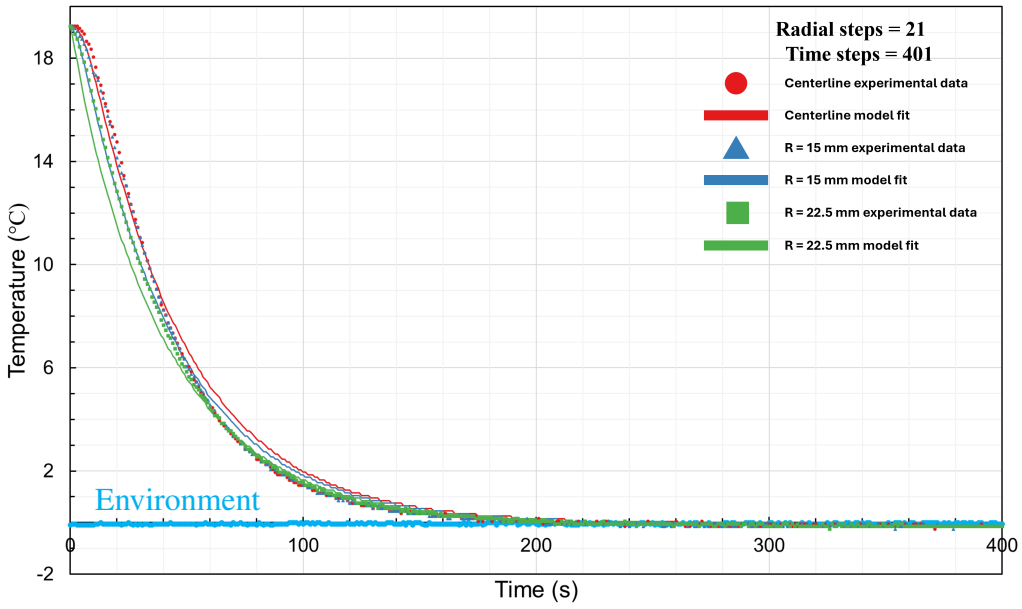

Figure 2.170: Experimental temperature data of support D of a microfibrous media bed compared with a model fit of the data as the bed is taken from approximately 20 °C and submerged in an approximately 0 °C ice-water bath. The bed was pressurized to 50 psi gauge with oxygen at room temperature.

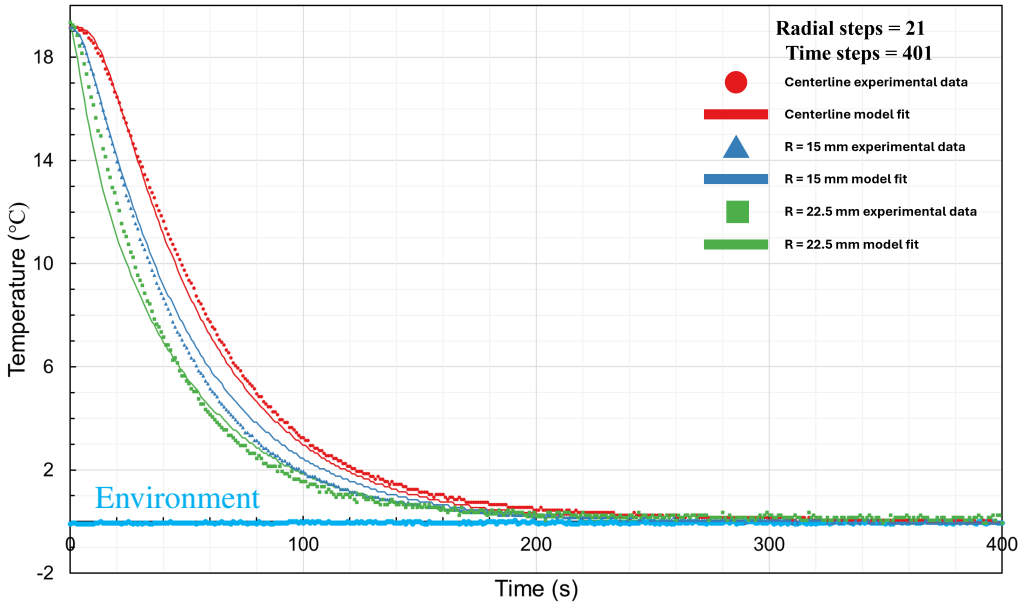

Figure 2.171: Experimental temperature data of support E of a microfibrous media bed compared with a model fit of the data as the bed is taken from approximately 20 °C and submerged in an approximately 0 °C ice-water bath. The bed was pressurized to 50 psi gauge with oxygen at room temperature.

2.44 Experimental and Model Comparisons for a Microfibrous Media (MFM) Bed Reduced to Vacuum and Taken from Approximately 22 °C and Submerged in a 70 °C Water Bath

Support E was fit using only 350 seconds due to thermocouple E3 failing to record temperature at least once after this point.

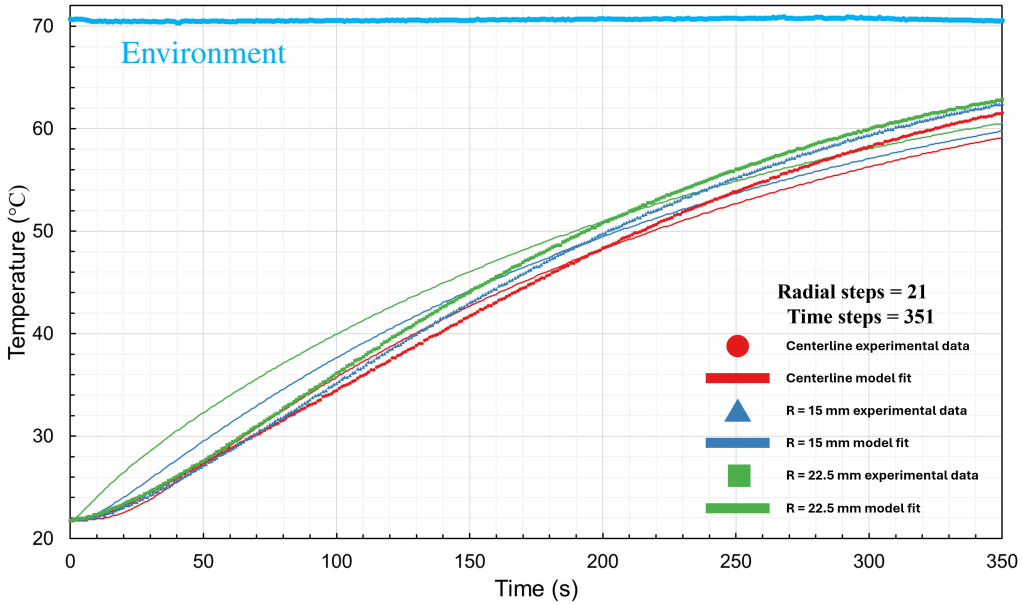

Figure 2.172: Experimental temperature data of support A of a microfibrous media bed compared with a model fit of the data as the bed is taken from approximately 22 °C and submerged in an approximately 70 °C water bath. The bed was reduced to 0.0033 mbar vacuum at room temperature.

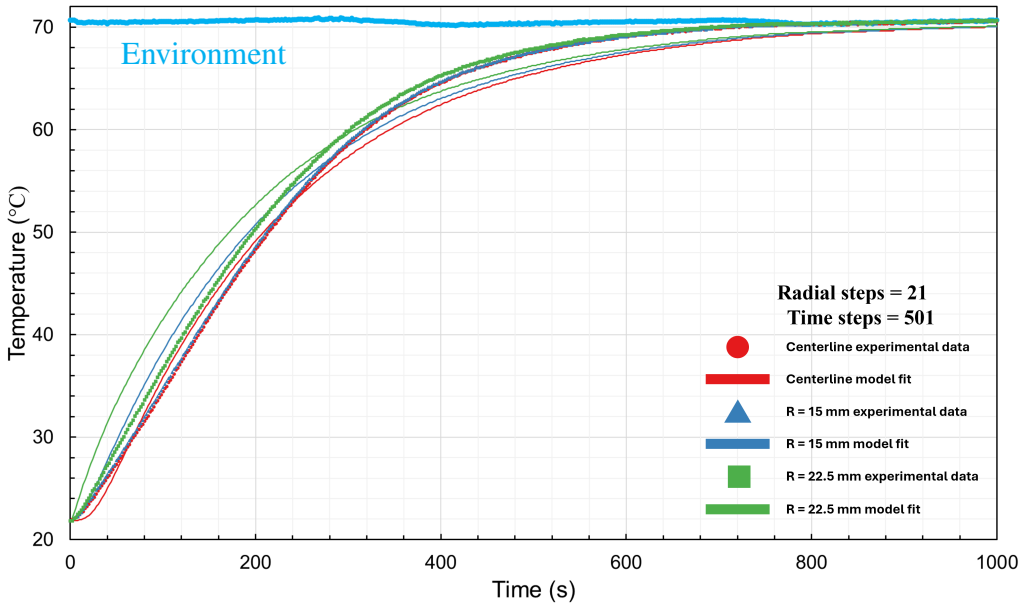

Figure 2.173: Experimental temperature data of support B of a microfibrous media bed compared with a model fit of the data as the bed is taken from approximately 22 °C and submerged in an approximately 70 °C water bath. The bed was reduced to 0.0033 mbar vacuum at room temperature.

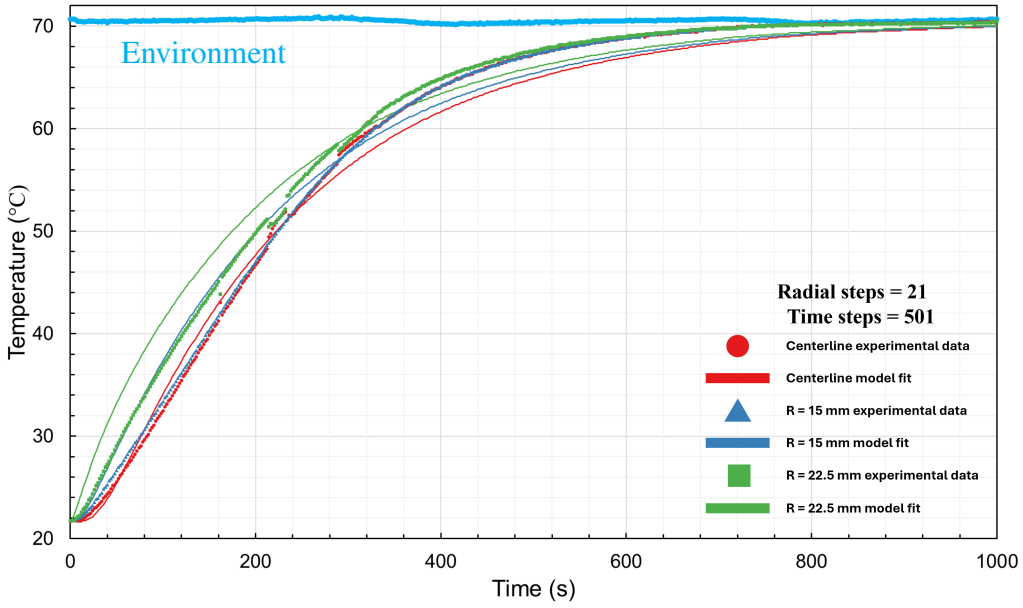

Figure 2.174: Experimental temperature data of support C of a microfibrous media bed compared with a model fit of the data as the bed is taken from approximately 22 °C and submerged in an approximately 70 °C water bath. The bed was reduced to 0.0033 mbar vacuum at room temperature.

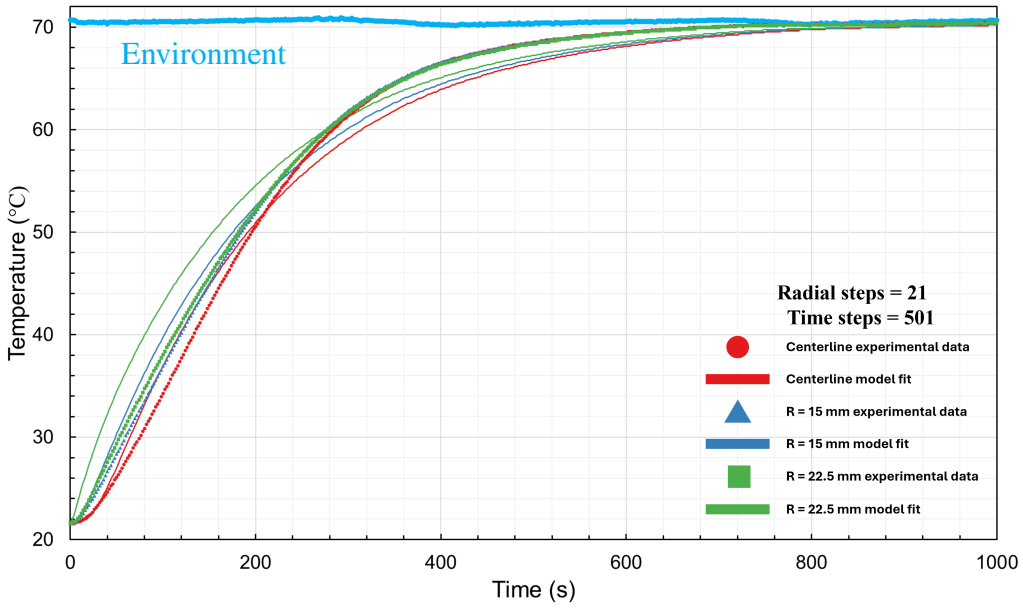

Figure 2.175: Experimental temperature data of support D of a microfibrous media bed compared with a model fit of the data as the bed is taken from approximately 22 °C and submerged in an approximately 70 °C water bath. The bed was reduced to 0.0033 mbar vacuum at room temperature.

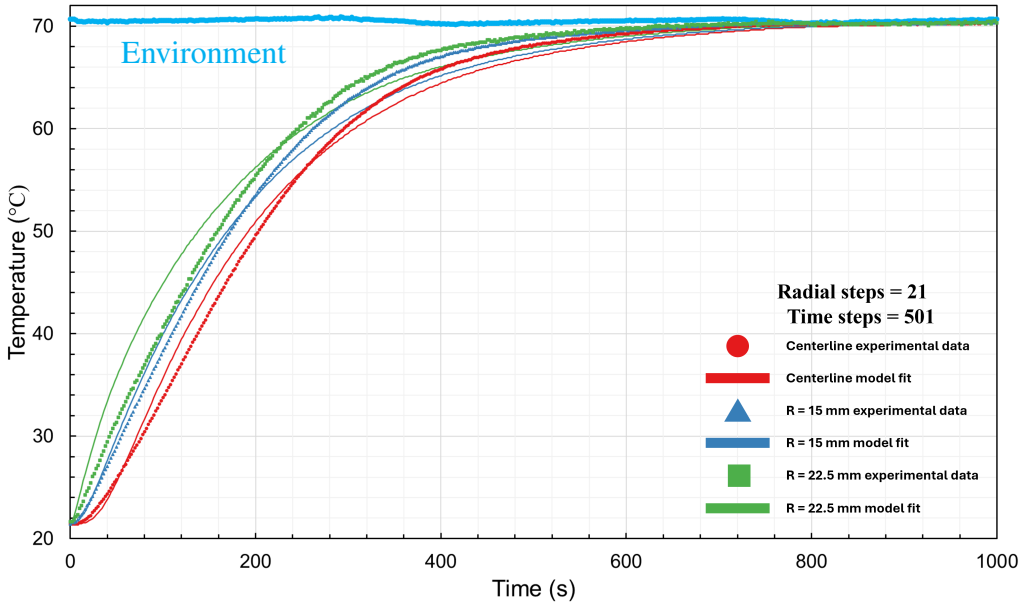

Figure 2.176: Experimental temperature data of support E of a microfibrous media bed compared with a model fit of the data as the bed is taken from approximately 22 °C and submerged in an approximately 70 °C water bath. The bed was reduced to 0.0033 mbar vacuum at room temperature.

2.45 Experimental and Model Comparisons for a Microfibrous Media (MFM) Bed Reduced to Vacuum and Taken from Approximately 70 °C and Submerged in a 19 °C Water Bath

Support E was fit using only 450 seconds due to thermocouple E3 failing to record temperature at occasional times after this point.

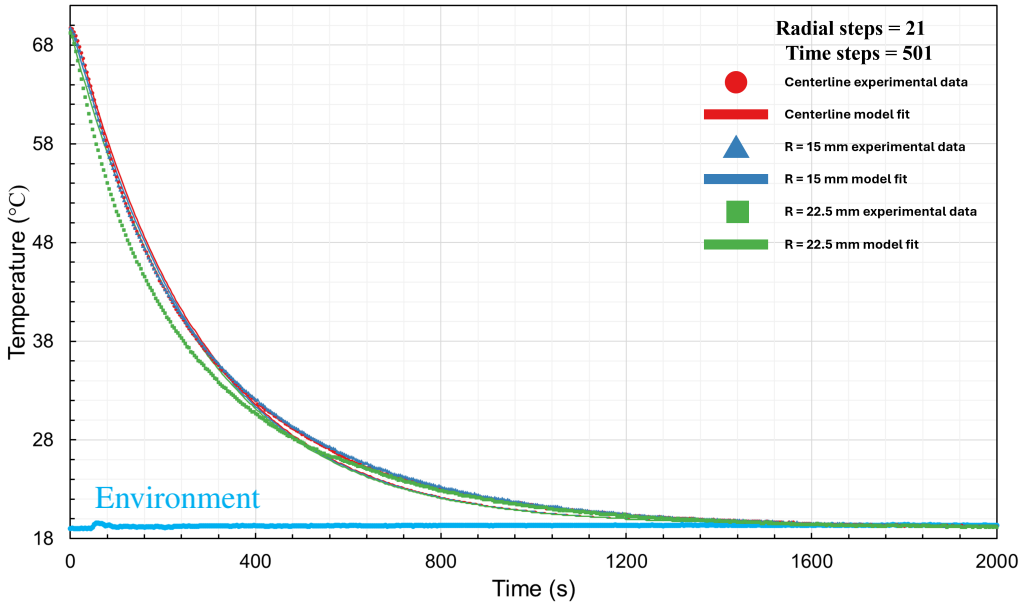

Figure 2.177: Experimental temperature data of support C of a microfibrous media bed compared with a model fit of the data as the bed is taken from approximately 70 °C and submerged in an approximately 19 °C water bath. The bed was reduced to 0.0033 mbar vacuum at room temperature.

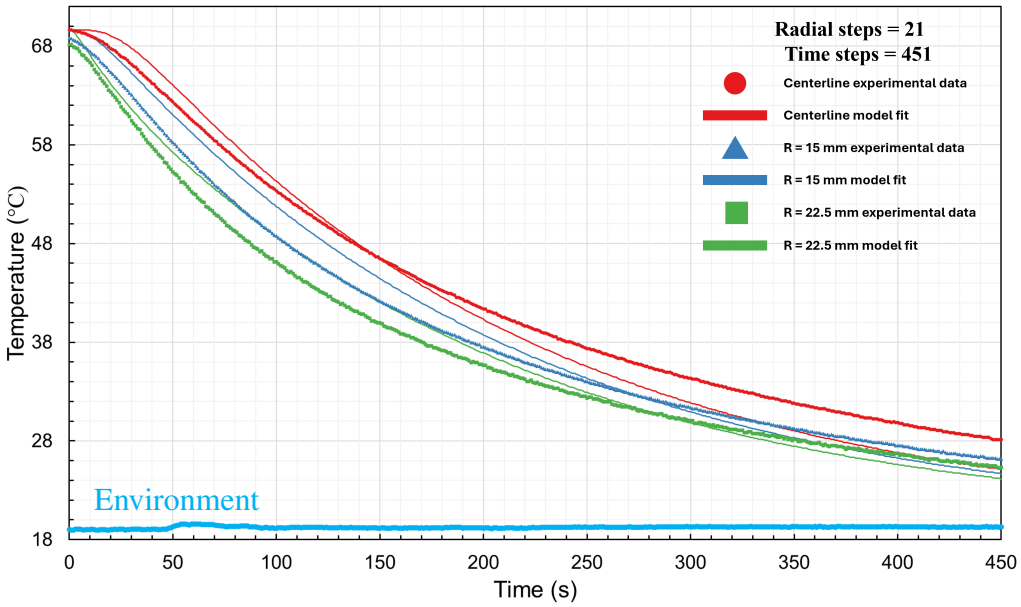

Figure 2.178: Experimental temperature data of support E of a microfibrous media bed compared with a model fit of the data as the bed is taken from approximately 70 °C and submerged in an approximately 19 °C water bath. The bed was reduced to 0.0033 mbar vacuum at room temperature.

2.46 Experimental and Model Comparisons for a Microfibrous Media (MFM) Bed Reduced to Vacuum and Taken from Approximately 0 °C and Submerged in a 19 °C Water Bath

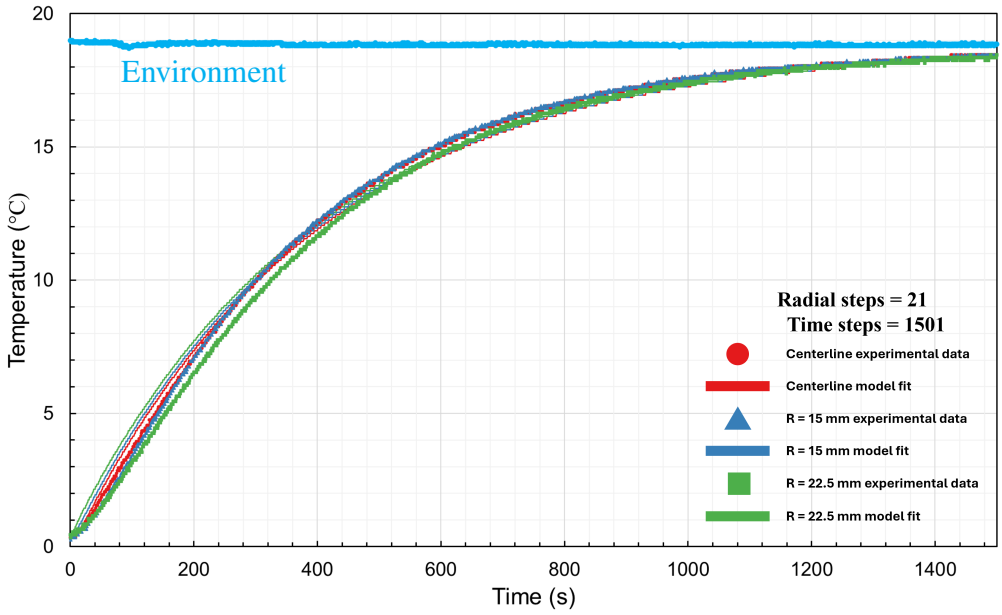

Figure 2.179: Experimental temperature data of support A of a microfibrous media bed compared with a model fit of the data as the bed is taken from approximately 0 °C and submerged in an approximately 19 °C water bath. The bed was reduced to 0.0029 mbar vacuum at room temperature.

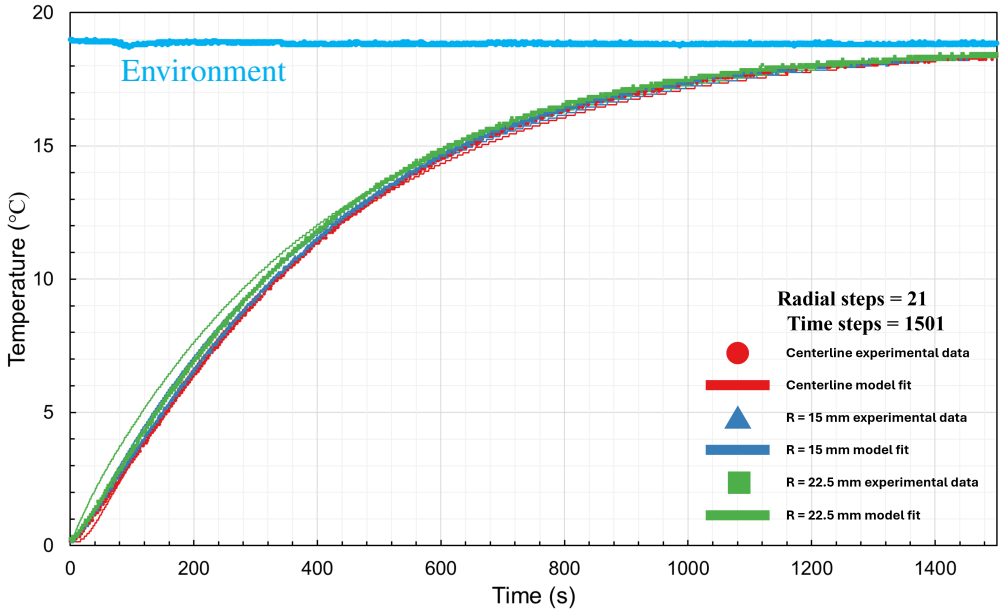

Figure 2.180: Experimental temperature data of support B of a microfibrous media bed compared with a model fit of the data as the bed is taken from approximately 0 °C and submerged in an approximately 19 °C water bath. The bed was reduced to 0.0029 mbar vacuum at room temperature.

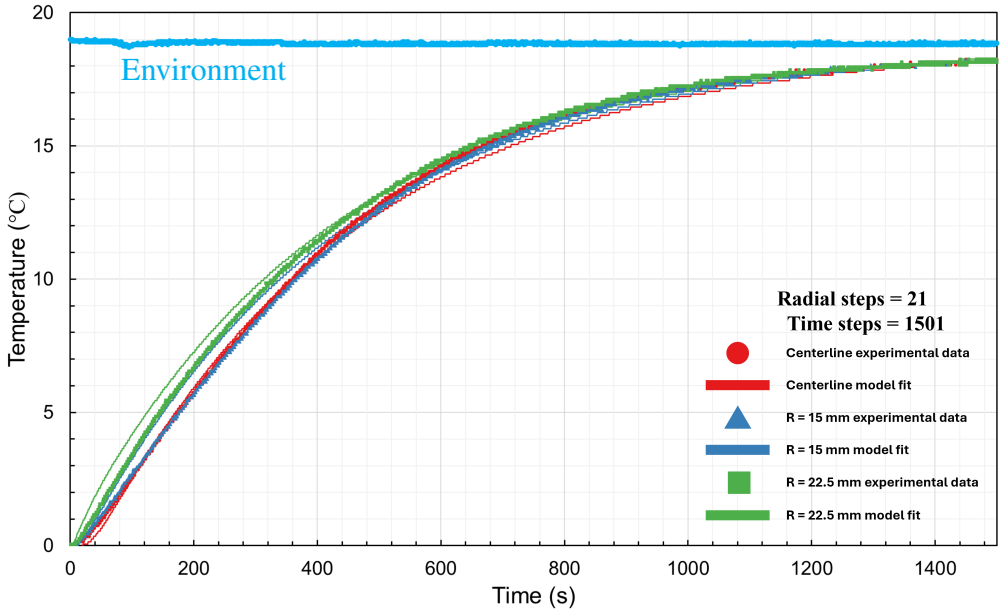

Figure 2.181: Experimental temperature data of support C of a microfibrous media bed compared with a model fit of the data as the bed is taken from approximately 0 °C and submerged in an approximately 19 °C water bath. The bed was reduced to 0.0029 mbar vacuum at room temperature.

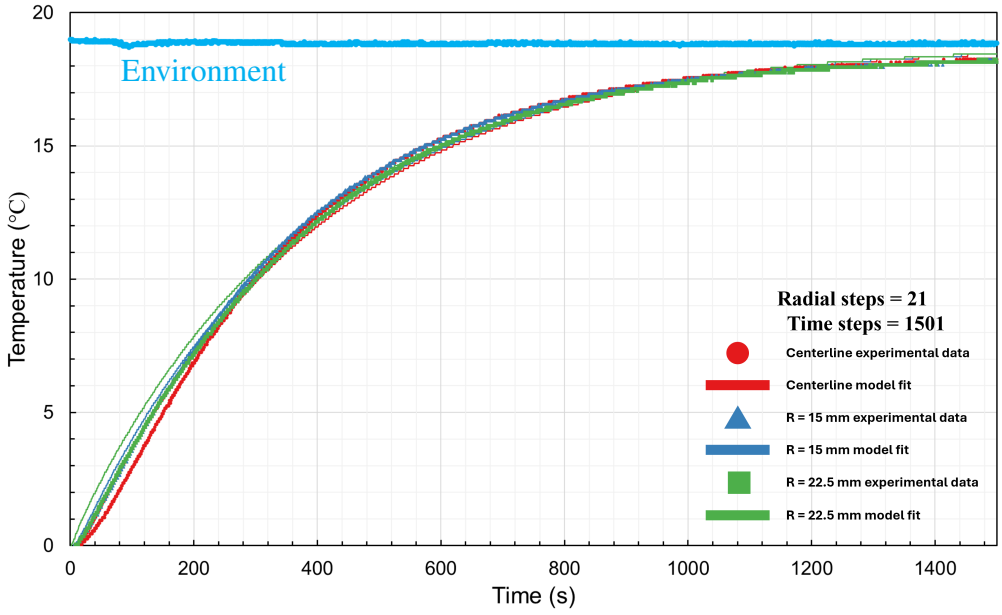

Figure 2.182: Experimental temperature data of support D of a microfibrous media bed compared with a model fit of the data as the bed is taken from approximately 0 °C and submerged in an approximately 19 °C water bath. The bed was reduced to 0.0029 mbar vacuum at room temperature.

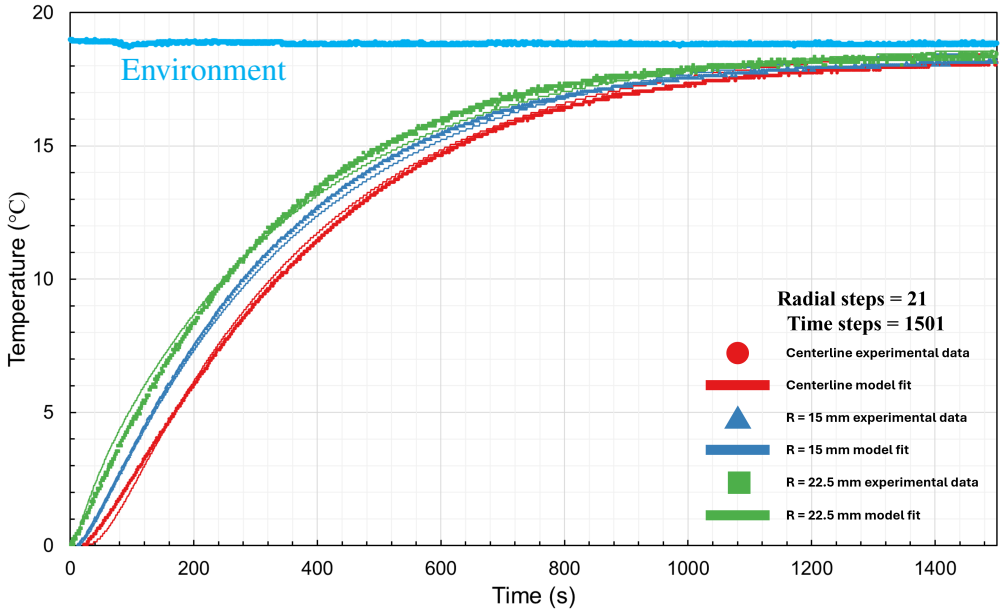

Figure 2.183: Experimental temperature data of support E of a microfibrous media bed compared with a model fit of the data as the bed is taken from approximately 0 °C and submerged in an approximately 19 °C water bath. The bed was reduced to 0.0029 mbar vacuum at room temperature.

2.47 Experimental and Model Comparisons for a Microfibrous Media (MFM) Bed Reduced to Vacuum and Taken from Approximately 22 °C and Submerged in a 0 °C Ice-Water Bath

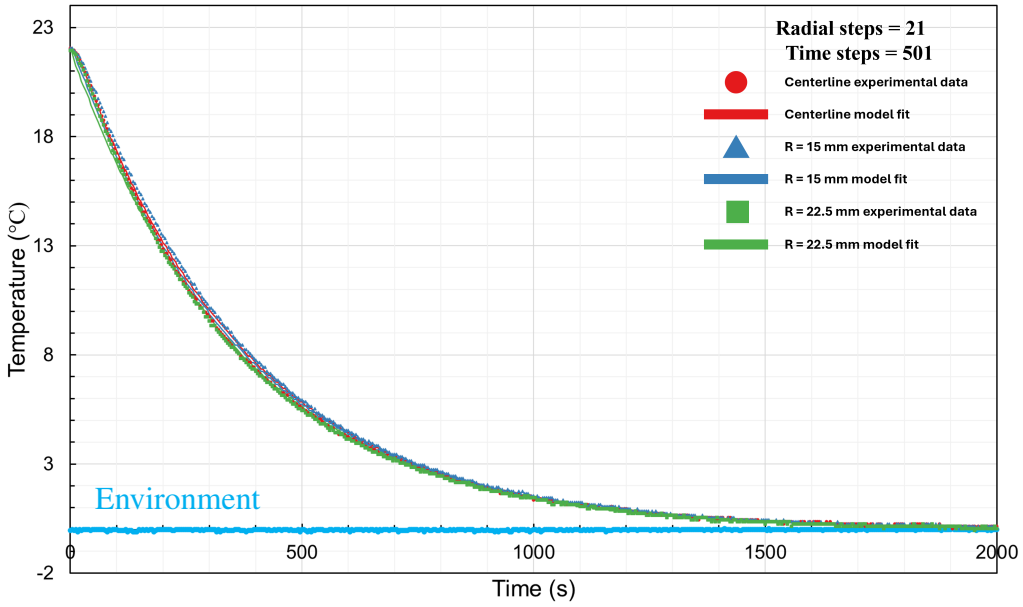

Figure 2.184: Experimental temperature data of support C of a microfibrous media bed compared with a model fit of the data as the bed is taken from approximately 22 °C and submerged in an approximately 0 °C ice-water bath. The bed was reduced to 0.0029 mbar vacuum at room temperature.

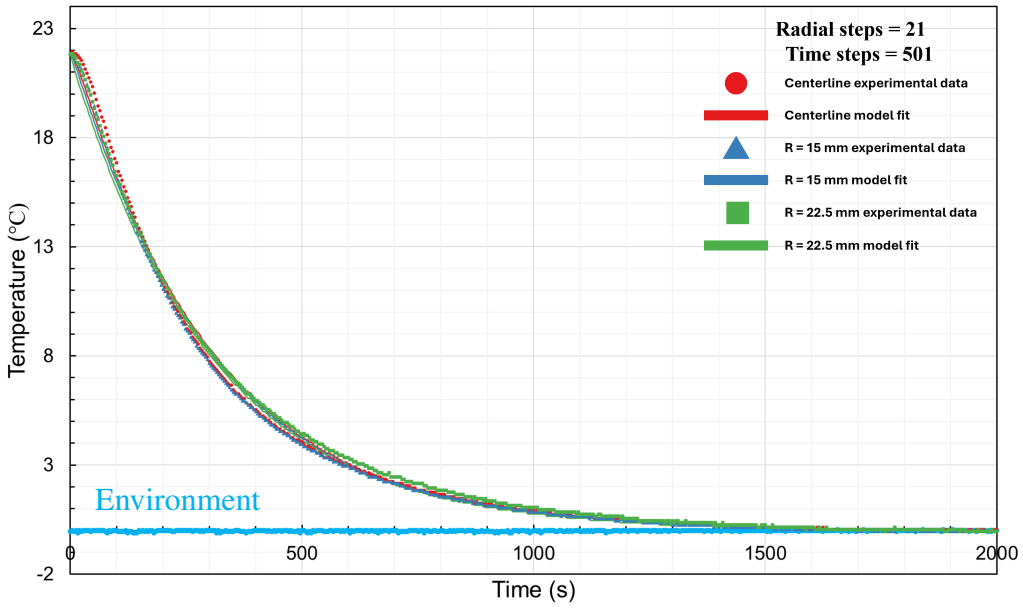

Figure 2.185: Experimental temperature data of support D of a microfibrous media bed compared with a model fit of the data as the bed is taken from approximately 22 °C and submerged in an approximately 0 °C ice-water bath. The bed was reduced to 0.0029 mbar vacuum at room temperature.

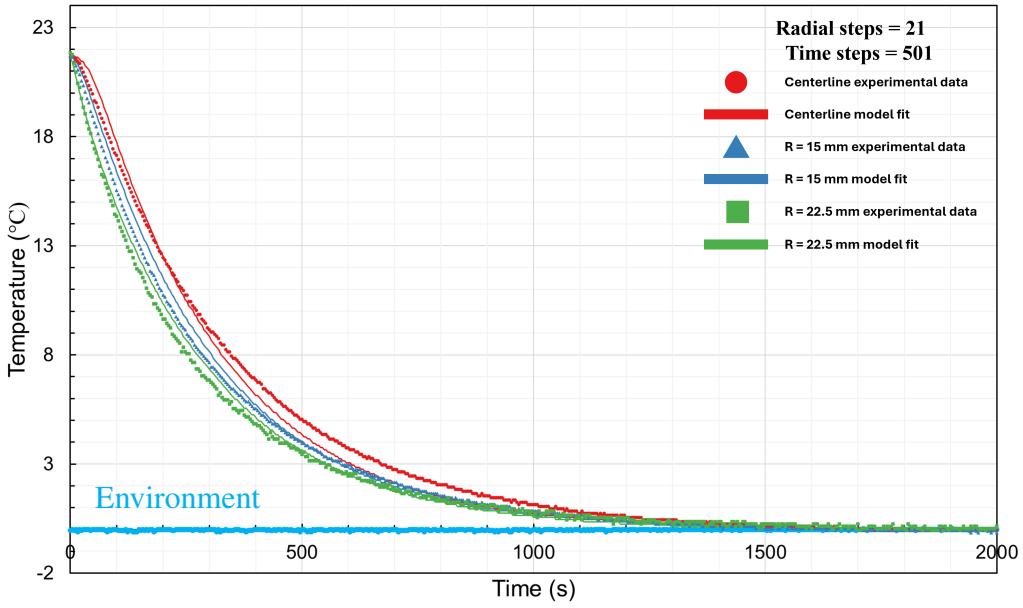

Figure 2.186: Experimental temperature data of support E of a microfibrous media bed compared with a model fit of the data as the bed is taken from approximately 22 °C and submerged in an approximately 0 °C ice-water bath. The bed was reduced to 0.0029 mbar vacuum at room temperature.

2.48 Stagnant Effective Thermal Conductivity

Numerous models have been suggested in literature to estimate the stagnant effective thermal conductivity of packed beds. A number of these model equations are shown in Table 2.23. The minimum and maximum stagnant effective thermal conductivities of a porous bed are given by the series and parallel models, respectively [47]. In Figure 2.187, it is shown how the effective thermal conductivity as calculated by the models in Table 2.23 varies with fluid thermal conductivity.

Table 2.24 applies these models to the tested alumina packed bed, and Table 2.25 applies the models to the tested microfibrous media (MFM) bed. A cursory comparison of the parameters estimated by the computational model and the parameters estimated via the models from literature suggests that of the models shown here the geometric mean [48] and Krupiczka [49–51] models best fit The packed bed experiments involving argon, nitrogen, and oxygen. The series [47, 48, 52], Maxwell-Euken [47, 53, 54], Chiew and Glandt [55], and EMT [56, 57] models best fit the experiments with helium and hydrogen. None of the literature models seemed to fit well with the results from the microfibrous media (MFM) bed experiments.

Table 2.23: Models for stagnant effective thermal conductivity of beds of solids within a fluid phase.

Series Model (Weighted Arithmetic Mean)	$k_e = \left(\frac{1-\epsilon}{k_s} + \frac{\epsilon}{k_f}\right)^{-1}$	[47, 48, 52]
Geometric Mean	$k_e = k_f^{\epsilon} k_s^{1-\epsilon}$	[48]
Parallel Model (Harmonic Mean)	$k_e = (1-\epsilon)\, k_s + \epsilon k_f$	[47, 48, 52]
Krupiczka	$k_e = k_f \left(\frac{k_s}{k_f}\right)^{0.28 - 0.757 \log \epsilon - 0.057 \log\left(\frac{k_s}{k_f}\right)}$	[49–51]
Maxwell-Euken	$k_e = k_f \frac{3k_s - 2\left(k_s - k_f\right)\epsilon}{3k_f + \left(k_s - k_f\right)\epsilon}$	[47, 53, 54]
Chiew and Glandt	$\frac{k_e}{k_f} = \frac{1 + 2\beta\phi + \left(K_2 - 3\beta^2\right)\phi^2}{1 - \beta\phi}$	[55]
Chiew and Glandt [a]	$\frac{k_e}{k_f} = \frac{1 + 2\beta\phi + \left(2\beta^3 - 0.1\beta\right)\phi^2 + \phi^3 0.05 \exp(4.5\beta)}{1 - \beta\phi}$	[55, 58]
	$\beta = \frac{k_s - k_f}{k_s + 2k_f}$	
Gonzo	$\frac{k_e}{k_f} = \alpha \frac{1 + 2\beta'(1-\phi)}{1 - \beta'(1-\phi)}$	[58]
	$\alpha = \frac{k_s}{k_f}$	
	$\beta' = \frac{k_f - k_s}{k_f + 2k_s}$	
Effective medium theory (EMT)	$k_e = \frac{1}{4}\Big\{(3\epsilon - 1)\, k_f + (3\phi - 1)\, k_s + \left(\left((3\epsilon - 1)\, k_f + (3\phi - 1)\, k_s\right)^2 + 8 k_s k_f\right)^{1/2}\Big\}$	[56, 57]
	$\phi = 1 - \epsilon$	

[a] As fitted in Gonzo [58].

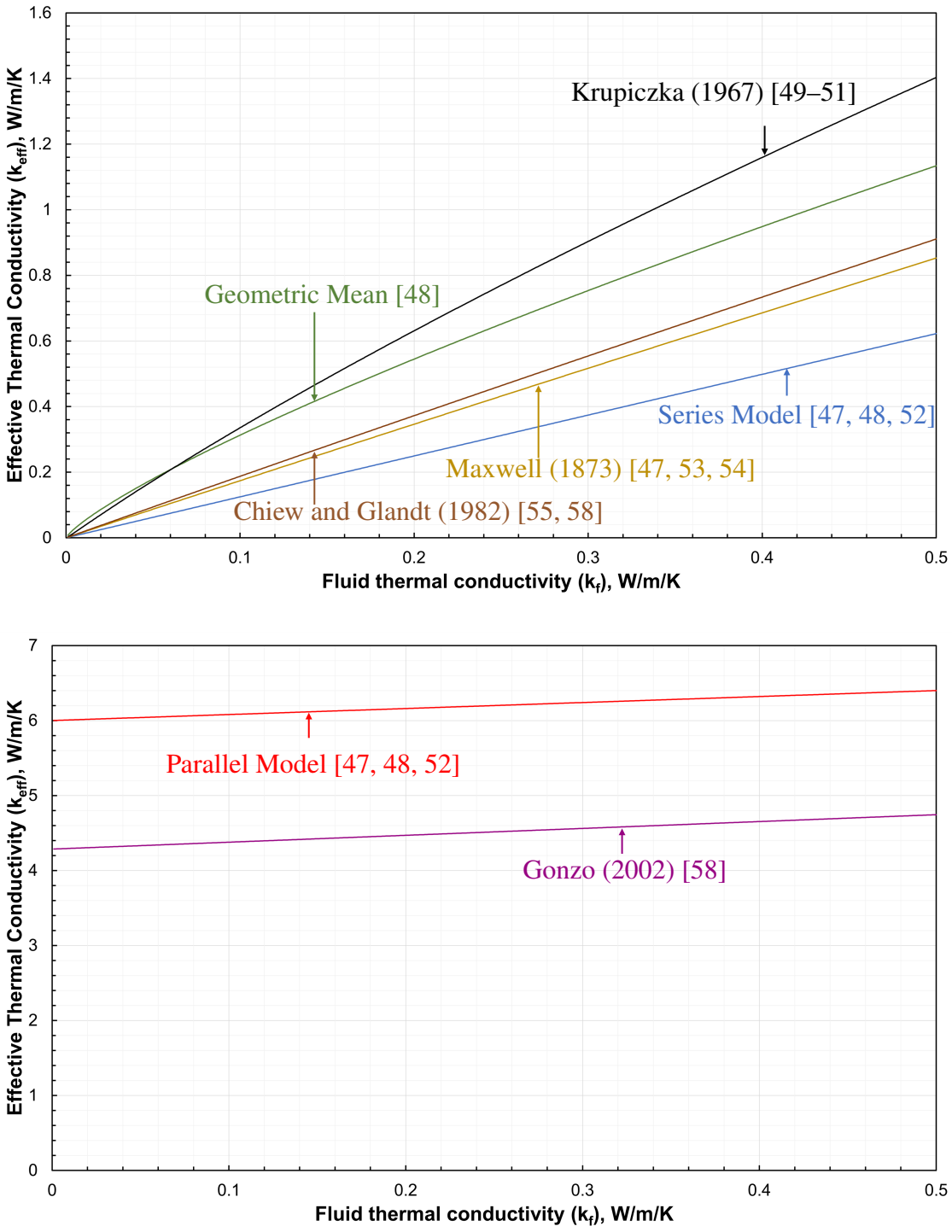

Figure 2.187: Models of stagnant effective thermal conductivity with solid thermal conductivity $k_s = 30 \frac{W}{mK}$ and void fraction $\varepsilon = 0.8$.

Table 2.24: Estimated stagnant effective thermal conductivity in $\frac{W}{m \cdot K}$ of a packed bed consisting of 11.7% $\frac{1}{8}$-in gamma alumina pellets and 88.3% void of various gasses.

Gas thermal conductivity $\frac{mW}{m \cdot K}$	Nitrogen 26	Argon 17.7	Oxygen 26.5	Helium 155.7	Hydrogen 186.6	Refs
Series Model	0.029	0.02	0.03	0.18	0.21	[47, 48, 52]
Parallel Model	4.1	4.1	4.1	4.2	4.3	[47, 48, 52]
Geometric Mean	0.06	0.043	0.061	0.29	0.34	[48]
Krupiczka	0.073	0.049	0.074	0.43	0.51	[49–51]
Maxwell-Euken	0.036	0.025	0.037	0.22	0.26	[47, 53, 54]
Chiew and Glandt	0.037	0.025	0.038	0.22	0.27	[55, 58]
Gonzo	2.9	2.9	2.9	3	3	[54, 58]
EMT	0.04	0.027	0.041	0.24	0.28	[56, 57]

[a] Thermal conductivity of 35 $\frac{W}{m \cdot K}$ used for alumina [59]

[b] Thermal conductivities for gases from Table 2.9

Table 2.25: Estimated stagnant effective thermal conductivity in $\frac{W}{m \cdot K}$ of a microfibrous bed consisting of 4.8% copper fibers and 95.2% void of various gasses.

Gas thermal conductivity $\frac{mW}{m \cdot K}$	Carbon dioxide 16.8	Argon 17.7	Oxygen 26.5	Helium 155.7	Hydrogen 186.6	Refs
Series Model	0.018	0.019	0.028	0.16	0.20	[47, 48, 52]
Parallel Model	19	19	19	19	19	[47, 48, 52]
Geometric Mean	0.027	0.029	0.042	0.23	0.27	[48]
Krupiczka	0.027	0.029	0.046	0.35	0.42	[49–51]
Maxwell-Euken	0.019	0.02	0.031	0.18	0.21	[47, 53, 54]
Chiew and Glandt	0.019	0.02	0.031	0.18	0.22	[55, 58]
Gonzo	13	13	13	13	13	[54, 58]
EMT	0.02	0.021	0.031	0.18	0.22	[56, 57]

[a] Thermal conductivity of 400 $\frac{W}{m \cdot K}$ used for copper

[b] Thermal conductivities for gases from Table 2.9

2.49 Discussion and Conclusions

This work has shown that microfibrous media (MFM) exhibits superior heat transfer characteristics than an alumina packed bed. This is in agreement with prior works on MFM [4, 15]. The heat transfer performance of microfibrous media beds were shown to be highly dependent on the thermal conductivity of the gas present within the bed. This is similar to previously reported results for packed beds [48, 52, 57, 58]. Furthermore, it is shown that MFM under vacuum (in the absence of fluid) is much worse at conducting heat than MFM with fluid. It is concluded that the inclusion of any fluid within the MFM vastly increases it's effective thermal conductivity over MFM alone.

Chapter 3

Effect of Flowing Gas on Heat Transfer in Microfibrous Media

Heat transfer experiments with flowing gas were carried out for the same microfibrous media (MFM) bed used for stagnant gas experiments (see section 2.1.4). However, the test apparatus was altered by adding insulation to the tubing and fittings before the bed in an attempt to maximize the temperature difference between the environment and the gas entering the bed. These experiments were conducted in a mixed water bath heated to 70 °C. Argon, helium, and oxygen were tested at flow rates of 10 to 100 standard liters per minute (SLPM) in increments of 10 SLPM.

Temperatures of all thermocouples were recorded once per second for the duration of the experiments. Flow rate changes were recorded using a binary event channel that was switched prior to changing the flow rate. The Reynolds number reported is the particle-based Reynolds number, and the characteristic length for the Reynolds number is calculated as in Ergun [17, 60]. The Sutherland equation was used to calculated the gas viscosity for calculating the Reynolds number [61, 62].

$$\mathrm{Re_p} \equiv \frac{\rho_f u L_c}{(1-\epsilon)\,\mu_f} \quad [17, 63] \tag{3.1}$$

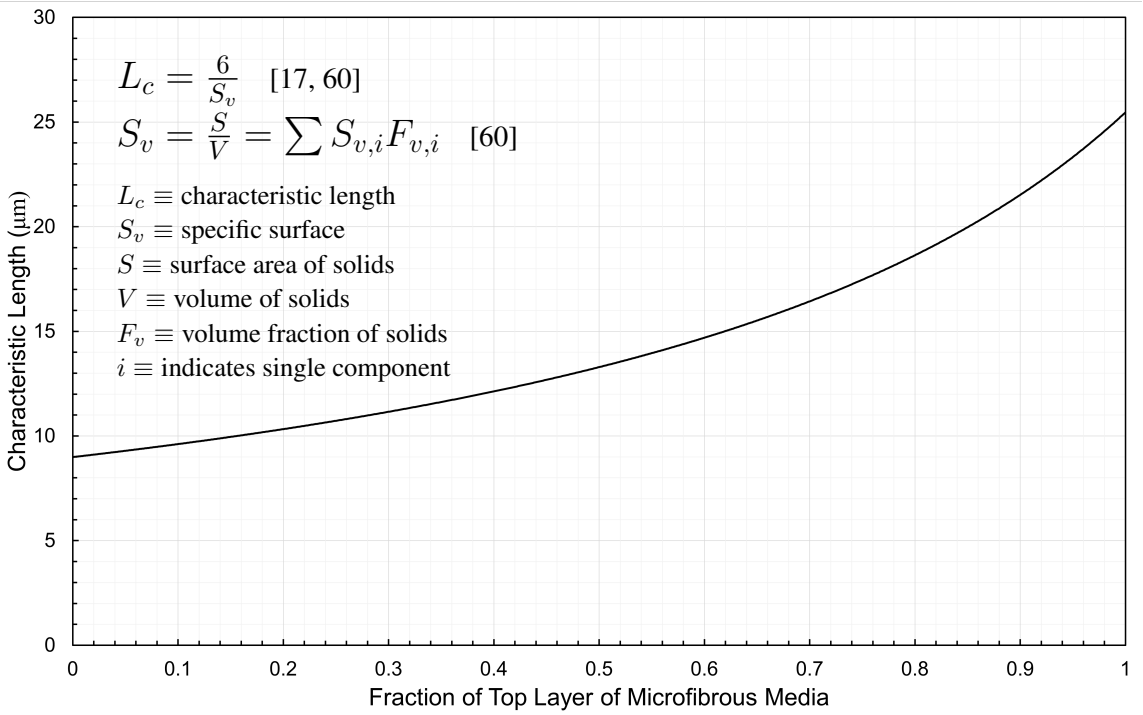

Figure 3.1: Characteristic length of microfibrous media composed of two layers of fibers with the top layer consisting of $17\,\mu\mathrm{m}$ diameter by $6\,\mathrm{mm}$ long fibers and the bottom layer consisting of $6\,\mu\mathrm{m}$ diameter by $3\,\mathrm{mm}$ long fibers.

3.1 Sutherland Constants

Sutherland constants were calculated for the gases presented in "Viscosity of gases" [64]. While only a few of the Sutherland constants were used within this work, all that were calculated are presented. Sutherland's equation is used to calculate the viscosity of a gas as a function of temperature [61]. The form of Sutherland's equation used here is that found in "Flow of Fluids through valves, fittings, and pipe" [62].

$$\mu = \mu_0 \left(\frac{T_0 + C}{T + C}\right) \left(\frac{T}{T_0}\right)^{\frac{3}{2}} \qquad \text{[62]} \tag{3.2}$$

Where

$$T = \text{Temperature in kelvin}$$

$$T_0 = \text{Reference temperature in kelvin}$$

$$\mu = \text{Viscosity at temperature } T$$

$$\mu_0 = \text{Viscosity at reference temperature } T_0$$

$$C = \text{Sutherland constant in kelvin}$$

To calculate the Sutherland coefficient of a gas, the Sutherland equation was used with a trial value of the Sutherland constant to calculate viscosities for the temperatures of that gas presented in "Viscosity of gases" [64].

The sum of squared residuals was then calculated for the gas as

$$\delta = \sum_{n=0}^{n=N} (\mu_n - \mu_n^*)^2 \tag{3.3}$$

Where

$\delta =$ Sum of squared residuals

$\mu_n =$ Viscosity at temperature n as calculated by the Sutherland equation

$\mu_n^* =$ Viscosity at temperature n as presented in [64]

$n =$ Temperature viscosity is calculated at

$N =$ Number of temperatures viscosity is calculated at

Microsoft Excel Solver was used to minimize the sum of squared residuals by varying the trial Sutherland constant. The result of this minimization was rounded to the nearest whole number and is reported as the Sutherland coefficient.

Table 3.1: Sutherland constants for gases presented in ”Viscosity of gases” [64].

	C (K)	T_{ref} (K)	μ_{ref} ($\mu Pa \cdot s$)
Air	107	100	7.1
Argon	139	100	8.1
Boron trifluoride	150	200	12.3
Hydrogen chloride	387	300	14.6
Sulfur hexafluoride	225	300	15.3
Normal hydrogen	54	100	4.1
Deuterium	48	100	5.9
Water	677	300	9.8
Deuterium oxide	688	300	10.1
Hydrogen sulfide	323	200	8.1
Ammonia	550	300	10.2
Helium	43	100	9.6
Krypton	161	100	8.9
Nitric oxide	118	200	13.8
Nitrogen	112	100	6.7
Nitrous oxide	258	200	10.0
Neon	54	100	14.4
Oxygen	119	100	7.7

[1] Data used to calculate the Sutherland constants from ”Viscosity of gases” [64].
[2] Sutherland constants rounded to the nearest whole number.

Table 3.2: Sutherland constants for gases presented in ”Viscosity of gases” [64] (cont.).

	C (K)	T_{ref} (K)	μ_{ref} (μPa · s)
Sulfur dioxide	320	200	8.6
Xenon	165	100	8.3
Carbon monoxide	110	100	6.7
Carbon dioxide	249	200	10.1
Chloroform	384	300	10.2
Methane	152	100	3.9
Methanol	320	200	6.6
Acetylene	257	300	10.4
Ethylene	244	200	7.0
Ethylene oxide	299	200	6.4
Ethane	167	100	3.3
Ethanol	399	400	11.6
Propane	314	300	8.2
n-Butane	370	300	7.4
Isobutane	328	300	7.5
Diethyl ether	328	300	7.6
n-Pentane	414	300	6.7
n-Hexane	410	400	8.4

[1] Data used to calculate the Sutherland constants from ”Viscosity of gases” [64].
[2] Sutherland constants rounded to the nearest whole number.

3.2 Results

The results of the experiments with flowing argon, helium, and oxygen are displayed in Figure 3.2 through Figure 3.10. The results from each experiment are split into three sets of plots; one each for temperatures recorded at the center line of the bed, temperatures 15 mm from the center line of the bed, and temperatures recorded 22.5 mm from the center line of the bed. Each set of plots contains one plot where the temperature is displayed in degrees Celsius and one plot where the the dimensionless temperature θ is displayed where $\theta = \frac{T}{T_0}$ and $T_0 = \frac{\text{Hot Water 1}+\text{Hot Water 2}}{2}$. "Hot Water 1" and "Hot Water 2" are the two temperature readings for the hot water bath. These temperatures are averages as T_0 which is used as the environment temperature.

3.2.1 Steady State Temperature Data for Heat Transfer Experiments in a Microfibrous Media Bed with Flowing Argon

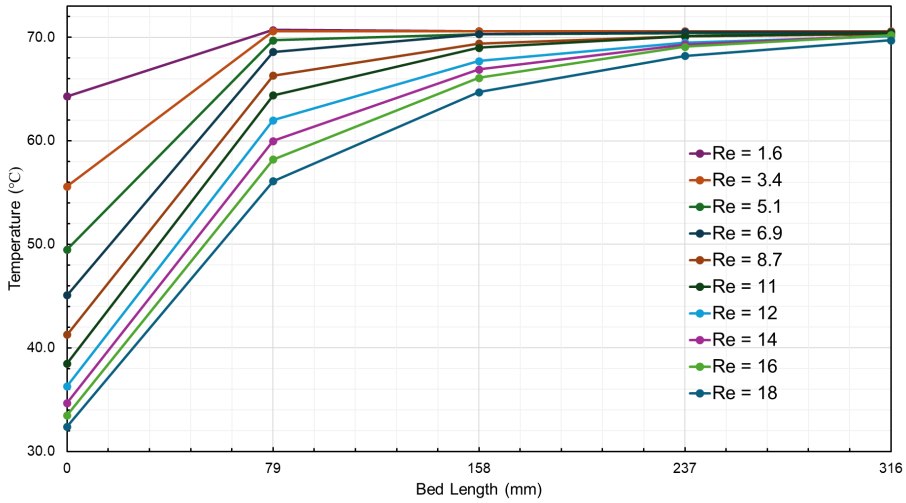

(a) Temperature profiles in degrees Celsius.

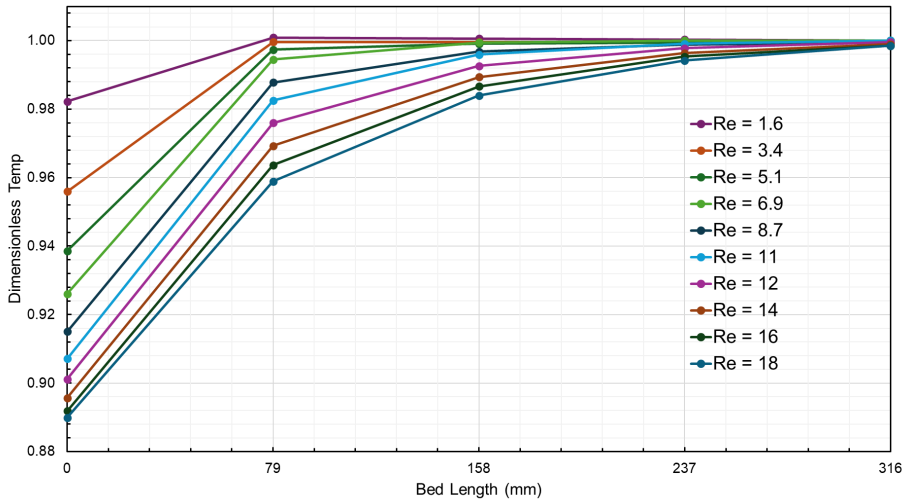

(b) Normalized temperature profiles in θ, where $\theta = \frac{T}{T_0}$ and $T_0 = \frac{\text{Hot Water 1}+\text{Hot Water 2}}{2}$.

Figure 3.2: Steady state temperatures at the center line for a microfibrous (MFM) bed with various flow rates of argon. The bed is submerged in a hot water bath at approximately 70 °C.

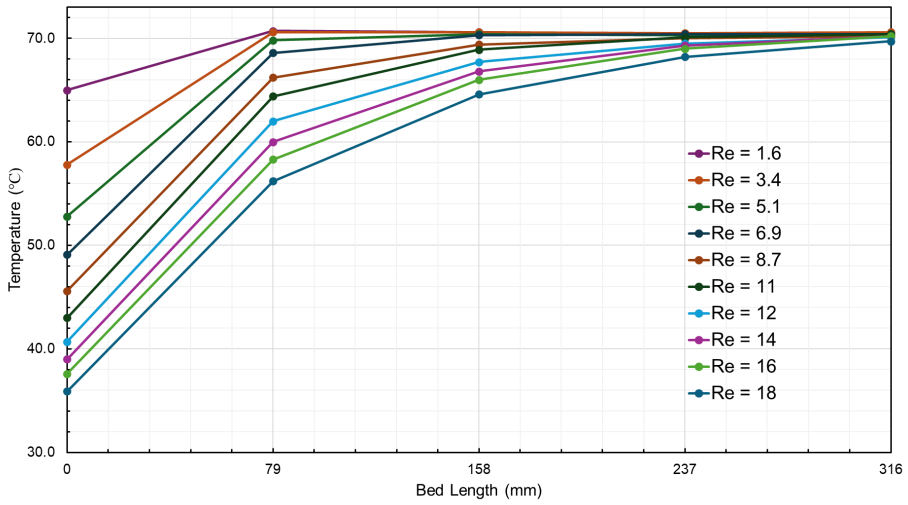

(a) Temperature profiles in degrees Celsius.

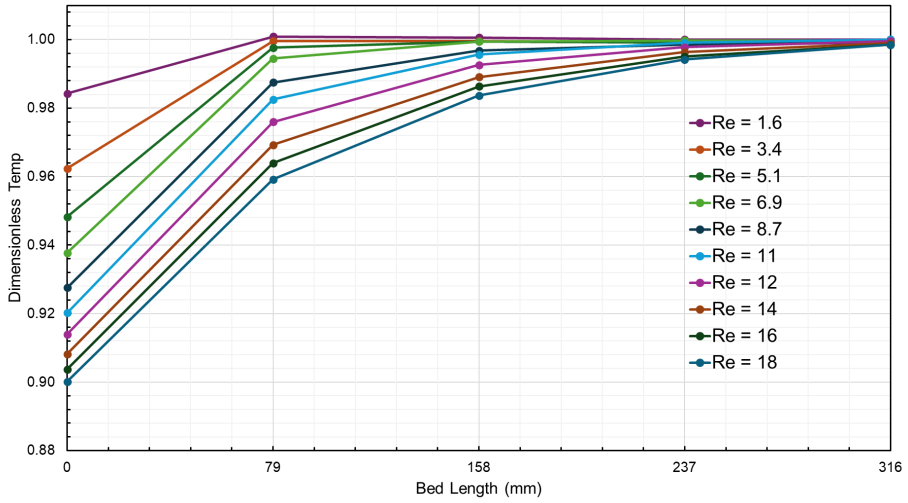

(b) Normalized temperature profiles in θ, where $\theta = \frac{T}{T_0}$ and $T_0 = \frac{\text{Hot Water 1}+\text{Hot Water 2}}{2}$.

Figure 3.3: Steady state temperatures at 15 mm from the center line for a microfibrous (MFM) bed with various flow rates of argon. The bed is submerged in a hot water bath at approximately 70 °C.

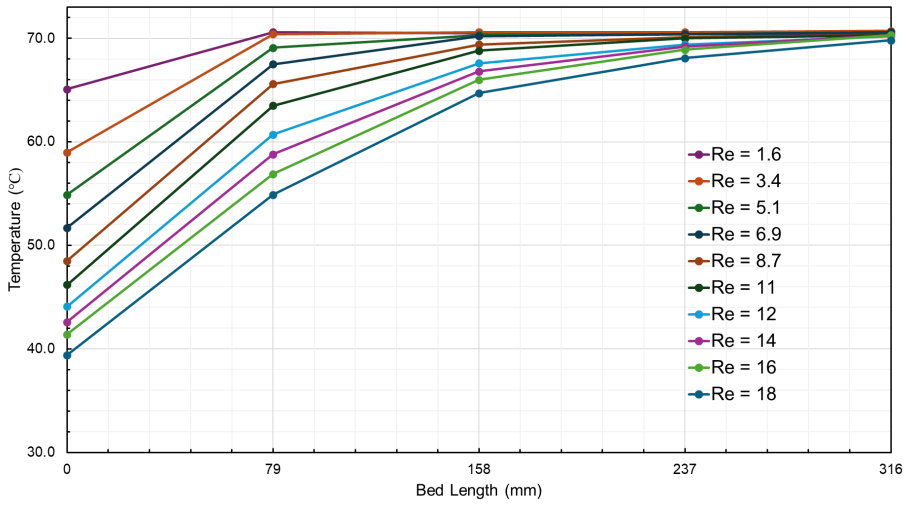

(a) Temperature profiles in degrees Celsius.

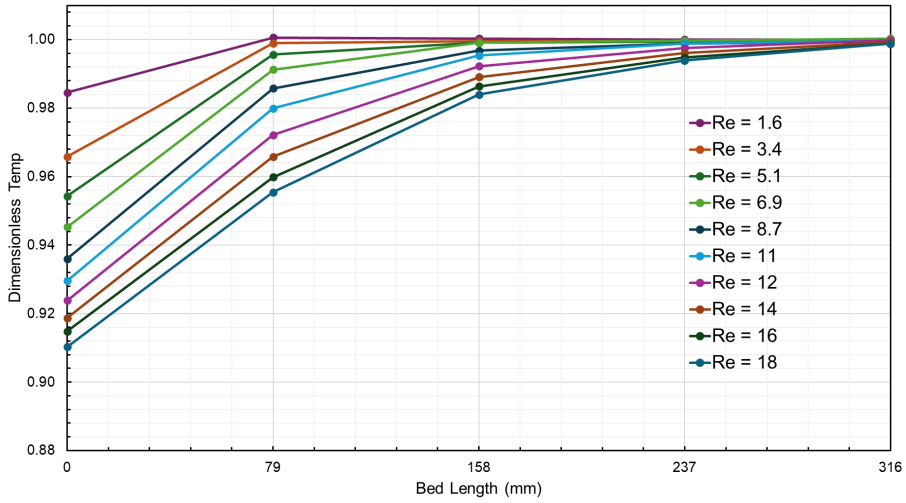

(b) Normalized temperature profiles in θ, where $\theta = \frac{T}{T_0}$ and $T_0 = \frac{\text{Hot Water 1}+\text{Hot Water 2}}{2}$.

Figure 3.4: Steady state temperatures at 22.5 mm from the center line for a microfibrous (MFM) bed with various flow rates of argon. The bed is submerged in a hot water bath at approximately 70 °C.

3.2.2 Steady State Temperature Data for Heat Transfer Experiments in a Microfibrous Media Bed with Flowing Helium

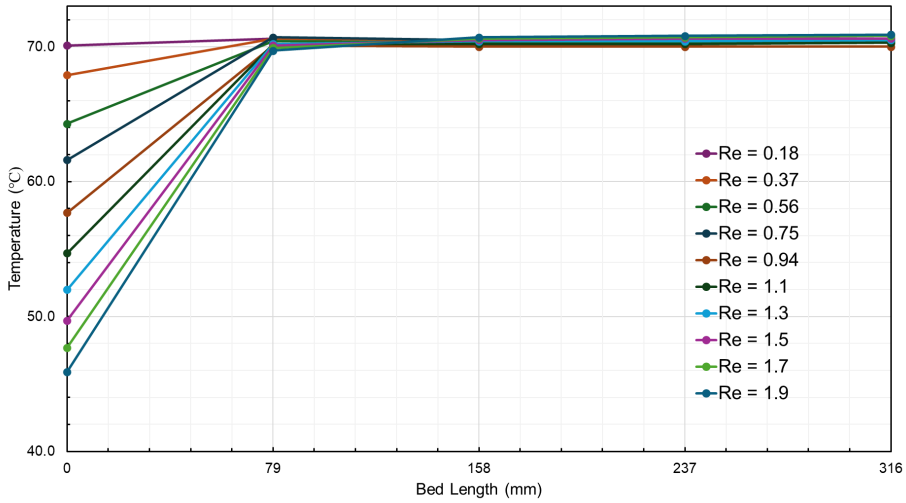

(a) Temperature profiles in degrees Celsius.

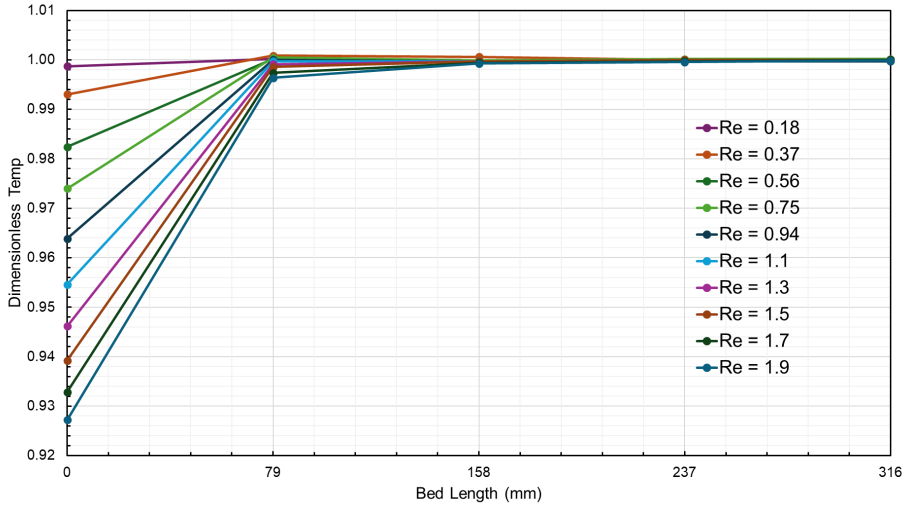

(b) Normalized temperature profiles in θ, where $\theta = \frac{T}{T_0}$ and $T_0 = \frac{\text{Hot Water 1+Hot Water 2}}{2}$.

Figure 3.5: Steady state temperatures at the center line for a microfibrous (MFM) bed with various flow rates of helium. The bed is submerged in a hot water bath at approximately 70 °C.

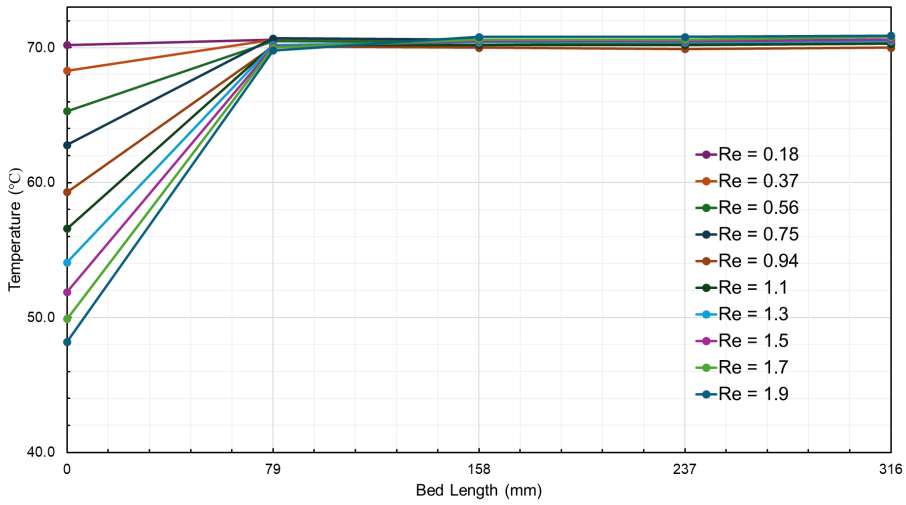

(a) Temperature profiles in degrees Celsius.

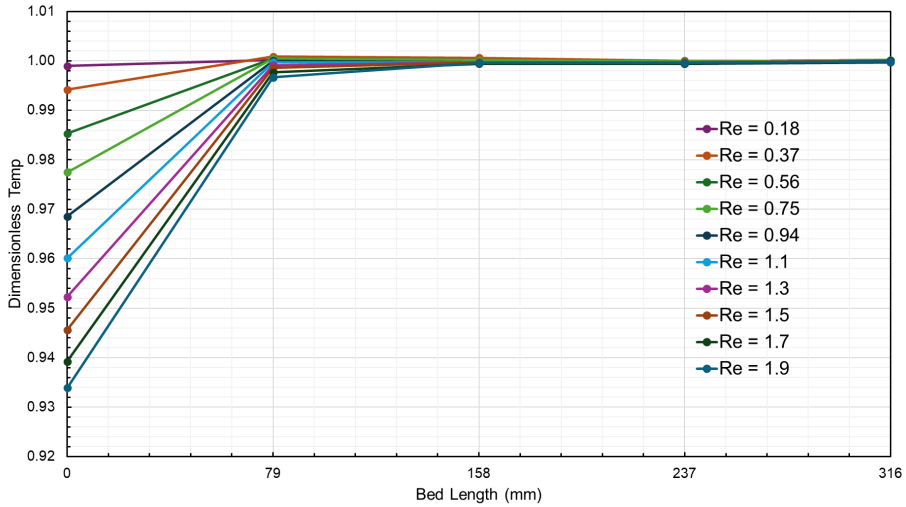

(b) Normalized temperature profiles in θ, where $\theta = \frac{T}{T_0}$ and $T_0 = \frac{\text{Hot Water 1}+\text{Hot Water 2}}{2}$.

Figure 3.6: Steady state temperatures at 15 mm from the center line for a microfibrous (MFM) bed with various flow rates of helium. The bed is submerged in a hot water bath at approximately 70 °C.

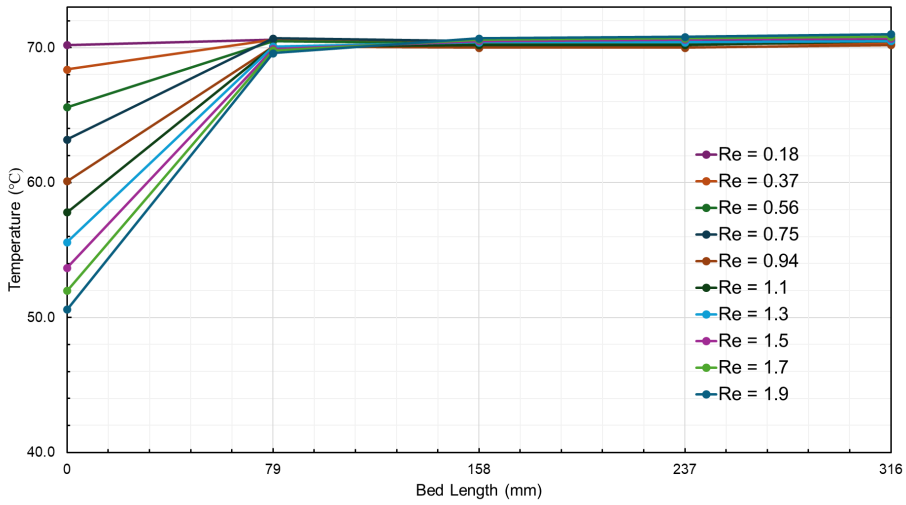

(a) Temperature profiles in degrees Celsius.

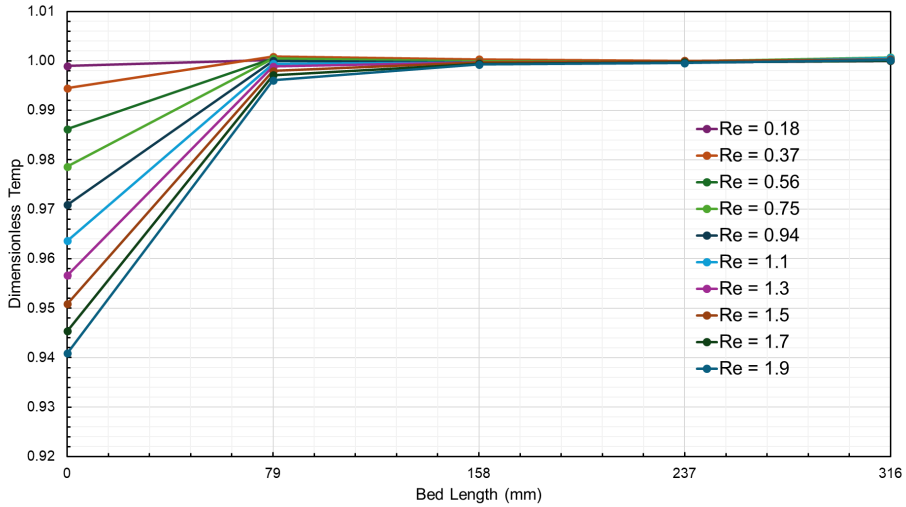

(b) Normalized temperature profiles in θ, where $\theta = \frac{T}{T_0}$ and $T_0 = \frac{\text{Hot Water 1}+\text{Hot Water 2}}{2}$.

Figure 3.7: Steady state temperatures at 22.5 mm from the center line for a microfibrous (MFM) bed with various flow rates of helium. The bed is submerged in a hot water bath at approximately 70 °C.

3.2.3 Steady State Temperature Data for Heat Transfer Experiments in a Microfibrous Media Bed with Flowing Oxygen

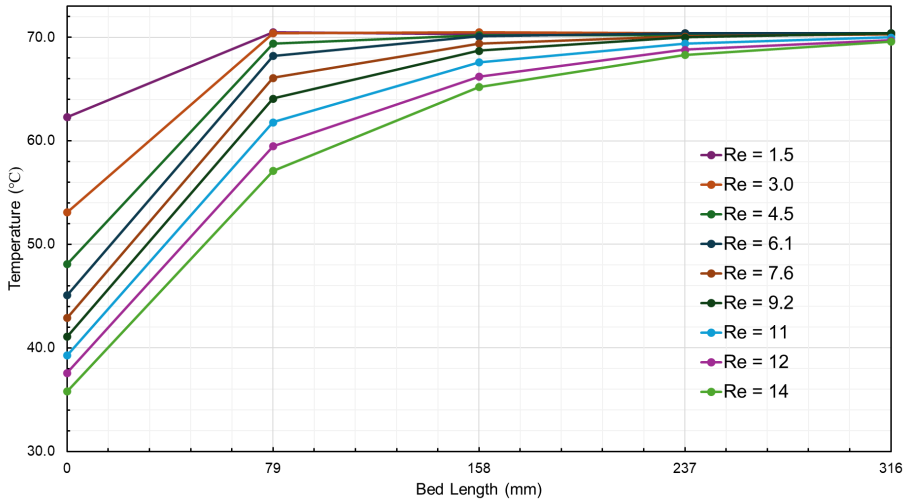

(a) Temperature profiles in degrees Celsius.

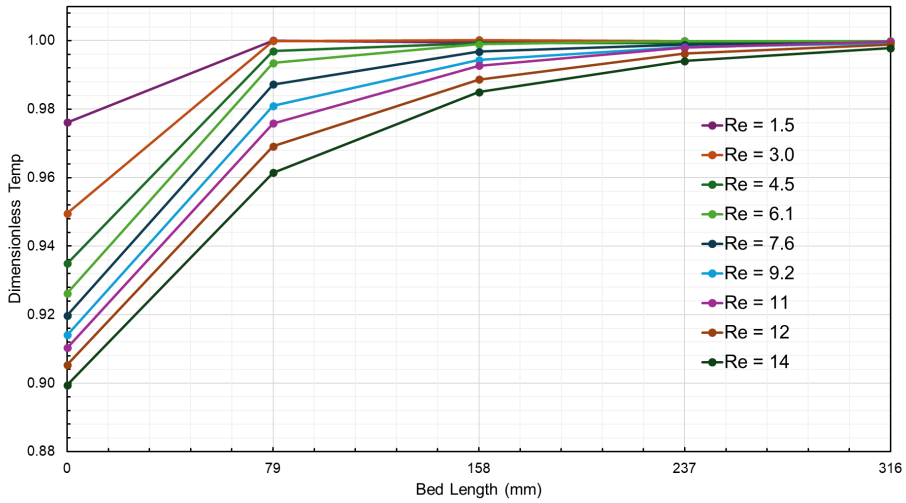

(b) Normalized temperature profiles in θ, where $\theta = \frac{T}{T_0}$ and $T_0 = \frac{\text{Hot Water 1}+\text{Hot Water 2}}{2}$.

Figure 3.8: Steady state temperatures at the center line for a microfibrous (MFM) bed with various flow rates of oxygen. The bed is submerged in a hot water bath at approximately 70 °C.

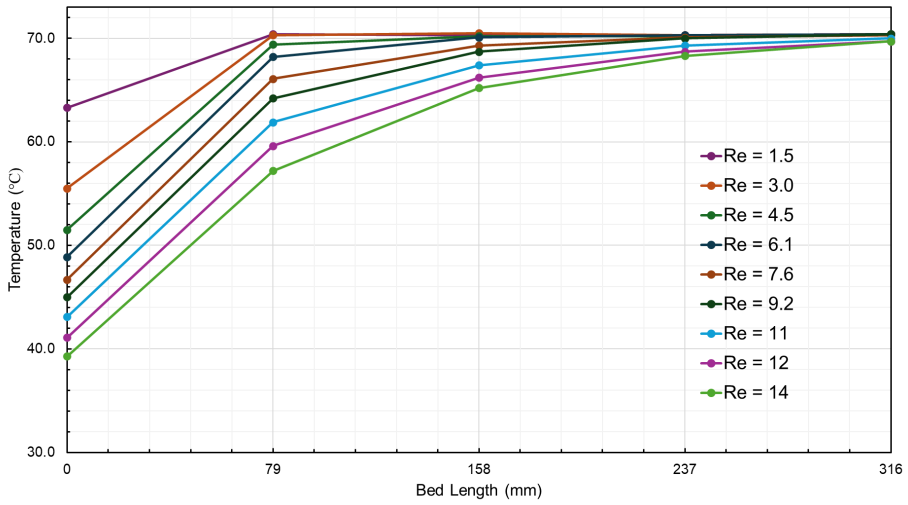

(a) Temperature profiles in degrees Celsius.

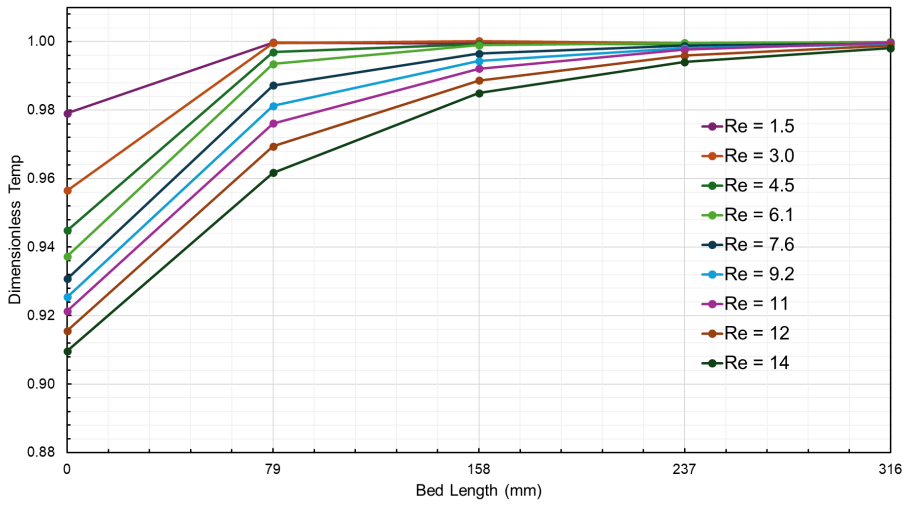

(b) Normalized temperature profiles in θ, where $\theta = \frac{T}{T_0}$ and $T_0 = \frac{\text{Hot Water 1}+\text{Hot Water 2}}{2}$.

Figure 3.9: Steady state temperatures at 15 mm from the center line for a microfibrous (MFM) bed with various flow rates of oxygen. The bed is submerged in a hot water bath at approximately 70 °C.

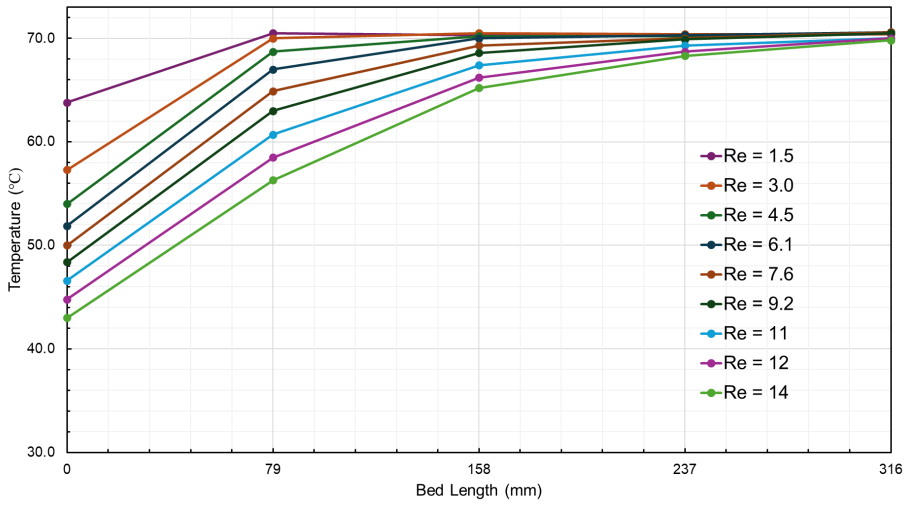

(a) Temperature profiles in degrees Celsius.

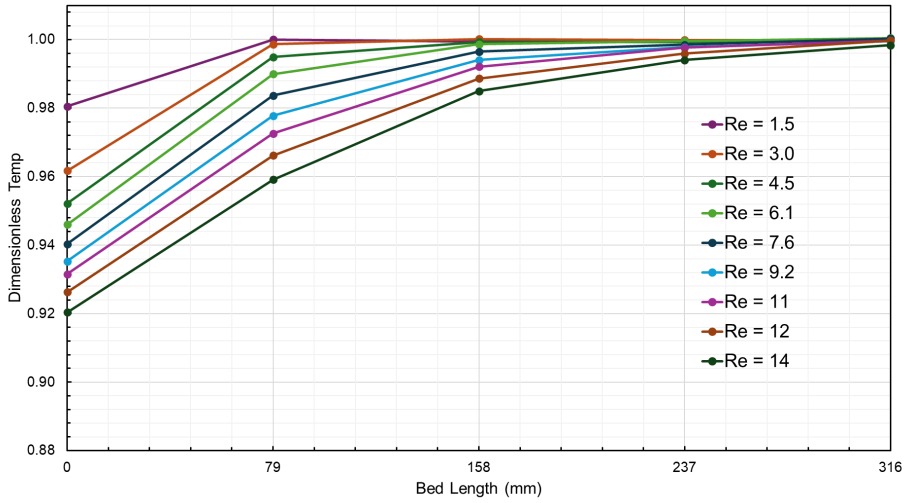

(b) Normalized temperature profiles in θ, where $\theta = \frac{T}{T_0}$ and $T_0 = \frac{\text{Hot Water 1}+\text{Hot Water 2}}{2}$.

Figure 3.10: Steady state temperatures at 22.5 mm from the center line for a microfibrous (MFM) bed with various flow rates of oxygen. The bed is submerged in a hot water bath at approximately 70 °C.

3.3 Discussion

The microfibrous media (MFM) heat transfer experiments with flowing gas were conducted with the intent of estimating the heat transfer parameters of the beds as a function of flow rate with different gases. Experiments were conducted at various flow rates of argon, helium, and oxygen. A computational model was produced to estimated the effective radial thermal conductivity, k_{er}, effective axial thermal conductivity k_{ea}, and overall heat transfer coefficient based on the inside wall, U_{id}.

Unfortunately, this model was not functional. It is assumed that the errors in the model are minor and can be fixed with further work. It was written in Python using the Sherpa application [43] and is left for future work to complete. The equations for this model are presented here for anyone continuing this work.

3.3.1 Computational Model of Microfibrous Media Bed Experiments with Flowing Gas

Energy Equation in Two Dimensions

The energy equation in radial coordinates is taken from Transport Phenomena [20] and simplified to two dimensions (radial and axial).

$$\rho \hat{C}_p \left[\frac{\partial T}{\partial t} + v_z \frac{\partial T}{\partial z} \right] = k \left[\frac{1}{r} \frac{\partial T}{\partial r} + \frac{\partial^2 T}{\partial r^2} + \frac{\partial^2 T}{\partial z^2} \right] \tag{3.4}$$

This equation is nondimensionalized as

$$\frac{\partial \theta}{\partial \tau} = \frac{1}{\xi} \frac{\partial \theta}{\partial \xi} + \frac{\partial^2 \theta}{\partial \xi^2} - \text{Pe} \frac{\partial \theta}{\partial \eta} + \text{A} \frac{\partial^2 \theta}{\partial \eta^2} \tag{3.5}$$

Nondimensional variable definitions

$$\tau = \frac{\alpha_r}{R^2}t \qquad \theta = \frac{T}{T_0} \qquad \xi = \frac{r}{R}$$
$$\eta = \frac{z}{L} \qquad \text{A} = \frac{\alpha_z R^2}{\alpha_r L^2} \qquad \text{Pe} = \frac{v_z R^2}{\alpha_r L}$$

The boundary conditions are

$$\text{at } \eta = 0\ ,\ \theta = \theta_0 \qquad \text{at } \eta = 1\ ,\ \frac{\partial \theta}{\partial \eta} = 0 \tag{3.6}$$

$$\text{at } \xi = 0\ ,\ \frac{\partial \theta}{\partial \xi} = 0 \qquad \text{at } \xi = 1\ ,\ \frac{\partial \theta}{\partial \xi} = \text{Bi}(\theta_\infty - \theta_b) \tag{3.7}$$

where

$$\text{Bi} = \frac{U_{\text{id}} R}{k_{\text{er}}}$$

$\theta_\infty \equiv$ temperature of the environment surrounding the outside wall

$\theta_b \equiv$ bulk temperature inside the bed ; taken as $\theta_b = \theta^{n+1}_{\xi-\Delta\xi,j}$

The derivatives in Equation 3.5 are approximated using the Taylor series. The time derivative is a forward first order approximation. The space derivatives are centered second order approximations.

$$\frac{\partial \theta}{\partial \tau} \approx \frac{\theta^{n+1}_{i,j} - \theta^{n}_{i,j}}{\Delta \tau} + \mathcal{O}[\Delta \tau] \tag{3.8}$$

$$\frac{\partial \theta}{\partial \xi} \approx \frac{\theta^{n+1}_{i+1,j} - \theta^{n+1}_{i-1,j}}{2(\Delta \xi)} + \mathcal{O}[(\Delta \xi)^2] \tag{3.9}$$

$$\frac{\partial \theta}{\partial \eta} \approx \frac{\theta^{n+1}_{i,j+1} - \theta^{n+1}_{i,j-1}}{2(\Delta \eta)} + \mathcal{O}[(\Delta \eta)^2] \tag{3.10}$$

$$\frac{\partial^2 \theta}{\partial \xi^2} \approx \frac{\theta^{n+1}_{i+1,j} - 2\theta^{n+1}_{i,j} + \theta^{n+1}_{i-1,j}}{(\Delta \xi)^2} + \mathcal{O}[(\Delta \xi)^2] \tag{3.11}$$

$$\frac{\partial^2\theta}{\partial\eta^2} \approx \frac{\theta_{i,j+1}^{n+1} - 2\theta_{i,j}^{n+1} + \theta_{i,j-1}^{n+1}}{(\Delta\eta)^2} + \mathcal{O}[(\Delta\eta)^2] \tag{3.12}$$

Combining Equations 3.5, 3.8, 3.9, 3.10, 3.11, and 3.12 results in an implicit finite difference equation for the energy equation in two dimension.

$$\begin{aligned}\frac{\theta_{i,j}^{n+1} - \theta_{i,j}^{n}}{\Delta\tau} = \frac{1}{\xi}\frac{\theta_{i+1,j}^{n+1} - \theta_{i-1,j}^{n+1}}{2(\Delta\xi)} - \mathrm{Pe}\frac{\theta_{i,j+1}^{n+1} - \theta_{i,j-1}^{n+1}}{2(\Delta\eta)} \\ + \frac{\theta_{i+1,j}^{n+1} - 2\theta_{i,j}^{n+1} + \theta_{i-1,j}^{n+1}}{(\Delta\xi)^2} + \mathrm{A}\frac{\theta_{i,j+1}^{n+1} - 2\theta_{i,j}^{n+1} + \theta_{i,j-1}^{n+1}}{(\Delta\eta)^2} \\ + \mathcal{O}[\Delta\tau, (\Delta\xi)^2, (\Delta\eta)^2]\end{aligned} \tag{3.13}$$

von Neumann Analysis of the Energy Equation in Two Dimensions

A von Neumann stability analysis [21] was performed for the two-dimensional heat transfer model as implemented. *Fundamental Algorithms in Computational Fluid Dynamics* [22] was referenced for implementing this analysis.

θ is taken to be of the form

$$\theta(\xi, \eta, \tau) = \lambda^n e^{ik\xi} e^{il\eta} \qquad [22] \tag{3.14}$$

$$e^{\alpha\Delta\tau} = \lambda^n \qquad [22] \tag{3.15}$$

The von Neumann stability criteria is

$$|\lambda| \leq 1 \qquad [22] \tag{3.16}$$

$$\frac{\lambda^{n+1}e^{ik\xi}e^{il\eta}-\lambda^{n}e^{ik\xi}e^{il\eta}}{\Delta\tau}=\frac{1}{\xi}\frac{\lambda^{n+1}e^{ik(\xi+\Delta\xi)}e^{il\eta}-\lambda^{n+1}e^{ik(\xi-\Delta\xi)}e^{il\eta}}{2(\Delta\xi)}$$
$$-\mathrm{Pe}\frac{\lambda^{n+1}e^{ik\xi}e^{il(\eta+\Delta\eta)}-\lambda^{n+1}e^{ik\xi}e^{il(\eta-\Delta\eta)}}{2(\Delta\eta)}$$
$$+\frac{\lambda^{n+1}e^{ik(\xi+\Delta\xi)}e^{il\eta}-2\lambda^{n+1}e^{ik\xi}e^{il\eta}+\lambda^{n+1}e^{ik(\xi-\Delta\xi)}e^{il\eta}}{(\Delta\xi)^2}$$
$$+\mathrm{A}\frac{\lambda^{n+1}e^{ik\xi}e^{il(\eta+\Delta\eta)}-2\lambda^{n+1}e^{ik\xi}e^{il\eta}+\lambda^{n+1}e^{ik\xi}e^{il(\eta-\Delta\eta)}}{(\Delta\eta)^2} \quad (3.17)$$

$$\frac{\lambda^{n+1}-\lambda^{n}}{\lambda^{n+1}(\Delta\tau)}=\frac{1}{\xi}\frac{e^{ik\Delta\xi}-e^{-ik\Delta\xi}}{2(\Delta\xi)}-\mathrm{Pe}\frac{e^{il\Delta\eta}-e^{-il\Delta\eta}}{2(\Delta\eta)}$$
$$+\frac{e^{ik\Delta\xi}-2+e^{-ik\Delta\xi}}{(\Delta\xi)^2}+\mathrm{A}\frac{e^{il\Delta\eta}-2+e^{-il\Delta\eta}}{(\Delta\eta)^2} \quad (3.18)$$

$$\frac{1}{\Delta\tau}\left(1-\frac{1}{\lambda}\right)=\frac{1}{\xi}\frac{e^{ik\Delta\xi}-e^{-ik\Delta\xi}}{2(\Delta\xi)}-\mathrm{Pe}\frac{e^{il\Delta\eta}-e^{-il\Delta\eta}}{2(\Delta\eta)}$$
$$+\frac{e^{ik\Delta\xi}-2+e^{-ik\Delta\xi}}{(\Delta\xi)^2}+\mathrm{A}\frac{e^{il\Delta\eta}-2+e^{-il\Delta\eta}}{(\Delta\eta)^2} \quad (3.19)$$

$$\frac{1}{\lambda}=1-\frac{\Delta\tau}{2\xi(\Delta\xi)}\left(e^{ik(\Delta\xi)}-e^{-ik(\Delta\xi)}\right)+\frac{\mathrm{Pe}(\Delta\tau)}{2(\Delta\eta)}\left(e^{il(\Delta\eta)}-e^{-il(\Delta\eta)}\right)$$
$$-\frac{\Delta\tau}{(\Delta\xi)^2}\left(e^{ik(\Delta\xi)}-2+e^{-ik(\Delta\xi)}\right)-\frac{\mathrm{A}(\Delta\tau)}{(\Delta\eta)^2}\left(e^{il(\Delta\eta)}-2+e^{-il(\Delta\eta)}\right) \quad (3.20)$$

$$\sin(x)=\frac{e^{ix}-e^{-ix}}{2i} \qquad \cos(x)=\frac{e^{ix}+e^{-ix}}{2}$$

$$\frac{1}{\lambda}=1-\frac{\Delta\tau}{\xi(\Delta\xi)}\sin(k(\Delta\xi))i+\frac{\mathrm{Pe}(\Delta\tau)}{\Delta\eta}\sin(l(\Delta\eta))i$$
$$-\frac{2(\Delta\tau)}{(\Delta\xi)^2}\left(\cos(k(\Delta\xi))-1\right)-\frac{2\mathrm{A}(\Delta\tau)}{(\Delta\eta)^2}\left(\cos(l(\Delta\eta))-1\right) \quad (3.21)$$

$$\frac{1}{\lambda} = 1 - \frac{2(\Delta\tau)}{(\Delta\xi)^2}\left(\cos(k(\Delta\xi)) - 1\right) - \frac{2\mathrm{A}(\Delta\tau)}{(\Delta\eta)^2}\left(\cos(l(\Delta\eta)) - 1\right) + \left[-\frac{\Delta\tau}{\xi(\Delta\xi)}\sin(k(\Delta\xi)) + \frac{\mathrm{Pe}(\Delta\tau)}{\Delta\eta}\sin(l(\Delta\eta))\right] i \quad (3.22)$$

For convenience, the following is defined.

$$C_1 = \frac{2(\Delta\tau)}{(\Delta\xi)^2} \qquad C_2 = \frac{2\mathrm{A}(\Delta\tau)}{(\Delta\eta)^2} \qquad C_3 = \frac{\Delta\tau}{\xi(\Delta\xi)} \qquad C_4 = \frac{\mathrm{Pe}(\Delta\tau)}{\Delta\eta}$$

$$\frac{1}{\lambda} = 1 - C_1\left(\cos(k(\Delta\xi)) - 1\right) - C_2\left(\cos(l(\Delta\eta)) - 1\right) + \left[-C_3\sin(k(\Delta\xi)) + C_4\sin(l(\Delta\eta))\right] i \quad (3.23)$$

$$\frac{1}{\lambda} = 1 - C_1\left(\cos(k(\Delta\xi)) - 1\right) - C_2\left(\cos(l(\Delta\eta)) - 1\right) + \left[C_4\sin(l(\Delta\eta)) - C_3\sin(k(\Delta\xi))\right] i \quad (3.24)$$

$$c = a + bi \quad (3.25)$$

$$|c| = \sqrt{a^2 + b^2} \quad (3.26)$$

Let $\gamma = \frac{1}{\lambda}$.

For $|\lambda| \leq 1$, it must be true that $|\gamma| \geq 1$.

To satisfy $|c| \leq 1$, $a^2 + b^2 \leq 1$. Applying this to 3.24 leads to

$$|\gamma|^2 = \left[1 - C_1\left(\cos(k(\Delta\xi)) - 1\right) - C_2\left(\cos(l(\Delta\eta)) - 1\right)\right]^2 + \left[C_4\sin(l(\Delta\eta)) - C_3\sin(k(\Delta\xi))\right]^2 \quad (3.27)$$

Breaking this into the parts

$$a^2 = \left[1 - C_1\left(\cos(k(\Delta\xi)) - 1\right) - C_2\left(\cos(l(\Delta\eta)) - 1\right)\right]^2$$

$$b^2 = \left[C_4 \sin(l(\Delta\eta)) - C_3 \sin(k(\Delta\xi))\right]^2$$

To satisfy $|\gamma| \geq 1$, it must be true that $a^2 + b^2 \geq 1$.

Sine and cosine are bound as

$$-1 \leq \sin(x) \leq 1$$

$$0 \leq \cos(x) \leq 1$$

Using this, it is known $1 \leq a^2 \leq (1 + C_1 + C_2)^2$.

Since C_1 and C_2 are both positive, it is always true that $a^2 \geq 1$.

$b^2 \geq 0$.

Combining this, it is always true that $a^2 + b^2 \geq 1$.

This means it is always true that $\gamma \geq 1$.

Which further leads to it always being true that $\lambda \leq 1$.

Meaning this scheme is unconditionally stable by von Neumman analysis.

3.3.2 Effective Thermal Conductivity of a Bed with Flow

As discussed at the beginning of this section, the desired results of this portion of the work were not achieved. However, information for what this work aimed to do is included for the use of anyone who continues this work in the future.

It has been shown by Sheng et all [4] that the effective thermal conductivity of microfibrous media increases with flow rate. Also, when comparing the experimental data in this work for flowing argon, helium, and oxygen it suggests that the effective thermal conductivity is a function both of the flow rate and the thermal conductivity of the gas. It

is shown in literature that the effective thermal conductivity of packed beds is a function of flow rate.

Presented here are various literature models for estimating the effective thermal conductivities of packed beds as a function of fluid flow rate. The goal was to assess these models applicability for microfibrous media. Unfortunately, this goal was not met.

Table 3.3: Models for effective radial thermal conductivity with flow of porous beds [49]. [a]

Authors	Equation	Conditions	Refs
Bunnell et al. [b]	$\frac{k_{er}}{k_f} = 5.0 + 0.061 Re_p$	Glass spheres	[49, 65]
Bey and Eigenberger	$\frac{k_{er}}{k_f} = \frac{k_0}{k_f} + \frac{Pe_p}{K_r}$	Glass and ceramic spheres $3.3 < \frac{d_t}{d_p} < 11$	[66]
Yagi and kunii	$\frac{k_{er}}{k_f} = \frac{k_0}{k_f} + \alpha Pe_p$		[67]
Bey and Eigenberger [b]	$\frac{k_{er}}{k_f} = \frac{k_0}{k_f} + 0.1 Pe_p$		[49, 66, 68, 69]
Demirel et al. [a]	$\frac{k_{er}}{k_f} = 2.894 + 0.068 Re_p$	Raschig rings $5.6 < \frac{d_t}{d_p} < 6.6$	[49, 70]
Demirel et al. [b]	$\frac{k_{er}}{k_f} = 10.432 + 0.0481 Re_p$	Polystyrene spheres $4.5 < \frac{d_t}{d_p} < 7.5$	[49, 70]
Béttega et al.	$k_{er}(r) = k_0(r) + k_d(r)$		[71]
Béttega et al.	$\frac{k_d}{k_f} = \gamma Re_p Pr \frac{U(r)}{U_0} \frac{L(r)}{D_p}$		[71, 72]
	$L(r) = \begin{cases} R - r, & R - r \leq D_p \\ D_p, & R - r > D_p \end{cases}$		[71, 72]
Hunt and Tien [c]	$\frac{k_0(r)}{k_f} = \frac{k_0(\infty)}{k_f} \left[1 + a' \exp\left(-b' \frac{R - r}{D_p} \right) \right]$		[71, 72]
Giudici [c]	$\frac{k_0(\infty)}{k_f} = (1 - \sqrt{1 - \epsilon}) + \frac{2\sqrt{1 - \epsilon}}{1 - B\frac{k_f}{k_s}} \theta$		[71, 73]
	$\theta = \frac{\left(1 - \frac{k_f}{k_s}\right) B}{\left(1 - B\frac{k_f}{k_s}\right)^2} \ln\left(\frac{1}{B\frac{k_f}{k_s}} \right) - \frac{B - 1}{1 - B\frac{k_f}{k_s}} - \frac{B(B + 1)}{2B}$		[71, 73]
	$B = \left(\frac{b'(1 - \epsilon)}{\epsilon} \right)^{10/9}$		[71, 73]
	$b' = 1.25$		[71, 73]
de Wasch and Froment [d]	$k_e = k_0 + \frac{0.0025}{1 + 46\left(\frac{d_t}{d_p}\right)^2} \left(\frac{4184}{3600} \right) Re$	various cylindrical catalysts with height = diameter	[74]

[a] This table is a duplication of and an extension to Table 2 in Wen and Ding [49].
[b] As recorded in [49].
[c] As recorded in [71].
[d] Equation originally in units of $\frac{\text{kcal}}{\text{m}\cdot\text{h}\cdot\text{K}}$ in de Wasch and Froment [74]. The $\frac{4184}{3600} \frac{\text{J}\cdot\text{h}}{\text{kcal}\cdot\text{s}}$ term is added to convert the second term on the right-hand side to $\frac{\text{W}}{\text{m}\cdot\text{K}}$.

If it is taken that $\gamma = 0.1$, $U(r) = U_0$, and $L(r) = D_p$ and it is noted that $Pe_p = Re_p Pr$, the equation for the dispersion thermal conductivity by Béttega et al. [71] reduces to the dispersion portion of the equation by Bey and Eigenberger [66] as written in Wen and

Ding [49]. Said simply, the equation reduces if changes in the radial direction are ignored and the constant for the porous medium is taken to be the same as used in Wen and Ding [49].

Table 3.4: Simple models for effective radial thermal conductivity with flow of porous beds

Authors	Equation	Conditions	Refs
Yagi and kunii	$\frac{k_{er}}{k_f} = \frac{k^0_{er}}{k_f} + \delta_r Pe_p$		[67]
Yagi and Kunii	$\delta_r = 0.1$ to 0.3	Various cylinders, tablets, raschig rings, saddles, and spheres	[67]
Vortmeyer and Winter	$\delta_r = 0.1$	Various authors and conditions	[49, 66, 68]

Table 3.5: Models for effective axial thermal conductivity with flow of porous beds.

Authors	Equation	Conditions	Refs
Yagi et al.	$\frac{k_{ea}}{k_f} = \frac{k^0_{ea}}{k_f} + \delta_a Pe_p$		[69]
Yagi et al.	$\delta_a = 0.7$ to 0.8	Glass beads Steel balls Limestone broken pieces Porcelain raschig rings	[69]
Wen and Ding	$\delta_a = 0.5$	$5\,\mathrm{mm}$ glass balls	[49]

Chapter 4

Future Work

4.1 Introduction to Future Work

Just as this work is built upon previous work, there is more to be done. Here is presented incomplete work with direction for completion.

A series of resistance models and unit cells to represent microfibrous media (MFM) have been developed. These models have been built in Microsoft Excel, but they're usefulness has not been examined. Determining if these models have any applicability is left for the future.

The effect of the distance between fibers that do not touch was also investigated. This was not extended for use in the aforementioned models or otherwise considered in conjunction with other aspects of MFM. Further research into the effect of non-touching fibers is left for the future.

Finally, a computational model of a unit cell consisting of one fiber of variable angle is discussed. It is desired to understand the impact on the effective heat transfer coefficient of fibers that do not align directly in the preferred direction of heat transfer. This computational model was built using Python; however, is was not functional. There appeared to be an error with the boundary conditions. Completion of this model is left for future work.

4.2 Resistance Networks for Microfibrous Media

The thermal resistance of a non-homogeneous body can be modeled as a network of series and parallel resistances. From this network of resistances, an equivalent resistances can be calculated. An equivalent thermal conductivity can then be calculated from the equivalent resistance.

The equation of resistance is taken from University Physics Volume 2 (chapter 9.3 Resistivity and Resistance) [75].

$$R = \rho \frac{L}{A} \qquad [75] \tag{4.1}$$

Which can also be written as

$$R = \frac{1}{k} \frac{L}{A} \qquad [75] \tag{4.2}$$

Rearranged for an equivalent thermal conductivity as

$$k_{\text{eq}} = \frac{1}{R_{\text{eq}}} \frac{L}{A} \qquad [75] \tag{4.3}$$

Where

$R =$ resistance

$\rho =$ thermal resistivity

$k =$ thermal conductivity

$L =$ length

$A =$ cross-sectional area

eq = equivalent

MFM can be viewed as a grid of thermal resistances where some resistances are oriented in the desired direction of heat transfer and others are oriented perpendicular to the desired direction. This idea was shown in an unpublished working paper from IntraMicron authored by Dr. Hongyun Yang [76]. These resistances include those for the MFM fibers as well as the fluid within the MFM in use. Figure 4.1 shows four cells of resistances for MFM with one cell highlighted.

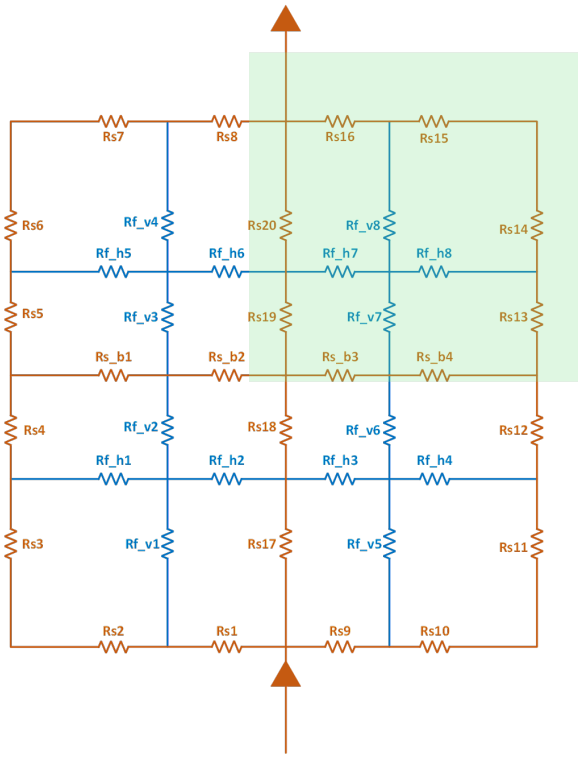

Figure 4.1: Grid of resistances for fibers and fluid within microfibrous media. Four unit cells of resistances are show with one cell highlighted. Resistance labels containing 'f' refer to fluid, and those containing 's' refer to fiber (solid). Labels containing 'v' refer to vertical (parallel to the direction of heat flow) and 'h' refer to horizontal (perpendicular to the direction of heat flow).

Simplifications are now made to the resistance grid shown in Figure 4.1. The first simplification made is removing the junction between vertical and horizontal fluid paths within each resistance cell. Further, the horizontal and vertical resistances are assumed to me numerous resistances originating from a single points and ending at single points. This

allows multiple fluid resistances in each direction to be calculated in parallel as equivalent resistances. This is shown for a single cell in Figure 4.2.

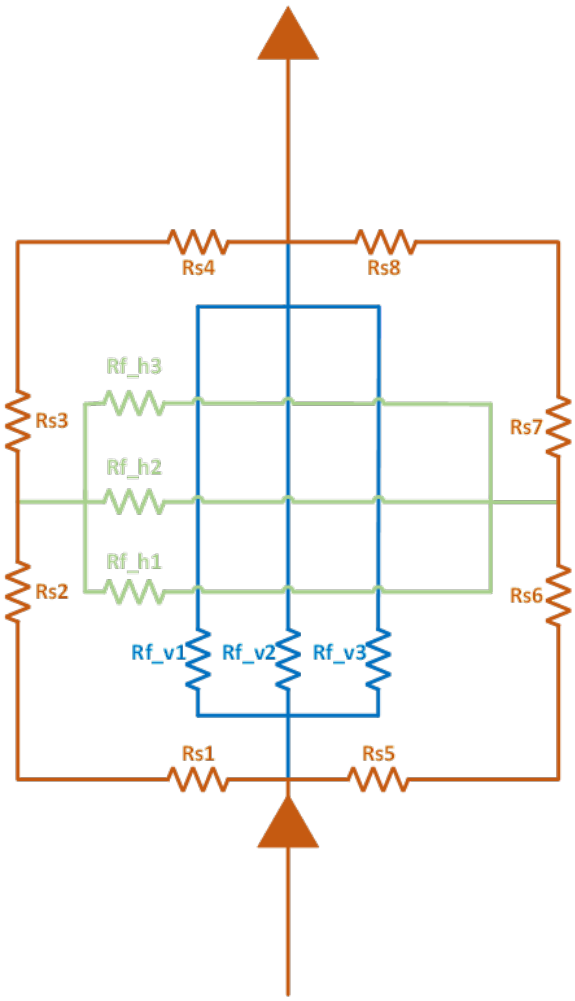

Figure 4.2: Single cell of resistances within microfibrous media with simplified fluid resistances in parallel.

Further, horizontal resistances can treated as wheatstone bridges. A wheatstone bridge is a resistance such as that depicted in 4.3 as Rs_b, and the bridge is considered balanced when no current passes through the bridge [77]. The balanced condition of the bridge in Figure 4.3 is shown in Equation 4.4. Applying this to Figure 4.1 results in Figure 4.4.

Equivalent thermal connectives were calculated for the resistance network shown in Figure 4.4 with various thermal conductivities for the fiber and fluid. Calculations were done with and without the inclusion of fluid resistances. The fluid resistances shown in

4.4 are calculated as equivalent resistances of multiple parallel fluid resistances as shown in 4.2. It is found that the addition of fluid pathways improves the equivalent thermal conductivity, and the equivalent thermal conductivity increases with increasing number of fluid resistances calculated in parallel to an asymptotic value of $k_{\text{eq}} = 2.5k_{\text{s}}$ (where k_{eq} is equivalent thermal conductivity and k_{s} is the fiber thermal conductivity).

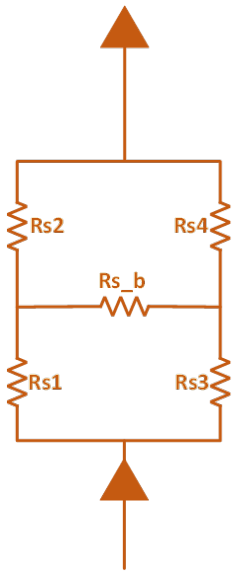

Figure 4.3: Diagram of a wheatstone bridge. RS_b is the bridge resistance.

$$\frac{R_2}{R_1} = \frac{R_4}{R_3} \tag{4.4}$$

4.3 Unit Cells for Microfibrous Media

It is desired to produce a simple model representation for microfibrous media. Toward that end, a number of simple unit cells are presented. The first simplification made is that fibers of circular cross section were approximated as fibers of square cross section with equal cross-sectional area.

The side length of the equivalent square fiber is calculated as

$$S_f = \frac{D_f\sqrt{\pi}}{2} \tag{4.5}$$

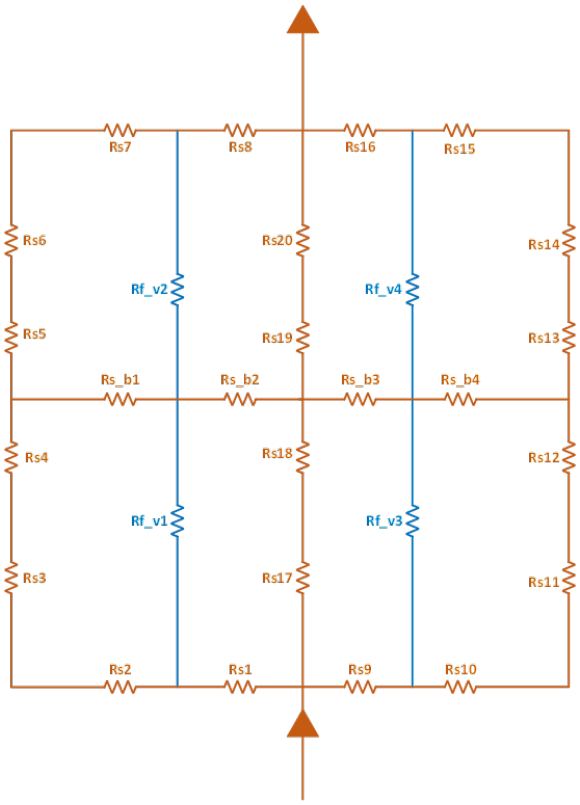

Figure 4.4: Simplified resistance diagram of resistances within microfibrous media with fluid.

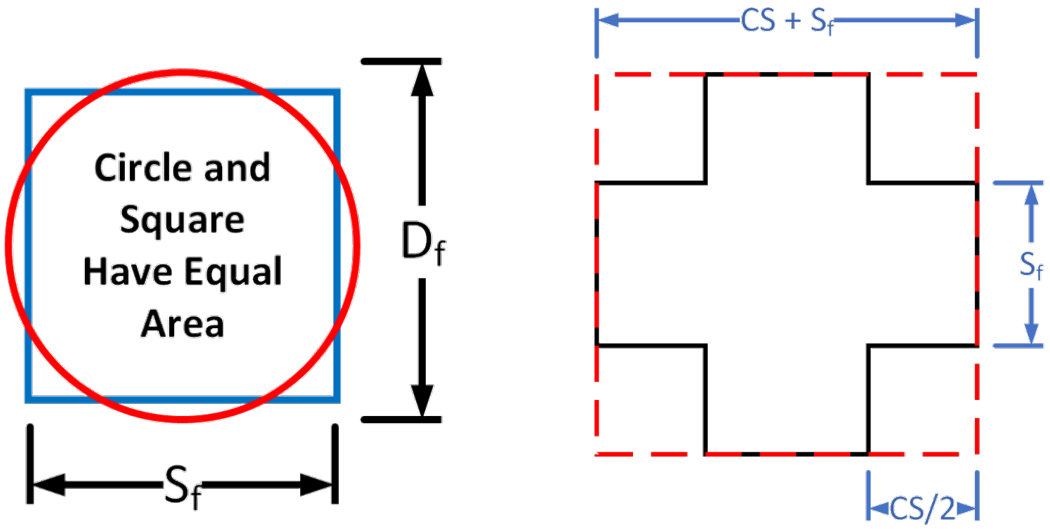

(a) Square fiber side compared to circular fiber diameter.

(b) Cage size of microfibrous media.

Figure 4.5: Representative square fiber compared to circular fiber and mesh cage size.

Where,

$$S_f = \text{side length of square-fiber cross-section}$$

$$D_f = \text{diameter of circular-fiber cross-section}$$

$$CS = \text{cage size}$$

A unit cell containing one straight fiber within a fluid is created. This case demonstrates the maximum stagnant effective thermal conductivity as determined by the parallel model [47, 48, 52].

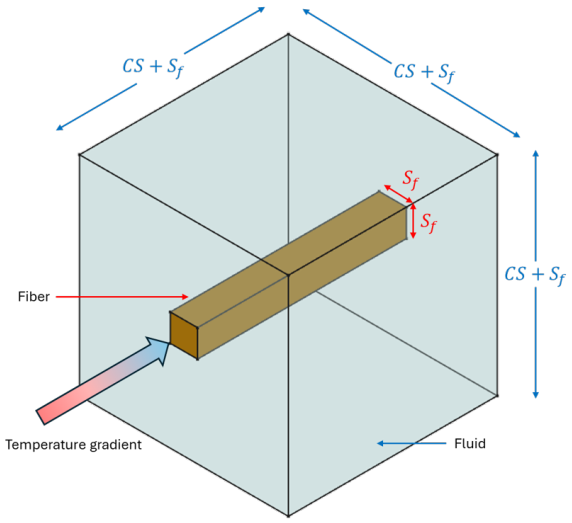

Figure 4.6: Cube unit cell of 1 fiber in fluid.

The next simplest unit cell presented is the cubic cell in Figure 4.7. This and the following unit cells consist of three intersecting perpendicular fibers. The simplification is made that these fibers pass through each other and are effectively one continuous medium. Figure 4.7b shows how the equivalent resistance of the unit cell is calculated. First, equivalent resistances are calculated for the three sections (1, 2, and 3) of the unit cell by adding the solid and fluid resistances in the section in parallel. Then, an equivalent resistance for the entire unit cell is calculated by adding the the three sections in series.

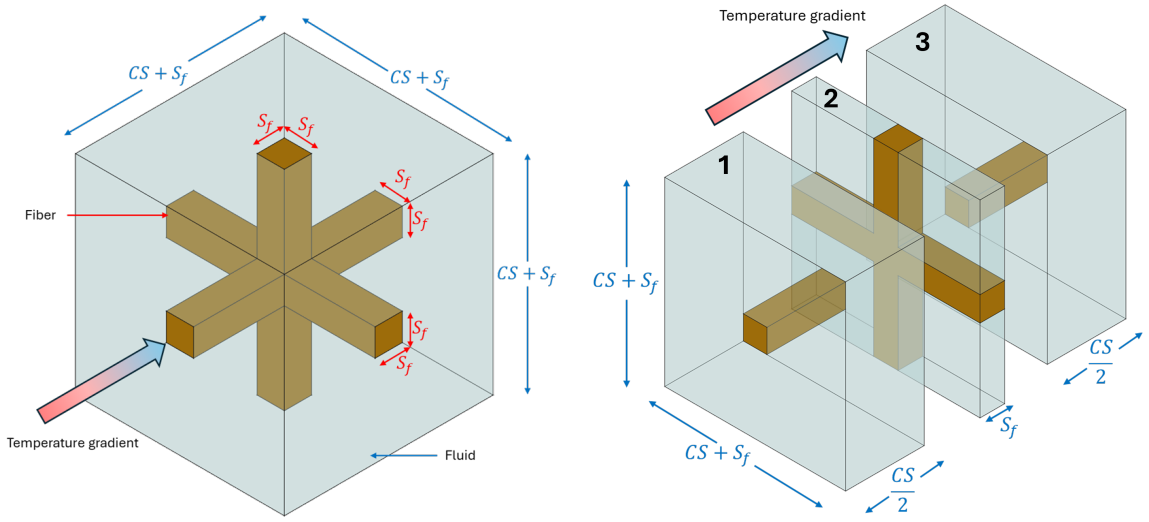

(a) Cube unit cell.

(b) Cube unit cell exploded view.

Figure 4.7: Cube unit cell for microfibrous media.

The simplification that the fibers pass through one another removes the resistance of the imperfect contacts that would exist in microfibrous media. To account for imperfect contact at sintered junctions between fibers, a junction factor is used. This is modeled as decrease in the diameter of the fibers at their intersection. A junction factor has previously been used by Sheng et al. [18], where it is defined as

$$\phi_{\text{Sheng}} = \frac{\text{crossing area of junction}}{\text{crossing area of bulk metal}}$$

In this work the junction factor will be defined as

$$\phi = \frac{\text{cross-sectional area of junction}}{\text{cross-sectional area of body fiber}}$$

Sheng et al. assumed the junction to be of infinitely small length [18]. In this work, the junction is assumed to be of length equal to side length of an equivalent square fiber. The junction factor implementation is shown in Figure 4.8.

Since microfibrous media is produced via paper-making techniques, the fibers in the media are preferentially oriented within a single plane. To adjust the cubic model to account

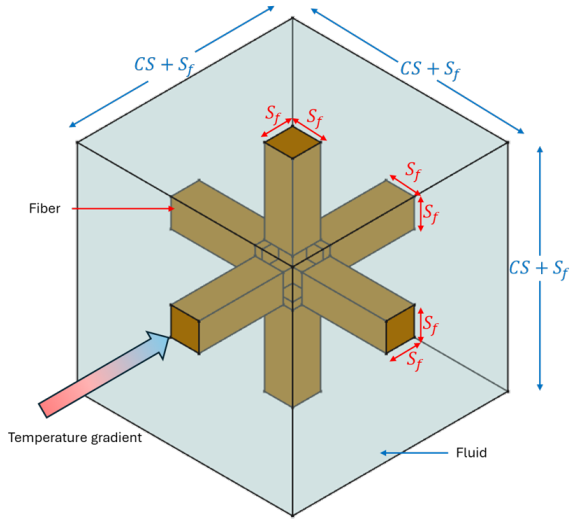

Figure 4.8: Cube unit cell for microfibrous media incorporating fiber junction.

for this, one dimension is made shorter than the other two. This shorter dimension is in the direction normal to the plane of preferential orientation. The two dimensions representing the directions of the plane of preferential orientation are equal. This unit cell is shown in Figure 4.9.

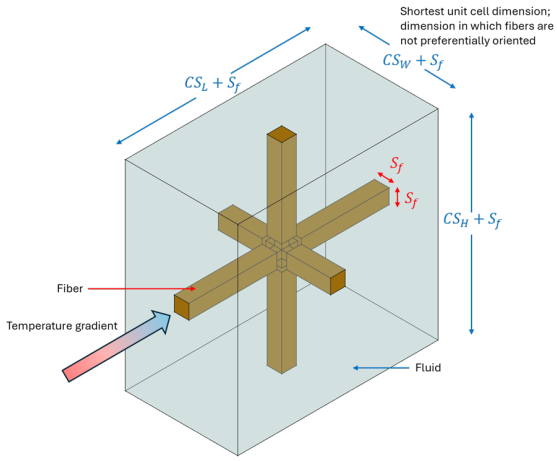

Figure 4.9: Rectangle unit cell for microfibrous media incorporating fiber junction.

4.3.1 Microfibrous Media (MFM) Fiber gap

The unit cells make the simplification that the fibers pass through one another where they intersect. However, in reality they are sintered junctions, and some fibers will pass near

another without actually being in contact with one another. Additionally, if the unit cells are stacked they create fibers of infinite length. The real fibers are of finite length, so there will likely be a gap distance between the ends of the fibers and the next closest fiber. Both of these illustrate why for microfibrous media there is an interest in knowing how the distance between fibers affects the effective thermal conductivity.

Figure 4.10 investigates the effect of gap distance between two fibers. A system of two fibers separated by fluid is modeled. The fibers are of equal and constant length, and the length of the fluid filled gap is varied. The system resistance is then calculated as the fiber and fluid resistances in series, and that is then used to calculate the system equivalent thermal conductivity.

The equation of resistance is taken from University Physics Volume 2 (chapter 9.3 Resistivity and Resistance) [75].

$$R = \rho \frac{L}{A} \qquad \text{[75]} \tag{4.6}$$

Which can also be written as

$$R = \frac{1}{k} \frac{L}{A} \qquad \text{[75]} \tag{4.7}$$

Where

$R =$ resistance

$\rho =$ thermal resistivity

$k =$ thermal conductivity

$L =$ length

$A =$ cross-sectional area

As mentioned, this method is based upon simply adding series resistances. It is noteworthy that it is likely more appropriate to calculate the system resistance using Newton's law of cooling at the solid fluid interfaces. This is left to future work.

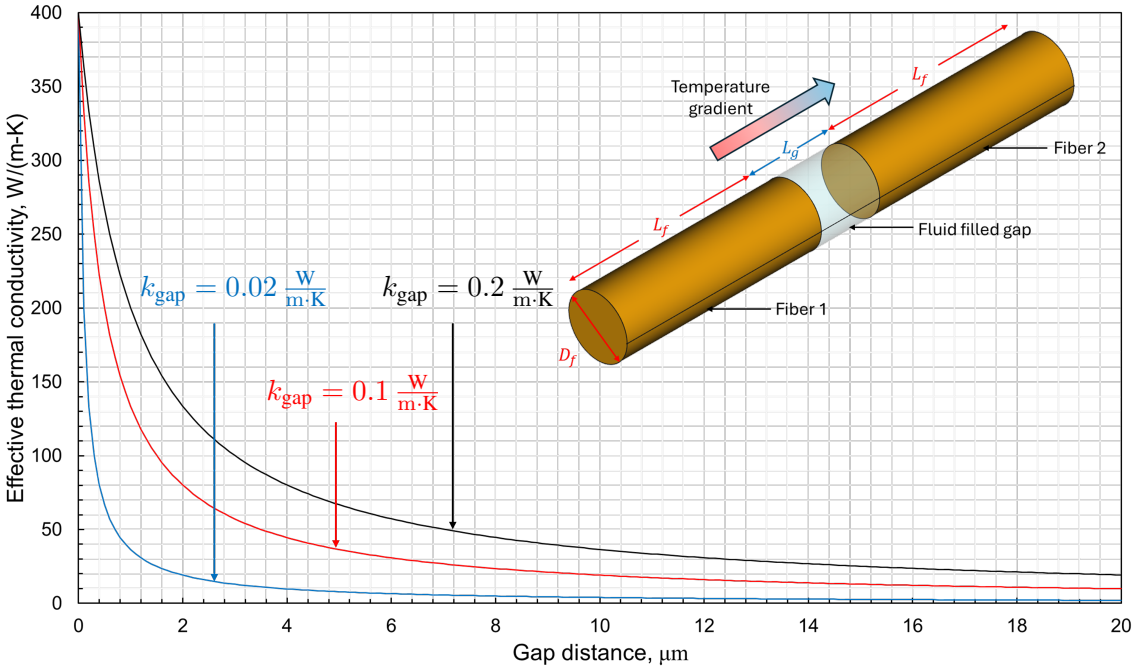

Figure 4.10: Effective thermal conductivity of a system of two fibers separated by a gap as a function of the length of the gap. Each fiber is $1000\,\mu m$ in length and $15.625\,\mu m$ in diameter. The fibers have a thermal conductivity of $400\,\frac{W}{m \cdot K}$.

In Equation 4.11 the mean free path of hydrogen is calculated from the equation given in Transport Phenomena [20], and the kinetic diameter of hydrogen is from Scholes et al. [78].

$$\lambda = \frac{1}{\sqrt{2}\pi d^2 n} \qquad [20] \tag{4.8}$$

Where

$\lambda =$ mean free path

$d =$ kinetic diameter

$n =$ Number of molecules per unit area

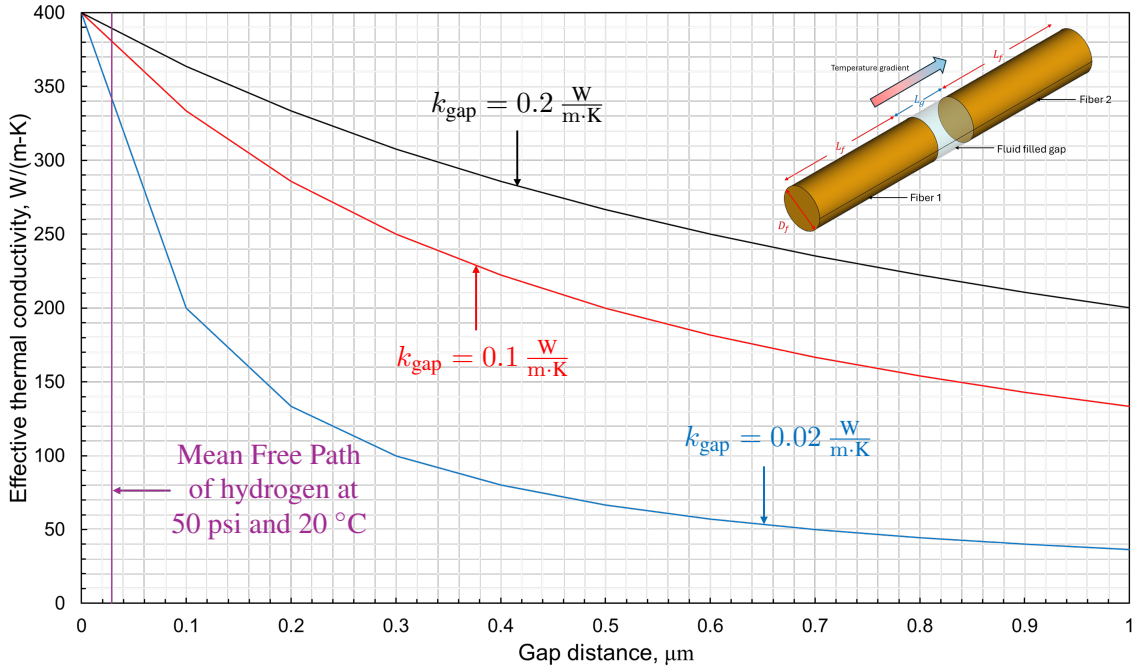

Figure 4.11: Effective thermal conductivity of a system of two fibers separated by a gap as a function of the length of the gap. Each fiber is $1000\,\mu m$ in length and $15.625\,\mu m$ in diameter. The fibers have a thermal conductivity of $400\,\frac{W}{m \cdot K}$. The mean free path of hydrogen is added for comparison against the gap distance.

4.4 Proposed Computational Model of a Unit Cell of Microfibrous Media

It is known that the fibers within microfibrous media are preferentially oriented in a single plane. However, in that plane not all fibers are oriented in the direction of desired heat flow. It is sought to understand the effect on effective thermal conductivity of the orientation of the fibers. This could be useful in predicting and understanding the effective thermal conductivity of microfibrous media. A method for determining the effect of fiber angle is suggested here.

A two-dimensional unit cell is constructed in Cartesian coordinates as shown in Figure 4.12. This cell is composed of a single fiber surrounded by a second material (may be solid or fluid depending and will change interface boundary condition). Using computation fluid dynamics, the average heat flux is determined, and from the average heat flux a thermal conductivity of an equivalent homogeneous material is calculated. By calculating the equivalent thermal conductivity from 0°(perpendicular to the direction of interest) to 90°(parallel to the direction of interest), the effect of the orientation of a single fiber is determined.

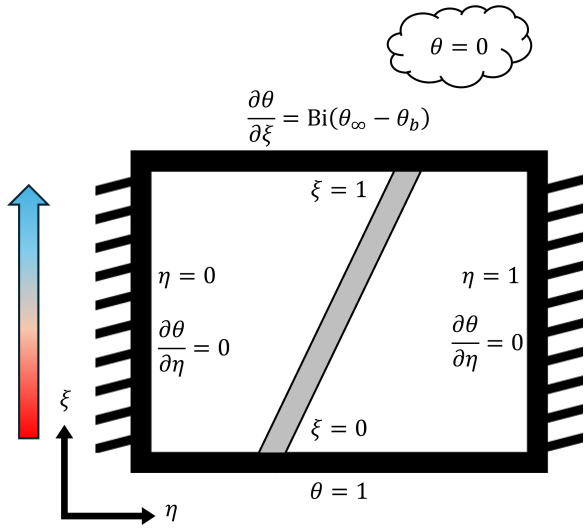

Figure 4.12: A two-dimensional cell consisting of a single fiber, surrounding materials, and walls.

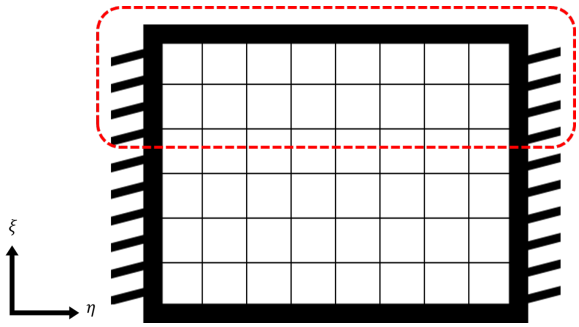

Figure 4.13: A representation of a discretized grid for Figure 4.12 with the positions used for calculating k_{eq} circled.

The energy equation in Cartesian coordinates is taken from Transport Phenomena [20]. For this problem, the energy equation simplifies to

$$\frac{\partial \theta}{\partial \tau} = \frac{\partial^2 \theta}{\partial \xi^2} + \beta \frac{\partial^2 \theta}{\partial \eta^2} \tag{4.9}$$

The boundary conditions for this problem are

$$\begin{aligned}
&\text{at } \xi = 0 \text{ , } \theta = 1 \\
&\text{at } \xi = 1 \text{ , } \frac{\partial \theta}{\partial \xi} = \text{Bi}(\theta_\infty - \theta_\text{b}) \\
&\text{at } \eta = 0 \text{ , } \frac{\partial \theta}{\partial \eta} = 0 \\
&\text{at } \eta = 1 \text{ , } \frac{\partial \theta}{\partial \eta} = 0 \\
&\text{at } \eta = \text{fiber/fill interface , } k_- \left.\frac{\partial \theta}{\partial \eta}\right|_- = k_+ \left.\frac{\partial \theta}{\partial \eta}\right|_+
\end{aligned}$$

The dimensionless variables are defined as follows:

$$\theta \equiv \frac{T_\infty - T}{T_\infty - T_0}$$
$$\beta \equiv \frac{L^2}{W^2}$$
$$\tau \equiv \frac{\alpha}{L^2} t$$
$$\xi \equiv \frac{x}{L}$$
$$\eta \equiv \frac{y}{W}$$

An implicit discretization of the energy equation for this problem is presented here. The time derivative is a forward time first order approximation, and the space derivatives are centered second order approximations.

$$\frac{\partial \theta}{\partial \tau} \approx \frac{\theta_{i,j}^{n+1} - \theta_{i,j}^{n}}{\Delta \tau} + \mathcal{O}[\Delta \tau] \tag{4.10}$$

$$\frac{\partial^2 \theta}{\partial \xi^2} \approx \frac{\theta_{i+1,j}^{n+1} - 2\theta_{i,j}^{n+1} + \theta_{i-1,j}^{n+1}}{(\Delta \xi)^2} + \mathcal{O}[(\Delta \xi)^2] \tag{4.11}$$

$$\frac{\partial^2 \theta}{\partial \eta^2} \approx \frac{\theta_{i,j+1}^{n+1} - 2\theta_{i,j}^{n+1} + \theta_{i,j-1}^{n+1}}{(\Delta \eta)^2} + \mathcal{O}[(\Delta \eta)^2] \tag{4.12}$$

The model equation is then converted to a finite difference equation using the finite difference approximations.

$$\frac{\theta_{i,j}^{n+1} - \theta_{i,j}^{n}}{\Delta \tau} = \frac{\theta_{i+1,j}^{n+1} - 2\theta_{i,j}^{n+1} + \theta_{i-1,j}^{n+1}}{(\Delta \xi)^2} + \beta \frac{\theta_{i,j+1}^{n+1} - 2\theta_{i,j}^{n+1} + \theta_{i,j-1}^{n+1}}{(\Delta \eta)^2} + \mathcal{O}[\Delta \tau, (\Delta \xi)^2, (\Delta \eta)^2] \tag{4.13}$$

It is proposed to determine the average heat flux at $\xi = 1$ of the unit cell, then use Fourier's law to calculate the equivalent thermal conductivity of a homogeneous material from the

average heat flux. The equation for the average heat flux is

$$q_{\text{avg}} = q_0 \left(\frac{\Delta\eta}{2}\right) + q_{N-1} \left(\frac{\Delta\eta}{2}\right) + \sum_{j=1}^{j=N-2} q_j \left(\Delta\eta\right) \tag{4.14}$$

Fourier's law applied to the average heat flux is

$$q_{\text{avg}} = \frac{k_{\text{eq}} \left(T_\infty - T_0\right)}{L} \left.\frac{\partial\theta}{\partial\xi}\right|_{\text{avg}} \tag{4.15}$$

Rearranging Fourier's law to solve for equivalent thermal conductivity.

$$k_{\text{eq}} = \left(\frac{\left(T_\infty - T_0\right)}{q_{\text{avg}} L} \left.\frac{\partial\theta}{\partial\xi}\right|_{\text{avg}}\right)^{-1} \tag{4.16}$$

A second-order, one-sided difference at a position (i, j) for the derivative in Fourier's law is

$$\left.\frac{\partial\theta}{\partial\xi}\right|_{i,j}^{n} \approx \frac{3\theta_{i,j}^{n} - 4\theta_{i-1,j}^{n} + \theta_{i-2,j}^{n}}{2\left(\Delta\xi\right)} + \mathcal{O}[(\Delta\xi)^2] \tag{4.17}$$

The proposed method for averaging the derivative across all η positions is

$$\left.\frac{\partial\theta}{\partial\xi}\right|_{\text{avg}} = \frac{1}{N} \sum_{j=1}^{N} \left(\left.\frac{\partial\theta}{\partial\xi}\right|_{j}\right) = \frac{1}{2(\Delta\xi)N} \sum_{j=1}^{N} \left(3\theta_{i,j} - 4\theta_{i-1,j} + \theta_{i-2,j}\right) + \mathcal{O}[(\Delta\xi)^2] \tag{4.18}$$

This leads to the equation for determining the equivalent thermal conductivity.

$$k_{\text{eq}} = 2(\Delta\xi) U_{\text{id}} L \frac{\sum_{j=1}^{N} (\theta_\infty - \theta_{\text{b}})}{\sum_{j=1}^{N} \left(3\theta_{i,j} - 4\theta_{i-1,j} + \theta_{i-2,j}\right)} \tag{4.19}$$

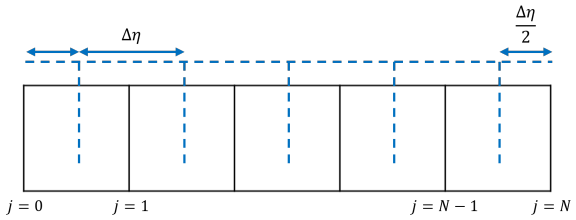

Figure 4.14: A visual representation of how the average heat flux is determined at $\xi = 1$.

Bibliography

[1] David Kohler et al. “Metal-Carbon Composite Materials from Fiber Precursors”. In: *Journal of The Electrochemical Society* 137 (1 Jan. 1990), pp. 136–141. ISSN: 00134651. DOI: 10.1149/1.2086793.

[2] J N Zabasajja et al. “Fabrication Of Composite Materials From Fibrous Precursors Using Paper Making Procedures”. In: *Materials Research Society Symposium Proceedings*. 1990, pp. 297–306.

[3] Bruce J. Tatarchuk et al. “Mixed fiber composite structures high surface area-high conductivity mixtures”. US Patent 5,080,963. Jan. 1992.

[4] Min Sheng et al. “Novel catalyst structures with enhanced heat transfer characteristics”. In: *Journal of Catalysis* 281 (2 2011), pp. 254–262. DOI: 10.1016/j.jcat.2011.05.006. URL: http://dx.doi.org/10.1016/j.jcat.2011.05.006.

[5] David Kohler et al. “Metal-Carbon Composite Electrodes from Fiber Precursors”. In: *Journal of The Electrochemical Society* 137 (6 June 1990), pp. 1750–1757. ISSN: 00134651. DOI: 10.1149/1.2086793.

[6] Bruce J. Tatarchuk et al. “Microfibrous entrapment of small reactive particulates and fibers for high contacting efficiency removal of contaminants from gaseous or liquid streams”. Patent Application Publication US 2005/016820 A1. Aug. 4, 2005.

[7] Hongyun Yang et al. “Methods for preparing highly porous microfibrous media with functional particles immobilized inside”. Patent Application Publication US 2015/0176894 A1. June 25, 2015.

[8] Ravi K. Duggirala et al. “Joint Numerical–Experimental Investigation of Enhanced Chemical Reactivity in Microfibrous Materials for Desulfurization”. In: *Journal of Fluids Engineering* 137 (3 2015). ISSN: 0098-2202. DOI: 10.1115/1.4028602. URL: http://fluidsengineering.asmedigitalcollection.asme.org/article.aspx?doi=10.1115/1.4028602.

[9] Xinquan Cheng, Hongyun Yang, and Bruce J. Tatarchuk. “Microfibrous entrapped hybrid iron-based catalysts for Fischer–Tropsch synthesis”. In: *Catalysis Today* 273 (Mar. 2016), pp. 62–71. DOI: 10.1016/j.cattod.2016.02.048. URL: http://dx.doi.org/10.1016/j.cattod.2016.02.048.

[10] Shirish S. Punde and Bruce J. Tatarchuk. “Microfibrous entrapped catalysts for low temperature CO oxidation in humid air”. In: *Catalysis Communications* 27 (2012), pp. 9–12. ISSN: 15667367. DOI: 10.1016/j.catcom.2012.06.011. URL: http://dx.doi.org/10.1016/j.catcom.2012.06.011.

[11] Shirish S. Punde and Bruce J. Tatarchuk. “Metal microfibers entrapped catalysts as effective ambient temperature CO oxidation catalysts”. In: *Applied Catalysis A: General* 441-442 (2012), pp. 54–64. ISSN: 0926860X. DOI: 10.1016/j.apcata.2012.07.021. URL: http://dx.doi.org/10.1016/j.apcata.2012.07.021.

[12] Qiang Gu, Robert T. Henderson, and Bruce J. Tatarchuk. “A CFD pressure drop model for microfibrous entrapped catalyst filters using micro-scale imaging”. In: *Engineering Applications of Computational Fluid Mechanics* 9 (1 2015), pp. 567–576. ISSN: 1997003X. DOI: 10.1080/19942060.2015.1094415.

[13] Donald R. Cahela and Bruce J. Tatarchuk. “Permeability of sintered microfibrous composites for heterogeneous catalysis and other chemical processing opportunities”. In: *Catalysis Today* 69 (1-4 Sept. 2001), pp. 33–39. ISSN: 09205861. DOI: 10.1016/S0920-5861(01)00352-2.

[14] Min Sheng et al. “Micro scale heat transfer comparison between packed beds and microfibrous entrapped catalysts”. In: *Engineering Applications of Computational Fluid Mechanics* 7 (4 2013), pp. 471–485. ISSN: 1997003X. DOI: 10.1080/19942060.2013.11015486.

[15] Min Sheng et al. “High conductivity catalyst structures for applications in exothermic reactions”. In: *Applied Catalysis A: General* 445-446 (2012), pp. 143–152. ISSN: 0926860X. DOI: 10.1016/j.apcata.2012.08.012. URL: http://dx.doi.org/10.1016/j.apcata.2012.08.012.

[16] Wenhua H. Zhu et al. “A novel cooling structure with a matrix block of microfibrous media / phase change materials for heat transfer enhancement in high power Li-ion battery packs”. In: *Journal of Cleaner Production* 210 (Feb. 2019), pp. 542–551. ISSN: 09596526. DOI: 10.1016/j.jclepro.2018.11.043.

[17] Min Sheng. “Enhanced Heat Transfer Catalyst Structures for Fischer-Tropsch Synthesis”. PhD thesis. Auburn University, 2011.

[18] Min Sheng et al. “Effective thermal conductivity and junction factor for sintered microfibrous materials”. In: *International Journal of Heat and Mass Transfer* 56 (1-2 2013), pp. 10–19. ISSN: 00179310. DOI: 10.1016/j.ijheatmasstransfer.2012.08.015. URL: http://dx.doi.org/10.1016/j.ijheatmasstransfer.2012.08.015.

[19] ASTM International. *Standard Specification for Standard Nominal Diameters and Cross-Sectional Areas of AWG Sizes of Solid Round Wires Used as Electrical Conductors*. ASTM Standard B258-18. Oct. 2018. DOI: 10.1520/B0258-18. URL: www.astm.org.

[20] R. B. Bird, Warren E. Stewart, and Edwin N. Lightfoot. *Transport Phenomena*. Ed. by Wayne; Anderson and Petrina Kulek. Revised Se. John Wiley & Sons, 2007. ISBN: 9780470115398.

[21] J. G. Charney, R. Fjörtoft, and J. von Neumann. "Numerical Integration of the Barotropic Vorticity Equation". In: *Tellus* 2 (4 Nov. 1950), pp. 237–254. ISSN: 00402826. DOI: 10.1111/j.2153-3490.1950.tb00336.x.

[22] Thomas H. Pulliam and David W. Zingg. *Fundamental Algorithms in Computational Fluid Dynamics*. Ed. by J.-J. Chattot et al. Springer International Publishing, 2014. ISBN: 978-3-319-05052-2. DOI: 10.1007/978-3-319-05053-9.

[23] John M. Prausnitz, Rüdiger N. Lichtenthaler, and Edmundo Gomes de Azevedo. *Molecular Thermodynamics of Fluid-Phase Equilibria*. Ed. by Neal R. Amundson et al. Third. Prentice Hall, 1999, p. 860. ISBN: 0-13-977745-8.

[24] J. H. Dymond and E. B. Smith. *The Virial Coefficients of Pure Gases and Mixtures A Critical Compilation*. Oxford University Press, 1980, p. 518. ISBN: 0-19-855361-7.

[25] S. Angus, B. Armstrong, and K. M. de Reuck. *International Thermodynamic Tables of the Fluid State Carbon Dioxide*. Pergamon Press, 1976. ISBN: 9780080209241. URL: https://search.worldcat.org/title/79693556.

[26] A. Michels et al. "Isotherms of carbon monoxide between 0°C and 150°C and at pressures up, to 3000 atmospheres". In: *Physica* 18 (2 Feb. 1952), pp. 121–127. ISSN: 0031-8914. DOI: 10.1016/S0031-8914(52)80275-7.

[27] A. E. Sherwood and J. M. Prausnitz. “Intermolecular potential functions and the second and third virial coefficients”. In: *The Journal of Chemical Physics* 41 (2 1964), pp. 429–437. ISSN: 00219606. DOI: 10.1063/1.1725884.

[28] Marcia L. Huber and Allan H. Harvey. “Thermal Conductivity of Gases”. In: *CRC Handbook of Chemistry and Physics*. 92nd ed. CRC-Press, 2011. Chap. 6, pp. 240–241.

[29] V. Vesovic et al. “The Transport Properties of Carbon Dioxide”. In: *Journal of Physical and Chemical Reference Data* 19 (3 May 1990), pp. 763–808. ISSN: 0047-2689. DOI: 10.1063/1.555875. URL: /aip/jpr/article/19/3/763/457276/The-Transport-Properties-of-Carbon.

[30] Eckhard Vogel et al. “Ab initio pair potential energy curve for the argon atom pair and thermophysical properties for the dilute argon gas. II. Thermophysical properties for low-density argon”. In: *Molecular Physics* 108 (24 Dec. 2010), pp. 3335–3352. ISSN: 00268976. DOI: 10.1080/00268976.2010.507557. URL: https://www.tandfonline.com/doi/abs/10.1080/00268976.2010.507557.

[31] Eric F. May, Robert F. Berg, and Michael R. Moldover. “Reference viscosities of H 2, CH 4, Ar, and Xe at low densities”. In: *International Journal of Thermophysics* 28 (4 Aug. 2007), pp. 1085–1110. ISSN: 0195928X. DOI: 10.1007/S10765-007-0198-7/METRICS. URL: https://link.springer.com/article/10.1007/s10765-007-0198-7.

[32] E. W. Lemmon and R. T. Jacobsen. “Viscosity and thermal conductivity equations for nitrogen, oxygen, argon, and air”. In: *International Journal of Thermophysics* 25 (1 Jan. 2004), pp. 21–69. ISSN: 0195928X. DOI: 10.1023/B:IJOT.0000022327.04529.F3. URL: https://www.researchgate.net/publication/

226578149_Viscosity_and_Thermal_Conductivity_Equations_for_Nitrogen_Oxygen_Argon_and_Air.

[33] John J. Hurly and James B. Mehl. "He Thermophysical Properties: New Ab Initio Calculations". In: *Journal of research of the National Institute of Standards and Technology* 112 (2 2007), pp. 75–94. ISSN: 1044-677X. DOI: 10.6028/JRES.112.006. URL: https://pubmed.ncbi.nlm.nih.gov/27110456/.

[34] James B. Mehl, Marcia L. Huber, and Allan H. Harvey. "Ab initio transport coefficients of gaseous hydrogen". In: *International Journal of Thermophysics* 31 (4-5 May 2010), pp. 740–755. ISSN: 0195928X. DOI: 10.1007/S10765-009-0697-9/METRICS. URL: https://link.springer.com/article/10.1007/s10765-009-0697-9.

[35] Eite Tiesinga et al. "Codata recommended values of the fundamental physical constants: 2018". In: *Reviews of Modern Physics* 93 (2 June 2021). ISSN: 15390756. DOI: 10.1103/RevModPhys.93.025010.

[36] National Institute of Standards and Technology (U.S. Department of Commerce). *Carbon dioxide*. Accessed on May 2, 2023. URL: https://webbook.nist.gov/cgi/inchi/InChI%3D1S/CO2/c2-1-3.

[37] National Institute of Standards and Technology (U.S. Department of Commerce). *Argon*. Accessed on May 2, 2023. URL: https://webbook.nist.gov/cgi/inchi/InChI%3D1S/Ar.

[38] National Institute of Standards and Technology (U.S. Department of Commerce). *Nitrogen*. Accessed on May 2, 2023. URL: https://webbook.nist.gov/cgi/inchi/InChI%3D1S/N2/c1-2.

[39] National Institute of Standards and Technology (U.S. Department of Commerce). *Oxygen*. Accessed on May 2, 2023. URL: https://webbook.nist.gov/cgi/inchi/InChI%3D1S/O2/c1-2.

[40] National Institute of Standards and Technology (U.S. Department of Commerce). *Helium*. Accessed on May 2, 2023. URL: https://webbook.nist.gov/cgi/inchi/InChI%3D1S/He.

[41] National Institute of Standards and Technology (U.S. Department of Commerce). *Hydrogen*. Accessed on May 2, 2023. URL: https://webbook.nist.gov/cgi/inchi/InChI%3D1S/H2/h1H.

[42] George S. Parks and C. Howard Shomate. "Some heat capacity data for isopropyl alcohol vapor". In: *The Journal of Chemical Physics* 8 (5 1940), pp. 429–429. ISSN: 00219606. DOI: 10.1063/1.1750679. URL: https://aip.scitation.org/doi/abs/10.1063/1.1750679.

[43] Peter Freeman, Stephen Doe, and Aneta Siemiginowska. "Sherpa: a mission-independent data analysis application". In: *Proceedings of SPIE*. Vol. 4477. Astronomical Data Analysis. Nov. 1, 2001, pp. 76–87. DOI: 10.1117/12.447161.

[44] Michael T. Heath. *Scientific Computing An Introductory Survey*. Second Edi. McGraw-Hill, 2002. ISBN: 0072399104.

[45] Smithsonian Astrophysical Observatory Chandra X-ray Center. *A quick guide to modeling and fitting in Sherpa — Sherpa 4.16.1 documentation*. Accessed on July 17, 2024. URL: https://sherpa.readthedocs.io/en/4.16.1/quick.html.

[46] Smithsonian Astrophysical Observatory Chandra X-ray Center. *LevMar — Sherpa 4.16.1 documentation*. Accessed on July 17, 2024. URL: https://sherpa.readthedocs.io/en/4.16.1/optimisers/api/sherpa.optmethods.LevMar.html#sherpa.optmethods.LevMar.ftol.

[47] Xuan Qin and Wanjun Yin. "A novel fractal model for effective thermal conductivity in granular porous media". In: *Geothermics* 108 (Feb. 2023), p. 102625. ISSN: 0375-6505. DOI: 10.1016/J.GEOTHERMICS.2022.102625.

[48] D. A. Nield. “Estimation of the stagnant thermal conductivity of saturated porous media”. In: *International Journal of Heat and Mass Transfer* 34 (6 June 1991), pp. 1575–1576. ISSN: 0017-9310. DOI: 10.1016/0017-9310(91)90300-4.

[49] Dongsheng Wen and Yulong Ding. “Heat transfer of gas flow through a packed bed”. In: *Chemical Engineering Science* 61 (11 June 2006), pp. 3532–3542. ISSN: 0009-2509. DOI: 10.1016/J.CES.2005.12.027.

[50] I. H. Tavman. “Effective thermal conductivity of granular porous materials”. In: *International Communications in Heat and Mass Transfer* 23 (2 1996), pp. 169–176. ISSN: 07351933. DOI: 10.1016/0735-1933(96)00003-6. URL: https://www.researchgate.net/publication/222602873_Effective_thermal_conductivity_of_granular_porous_materials.

[51] R. Krupiczka. “Analysis of thermal conductivity in granular materials”. In: *International Chemical Engineering* 7 (1 1967), pp. 122–144.

[52] R. G. Deissler and J. S. Boegli. “An Investigation of Effective Thermal Conductivities of Powders in Various Gases”. In: *Journal of Fluids Engineering* 80 (7 Oct. 1958), pp. 1417–1423. ISSN: 0097-6822. DOI: 10.1115/1.4012740.

[53] Jianfeng Wang et al. “A new approach to modelling the effective thermal conductivity of heterogeneous materials”. In: *International Journal of Heat and Mass Transfer* 49 (17-18 Aug. 2006), pp. 3075–3083. ISSN: 00179310. DOI: 10.1016/J.IJHEATMASSTRANSFER.2006.02.007.

[54] James Clerk Maxwell. *A Treatise on Electricity and Magnetism*. Vol. I. Macmillan and Co., 1873, p. 365.

[55] Y C Chiew and E D Glandt. “The Effect of Structure on the Conductivity of a Dispersion”. In: *Journal of Colloid and Interface Science* 94 (1 July 1983), pp. 90–104.

[56] Rolf Landauer. “The Electrical Resistance of Binary Metallic Mixtures”. In: *Journal of Applied Physics* 23 (7 July 1952), pp. 779–784. ISSN: 0021-8979. DOI: 10.1063/1.1702301. URL: /aip/jap/article/23/7/779/159999/The-Electrical-Resistance-of-Binary-Metallic.

[57] A. D. Brailsford et al. “The thermal conductivity of aggregates of several phases, including porous materials”. In: *British Journal of Applied Physics* 15 (3 1964), pp. 313–319. ISSN: 0052-1123. DOI: 10.1088/0508-3443/15/3/311. URL: https://ui.adsabs.harvard.edu/abs/1964BJAP...15..313B/abstract.

[58] Elio E Gonzo. “Estimating correlations for the effective thermal conductivity of granular materials”. In: *Chemical Engineering Journal* 90 (2002), pp. 299–302.

[59] Mohammadhassan Vasheghani et al. “Effect of Al_2O_3 phases on the enhancement of thermal conductivity and viscosity of nanofluids in engine oil”. In: *Heat and Mass Transfer/Wärme- und Stoffübertragung* 47 (11 May 2011), pp. 1401–1405. ISSN: 09477411. DOI: 10.1007/s00231-011-0806-8.

[60] Sabri Ergun. “Fluid Flow Through Packed Columns”. In: *Chemical Engineering Progress* 48 (2 1952), pp. 89–94.

[61] William Sutherland. “LII. The viscosity of gases and molecular force”. In: *The London, Edinburgh, and Dublin Philosophical Magazine and Journal of Science* 36 (223 Dec. 1893), pp. 507–531. ISSN: 1941-5982. DOI: 10.1080/14786449308620508.

[62] Crane Company. *Flow of fluids through valves, fittings and pipe*. 1982.

[63] M. Molenda et al. “Airflow Resistance Of Seeds At Different Bulk Densities Using Ergun’s Equation”. In: *Transactions of the American Society of Agricultural Engineers* 48 (3 May 2005), pp. 1137–1145. ISSN: 00012351. DOI: 10.13031/2013.18487. URL: https://elibrary.asabe.org/azdez.asp?JID=3&AID=18487&CID=t2005&v=48&i=3&T=1.

[64] Marcia L. Huber. “Viscosity Of Gases”. In: *CRC Handbook of Chemistry and Physics*. CRC Press, 2019. URL: https://www.nist.gov/publications/viscosity-gases-0.

[65] D. G. Bunnell et al. “Effective Thermal Conductivities in Gas-Solid Systems”. In: *Industrial & Engineering Chemistry* 41 (9 Sept. 1949), pp. 1977–1981. ISSN: 0019-7866. DOI: 10.1021/IE50477A033. URL: https://pubs.acs.org/doi/abs/10.1021/ie50477a033.

[66] Oliver Bey and Gerhart Eigenberger. “Gas flow and heat transfer through catalyst filled tubes”. In: *International Journal of Thermal Sciences* 40 (2 Feb. 2001), pp. 152–164. ISSN: 1290-0729. DOI: 10.1016/S1290-0729(00)01204-7.

[67] Sakae Yagi and Daizo Kunii. “Studies on effective thermal conductivities in packed beds”. In: *AIChE Journal* 3 (3 Sept. 1957), pp. 373–381. ISSN: 1547-5905. DOI: 10.1002/AIC.690030317. URL: https://onlinelibrary.wiley.com/doi/full/10.1002/aic.690030317.

[68] D. VORTMEYER and R. P. WINTER. “Impact of Porosity and Velocity Distribution on the Theoretical Prediction of Fixed-Bed Chemical Reactor Performance”. In: *Chemical Reaction Engineering—Boston*. Chap. 5, pp. 49–61. DOI: 10.1021/bk-1982-0196.ch005. eprint: https://pubs.acs.org/doi/pdf/10.1021/bk-1982-0196.ch005.

[69] Sakae Yagi, Daizo Kunii, and Noriaki Wakao. “Studies on axial effective thermal conductivities in packed beds”. In: *AIChE Journal* 6 (4 Dec. 1960), pp. 543–546. ISSN: 1547-5905. DOI: 10.1002/AIC.690060407. URL: https://onlinelibrary.wiley.com/doi/full/10.1002/aic.690060407.

[70] Y. Demirel, R. N. Sharma, and H. H. Al-Ali. “On the effective heat transfer parameters in a packed bed”. In: *International Journal of Heat and Mass Transfer* 43 (2

Jan. 2000), pp. 327–332. ISSN: 0017-9310. DOI: 10.1016/S0017-9310(99)00126-X.

[71] Rodrigo Béttega et al. “Mathematical simulation of radial heat transfer in packed beds by pseudohomogeneous modeling”. In: *Particuology* 9 (2 Apr. 2011), pp. 107–113. ISSN: 16742001. DOI: 10.1016/j.partic.2010.09.009.

[72] M. L. Hunt and C. L. Tien. “Non-Darcian Convection in Cylindrical Packed Beds”. In: *Journal of Heat Transfer* 110 (2 May 1988), pp. 378–384. ISSN: 0022-1481. DOI: 10.1115/1.3250495. URL: https://dx.doi.org/10.1115/1.3250495.

[73] Reinaldo Giudici. “Transferencia de calor em reator de leito fixo: modelo que incorpora nao-uniformidades radiais do leito”. In: *Proceedings of XIX Encontro sobre Escoamento em Meios Porosos*. 1991, pp. 262–273. URL: https://repositorio.usp.br/item/000838848.

[74] A. P. de Wasch and G. F. Froment. “Heat transfer in packed beds”. In: *Chemical Engineering Science* 27 (3 Mar. 1972), pp. 567–576. ISSN: 0009-2509. DOI: 10.1016/0009-2509(72)87012-X.

[75] Samuel J. Ling, William Moebs, and Jeff Sanny. *University Physics Volume 2*. Accessed on May 4, 2024. OpenStax, Oct. 2016. URL: https://openstax.org/books/university-physics-volume-2/pages/preface.

[76] Hongyun Yang. “Heat Transfer Experiment”. Unpublished.

[77] ElectronicsTutorials. *Wheatstone Bridge*. Accessed on June 4, 2024. URL: https://www.electronics-tutorials.ws/blog/wheatstone-bridge.html.

[78] Colin A. Scholes, Sandra E. Kentish, and Geoff W. Stevens. “Carbon Dioxide Separation through Polymeric Membrane Systems for Flue Gas Applications”. In: *Recent*

Patents on Chemical Engineering 1 (1 Jan. 2010), pp. 52–66. ISSN: 18744788. DOI: 10.2174/1874478810801010052.